



# Isotopic Fingerprints of Organic Pollutants

Quantifying sources and sinks of organic pollutants  
with isotope analysis from aquifer to catchment scale

Stefanie R. Lutz

**Isotopic Fingerprints of Organic Pollutants**  
**Quantifying Sources and Sinks of Organic**  
**Pollutants with Isotope Analysis from Aquifer to**  
**Catchment Scale**

Stefanie Rayana Lutz

Cover page: Dorothea Konkol

Isotopic Fingerprints of Organic Pollutants  
(PhD Thesis, VU University Amsterdam)

© S.R. Lutz, 2015

This research has been financially supported by the European Union under the 7th Framework Programme (project acronym CSI:ENVIRONMENT, contract number PITN-GA-2010-264329.)

VRIJE UNIVERSITEIT

# Isotopic Fingerprints of Organic Pollutants

Quantifying Sources and Sinks of Organic Pollutants with Isotope  
Analysis from Aquifer to Catchment Scale

ACADEMISCH PROEFSCHRIFT

ter verkrijging van de graad Doctor aan  
de Vrije Universiteit Amsterdam,  
op gezag van de rector magnificus  
prof.dr. F.A. van der Duyn Schouten,  
in het openbaar te verdedigen  
ten overstaan van de promotiecommissie  
van de Faculteit der Aard- en Levenswetenschappen  
op woensdag 4 maart 2015 om 9.45 uur  
in de aula van de universiteit,  
De Boelelaan 1105

door

Stefanie Rayana Lutz

geboren te Frankfurt am Main, Duitsland

promotor: prof.dr. P.J. Stuyfzand  
copromotoren: dr. B.M. van Breukelen  
dr. H.J. van Meerveld

reading committee: dr. H.P. Broers  
dr. M. Elsner  
prof.dr. D. Hunkeler  
prof.dr. S. Uhlenbrook  
prof.dr. S.E.A.T.M. van der Zee

Twenty years from now you will be more disappointed by the things you didn't do than by the ones you did do. So throw off the bowlines. Sail away from the safe harbor. Catch the trade winds in your sails. Explore. Dream. Discover.

*H. Jackson Brown Jr.'s mother*

# Contents

<b>Samenvatting</b>	<b>1</b>
<b>Zusammenfassung</b>	<b>5</b>
<b>1 General Introduction</b>	<b>9</b>
1.1 Background . . . . .	10
1.1.1 Organic contaminants: isotope-based assessment of sources and sinks . . . . .	10
1.1.2 Sources and sinks of pesticides at catchment scale . . . . .	12
1.1.3 Modeling of sources and sinks of organic water pollutants . .	14
1.2 Thesis objectives . . . . .	15
1.3 Thesis outline . . . . .	15
<b>2 A stable isotope model for combined source apportionment and degradation quantification of organic pollutants: model derivation</b>	<b>17</b>
2.1 Introduction . . . . .	18
2.2 Theoretical background . . . . .	19
2.2.1 The Rayleigh equation: calculation of pollutant degradation .	19
2.2.2 Stable isotope mixing model: source apportionment . . . . .	20
2.3 Results and Discussion . . . . .	21
2.3.1 Derivation of the Stable Isotope Sources and Sinks Model . .	21
2.3.2 Degradation follows mixing: single-element CSIA . . . . .	22
2.3.3 Degradation follows mixing: dual-element CSIA . . . . .	23
2.3.4 Mixing follows degradation: dual-element CSIA . . . . .	25
2.3.5 Unequivocal source apportionment with dual-element CSIA .	29
2.4 Conclusions . . . . .	31
Supplementary information . . . . .	32
<b>3 A stable isotope model for combined source apportionment and degradation quantification of organic pollutants: model valida- tion and application</b>	<b>45</b>
3.1 Introduction . . . . .	46
3.2 Methods . . . . .	47
3.2.1 Summary of the SISS model . . . . .	47

---

3.2.2	Reactive transport model setup . . . . .	48
3.3	Results and Discussion . . . . .	49
3.3.1	Model validation: virtual data set . . . . .	49
3.3.2	Model validation: extent of degradation . . . . .	49
3.3.3	Model validation: source apportionment . . . . .	51
3.3.4	Model application: description of the case study . . . . .	52
3.3.5	Model application: preliminary qualitative analysis . . . . .	52
3.3.6	Model application: SA and QED in the mixing zone . . . . .	55
3.3.7	Uncertainties and complications in the use of the SISS model . . . . .	58
3.4	Conclusions . . . . .	59
	Supplementary information . . . . .	61
<b>4</b>	<b>A model-based assessment of the potential use of CSIA in the analysis of diffuse pesticide pollution</b>	<b>67</b>
4.1	Introduction . . . . .	68
4.2	Methods . . . . .	70
4.2.1	Model code description: HydroGeoSphere . . . . .	70
4.2.2	Hillslope geometry and model grid . . . . .	70
4.2.3	Hydraulic properties and flow simulation . . . . .	71
4.2.4	Reactive solute transport . . . . .	72
4.2.5	Simulation of isotope fractionation effects . . . . .	73
4.2.6	Simulated scenarios . . . . .	75
4.2.7	Post-model calculations . . . . .	77
4.3	Results . . . . .	78
4.3.1	Scenario 1: steady-state flow conditions . . . . .	78
4.3.2	Scenario 2: extreme rainfall event . . . . .	80
4.3.3	Scenario 3: transient simulation for water flow and solute input . . . . .	81
4.4	Discussion . . . . .	83
4.4.1	Pesticide movement through the hillslope . . . . .	83
4.4.2	Carbon and hydrogen isotope ratios . . . . .	84
4.4.3	Responses to rainfall events . . . . .	86
4.4.4	Validity of model assumptions . . . . .	88
4.4.5	Implications for the applicability of CSIA to assess pesticide transport and transformation . . . . .	89
4.5	Conclusions . . . . .	92
<b>5</b>	<b>CSIA of pesticides: a combined monitoring and modeling approach to assess pesticide fate and degradation at catchment scale</b>	<b>95</b>
5.1	Introduction . . . . .	96
5.2	Methods . . . . .	97
5.2.1	Field measurements . . . . .	97
5.2.2	Hydrological model . . . . .	101
5.2.3	Pesticide model . . . . .	102
5.2.4	Input data and calibration . . . . .	104
5.3	Results and Discussion . . . . .	106

---

5.3.1	Monitoring results . . . . .	106
5.3.2	Modeling results . . . . .	111
5.4	Conclusions . . . . .	119
	Supplementary information . . . . .	121
<b>6</b>	<b>Synthesis</b>	<b>125</b>
6.1	Summary . . . . .	126
6.2	Implications and Outlook . . . . .	128
6.2.1	Assessment of contaminant sources and sinks with the SISS model . . . . .	128
6.2.2	Applicability of CSIA for diffuse pollutants . . . . .	129
6.2.3	Recommendations for modeling of CSIA of diffuse pollutants	130
	<b>Acknowledgments</b>	<b>133</b>



# List of Figures

1.1	Conceptualization of degradation-induced changes in the isotopic composition of an organic contaminant. . . . .	11
1.2	Use of dual-element isotope analysis for source apportionment between two sources and distinction between two reaction pathways, and complications in the use of dual-element CSIA due to the combined effect of mixing between sources and isotope-fractionation. . . . .	11
1.3	Schematic overview of pesticide transport routes and transformation processes. . . . .	13
2.1	Schematic representation of the temporal sequence of mixing and degradation processes in the two discussed scenarios. . . . .	22
2.2	Two-dimensional isotope plot of a scenario of degradation that follows mixing of two emission sources. . . . .	23
2.3	Two-dimensional isotope plot of a scenario of mixing that follows independent degradation of two contaminant pools. . . . .	27
2.4	Calculation of the minima of the non-degraded fractions from sources A and B based on the dual-element isotope plot. . . . .	28
2.5	Source apportionment of the groundwater contaminant perchlorate. . . . .	30
S2.1	One-dimensional isotope plot of a scenario where mixing follows degradation. . . . .	33
S2.2	Two-dimensional isotope plot of the degradation trajectory. . . . .	34
S2.3	Illustration of the conservative estimate obtained from scenario 1. . . . .	37
S2.4	Approximation of degradation trajectories by straight lines. . . . .	38
S2.5	Application of the Thales' theorem to three parallel trajectories and two mixing lines in the two-dimensional isotope plot. . . . .	39
S2.6	Illustration of mixing between two sources and degradation via two competing reaction pathways in the two-dimensional isotope plot. . . . .	40
S2.7	Illustration of the parameter $F$ for different isotopic elements in a scenario of degradation via two competing reaction pathways. . . . .	41
S2.8	Illustration of mixing between three sources and degradation in the three-dimensional isotope plot. . . . .	43
S2.9	Illustration of mixing between three sources and degradation in the two-dimensional isotope plot. . . . .	44
3.1	Plan view of the model domain of the two-dimensional PHAST simulations. . . . .	48
3.2	Virtual data (RTM simulation results) from the simulation of two partially overlapping groundwater pollution plumes. . . . .	50

3.3	Virtual data (RTM simulation results) and SISS-model calculations for the extent of degradation and source apportionment. . . . .	51
3.4	BTEX-contaminated field site analyzed in the SISS-model application.	53
3.5	Dual-element isotope plot of field CSIA data analyzed in the SISS-model application. . . . .	54
3.6	Dual-element isotope plot of CSIA data at the well filters analyzed in the SISS-model application. . . . .	56
3.7	Uncertainties and complications in the SISS-model application illustrated in the two-dimensional isotope plot. . . . .	59
S3.1	Plan view of the alternative RTM simulation with a greater distance between the sources. . . . .	61
S3.2	Illustration of SISS-model estimates of the non-degraded fraction for the virtual data. . . . .	62
S3.3	Two-dimensional isotope plot with a large area of overlap between possible trajectories from sources A and B. . . . .	64
S3.4	Two extreme configurations of the angle between the mixing line and degradation trajectories. . . . .	65
4.1	Model domain of the hillslope model. . . . .	71
4.2	Meteorological data used in the hillslope model. . . . .	77
4.3	Steady-state results of the hillslope model. . . . .	79
4.4	Response to the extreme rainfall event at the hillslope outlet. . . . .	80
4.5	Pesticide plume before and after the last application. . . . .	81
4.6	Results of the last five years of the transient simulation at the hillslope outlet. . . . .	82
5.1	Scheme of the Alteckendorf study catchment. . . . .	98
5.2	Scheme of the parsimonious flow and pesticide transport model. . . . .	102
5.3	Pesticide concentrations and carbon isotope ratios at the plot, drain, and catchment outlet. . . . .	107
5.4	Results of the model calibration to discharge, concentration and CSIA data. . . . .	113
5.5	Distribution of the model parameters $S_{\max}$ and $R_{\max}$ . . . . .	117
5.6	Distribution of the calculated extent of degradation in the shallow and groundwater reservoir in 2011. . . . .	117

# List of Tables

3.1	Results of the SISS-model application to the well filters in the mixing zone. . . . .	57
S3.1	Hydrochemical parameters of the aquifer analyzed in the SISS-model application. . . . .	62
S3.2	Benzene concentrations and CSIA data from the aquifer analyzed in the SISS-model application. . . . .	63
4.1	Hydraulic properties of the hillslope subsurface domain. . . . .	72
4.2	Parameters for degradation and isotope fractionation in the hillslope model. . . . .	73
5.1	Compound properties of the two study compounds S-metolachlor and acetochlor. . . . .	99
5.2	Parameter values of the hydrological and pesticide model. . . . .	105
5.3	Mass balance of the pesticide model for the years 2011, 2012, and the study period. . . . .	115
S5.1	Governing equations of the hydrological model. . . . .	122
S5.2	Governing equations of the pesticide model. . . . .	123



# Samenvatting

Onze leefomgeving wordt vervuild door een verscheidenheid aan organische stoffen, zoals bestrijdingsmiddelen en andere chemicaliën, die in het oppervlakte- en grondwater terecht komen. Alleen afbraakprocessen kunnen deze stoffen definitief verwijderen en daarmee schadeloos maken. Het is dus belangrijk zowel de herkomst ("sources") van organische vervuilende stoffen in het milieu te kunnen vaststellen, alsmede de processen die leiden tot hun verwijdering ("sinks"). In deze context blijkt componentspecifieke isotopenanalyse ("compound-specific isotope analysis"), ofwel CSIA, een nuttig instrument.

CSIA meet de verhouding van zware en lichte isotopen van elementen in verbindingen. Aangezien de isotopenverhouding toeneemt tijdens de afbraak van organische stoffen (dit proces wordt isotopenfractionering genoemd), kan CSIA gebruikt worden om aan te tonen dat organische vervuilende stoffen uit de leefomgeving verdwijnen. De mate van isotopenfractionering verschilt doorgaans per element in een verbinding, en wordt meestal ook bepaald door het specifieke afbraakmechanisme. Het uitvoeren van CSIA aan meerdere elementen die in de verbinding aanwezig zijn, zoals naast koolstof ook waterstof en bijvoorbeeld chloor in gechloreerde koolwaterstoffen, kan daardoor inzicht geven in het specifieke afbraakmechanisme. Daarmee kan ook de mate van afbraak nauwkeuriger worden bepaald. Als verschillende vervuilingbronnen gekarakteriseerd worden door specifieke unieke isotopenverhoudingen, kan CSIA bovendien gebruikt worden om deze bronnen te identificeren, en hun aandeel in de totale vervuiling te berekenen.

Eerdere studies gingen ervan uit dat CSIA niet geschikt zou zijn om de herkomst van een stof vast te stellen indien de stof afkomstig is van verschillende bronnen met specifieke isotopensamenstelling, en tegelijkertijd ook afbraak van deze stof optreedt. De isotopensamenstelling van deze stof verandert namelijk dan zowel door afbraak, als door het mengen van verschillende emissiebronnen. In hoofdstukken 2 en 3 worden dit soort gevallen besproken en wordt er een nieuw wiskundig model (het stable isotopes sources and sinks, SISS model) gepresenteerd. Het SISS model maakt gebruik van CSIA van meerdere elementen om zowel de herkomstverdeling, als de mate van afbraak van de betreffende stof vast te stellen. Het model levert een conservatieve schatting op van de mate van afbraak, en kan het aandeel van verschillende vervuilingbronnen accuraat berekenen, zelfs als het mengen van deze bronnen gelijktijdig met afbraak optreedt. Deze studie toont aan dat, in tegenstelling tot eerdere veronderstellingen, de bronverdeling wel degelijk berekend kan worden in situaties waar de isotoopsamenstelling ook verandert door afbraak.

In hoofdstuk twee wordt de berekening van de bronverdeling met het SISS model toegepast op CSIA gegevens van de stof perchloraat. Hoofdstuk drie valideert het SISS model ten opzichte van resultaten van een reactief transportmodel, en laat zien hoe het SISS model toegepast kan worden op een eerder onderzochte veldlocatie waar het grondwater verontreinigd is door twee verschillende benzeenbronnen. Hoewel de toepassing van het SISS model bemoeilijkt wordt door de onzekerheid van de

koolstof en waterstof CSIA gegevens en de fysieke heterogeniteit van het terrein, is het SISS model succesvol in het identificeren van de voornaamste van de twee vervuilingsbronnen en het berekenen van een boven- en ondergrens van de mate van afbraak die optreedt in het grondwater. Dit laatste is specifiek belangrijk, aangezien de klassieke Rayleigh vergelijking, die uitgaat van één herkomstbron, onnauwkeurige schattingen van benzeenafbraak op deze locatie geeft.

In dit proefschrift wordt aangetoond dat toepassing van het SISS model het mogelijk maakt meer informatie uit CSIA gegevens te verkrijgen dan tot nu toe gewoon was. Dit is zowel wetenschappelijk als commercieel van belang. Naast toepassingen in grondwater heeft dit model bovendien voordelen bij de analyse van diffuse vervuiling door bijvoorbeeld pesticiden in oppervlaktewater of van stoffen in de atmosfeer. Dit proefschrift laat verder zien hoe het SISS model van toepassing kan zijn voor situaties met meer dan één reactiepad of meer dan twee emissiebronnen. Het SISS model heeft CSIA gegevens nodig van een extra element voor elke bron en/of afbraak route die extra bepaald dient te worden. Voor verbindingen die uit meerdere elementen bestaan kunnen dus theoretisch ook meer bronnen en/of afbraakroutes worden aangetoond. Toekomstig onderzoek kan daarom verder gericht worden op de toepassing van het SISS model in dergelijke situaties.

Hoofdstuk 4 en 5 bespreken het potentiële nut van CSIA voor diffuse verontreiniging zoals door bestrijdingsmiddelen in de landbouw. CSIA gegevens van pesticiden zijn zeldzaam, en er zijn geen doorlopende CSIA gegevens verzameld om de afbraak van pesticiden op stroomgebiedsschaal vast te stellen. Om de variatie van CSIA gegevens onder verschillende hydrologische omstandigheden te voorspellen, zijn in hoofdstuk 4 computersimulaties gedaan van de verspreiding en afbraak, inclusief de isotopenfractionering, van een denkbeeldig bestrijdingsmiddel op de schaal van een helling ("hillslope") die hoger gelegen gronden verbindt met een rivier. Deze simulaties zijn uitgevoerd met het fysisch-gebaseerd gekoppeld grond- en oppervlaktewatermodel HydroGeoSphere. De simulaties wijzen op de nuttigheid en toepasbaarheid van CSIA voor de analyse van bestrijdingsmiddelen: (i) de mate van gesimuleerde isotopenfractionering in de rivier is groot genoeg om gemeten te worden met de huidige analytische methoden, en (ii) drastische wijziging van de isotopensamenstelling tijdens regenval in de richting van de oorspronkelijke isotopensamenstelling van het bestrijdingsmiddel geeft aan dat het bestrijdingsmiddel in de rivier is gekomen door snelle oppervlakkige afvoer. Aangezien in de simulaties grondwater dominant was ten opzichte van oppervlakkige afvoer voor de voeding van de rivier, voorspelde het model dat zelfs onder variabele hydrologische condities de veranderingen in isotopensamenstelling in de rivier niet detecteerbaar zijn. Dit geeft aan dat een lage frequentie van CSIA metingen voldoende kan zijn om de afbraak van bestrijdingsmiddelen te kunnen bepalen voor stroomgebieden die goed gedraineerd zijn en waar grondwater aanzienlijk bijdraagt aan rivierafvoer.

In hoofdstuk 5 worden de eerste systematische CSIA metingen van bestrijdingsmiddelen in een stroomgebied geanalyseerd. Gedurende het groeiseizoen van 2012 zijn de concentraties en koolstof isotopensamenstellingen van twee herbiciden (S-metolachlor en acetochlor) gemeten in een klein agrarisch stroomgebied (47 ha) in de Alsace, Frankrijk. Door omvangrijke oppervlakkige afvoer en erosie waren de concentraties in de uitlaat van het stroomgebied het hoogst ( $65 \mu\text{gL}^{-1}$ ) na een

extreme regenbui (54 mm) die twee weken na het aanbrengen van de herbiciden plaatsvond. Koolstof isotopenverhoudingen stegen geleidelijk gedurende het groei-seizoen, wat aangeeft dat herbiciden in de bodem en tijdens het transport naar de uitlaat van het stroomgebied worden afgebroken.

Om de kwantitatieve interpretatie van de CSIA gegevens van de bestrijdingsmiddelen mogelijk te maken, zijn de rivierafvoer, de concentraties en CSIA gegevens van het bestrijdingsmiddel S-metolachlor met een conceptueel wiskundig hydrologisch model gesimuleerd (hoofdstuk 5). Model calibratie laat zien dat de beschikbaarheid van CSIA gegevens resulteert in een lagere mate van onzekerheid van sommige model parameters en een nauwkeuriger schatting van de mate van afbraak in het stroomgebied. Hoofdstuk 5 demonstreert dat de combinatie van waarnemingen en modelleren van CSIA gegevens een belangrijk voordeel oplevert bij het begrijpen van afbraak en transport processen van bestrijdingsmiddelen in stroomgebieden.

Aangezien CSIA van watermonsters uit het milieu grote monstervolumes vereist, is de gebruikte dataset in hoofdstuk 5 beperkt tot een gelimiteerd aantal metingen in de tijd. Dit bemoeilijkt een gedetailleerde interpretatie van deze gegevens, evenals de berekening van de afbraak van het bestrijdingsmiddel, zeker aangezien het model voorspelt dat er grote temporele fluctuaties optreden in isotopenverhoudingen door de gevoeligheid voor oppervlakkige afvoer in het bestudeerde stroomgebied. Toekomstige studies naar vergelijkbare stroomgebieden zouden daarom idealiter een hogere temporele resolutie van CSIA gegevens moeten nastreven. Bijvoorbeeld metingen van de isotopenverhouding van het aangebrachte bestrijdingsmiddel, gedurende periodes van basisafvoer, en gedurende specifieke regenbuien. Zoals in hoofdstuk 5 gebleken is, zijn extra gegevens bovendien gunstig voor het beter kalibreren van pesticidenmodellen. Hoofdstuk 5 benadrukt ook dat verdere laboratoriumstudies naar de isotopen fractionering van bestrijdingsmiddelen essentieel zijn om CSIA veldgegevens gedetailleerder te kunnen interpreteren en om pesticidenmodellen beter te kunnen parametriseren. Desondanks onderstrepen hoofdstuk 4 en 5 dat CSIA een veelbelovende methode is om de verspreiding en de afbraak van diffuse verontreiniging op stroomgebiedsschaal te kunnen karakteriseren.



# Zusammenfassung

Unsere Umwelt wird durch eine Reihe organischer Stoffe wie beispielsweise Pestizide oder Grundwasserschadstoffe beeinträchtigt. Wenn diese Stoffe in die Umwelt gelangen, können sie nur durch Abbauprozesse unumkehrbar entfernt und damit schadlos gemacht werden. Es ist daher von Bedeutung, die Quellen ("sources") und Senken (d.h. Abbau, "sinks") von organischen Schadstoffen in der Umwelt charakterisieren zu können. In diesem Kontext hat sich die sogenannte substanzspezifische Isotopenanalyse ("compound-specific isotope analysis", kurz CSIA) als nützliche Methode erwiesen.

CSIA bezeichnet die Messung der relativen Häufigkeit von leichten und schweren stabilen Isotopen (d.h. das Isotopenverhältnis) eines Elements in der chemischen Substanz. Da das Isotopenverhältnis unter dem Einfluss von Abbauprozessen in der Regel ansteigt (dieser Prozess wird Isotopenfraktionierung genannt), kann CSIA einen eindeutigen Hinweis auf den Abbau von Schadstoffen liefern. Das Ausmaß dieser Isotopenfraktionierung ist einerseits meist abhängig vom jeweiligen Element in der Substanz, dessen Isotope untersucht werden, und andererseits vom jeweiligen Abbaumechanismus. Wird die Isotopenanalyse auf mehrere Elemente in der Substanz ausgeweitet (z.B. in chlorierten Kohlenwasserstoffen neben Kohlenstoff auch Wasserstoff und Chlor), so kann CSIA folglich auch verwendet werden, um zwischen unterschiedlichen Abbaumechanismen zu differenzieren. CSIA erlaubt außerdem, verschiedene Emissionsquellen zu identifizieren und ihren Anteil an der Gesamtverschmutzung zu berechnen, vorausgesetzt dass diese Quellen durch eindeutige isotopische Zusammensetzungen charakterisiert werden können.

Vorangegangene Studien haben die Anwendbarkeit von CSIA zur Identifikation von Emissionsquellen für solche Fälle angezweifelt, in denen der Schadstoff aus mehreren Quellen stammt und gleichzeitig Abbau des Schadstoffes stattfindet. Ein derartiges Szenario hat nämlich zur Folge, dass die isotopische Zusammensetzung des Schadstoffes sowohl durch Abbau als auch das Mischen von verschiedenen Schadstoffquellen beeinflusst wird. Diese Fälle werden in Kapitel 2 und 3 behandelt, in denen ein mathematisches Modell basierend auf CSIA zur kombinierten Abschätzung von Quellen und Senken von organischen Schadstoffen (das "stable isotopes sources and sinks model", kurz SISS-Modell) entwickelt und besprochen wird. Das SISS-Modell kann mit Hilfe von CSIA von mehreren Elementen sowohl das Ausmaß des Abbaus des betreffenden Stoffes ermitteln, als auch die Herkunftsverteilung zwischen verschiedenen Emissionsquellen bestimmen. Diese Erkenntnis steht im Kontrast zu vorherigen Studien, die die Anwendbarkeit von CSIA zur Identifizierung von Schadstoffquellen anzweifeln, wenn gleichzeitig Isotopenfraktionierung durch Abbauprozesse stattfindet.

In Kapitel 2 wird die Berechnung der Herkunftsverteilung zwischen Emissionsquellen mit dem SISS-Modell anhand von CSIA-Daten für den Grundwasserschadstoff Perchlorat dargestellt. In Kapitel 3 wird das SISS-Modell mit Hilfe von Simulationsresultaten eines reaktiven Stofftransportmodells validiert. Zudem wird das

SISS-Modell auf einen bereits untersuchten Standort angewandt, der durch zwei verschiedene Benzolquellen verseucht ist. Obwohl die Anwendung des SISS-Modells durch Unsicherheiten in den CSIA-Felddaten und die physikalische Heterogenität des Standorts erschwert wird, erlaubt das Modell dennoch die Identifikation der Hauptemissionsquelle und die Berechnung des minimalen und maximalen Ausmaßes von Benzolabbau. Letzteres erweist sich als besonders vorteilhaft in Anbetracht der Tatsache, dass die klassische Rayleigh-Gleichung ungenaue Abschätzungen des Abbau-Ausmaßes am Standort liefert.

Wie in dieser Arbeit dargestellt, ermöglicht das SISS-Modell, mehr Informationen aus CSIA-Daten zu erhalten. Dies ist sowohl von wissenschaftlichem als auch kommerziellem Interesse. Darüber hinaus ist anzunehmen, dass das SISS-Modell auch der Analyse von diffuser Verschmutzung durch z.B. Pestizide oder atmosphärische Schadstoffe zugutekommt. Da das Modell auch für mehr als zwei Emissionsquellen und mehr als einen Abbaumechanismus beschrieben wird, könnte zukünftige Forschung zudem auf die Anwendung des SISS-Modells auf eine Kombination von mehreren Emissionsquellen und Reaktionswegen abzielen. Dabei erfordert das SISS-Modell für jede zusätzliche Emissionsquelle und/oder Abbaumechanismus die Bestimmung von CSIA-Daten von einem zusätzlichen Element, das in dem zu untersuchenden Stoff vorhanden ist.

In den Kapiteln 4 und 5 wird die mögliche Anwendung von Methoden basierend auf CSIA in der Abschätzung von diffuser Verschmutzung (z.B. durch Pestizide in der Landwirtschaft) behandelt. CSIA-Daten von Pestiziden sind kaum vorhanden und wurden bis dato noch nicht auf systematische Weise gemessen, um den Abbau von Pestiziden auf Einzugsgebietsebene zu ermitteln. Um den zeitlichen und räumlichen Verlauf solcher Daten unter verschiedensten hydrologischen Bedingungen zu prognostizieren, werden daher Computersimulationen von Verbreitung (Transport), Abbau und Isotopenfraktionierung auf der Ebene einer Hangneigung ("hillslope"), die höher gelegenes Gebiet mit einem Fluss verbindet, durchgeführt. Dies geschieht mit Hilfe des physikalisch basierten gekoppelten Untergrund- und Oberflächenwassermodells HydroGeoSphere (Kapitel 4). Die Simulationsergebnisse deuten in zweierlei Hinsicht auf die Nützlichkeit und Durchführbarkeit von CSIA in der Analyse von diffuser Verschmutzung hin: (i) die simulierte Isotopenfraktionierung ist signifikant genug, um mit derzeitigen analytischen Methoden nachgewiesen werden zu können, und (ii) Veränderungen im Isotopenverhältnis während Regenfällen kennzeichnen Pestizidtransport über schnellen Oberflächenabfluss. Darüber hinaus verändert sich das Isotopenverhältnis selbst unter variablen hydrologischen Bedingungen nur in geringem Maße. Dies weist darauf hin, dass vereinzelte CSIA-Proben ausreichen, um den Abbau von Pestiziden in Einzugsgebieten zu charakterisieren, in denen Niederschlag schnell in tiefere Schichten abfließt und Grundwasser einen bedeutenden Teil des Flusswassers ausmacht.

In Kapitel 5 werden erstmals systematisch auf Einzugsgebietsebene erhobene CSIA-Daten von Pestiziden erörtert. In diesem Kapitel wird untersucht, inwiefern Konzentrationen und Kohlenstoff-Isotopenverhältnisse von zwei Herbiziden (S-Metolachlor und Acetochlor) während der Wachstumsaison in einem kleinen landwirtschaftlichen Einzugsgebiet (47 ha) im Elsass, Frankreich, variieren. Bedingt durch ausgedehnten Oberflächenabfluss und Erosion werden die höchsten Konzentrationen ( $65 \mu\text{gL}^{-1}$ )

in Folge eines extremen Niederschlagsereignisses (54 mm) im ersten Monat nach der Aufbringung der Pestizide erreicht. Ferner steigt das Kohlenstoff-Isotopenverhältnis der Herbizide im Laufe des Messzeitraums sukzessive an, was auf Abbau im Boden und während des Transports durch das Einzugsgebiet hinweist.

Um eine quantitative Betrachtung der CSIA-Daten der Pestizide zu ermöglichen, werden Abflussmenge, Pestizidkonzentrationen und -Isotopenverhältnisse mit Hilfe eines konzeptuellen hydrologischen Modells simuliert (Kapitel 5). Zur Kalibrierung dieses Modells werden die gemessenen Abflussdaten, Pestizidkonzentrationen und CSIA-Daten verwendet. Daraus wird ersichtlich, dass die Unsicherheit in den kalibrierten Parameterwerten und im berechneten Abbau-Ausmaß durch die Einbindung von CSIA-Daten in den Kalibrierungsprozess verringert wird. Ferner veranschaulichen die gemessenen Konzentrationswerte und CSIA-Daten, welche Prozesse in das Modell miteinbezogen werden müssen, während die Simulationsergebnisse eine Abschätzung des Pestizidabbaus ermöglichen. Kapitel 5 verdeutlicht demnach, dass ein kombinierter Mess- und Modellierungsansatz von CSIA-Daten Vorteile in der Analyse von Transport und Abbau von Pestiziden auf Einzugsgebietsebene verschafft.

Da Isotopenanalyse von Wasserproben aus der Umwelt große Probenvolumen erfordert, sind die CSIA-Daten in Kapitel 5 auf wenige Datenpunkte beschränkt. Dies erschwert eine detaillierte Interpretation dieser Daten mitsamt der Abschätzung des Pestizidabbaus, zumal das Modell auf starke Schwankungen im Isotopenverhältnis aufgrund des häufigen Auftretens von Oberflächenabfluss im betrachteten Einzugsgebiet hinweist. Zukünftige Studien in vergleichbaren Einzugsgebieten sollten demnach eine feinere zeitliche Auflösung der CSIA-Daten von Pestiziden anstreben (d.h. beispielsweise die Messung von Isotopenverhältnissen vor der Aufbringung des Pestizids, während Niedrigwasserabfluss, oder während einzelner Niederschlagsereignisse). Wie auch aus Kapitel 5 ersichtlich wird, ist weiterhin zu erwarten, dass sich zusätzliche CSIA-Messpunkte als vorteilhaft für die Kalibrierung von Pestizidmodellen erweisen. In Kapitel 5 wird zudem deutlich, dass weitere Laborstudien über die Isotopenfraktionierung von Pestiziden für eine detaillierte Interpretation von Feld-CSIA-Daten und genauere Parametrisierung von Pestizidmodellen erforderlich sind. Nichtsdestotrotz demonstrieren die Ergebnisse aus Kapitel 4 und 5, dass CSIA als vielversprechende Methode in der Charakterisierung von Verbreitung und Abbau diffuser Schadstoffe auf Einzugsgebietsebene angesehen werden kann.



# 1

## General Introduction

## 1.1 Background

### 1.1.1 Organic contaminants: isotope-based assessment of sources and sinks

Organic contaminants are ubiquitous pollutants in the environment. Their emission into the environment often occurs by accident. For example, organic contaminants are frequently detected in groundwater below industrial sites (Blum et al., 2009; Sherwood Lollar et al., 2001; Zwank et al., 2005). Organic pollutants can also be emitted by fossil fuel combustion or forest fires, and deteriorate air quality (Giebel et al., 2011; Okuda et al., 2002; Thompson et al., 2003). In other cases, organic contaminants are deliberately released into the environment to fulfill a certain function (e.g., weed or insect control by pesticides). Once they enter the environment, organic contaminants can undergo a variety of transport, redistribution, and transformation processes. Among these processes, only transformation can irreversibly remove the contaminant and render it harmless to the environment, provided that the contaminant is completely mineralized and does not form harmful metabolites. It is, therefore, crucial to understand and characterize sources and sinks (i.e., degradation) of organic pollutants in the environment. In this context, compound-specific stable isotope analysis (CSIA) has proven a useful tool. CSIA is the measurement of the relative abundance of light and heavy stable isotopes (i.e., the isotopic composition) of an element contained in the compound. Stable isotopes of an element contain the same number of protons, but vary in the number of neutrons. For example, carbon occurs as the two stable isotopes  $^{12}_6\text{C}$  and  $^{13}_6\text{C}$ . The lighter isotope (i.e.,  $^{12}_6\text{C}$ ) has six neutrons and six protons, and accounts for 98.89% of carbon in nature, whereas the heavier isotope (i.e.,  $^{13}_6\text{C}$ ) comprises one additional neutron, and only accounts for 1.11% (Schmidt and Jochmann, 2012).

CSIA is of interest for the assessment of contaminant degradation, as the isotopic composition tends to change under the influence of degradation processes (Elsner, 2010; Meckenstock et al., 2004, Fig. 1.1). This change in isotopic composition is called isotope fractionation, and is a function of reaction progress. It depends on the isotope fractionation factor, which differs for each compound, reaction mechanism, and element. Isotope fractionation is described by the Rayleigh equation, which allows to quantify transformation of organic contaminants either by considering the temporal change in isotopic composition over time, or by comparing the isotopic composition of an environmental sample to the emission source. Whereas changes in concentrations can also result from dilution (Fig. 1.1), CSIA provides clear evidence of contaminant degradation, which thus represents a major advantage of CSIA over concentration measurements only.

In addition to the assessment of contaminant degradation, CSIA can also provide insights into sources of organic contaminants: it allows for the discrimination between different pollution sources or commercial products of a compound, provided that these have distinctly different isotopic compositions (Elsner et al., 2012; Schmidt et al., 2004). In cases where the isotopic composition of an element is similar for the considered sources, it might be required to analyze an additional element in order to distinguish between the sources, i.e., to perform multi-element (multi-dimensional)

CSIA. More specifically, by using the linear stable isotope mixing model, this does not only allow distinction, but also quantification of the relative contribution of each source to the environmental sample (i.e., source apportionment). Multi-element CSIA can also be used for the identification of specific reaction mechanisms (Zwank et al., 2005; Fischer et al., 2008; Meyer et al., 2009), and even the calculation of the contribution of each reaction mechanism to overall degradation (van Breukelen, 2007a). The two-dimensional isotope plot in Fig. 1.2 illustrates the use of multi-element CSIA for source apportionment between sources A and B (panel a), and distinction between two competing reaction pathways (panel b).

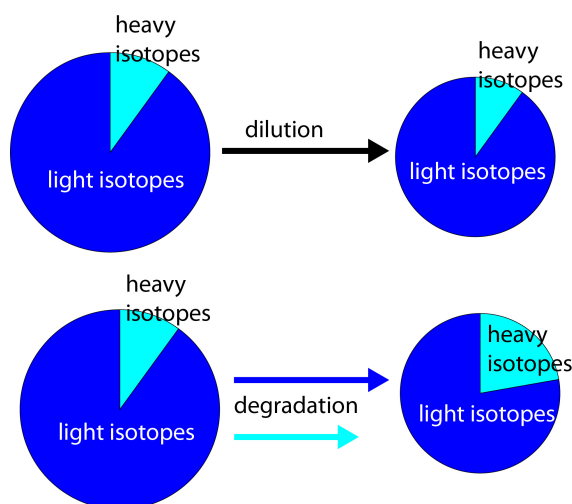


Figure 1.1: Conceptualization of the proportion of light (dark blue) and heavy (green) isotopes (i.e., isotopic composition) in an organic contaminant. Dilution does not alter the isotopic composition (top), whereas degradation generally leads to an enrichment in heavy isotopes of the remaining contaminant (bottom).

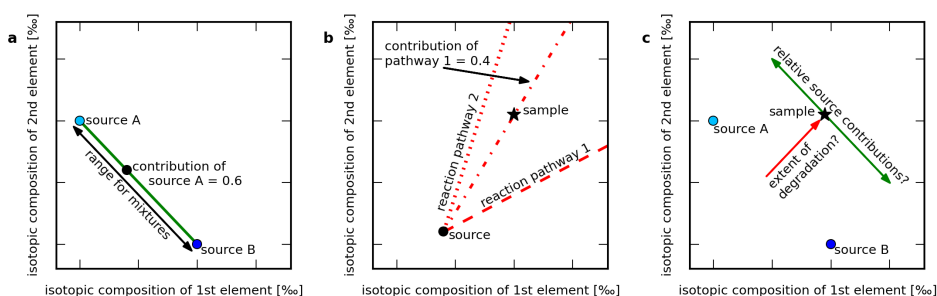


Figure 1.2: Panel a: use of dual-element isotope analysis for source apportionment between two sources (green line); panel b: distinction between two reaction pathways (dashed line: degradation via reaction pathway 1, dotted line: degradation via reaction pathway 2, dash-dotted line: degradation via a combination of both pathways with a contribution of 0.4 of pathway 1); and panel c: complications in the use of dual-element isotope analysis for an environmental sample that might be subject to both mixing between sources and isotope-fractionation induced by degradation via one pathway.

Many field sites where CSIA data have been collected are characterized by several pollution sources (Blessing et al., 2009; Mancini et al., 2002; Sherwood Lollar et al., 2001) and more than one potential mechanism for contaminant degradation (D’Affonseca et al., 2011; van Breukelen, 2007a; van Keer et al., 2012). Quantification of degradation in these systems can be complex, as mixing of several pollution sources with distinct isotopic compositions might obscure degradation-induced changes in isotope ratios. Similarly, previous studies have illustrated that simultaneous occurrence of degradation processes complicates CSIA-based source identification and apportionment (Moore and Semmens, 2008; Seiler, 2005; van Keer et al., 2012). These complications are shown in Fig. 1.2c, where the hypothetical sample signature results from a combination of source mixing and degradation-induced isotope fractionation. There is currently no simple CSIA-based model that can link sources and sinks of organic pollutants.

So far, CSIA has mainly been applied to analyze degradation of various groundwater pollutants (Blum et al., 2009; Hunkeler et al., 2005; Sherwood Lollar et al., 2001; Sturchio et al., 2012; Zwank et al., 2005). Furthermore, it has been used in source identification and apportionment of organic groundwater contaminants (Eberts et al., 2008; Mancini et al., 2008), and nitrate (Deutsch et al., 2006; Divers et al., 2014; Liu et al., 2013). Recently, analytical methods for CSIA of different pesticides have been developed as well (Badea et al., 2009; Elsayed et al., 2014; Hartenbach et al., 2008; Meyer et al., 2008; Penning and Elsner, 2007; Wu et al., 2014). CSIA can provide an important line of evidence for pesticide degradation (Fenner et al., 2013). Moreover, appropriate sampling and pre-concentration techniques allow CSIA of pesticides at low (environmental) concentrations (Jochmann et al., 2006; Zwank et al., 2003). Nonetheless, field CSIA data of pesticides remain extremely scarce (Milosevic et al., 2013; Schreglmann et al., 2013), and have not yet been specifically used to assess pesticide degradation at catchment scale. This emphasizes the need to evaluate the feasibility of CSIA in the analysis of pesticide pollution at catchment scale.

### **1.1.2 Sources and sinks of pesticides at catchment scale**

Pesticides are an important group of organic contaminants, as modern agriculture makes use of a variety of pesticides to increase crop yield, and reduce the growth of weeds or spreading of other pests (e.g., insects or fungi). Diffuse pollution by pesticides can pose a risk for the terrestrial and aquatic environment, as pesticide residuals and their metabolites have been found in groundwater and surface water. Pesticides might also be of concern for human health if they affect drinking water (direct exposure; Donald et al., 2007; Kjær et al., 2005; Kolpin et al., 1998) or water used for farming (indirect exposure). It is therefore vital to identify pesticide fate and degradation in agricultural catchments (Fenner et al., 2013).

After pesticide application, transfer and transformation processes at the surface lead to the reduction of the amount of pesticide that is available for transport in the soil (Fig. 1.3). Pesticide transfer to the atmosphere (i.e., volatilization) can occur during application as spray drift, or after the pesticide has settled on the ground surface or the crop (van den Berg et al., 1999). Following volatilization, the

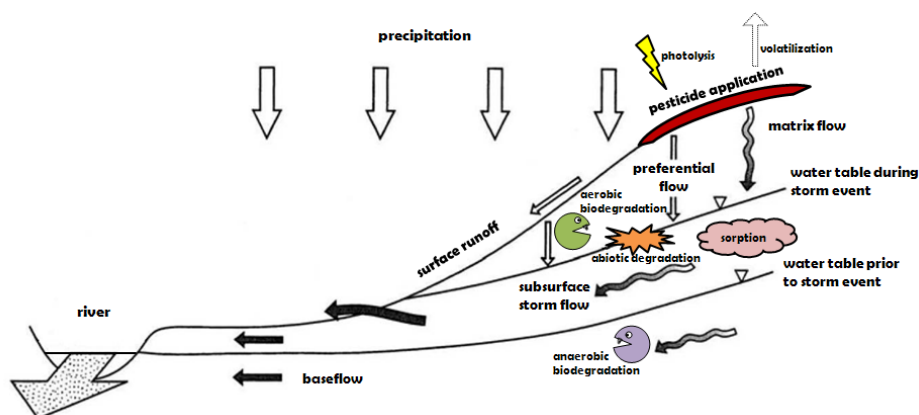


Figure 1.3: Schematic overview of pesticide transport routes and transformation processes (modified from Burt and Pinay 2005).

pesticide can be subject to aerial transport and atmospheric deposition. Besides, aerial transport and subsequent deposition of contaminated soil dust can also cause atmospheric pesticide input. Such transfer processes have been found to cause high pesticide concentrations in surface water during low flow periods (Rawn and Muir, 1999).

While volatilization leads to the transfer between the soil surface and atmosphere, sorption causes the transfer from the liquid to the solid phase of the soil matrix (Fig. 1.3). Sorption can, therefore, account for a substantial retention of pesticides in the subsurface. This can limit the availability of the sorbed molecules for degradation (Si et al., 2009), but also prolong the residence time of pesticides in microbially active layers and, consequently, enhance pesticide degradation. The relevance of sorption depends on the tendency of a pesticide to be attached to the soil matrix or suspended sediments in the water phase. Transfer into the solid soil phase is especially relevant if pesticides are applied shortly before a heavy rainfall event that leads to surface runoff, which can, consequently, entrain a substantial amount of sediment and sorbed pesticides (Squillace and Thurman, 1992; Taghavi et al., 2011; Wu et al., 2004).

Transformation processes on the ground surface and in the soil represent sinks of pesticides in agricultural catchments. The transformation of pesticides can be ascribed to microbial activity or abiotic processes, or both (Fig. 1.3). Depending on the oxygen content, microbial degradation in the soil matrix can occur under aerobic or anaerobic conditions. Abiotic processes comprise hydrolysis, redox-reactions, and direct or indirect photolysis (Gavrilescu, 2005; Hartenbach et al., 2008; Jones and Norris, 1998; Penning et al., 2010). Photolysis has been detected in surface water, at the soil surface, and in the topsoil up to a depth of a few millimeters below the surface (Konstantinou et al., 2001). Whether a specific reaction mechanism occurs, depends – apart from the properties of the compound itself – on environmental parameters such as the soil type or the climatic conditions (Arias-Estévez et al., 2008; Gavrilescu, 2005; Leu et al., 2004b). This variety of potential transformation processes highlights the need for methods that can confirm pesticide degradation

and even allow for quantification of the extent of degradation.

The part of the applied pesticide that has neither been transformed nor transferred into the gaseous or solid phase will be subject to transport processes in the aqueous phase. The transport to surface water bodies can occur via surface runoff or via lateral subsurface flow (Fig. 1.3). Vertical subsurface flow transports pesticide from the topsoil to deeper soil layers and groundwater; it can occur as a slow movement through the soil matrix or rapid vertical movement via preferential flow (e.g., in earthworm burrows and cracks; Doppler et al. 2012; Gavrilesco 2005; Zehe et al. 2001). Preferential flow is assumed to be a prominent leaching process for pesticides because it bypasses the soil matrix and can thus result in rapid transport of pesticides from the topsoil to artificial drainage systems. Drainage systems and subsurface storm flow can, thereupon, cause fast transport to surface water (Gavrilesco, 2005; Leu et al., 2004b; Müller et al., 2003). In summary, pesticides can be transported via various pathways, which underlines the importance of a tool that allows identification of pesticide sources and transport routes in a catchment.

### 1.1.3 Modeling of sources and sinks of organic water pollutants

Complementary to the analysis of field data, numerical hydrological models can assist and facilitate the characterization of sources and sinks of organic contaminants. A variety of hydrological models is available for different applications. A classification can be made according to different characteristics: the spatial scale that can be simulated, the time span and temporal discretization that the model is able to represent, or the spatial variability in input parameters and processes that the model accounts for (Quilbe et al., 2006). Distributed physically-based models are the model type with the highest complexity; they allow for the simulation of hydrological processes in different flow domains in a detailed and spatially explicit way (Kampf and Burges, 2007). They have been applied to model nitrate (e.g., Flipo et al. 2007; Wriedt et al. 2007) and pesticide transport (e.g., Christiansen et al. 2004; Fauser et al. 2008; Gassmann et al. 2013; Zehe et al. 2001). However, only a few distributed physically-based models comprise the simulation of both flow and transport processes (Payraudeau and Gregoire, 2012).

Parsimonious (lumped) models follow a fundamentally different approach from physically-based models: they describe the catchment as a series of a few connected subsystems, and are, therefore, also referred to as conceptual models (Payraudeau and Gregoire, 2012). The mass-balance equations of the subsystems can then be combined with a travel-time formulation of transport, which allows calculating flux concentrations and mass fluxes of conservative and reactive solutes with relatively few parameters (Botter et al., 2010; van der Velde et al., 2012). This has been, e.g., applied to simulate atrazine and chloride transport in agricultural catchments (Benettin et al., 2013; Bertuzzo et al., 2013).

Hydrological models are also frequently used in the characterization of point-source pollution in groundwater systems. In this context, models that simulate isotope fractionation processes (isotope-fractionation reactive transport models, IF-RTMs)

have become a popular method to model and interpret CSIA data from aquifers (Atteia et al., 2008; D’Affonseca et al., 2011; Pooley et al., 2009; Prommer et al., 2009; van Breukelen et al., 2005). However, although the Rayleigh equation approach is an attractive tool in the assessment of contaminant degradation, it tends to result in an underestimation of the extent of degradation when applied to open flow systems due to their physical heterogeneity. Therefore, IF-RTMs have also been used to test the performance of the Rayleigh equation for such systems (Abe and Hunkeler, 2006; Thullner et al., 2012; van Breukelen and Prommer, 2008). In contrast, the simulation of diffuse pollution with IF-RTMs has so far been limited to a few studies of riparian transformation of nitrate (Chen and MacQuarrie, 2004; Green et al., 2010). To date, it has not yet been examined whether modeling of isotope fractionation of contaminants at catchment scale can provide additional information in the assessment of sources and sinks of diffuse pollutants.

## 1.2 Thesis objectives

This thesis aims at advancing the use of CSIA in the assessment of sources and sinks of organic contaminants. In view of the aforementioned open questions in monitoring and modeling of organic pollution and related CSIA data, the specific objectives of this thesis are to:

- i. Develop a simple CSIA-based mathematical model that allows combined source apportionment and assessment of contaminant degradation for systems where mixing between sources and degradation can occur simultaneously (Fig. 1.2c). This model should be applicable independently of the spatial scope and to all organic contaminants, be it in the characterization of groundwater, surface water, or atmospheric pollution.
- ii. Validate the model from point (i) with a field site application and discuss factors of model uncertainty.
- iii. Bridge the gap between CSIA and the analysis of diffuse pollution at catchment scale by modeling how isotope ratios of pesticides might evolve under varying hydrological conditions; and provide recommendations for sampling and interpretation of CSIA data of diffuse pollutants.
- iv. Investigate how measured concentration and CSIA data can be combined to gain more insights into sources and sinks of pesticides at catchment scale; and provide recommendations for sampling and interpretation of CSIA data of diffuse pollutants.
- v. Evaluate the added value of CSIA data in monitoring and modeling of diffuse pollution at catchment scale. The aim is especially to identify how the interpretation of field CSIA data can inform modeling of diffuse pollutants, and vice versa.

## 1.3 Thesis outline

The thesis is structured as follows:

- i. Chapter 2 describes and discusses a CSIA-based mathematical model for combined source apportionment and degradation quantification (stable isotopes sources and sinks model; SISS model). The model is derived for the specific case of two contaminant sources and one degradation mechanism; its application is also outlined for multiple sources and degradation pathways. Following model derivation, source apportionment with the SISS model is illustrated for the groundwater contaminant perchlorate.
- ii. Chapter 3 presents a validation of the SISS model against virtual CSIA data produced with a reactive transport model that includes isotope fractionation effects (IF-RTM). The chapter further evaluates the model in a field application with isotope data from a benzene-contaminated aquifer, and discusses model uncertainties and complications resulting from, e.g., uncertainties in field CSIA data.
- iii. Chapter 4 shows the results of numerical experiments with a distributed physically-based coupled subsurface-surface model that simulates isotope fractionation of a pesticide at hillslope scale. These virtual experiments are discussed in view of evaluating the potential use of CSIA for diffuse pollutants in ground and surface water.
- iv. Chapter 5 describes the first field CSIA data of pesticides in stream water from an agricultural catchment. Moreover, it provides a combined measurement and modeling approach of pesticide concentrations and CSIA data. The chapter first discusses concentrations and carbon isotope ratios of two herbicides measured during the growing season in an agricultural headwater catchment. Subsequently, it shows the simulation of these field data with a parsimonious model based on travel-time distributions. This leads to a discussion of the usefulness of such a combined monitoring and modeling approach in the analysis of pesticide pollution.
- v. Chapter 6 completes the thesis with a summary of the main findings and conclusions of the previous chapters, and presents recommendations for future research and application of the developed models and approaches.

# 2

## A stable isotope model for combined source apportionment and degradation quantification of organic pollutants: model derivation\*

**Abstract.** Compound-specific stable isotope analysis (CSIA) serves as a tool for source apportionment (SA) and for the quantification of the extent of degradation (QED) of organic pollutants. However, simultaneous occurrence of mixing of sources and degradation is generally believed to hamper both SA and QED. On the basis of the linear stable isotope mixing model and the Rayleigh equation, we developed the stable isotope sources and sinks model, which allows for simultaneous SA and QED of a pollutant that is emitted by two sources and degrades via one transformation process. It was shown that the model necessitates at least dual-element CSIA for unequivocal SA in the presence of degradation-induced isotope fractionation, as illustrated for perchlorate in groundwater. The model also enables QED, provided degradation follows instantaneous mixing of two sources. If mixing occurs after two sources have degraded separately, the model can still provide a conservative estimate of the overall extent of degradation. The model can be extended to a larger number of sources and sinks as outlined. It may aid in forensics and natural attenuation assessment of soil, groundwater, surface water, or atmospheric pollution.

---

\*This chapter is an edited version of: Lutz, S. R. and van Breukelen, B. M. Combined Source Apportionment and Degradation Quantification of Organic Pollutants with CSIA: 1. Model Derivation. *Environmental Science & Technology*, 48(11):6220-6228, 2014.

## 2.1 Introduction

Compound-specific stable isotope analysis (CSIA) is an emerging and promising technique in the analysis of organic pollutants. It consists of the measurement of the relative abundance of the stable isotopes of an element in the pollutant (e.g.,  $^{13}\text{C}$  and  $^{12}\text{C}$  or  $^2\text{H}$  and  $^1\text{H}$  in benzene,  $\text{C}_6\text{H}_6$ ). This isotopic composition is prone to change under the influence of transformation processes, i.e., to undergo isotope fractionation effects. In contrast, nondestructive processes such as dispersion, sorption, or diffusion generally induce negligible isotope fractionation effects, except under specific conditions (Aeppli et al., 2009; Bouchard et al., 2008; van Breukelen and Prommer, 2008; van Breukelen and Rolle, 2012). Therefore, CSIA allows for the distinction between destructive and nondestructive processes and can be used to determine the extent of in situ degradation (ED; Elsner et al., 2012; Schmidt et al., 2004; Thullner et al., 2012). This represents an advantage over concentration analysis, which usually cannot be used to calculate the ED, as concentration differences between the source and sample also result from dilution. Assuming release from a unique and clearly defined emission source, CSIA has been primarily applied for the quantification of the ED (QED) of organic groundwater contaminants, such as chlorinated ethenes (Aeppli et al., 2010; Amaral et al., 2011; Hunkeler et al., 2005; Sherwood Lollar et al., 2001; Wiegert et al., 2012), aromatic hydrocarbons (Blum et al., 2009; Mancini et al., 2002; Morasch et al., 2011), and the fuel additive MTBE (Kuder et al., 2004; Zwank et al., 2005). Isotope analysis has also been used for the QED of inorganic groundwater contaminants such as chromium(VI) (Wanner et al., 2012a).

In addition to the QED, CSIA serves as a tool for source identification and source apportionment (SA). Source identification can also be based on concentrations, but as these are affected by processes such as mixing or dilution, they only allow for clear source identification at local scale and when measured at high spatial resolution. In contrast, provided the compound does not undergo degradation-induced isotope fractionation, isotope data can be used as distinct tracer for pollution sources. In particular, if the individual isotopic compositions of different sources are known, CSIA can allow for the assessment of the relative contribution of each source to a sample (Elsner et al., 2012; Le Bot et al., 2011; Schmidt et al., 2004). Source identification and apportionment in contaminant hydrology based on CSIA data have been, for example, applied to attribute the presence of phthalates, isopropyl palmitate, and synthetic musks in rivers to the discharge of different tributaries (Kronimus et al., 2006), distinguish sources of diffuse nitrate pollution (Divers et al., 2014; Deutsch et al., 2006; Seiler, 2005), quantify riverine and coastal emission of dissolved organic carbon in estuaries (Cifuentes and Eldridge, 1998), and identify the origin of aromatic and halogenated hydrocarbons in groundwater (Blessing et al., 2009; Mancini et al., 2008). CSIA has also been employed in SA of volatile and semi-volatile organic compounds in air, such as polycyclic aromatic hydrocarbons (Okuda et al., 2002) and ethanol in fuel (Giebel et al., 2011).

If the isotopic composition of a given element is similar for different pollution sources, it might be required to measure the isotope ratio of other elements in the compound, i.e., to perform a multidimensional isotope analysis. This can allow for the identification of unique patterns in the isotopic composition that are

characteristic of specific sources (Annable et al., 2007; Sturchio et al., 2012; Wang et al., 2004). Likewise, multidimensional CSIA proves beneficial in identifying reaction mechanisms, as these are typically associated with a specific proportion between isotope fractionation effects of different elements (Fischer et al., 2008; Meyer et al., 2009; Zwank et al., 2005). Moreover, in a system of  $n$  simultaneously occurring irreversible reaction pathways, the overall ED and proportional contribution of each transformation pathway can be quantified with CSIA of  $n$  elements (van Breukelen, 2007a). In comparison, CSIA of  $n$  elements allows for SA between  $n + 1$  sources (Phillips and Gregg, 2001).

Various field sites are characterized by mixing of contaminant plumes from adjacent source areas (Blessing et al., 2009; Mancini et al., 2002; Sherwood Lollar et al., 2001) and contaminant transformation by more than one metabolic pathway (D’Affonseca et al., 2011; van Breukelen, 2007a; van Keer et al., 2012). However, combined SA and QED has not yet been described for the case of several sources and reaction pathways. In fact, Moore and Semmens (2008) and Xue et al. (2009) emphasized that isotope fractionation due to transformation processes impedes source identification and apportionment with CSIA. For example, CSIA of two elements did not allow for unambiguous identification of BTEX sources at a field site with two emission sources because both mixing of the two contaminant plumes and degradation-induced isotope fractionation presumably influenced CSIA values (van Keer et al., 2012). Similarly, since isotope fractionation effects during denitrification had to be taken into account, Seiler (2005) could not clearly attribute nitrate contamination of groundwater wells to the potential sources fertilizer, wastewater, and natural nitrate, or a mixture of those. For the same reason, Kellman and Hillaire-Marcel (2003) questioned the use of nitrate isotope data in source identification, whereas Liu et al. (2013) disregarded isotope fractionation due to denitrification in order to facilitate CSIA-based source apportionment. In these studies, it was thus assumed that the occurrence of degradation-induced isotope fractionation considerably hampers the use of CSIA data for source identification and apportionment.

To bridge the gap between CSIA-based forensics and degradation assessment, this study aimed at analyzing how and to what extent source apportionment and quantification of in situ degradation are feasible in the presence of both mixing of sources and degradation. To this extent, we derived a CSIA-based mathematical model (stable isotope sources and sinks model; SISS model) that allows for SA and QED in the case of two mixing contaminant sources that are additionally exposed to one degradation pathway. Furthermore, we will discuss the impact of data uncertainty on the accuracy of SISS model estimates, and outline the use of the SISS model for more than two sources and one reaction mechanism.

## 2.2 Theoretical background

### 2.2.1 The Rayleigh equation: calculation of pollutant degradation

The Rayleigh equation describes the change in isotope ratio as a function of reaction progress of an irreversible transformation process in a closed system (Mariotti et al.,

1981):

$$\frac{R_t}{R_0} = f_{\text{deg}}^{(\alpha-1)} \quad (2.1)$$

where  $R$  represents the ratio between the abundance of a heavy and a light isotope of an element in a compound at time  $t$  ( $R_t$ ) and at time 0 ( $R_0$ ), respectively, and  $f_{\text{deg}}$  denotes the non-degraded fraction (NDF) of the compound in the system at time  $t$ . The parameter  $\alpha$  is the kinetic isotope fractionation factor, which determines the strength of isotope fractionation for the considered reaction. It typically has a value of close to one and is therefore reported in per mil (‰) as the kinetic isotopic enrichment factor  $\varepsilon = (\alpha - 1)$  (Coplen, 2011). The Rayleigh equation is the common model to fit laboratory experiments on transformation of organic pollutants irrespective of the type of degradation kinetics (e.g., Michaelis-Menten or first-order). In applications to environmental systems (e.g., an aquifer), it is used to compare the isotope ratio of the compound at the emission source (equivalent to  $R_0$ ) to the one in a sample in the environmental system (equivalent to  $R_t$ ). This usually results in an underestimation of the ED due to the attenuating effect of hydrodynamic dispersion on isotope ratios in environmental systems (Abe and Hunkeler, 2006; van Breukelen and Prommer, 2008; see also section 4.4.5).

To facilitate intersample comparison, the isotope ratio of an element  $E$  in a compound in a sample ( $R_S$ ) is expressed in the  $\delta$ -notation, which gives the relative difference from a standard ratio  $R_{\text{ref}}$  (Schmidt and Jochmann, 2012):

$$\delta(E)_S = \frac{R_S - R_{\text{ref}}}{R_{\text{ref}}} = \frac{R_S}{R_{\text{ref}}} - 1 \quad (2.2)$$

The  $\delta$ -value or isotopic signature is commonly reported in per mil (‰) as done in the following.

According to Eqs. 2.1 and 2.2, the NDF of the contaminant in the sample ( $f_{\text{deg}}$ ) is given by

$$f_{\text{deg}} = \left( \frac{10^{-3} \cdot \delta_S + 1}{10^{-3} \cdot \delta_0 + 1} \right)^{1000/\varepsilon} \quad (2.3)$$

where  $\delta_S$  and  $\delta_0$  represent the isotopic signature of the compound in the sample and at the emission source, respectively ( $\delta_S$ ,  $\delta_0$ , and  $\varepsilon$  expressed in per mil). If the NDF is known, the extent of in situ degradation of a sample can be determined as follows:

$$ED (\%) = (1 - f_{\text{deg}}) \cdot 100 \quad (2.4)$$

### 2.2.2 Stable isotope mixing model: source apportionment

Linear stable isotope mixing models are used to quantify the contribution of different end members (i.e., sources with distinct isotopic compositions) in a mixture (i.e., the environmental sample). If the number of available signatures of isotopic markers is  $n$ , they yield unique solutions for the proportional contribution of a maximum

of  $n + 1$  end members (Phillips and Gregg, 2001). The mixing model for two end members and one isotope is described by the following system of equations:

$$\delta_M = f_A \delta_A + f_B \delta_B \quad (2.5)$$

$$1 = f_A + f_B \quad (2.6)$$

with  $\delta_M$ ,  $\delta_A$ , and  $\delta_B$  being the isotopic signature of the mixture, source A, and source B, respectively. The fractions  $f_A$  and  $f_B$  denote the proportional contribution of the sources A and B, respectively, to the mixture M in terms of the number of molecules. The linear stable isotope mixing model is mainly applied in the context of atmospheric pollutants (Giebel et al., 2011; Okuda et al., 2002). Its use in contaminant hydrology has been illustrated for an industrial site with overlapping PCE plumes, where  $\delta_A$  and  $\delta_B$  in Eq. 2.5 corresponded to the carbon isotopic signatures of freshly dissolved and already degraded PCE (Blessing et al., 2009).

## 2.3 Results and Discussion

### 2.3.1 Derivation of the Stable Isotope Sources and Sinks Model

The scope of the SISS model are organic pollutants and inorganic compounds such as nitrate, as degradation of these compounds follows the Rayleigh equation model. The SISS model describes mixing of two sources with different isotopic compositions in the presence of degradation via one reaction pathway, whose associated isotope fractionation effect is constant in the entire system. We considered two scenarios that differ in the temporal order of mixing and degradation. In the first scenario, the two mixing sources are located close to each other such that the ED before mixing is negligible (Fig. 2.1a). After mixing, the contaminant mixture is transported to the CSIA sampling point. During transport, it is subject to degradation-induced isotope fractionation. The unknowns are thus the contribution of each source to the sample, which remains constant during degradation, and the ED that the mixture has undergone between mixing and sampling. For example, such a situation might occur in aquifers with an upgradient and a downgradient contaminant plume with respect to the groundwater flow direction (see chapter 3), or if two neighboring industrial sites discharge a pollutant into the same reach of a river.

In the second scenario, mixing of the two sources does not occur immediately, but at a later point after independent degradation of the two contaminant pools (Fig. 2.1b). The ED before mixing is therefore significant and can differ between the two contaminant pools, whereas it is negligible between mixing and sampling. It is thus of interest to determine the overall ED of the sample and the relative contribution of each source to the sample. This scenario is, for instance, applicable if isotope ratios are measured at a confluence of two rivers, or if two sources are located on opposing hillslopes and CSIA is performed in-stream at the assumed mixing point of discharge from the two hillslopes.

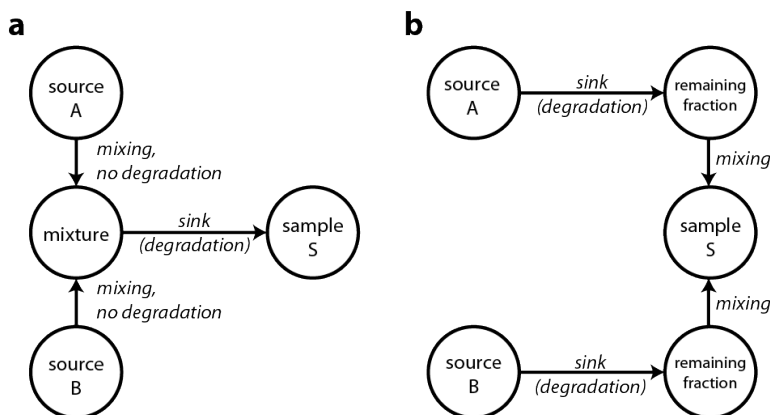


Figure 2.1: Schematic representation of the temporal sequence of mixing and degradation processes in the two discussed scenarios: degradation follows instantaneous mixing of two contaminant pools (scenario 1; a); and mixing follows independent degradation of two contaminant pools (scenario 2; b).

The classification of the temporal sequence of mixing and degradation according to scenarios 1 and 2 is clearly a simplified representation of real field conditions, as mixing and degradation processes will alternate, and occur only partially or gradually in most environmental systems. We suggest that if the considered system cannot be categorized into either scenario 1 or 2, it might still be possible to describe it by sequential subsystems that closely adhere to one of these scenarios. Nonetheless, it is required to validate this conceptualization in systems with known source contributions and extent of degradation (see chapter 3).

### 2.3.2 Degradation follows mixing: single-element CSIA

We considered the use of single-element CSIA in combined SA and QED for scenario 1 (see section S2.1 in the supplementary information to this chapter for scenario 2), since this is sufficient for SA between two sources for a non-degrading compound or QED for one reaction pathway in the presence of only one emission source. If the carbon isotopic signatures of the sources and the sample are known, the  $\delta^{13}\text{C}$ -value of the mixture prior to degradation is, according to Eq. 2.5:

$$\delta^{13}\text{C}_M = f_A \delta^{13}\text{C}_A + (1 - f_A) \delta^{13}\text{C}_B \quad (2.7)$$

After mixing, isotope fractionation during degradation leads to an enrichment in  $^{13}\text{C}$ -isotopes, which results, according to Eq. 2.3, in a sample signature of

$$\delta^{13}\text{C}_S = f_{\text{deg},S}^{\varepsilon_C/1000} \cdot (\delta^{13}\text{C}_M + 1000) - 1000 \quad (2.8)$$

where  $\varepsilon_C$  is the carbon isotopic enrichment factor,  $\delta^{13}\text{C}_S$  is the carbon isotopic signature of the sample S (Fig. 2.1a), and  $f_{\text{deg},S}$  is the NDF since mixing occurred. Substitution of Eq. 2.7 into 2.8 results in a single equation with the two unknowns  $f_A$  and  $f_{\text{deg},S}$ . Therefore, single-element CSIA does not yield an unequivocal solution

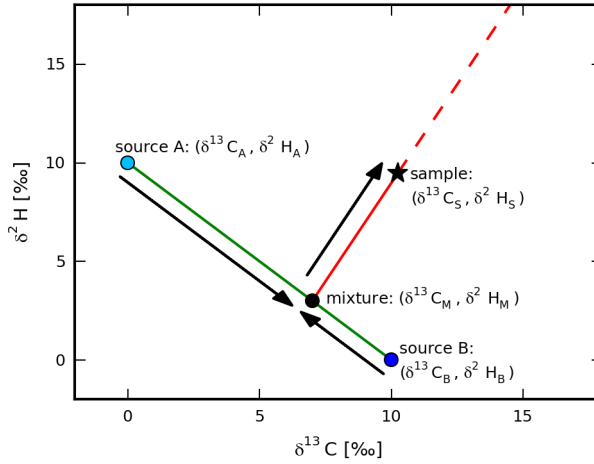


Figure 2.2: Two-dimensional isotope plot of a scenario of degradation that follows mixing of two emission sources. Mixing leads to an isotopic signature of  $(\delta^{13}C_M, \delta^2H_M)$ . Subsequently, degradation-induced isotope fractionation leads to a sample signature of  $(\delta^{13}C_S, \delta^2H_S)$ . Enrichment factors are  $\varepsilon_H = -4 \text{ ‰}$  and  $\varepsilon_C = -2 \text{ ‰}$ .

in combined SA and QED. The same holds for scenario 2 (see section S2.1 in the supplementary information). Note that additional consideration of concentration data does not allow precise SA or QED either, as nondestructive processes such as dilution affect concentrations to an unknown extent.

### 2.3.3 Degradation follows mixing: dual-element CSIA

Since single-element CSIA does not allow for combined SA and QED, we extended the SISS model to dual-element CSIA, e.g., carbon and hydrogen CSIA. The system of Eqs. 2.5 and 2.6 then becomes

$$\delta^{13}C_M = f_A \delta^{13}C_A + (1 - f_A) \delta^{13}C_B \quad (2.9)$$

$$\delta^2H_M = f_A \delta^2H_A + (1 - f_A) \delta^2H_B \quad (2.10)$$

$$f_B = (1 - f_A) \quad (2.11)$$

Equations 2.9-2.11 define a straight line through the source signatures  $(\delta^{13}C_A, \delta^2H_A)$  and  $(\delta^{13}C_B, \delta^2H_B)$ . This line is called the mixing line and describes, in this example, all possible combinations of  $\delta^{13}C$ - and  $\delta^2H$ -values for a mixture between sources A and B (green line in Fig. 2.2). Note that isotopes of the second element (Eq. 2.10) are not needed for SA between two sources solely, but they become relevant when considering degradation-induced isotope fractionation as shown below.

Following mixing, the signature of the mixture  $(\delta^{13}C_M, \delta^2H_M)$  shifts to the sample value  $(\delta^{13}C_S, \delta^2H_S)$  as a result of degradation-induced isotope fractionation. This

shift toward more enriched  $\delta$ -values can be described by the following equation, which gives the  $\delta^2\text{H}$ -values as a function of the  $\delta^{13}\text{C}$ -values (see the supplementary information, Eqs. S2.5–S2.7, for the derivation of Eq. 2.12):

$$\delta^2\text{H}_\text{S} = \left( \frac{\delta^{13}\text{C}_\text{S} + 1000}{\delta^{13}\text{C}_\text{M} + 1000} \right)^\Phi \cdot (\delta^2\text{H}_\text{M} + 1000) - 1000 \quad (2.12)$$

where  $\Phi = \varepsilon_\text{H}/\varepsilon_\text{C}$  represents the ratio between the enrichment factors (in per mil) for hydrogen and carbon isotopes that are associated with the specific reaction,  $\delta^{13}\text{C}_\text{S}$  and  $\delta^{13}\text{C}_\text{M}$  are the carbon isotopic signatures (in per mil) of the sample and at the mixing point, respectively, and  $\delta^2\text{H}_\text{S}$  and  $\delta^2\text{H}_\text{M}$  are the hydrogen isotopic signatures of the sample and at the mixing point, respectively. Equation 2.12 thus determines the trajectory of carbon and hydrogen isotope ratios under the influence of degradation-induced isotope fractionation (red solid line in Fig. 2.2).

In order to quantify the ED and source contributions, it is necessary to reconstruct the mixing signature ( $\delta^{13}\text{C}_\text{M}$ ,  $\delta^2\text{H}_\text{M}$ ) from the sample signature ( $\delta^{13}\text{C}_\text{S}$ ,  $\delta^2\text{H}_\text{S}$ ). This can be done by combining Eqs. 2.9, 2.10, and 2.12, as these equations comprise the three unknowns  $f_\text{A}$ ,  $\delta^{13}\text{C}_\text{M}$ , and  $\delta^2\text{H}_\text{M}$ . Alternatively, we can obtain the mixing signature by calculating the point of intersection between the trajectory of the fractionating mixture, given by Eq. 2.12, and the mixing line (Fig. 2.2). As the mixing line is a straight line, it is uniquely defined by two points (e.g., the source signatures). It can thus be described by a linear equation of the form  $y = mx + b$ , where  $m$  defines the slope and  $b$  the y-intercept of the mixing line. Plugging the source signatures ( $\delta^{13}\text{C}_\text{A}$ ,  $\delta^2\text{H}_\text{A}$ ) and ( $\delta^{13}\text{C}_\text{B}$ ,  $\delta^2\text{H}_\text{B}$ ) into the mixing line equation ( $y = mx + b$ ) yields the parameters  $m$  and  $b$ :

$$\delta^2\text{H}_\text{A} = m\delta^{13}\text{C}_\text{A} + b \quad (2.13)$$

$$\delta^2\text{H}_\text{B} = m\delta^{13}\text{C}_\text{B} + b \quad (2.14)$$

The factor  $m$  is thus equal to

$$m = \frac{\delta^2\text{H}_\text{A} - \delta^2\text{H}_\text{B}}{\delta^{13}\text{C}_\text{A} - \delta^{13}\text{C}_\text{B}} \quad (2.15)$$

and  $b$  is given by

$$b = \delta^2\text{H}_\text{A} - m\delta^{13}\text{C}_\text{A} \quad (2.16)$$

After obtaining  $m$  and  $b$ , the mixing signature ( $\delta^{13}\text{C}_\text{M}$ ,  $\delta^2\text{H}_\text{M}$ ) can be determined as the point of intersection between Eq. 2.12 and the following equation:

$$\delta^2\text{H}_\text{M} = m\delta^{13}\text{C}_\text{M} + b \quad (2.17)$$

In the case of differing enrichment factors for the two isotopes, thus for  $\Phi \neq 1$ , Eq. 2.12 is nonlinear, which might require a numerical solution of the system of Eqs. 2.12 and 2.17. If Eq. 2.12 takes a linear ( $\Phi = 1$ ) or quadratic form ( $\Phi = 2$ ), this system of two equations can be easily analytically solved for the two unknowns  $\delta^{13}\text{C}_\text{M}$  and  $\delta^2\text{H}_\text{M}$  (see sections S2.3 and S2.4 in the supplementary information to this chapter).

Following Eq. 2.9, the relative contribution of source A to the mixture is equal to

$$f_A = \frac{\delta^{13}C_M - \delta^{13}C_B}{\delta^{13}C_A - \delta^{13}C_B} \quad (2.18)$$

According to Eq. 2.8, the NDF of the sample can be determined as follows:

$$f_{\text{deg,S}} = \left( \frac{10^{-3} \cdot \delta^{13}C_S + 1}{10^{-3} \cdot \delta^{13}C_M + 1} \right)^{1000/\varepsilon_C} \quad (2.19)$$

As opposed to single-element CSIA, the use of dual-element CSIA in Eqs. 2.13-2.19 yields a unique solution for SA and QED of the sample, provided that degradation processes and thus isotope fractionation effects before mixing are negligible. Note that if degradation-induced isotope fractionation before mixing is, in fact, significant, this approach will yield an underestimation of the real ED. This underestimation generally decreases with increasing distance from the two source areas (see chapter 3), as the contribution of degradation before mixing to overall degradation decreases with further distance from the source areas, and, therefore, also the effect of the error introduced by assuming instantaneous mixing.

### 2.3.4 Mixing follows degradation: dual-element CSIA

This scenario considers the change in isotope ratios of the two contaminant pools resulting from degradation prior to mixing. The carbon isotope ratios of the two independently degrading pools prior to mixing are, according to Eq. 2.8, given by

$$\delta^{13}C_{A,t} = f_{\text{deg,A}}^{\varepsilon_C/1000} \cdot (\delta^{13}C_{A,0} + 1000) - 1000 \quad (2.20)$$

for source A, and by

$$\delta^{13}C_{B,t} = f_{\text{deg,B}}^{\varepsilon_C/1000} \cdot (\delta^{13}C_{B,0} + 1000) - 1000 \quad (2.21)$$

for source B, with  $\delta^{13}C_{A,t}$  and  $\delta^{13}C_{A,0}$  being the carbon isotopic signatures of the contaminant pool from source A at the time of mixing (subscript t) and emission (subscript 0),  $\delta^{13}C_{B,t}$  and  $\delta^{13}C_{B,0}$  being the respective values for source B, and  $f_{\text{deg,A}}$  and  $f_{\text{deg,B}}$  being the NDFs of sources A and B, respectively, at the time of mixing. Likewise, the hydrogen isotope ratios prior to mixing can be written as

$$\delta^2H_{A,t} = f_{\text{deg,A}}^{\varepsilon_H/1000} \cdot (\delta^2H_{A,0} + 1000) - 1000 \quad (2.22)$$

and

$$\delta^2H_{B,t} = f_{\text{deg,B}}^{\varepsilon_H/1000} \cdot (\delta^2H_{B,0} + 1000) - 1000 \quad (2.23)$$

where  $\delta^2H_{A,t}$  and  $\delta^2H_{A,0}$  are the hydrogen isotopic signatures of source A at the time of mixing (subscript t) and emission (subscript 0), respectively, and  $\delta^2H_{B,t}$  and  $\delta^2H_{B,0}$  are the respective values for source B. Equations 2.9 and 2.10 can then be adapted to scenario 2 as follows:

$$\delta^{13}C_S = f_A \delta^{13}C_{A,t} + (1 - f_A) \delta^{13}C_{B,t} \quad (2.24)$$

$$\delta^2\text{H}_S = f_A \delta^2\text{H}_{A,t} + (1 - f_A) \delta^2\text{H}_{B,t} \quad (2.25)$$

with  $(\delta^{13}\text{C}_S, \delta^2\text{H}_S)$  being the isotope ratio at the sampling point. Plugging Eqs. 2.20 and 2.21 into Eq. 2.24, and Eqs. 2.22 and 2.23 into Eq. 2.25 yields

$$\begin{aligned} \delta^{13}\text{C}_S = f_A \cdot [f_{\text{deg},A}^{\varepsilon_C/1000} (\delta^{13}\text{C}_{A,0} + 1000) - 1000] \\ + (1 - f_A) \cdot [f_{\text{deg},B}^{\varepsilon_C/1000} (\delta^{13}\text{C}_{B,0} + 1000) - 1000] \end{aligned} \quad (2.26)$$

$$\begin{aligned} \delta^2\text{H}_S = f_A \cdot [f_{\text{deg},A}^{\varepsilon_H/1000} (\delta^2\text{H}_{A,0} + 1000) - 1000] \\ + (1 - f_A) \cdot [f_{\text{deg},B}^{\varepsilon_H/1000} (\delta^2\text{H}_{B,0} + 1000) - 1000] \end{aligned} \quad (2.27)$$

Given the three unknowns  $f_A$ ,  $f_{\text{deg},A}$ , and  $f_{\text{deg},B}$  in Eqs. 2.26 and 2.27, a unique solution for the mixing line does not exist. However, as the sample signature is known and the mixing line between two end members is defined by two points, the specification of the isotopic signature before mixing either of the contaminant pool from source A  $(\delta^{13}\text{C}_{A,t}, \delta^2\text{H}_{A,t})$  or source B  $(\delta^{13}\text{C}_{B,t}, \delta^2\text{H}_{B,t})$  yields a unique solution for the mixing line equation. Without any additional information that could indicate the ED of one of the sources at the mixing point (e.g., its location in the aquifer or river with respect to the mixing zone), the choice of  $(\delta^{13}\text{C}_{A,t}, \delta^2\text{H}_{A,t})$  or  $(\delta^{13}\text{C}_{B,t}, \delta^2\text{H}_{B,t})$  is arbitrary. If we specify  $(\delta^{13}\text{C}_{B,t}, \delta^2\text{H}_{B,t})$ , or, in other words,  $f_{\text{deg},B}$ , Eqs. 2.13 and 2.14 become

$$\delta^2\text{H}_S = m \delta^{13}\text{C}_S + b \quad (2.28)$$

$$\delta^2\text{H}_{B,t} = m \delta^{13}\text{C}_{B,t} + b \quad (2.29)$$

Following the computation of  $m$  and  $b$  from Eqs. 2.28 and 2.29, the corresponding signature  $(\delta^{13}\text{C}_{A,t}, \delta^2\text{H}_{A,t})$  is given by the intersection of the mixing line and the trajectory of the contaminant pool from source A (Fig. 2.3):

$$\delta^2\text{H}_{A,t} = m \delta^{13}\text{C}_{A,t} + b \quad (2.30)$$

$$\delta^2\text{H}_{A,t} = \left( \frac{10^{-3} \cdot \delta^{13}\text{C}_{A,t} + 1}{10^{-3} \cdot \delta^{13}\text{C}_{A,0} + 1} \right)^\Phi \cdot (\delta^2\text{H}_{A,0} + 1000) - 1000 \quad (2.31)$$

According to Eq. 2.24, the contribution of source A to the sample is defined by

$$f_A = \frac{\delta^{13}\text{C}_S - \delta^{13}\text{C}_{B,t}}{\delta^{13}\text{C}_{A,t} - \delta^{13}\text{C}_{B,t}} \quad (2.32)$$

The total NDF at the sampling point in scenario 2 depends on the NDFs of sources A and B. As the NDFs of the two sources can take an indefinite number of values, it is not possible to obtain a unique solution for the total NDF. However, the following equation allows for the calculation of the total NDF in scenario 2 after specification

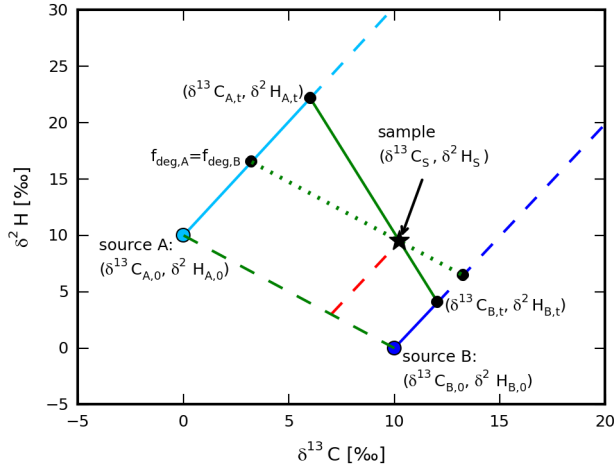


Figure 2.3: Two-dimensional isotope plot of a scenario of mixing that follows independent degradation of two contaminant pools. The a priori specification of point  $(\delta^{13}C_{B,t}, \delta^2H_{B,t})$  yields the mixing line equation and the corresponding signature of the contaminant pool from source A  $(\delta^{13}C_{A,t}, \delta^2H_{A,t})$ . The mixing line between sources A and B (dashed green line) is parallel to the mixing line for  $f_{deg,A} = f_{deg,B}$  (dotted green line). Enrichment factors are  $\varepsilon_H = -4 \text{ ‰}$  and  $\varepsilon_C = -2 \text{ ‰}$ .

of the NDFs from sources A and B (see section S2.5 in the supplementary information to this chapter for the derivation of Eq. 2.33):

$$f_{deg,tot} = \frac{1}{\frac{f_A}{f_{deg,A}} + \frac{(1-f_A)}{f_{deg,B}}} \quad (2.33)$$

where  $f_{deg,A}$  and  $f_{deg,B}$  are the NDFs of sources A and B, respectively, and  $f_A$  is the contribution of source A to the sample. Equation 2.33 allows for the calculation of the overall NDF for any possible combination of  $f_{deg,A}$  and  $f_{deg,B}$  without further information about source or sample concentrations. According to Eq. 2.33, the overall NDF is  $f_{deg,tot} = f_{deg,A} = f_{deg,B}$  if  $f_{deg,A} = f_{deg,B}$ , which corresponds to a mixing line through the sample signature  $(\delta^{13}C_S, \delta^2H_S)$  that is parallel to the mixing line between sources A and B (dotted and dashed green line, respectively, in Fig. 2.3). In this case, the degradation trajectories of sources A and B (line segments in Fig. 2.3 from  $(\delta^{13}C_{A,0}, \delta^2H_{A,0})$  to  $(\delta^{13}C_{A,t}, \delta^2H_{A,t})$ , and  $(\delta^{13}C_{B,0}, \delta^2H_{B,0})$  to  $(\delta^{13}C_{B,t}, \delta^2H_{B,t})$ , respectively) have the same length as the degradation trajectory of the mixture in scenario 1 (red solid line from  $(\delta^{13}C_M, \delta^2H_M)$  to  $(\delta^{13}C_S, \delta^2H_S)$  in Fig. 2.2, or red dashed line in Fig. 2.3). Consequently, if  $f_{deg,A} = f_{deg,B}$ , the NDF in scenario 2 is the same as under the assumption of instantaneous mixing followed by degradation (i.e., scenario 1). Moreover,  $f_{deg,A} = f_{deg,B}$  gives a smaller  $f_{deg,tot}$  than any other combination of  $f_{deg,A}$  and  $f_{deg,B}$  with  $f_{deg,A} \neq f_{deg,B}$ , as the latter results in an overcompensation of the lower ED of one of the sources by a much larger ED of the other source. Hence, scenario 1 always yields a conservative estimate of the ED in scenario 2 (see section S2.6 in the supplementary information). The underestimation of the actual ED increases with increasing difference between  $f_{deg,A}$  and  $f_{deg,B}$ , i.e., the more the slopes of the actual mixing line (solid green line

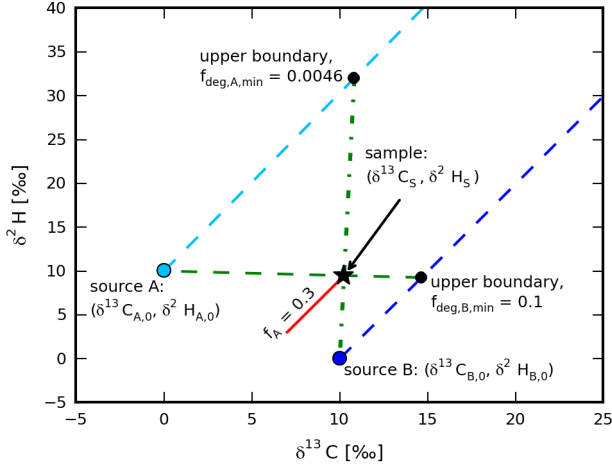


Figure 2.4: Minima of the NDFs from sources A and B that result in the sample signature  $(\delta^{13}\text{C}_S, \delta^2\text{H}_S)$ , and corresponding mixing lines (dashed green line: upper boundary of  $(\delta^{13}\text{C}_{B,t}, \delta^2\text{H}_{B,t})$ ; dash-dotted green line: upper boundary of  $(\delta^{13}\text{C}_{A,t}, \delta^2\text{H}_{A,t})$ ). Enrichment factors are  $\varepsilon_{\text{H}} = -4\text{‰}$  and  $\varepsilon_{\text{C}} = -2\text{‰}$ .

in Fig. 2.3) and the conservative mixing line (dotted green line in Fig. 2.3) differ. Note that the extension of the model equations for scenario 2 by the isotope ratios of a third element does not obviate the need for specification of either  $f_{\text{deg},A}$  or  $f_{\text{deg},B}$  (not shown).

As the SISS model for scenario 2 requires the definition of one of the isotopic signatures prior to mixing (such as  $(\delta^{13}\text{C}_{B,t}, \delta^2\text{H}_{B,t})$  in Eq. 2.29), one might be interested in the upper boundary of this signature beyond which a sample signature of  $(\delta^{13}\text{C}_S, \delta^2\text{H}_S)$  is impossible (Fig. 2.4). This upper boundary thus determines the maximum ED that a contaminant pool may have undergone before it mixes with the second contaminant pool. The upper boundary for the contaminant pool from source A can be obtained by setting  $(\delta^{13}\text{C}_{B,t}, \delta^2\text{H}_{B,t})$  in Eq. 2.29 to the source signature  $(\delta^{13}\text{C}_{B,0}, \delta^2\text{H}_{B,0})$ . The corresponding signature  $(\delta^{13}\text{C}_{A,t}, \delta^2\text{H}_{A,t})$  that results from solving Eqs. 2.30 and 2.31 then determines the smallest NDF possible (i.e., the largest ED) for the contaminant pool from source A prior to mixing ( $f_{\text{deg},A,\text{min}}$ ). In the example of Fig. 2.4,  $f_{\text{deg},A,\text{min}}$  is 0.0046, and the smallest NDF of source B is  $f_{\text{deg},B,\text{min}} = 0.1$ .

Taking the source and sample concentration into account allows for further constraining the plausible range of  $f_{\text{deg},A}$  and  $f_{\text{deg},B}$  given the upper boundaries  $f_{\text{deg},A,\text{min}}$  and  $f_{\text{deg},B,\text{min}}$ . In the absence of sorption processes, the source concentration  $C_{A,0}$  is defined by the sample concentration, the contribution of source A to the sample ( $f_A$ ; known from the SISS model), a dilution factor for source A ( $F_{\text{dil},A}$ ), and the NDF of source A ( $f_{\text{deg},A}$ ; see section S2.5 for derivation of Eq. 2.34):

$$C_{A,0} = \frac{F_{\text{dil},A} \cdot C_S \cdot f_A}{f_{\text{deg},A}} \quad (2.34)$$

Rearranging yields, given  $F_{\text{dil,A}} \geq 1$ :

$$f_{\text{deg,A,min}} = \frac{C_S \cdot f_A}{C_{A,0}} \quad (2.35)$$

Equation 2.35, therefore, gives the minimum NDF of source A in scenario 2, which can be larger than the minimum NDF obtained from isotope data only (i.e., by setting  $(\delta^{13}\text{C}_{\text{B,t}}, \delta^2\text{H}_{\text{B,t}})$  in Eq. 2.29 to the source signature  $(\delta^{13}\text{C}_{\text{B,0}}, \delta^2\text{H}_{\text{B,0}})$ ; see above). The same calculation can be done for  $f_{\text{B}}$  and  $C_{\text{B,0}}$  to further constrain the minimum NDF of source B ( $f_{\text{deg,B,min}}$ ). Similarly, by setting the dilution factor ( $F_{\text{dil}}$ ) to one, the minimum concentration of sources A and B can be derived from Eq. 2.34 for any combination of  $f_{\text{deg,A}}$  and  $f_{\text{deg,B}}$  (see Fig. S2.3d). When applied in the assessment of groundwater pollution, Eqs. 2.34 and 2.35 also hold for sorbing contaminants, provided the contaminant plume is at steady state (van Breukelen and Prommer, 2008).

### 2.3.5 Unequivocal source apportionment with dual-element CSIA

The trajectory given by Eqs. 2.12 or 2.31 can generally be approximated by a straight line in the two-dimensional isotope plot (see Fig. S2.4; Fischer et al., 2008; van Breukelen, 2007a) unless for a large ED or large  $\Phi$ -values (e.g.,  $\varepsilon_{\text{H}} \gg 100 \text{‰}$ ; Mariotti et al., 1981; Wijker et al., 2013). Assuming that the degradation trajectory is a straight line, we can derive from the Thales' theorem (Agricola et al., 2008) that the proportional contribution of source A is almost identical for all combinations of  $f_{\text{deg,A}}$  and  $f_{\text{deg,B}}$  that lead to the same sample signature. It follows that two sample signatures that lie on the same trajectory defined by Eqs. 2.12 or 2.31 are associated with the same  $f_{\text{A}}$  (see section S2.7 in the supplementary information for a more detailed discussion). The location of a sample signature in the two-dimensional isotope plot thus uniquely defines the relative source contributions. Therefore, it is irrelevant for SA with the SISS model whether the two sources mix instantaneously (scenario 1), or whether degradation occurs prior to mixing (scenario 2). This is illustrated in Fig. 2.5 for perchlorate, which can have a natural (source A) or synthetic (source B) origin. Figure 2.5a shows examples of degradation-trajectories in the  $(\delta^{18}\text{O}, \delta^{37}\text{Cl})$ -space based on reported source signatures (Sturchio et al., 2006) and enrichment factors for biodegradation of perchlorate (Sturchio et al., 2007). Points on the same trajectory approximately yield the same relative contribution of natural perchlorate ( $f_{\text{A}} = 0.1$  for the dotted,  $f_{\text{A}} = 0.5$  for the dash-dotted, and  $f_{\text{A}} = 0.95$  for the dashed line). Hence, SA with the SISS model does not require the a priori specification of the points  $(\delta^{18}\text{O}_{\text{A,t}}, \delta^{37}\text{Cl}_{\text{A,t}})$  or  $(\delta^{18}\text{O}_{\text{B,t}}, \delta^{37}\text{Cl}_{\text{B,t}})$  and use of Eqs. 2.28-2.32. Instead, it is sufficient to calculate the intersection point between the trajectory through the sample signature (given by Eq. 2.12) and the mixing line between sources A and B (as done in scenario 1) to obtain a good approximation of the actual  $f_{\text{A}}$  (given by Eq. 2.32). Similarly, three-dimensional isotope data uniquely determine the source contributions in a scenario of three mixing sources and one degradation pathway (see section S2.9 in the supplementary information). Hence, given that degradation trajectories are in good approximation straight lines in the dual-element isotope plot, the SISS model provides a tool for SA in cases

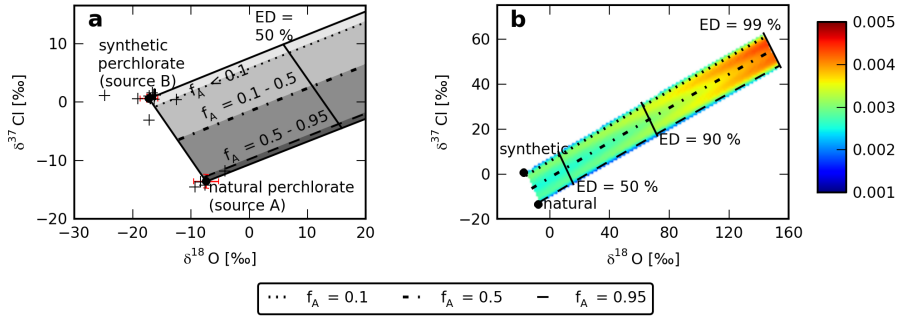


Figure 2.5: Partitioning of the  $(\delta^{18}\text{O}, \delta^{37}\text{Cl})$ -space according to the relative contribution of natural perchlorate ( $f_A$ ) (a); and uncertainty in  $f_A$  (95% confidence interval for 2500 Monte Carlo simulations at 693 sample locations interpolated in depicted  $(\delta^{18}\text{O}, \delta^{37}\text{Cl})$ -space) due to variation of isotopic signatures of perchlorate sources, and analytical uncertainties in enrichment factors and CSIA of samples (b). Shaded areas in (a) indicate degradation trajectories with a contribution of source A of  $>0.95$ ,  $0.5-0.95$ ,  $0.1-0.5$ , and  $<0.1$  according to the labels. The source signatures (black dots) were obtained as the mean of individual source signatures from Sturchio et al. (2006) (black crosses). Error bars (red) show 95%-confidence intervals of source signatures. Enrichment factors were set to the mean of  $\varepsilon$ -values from Sturchio et al. (2007) ( $\varepsilon_{\text{Cl}} = -13.3$  ‰ and  $\varepsilon_{\text{O}} = -33.4$  ‰,  $\Phi_{\text{Cl/O}} = 0.4 \pm 0.01$ ).

where degradation-induced isotope fractionation complicates the use of CSIA data for source identification and apportionment.

Figure 2.5b shows an uncertainty analysis for the calculated  $f_A$  (95% confidence interval) for perchlorate based on scenario 1 of the SISS model and numerical solution of Eqs. 2.12 and 2.17 (function `nsolve` in python package `SymPy`). The uncertainty in  $f_A$  was obtained from Monte Carlo simulations considering uncertainties in enrichment factors (Sturchio et al., 2007) and CSIA of samples (Sturchio et al., 2006), and variation of isotopic signatures of perchlorate sources (Sturchio et al., 2006). A similar approach has been taken by Andersson (2011) to illustrate the incorporation of source variability into mixing models. Values of  $f_A$  above 1 or below 0, which can result from these variations in the input parameters, were set to 1 or 0, respectively. This correction resulted in a small uncertainty in  $f_A$  for areas with a contribution of close to one from either source A or B. Note that the use of scenario 1 implies that potential inaccuracies introduced by the approximation of degradation trajectories by straight lines were not considered.

The overall uncertainty increases with increasing ED (Fig. 2.5b), as the uncertainty in  $\Phi$  becomes more relevant for more enriched isotope values ( $\Phi$  as exponent in Eq. 2.12); and decreases (apart from the areas with  $f_A \approx 1$  or  $f_B \approx 1$ ), at a given ED, toward the line of equal source contributions ( $f_A = 0.5$ ) where the variation in source signatures has less influence on  $f_A$  compared to areas with a predominant contribution of either source A or B. With a maximum value of below 0.005, the variations in the given input parameters did only cause a minor uncertainty in SA of perchlorate. This can be ascribed to the limited number of  $\varepsilon_{\text{O}}$  and  $\varepsilon_{\text{Cl}}$  values for perchlorate biodegradation (Sturchio et al., 2007), which led to a small uncertainty in  $\Phi_{\text{Cl/O}}$ ; the high analytical precision in oxygen and chlorine CSIA (standard deviation of 0.3 ‰; Sturchio et al., 2006); the low standard deviation of the mean

isotopic signature of natural and synthetic perchlorate; and the relatively large difference in the isotopic signatures of natural and synthetic perchlorate sources compared to the high analytical precision of  $\delta^{18}\text{O}$ - and  $\delta^{37}\text{Cl}$ -values.

As the degradation trajectories in the two-dimensional isotope plot form, to a good approximation, straight lines, a numerical solution of the system of Eqs. 2.12 and 2.17 can be avoided not only for  $\Phi = 1$  or  $\Phi = 2$ , but also for other  $\Phi$ -values. In this case, Eq. 2.12 or 2.17 can be approximated by a straight line with a slope of  $\Phi$ , such that the isotope ratio at mixing ( $\delta^{13}\text{C}_M$ ,  $\delta^2\text{H}_M$ ) is given by the intersection of two straight lines (the approximated trajectory and the mixing line). However, various mathematics software packages provide numerical methods for the solution of nonlinear systems, which obviates the need for linearization of Eq. 2.12.

## 2.4 Conclusions

The presented SISS model offers a tool for combined source apportionment and quantification of in situ degradation of organic pollutants (and inorganic compounds such as nitrate) with dual-element CSIA data in a scenario of two sources and one reaction pathway. In particular, it allows for accurate SA based on the location of the sample in the two-dimensional isotope plot, regardless of whether mixing occurs instantaneously after emission or after significant degradation of the two contaminant pools. Therefore, SA appears, in general, to be also feasible if the analyzed contaminant undergoes transformation processes that entail isotope fractionation effects. This is opposed to previous studies that challenge the use of isotope data in such a case. However, if mixing occurs following degradation of the individual contaminant pools, the SISS model can only provide a conservative estimate of the overall ED, since the same sample signature can result from different combinations of NDFs of the mixing contaminant pools. Nonetheless, the SISS model is, to our knowledge, the only approach that allows for an estimate of the ED in such a scenario.

The SISS model was derived for two emission sources and one degradation pathway. Future research could consider multiple emission sources and reaction pathways. In general, every additional reaction pathway or end member should necessitate CSIA of an additional element. As shown in the supplementary information to this chapter, this results in three-dimensional isotope analysis in the case of two emission sources and two simultaneously occurring reaction pathways (section S2.8), as well as in the case of three emission sources and one reaction pathway only (section S2.9).

There is a clear need for validation of the SISS model with reactive transport modeling, as the latter allows for precise SA and QED of the virtual data set (see chapter 3). Moreover, it is required to apply the SISS model to actual field data. For example, the model could be tested with dual-element CSIA data of organic groundwater contaminants (see chapter 3) or nitrate pollution of rivers. This would evaluate its robustness against uncertainties in measured CSIA data and applicability for environmental systems, which generally involve a high degree of heterogeneity.

## Supplementary information to chapter 2

### S2.1 Mixing follows degradation (scenario 2): single-element CSIA

We consider two mixing end members (sources A and B) in combination with CSIA data for carbon only. Analogous to Eq. 2.8, the  $\delta^{13}\text{C}$ -signatures of the mixing contaminant pools that stem from source A and B can be expressed as a function of the source signatures ( $\delta^{13}\text{C}_{\text{A},0}$  and  $\delta^{13}\text{C}_{\text{B},0}$ ) and the NDFs ( $f_{\text{deg,A}}$  and  $f_{\text{deg,B}}$ ) of the initial contaminant masses:

$$\delta^{13}\text{C}_{\text{A},t} = f_{\text{deg,A}}^{\varepsilon_{\text{C}}/1000} \cdot (\delta^{13}\text{C}_{\text{A},0} + 1000) - 1000 \quad (\text{S2.1})$$

$$\delta^{13}\text{C}_{\text{B},t} = f_{\text{deg,B}}^{\varepsilon_{\text{C}}/1000} \cdot (\delta^{13}\text{C}_{\text{B},0} + 1000) - 1000 \quad (\text{S2.2})$$

where  $\varepsilon_{\text{C}}$  is the carbon isotopic enrichment factor,  $\delta^{13}\text{C}_{\text{A},t}$  and  $\delta^{13}\text{C}_{\text{B},t}$  are the signatures of the two contaminant pools from source A and source B, respectively, at the time of mixing, and  $f_{\text{deg,A}}$  and  $f_{\text{deg,B}}$  are the NDFs of these contaminant pools at the time of mixing. Accordingly, the isotopic signature of the sample mixture ( $\delta^{13}\text{C}_{\text{S}}$ ) is

$$\delta^{13}\text{C}_{\text{S}} = f_{\text{A}}\delta^{13}\text{C}_{\text{A},t} + (1 - f_{\text{A}})\delta^{13}\text{C}_{\text{B},t} \quad (\text{S2.3})$$

with  $f_{\text{A}}$  being the proportional contribution of source A to the mixture. Substituting Eqs. S2.1 and S2.2 into Eq. S2.3 yields

$$\delta^{13}\text{C}_{\text{S}} = f_{\text{A}} \cdot [f_{\text{deg,A}}^{\varepsilon_{\text{C}}/1000} \cdot (\delta^{13}\text{C}_{\text{A},0} + 1000) - 1000] + (1 - f_{\text{A}}) \cdot [f_{\text{deg,B}}^{\varepsilon_{\text{C}}/1000} \cdot (\delta^{13}\text{C}_{\text{B},0} + 1000) - 1000] \quad (\text{S2.4})$$

Equation S2.4 has three unknowns, which means that there is an indefinite number of solutions for  $f_{\text{A}}$ ,  $f_{\text{deg,A}}$ , and  $f_{\text{deg,B}}$ . Even if the NDF of the part of the sample that originates from source A ( $f_{\text{deg,A}}$ ) is known, the equation still has the two unknowns  $f_{\text{A}}$  and  $f_{\text{deg,B}}$ . This situation is illustrated in the one-dimensional isotope plot in Fig. S2.1, which shows two different combinations of degradation and mixing for source B that result in the same sample signature (first combination with  $\delta^{13}\text{C}_{\text{B},t}$ : dotted blue and green lines; second combination with  $\delta^{13}\text{C}'_{\text{B},t}$ : dashed blue and green lines). Therefore, it is, as seen for instantaneous mixing after emission (scenario 1), not sufficient to solely look at one isotopic marker if one wants to quantify the overall ED and the contribution of the two sources to the sample mixture.

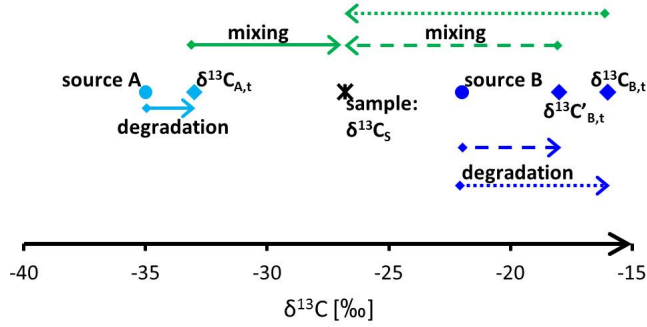


Figure S2.1: One-dimensional isotope plot of a scenario where mixing follows degradation. Although the ED of source A is specified (corresponding to the value  $\delta^{13}C_{A,t}$  before mixing), a unique solution for the proportional contribution of source B that leads to the sample signature  $\delta^{13}C_S$ , and thus for the overall ED does not exist (two possibilities are indicated by  $\delta^{13}C_{B,t}$  and  $\delta^{13}C'_{B,t}$ ).

## S2.2 Derivation of Equation 2.12: $\delta^2H$ -values as a function of $\delta^{13}C$ -values

According to Eq. 2.8, the  $\delta^2H$ -value of the sample is given by

$$\delta^2H_S = f_{\text{deg},S}^{\varepsilon_H/1000} \cdot (\delta^2H_M + 1000) - 1000 \quad (\text{S2.5})$$

where  $\varepsilon_H$  is the hydrogen isotopic enrichment factor,  $\delta^2H_S$  is the hydrogen isotopic signature of the sample S,  $\delta^2H_M$  is the hydrogen isotopic signature at the mixing point, and  $f_{\text{deg},S}$  is the NDF since mixing occurred.

Rearranging Eq. 2.8 yields the NDF of the sample based on the  $\delta^{13}C$ -values of the sample ( $\delta^{13}C_S$ ) and mixing point ( $\delta^{13}C_M$ ):

$$f_{\text{deg},S} = \left( \frac{\delta^{13}C_S + 1000}{\delta^{13}C_M + 1000} \right)^{1000/\varepsilon_C} \quad (\text{S2.6})$$

where  $\varepsilon_C$  is the carbon isotopic enrichment factor.

Plugging Eq. S2.6 into S2.5 thus gives the  $\delta^2H$ -values as a function of the  $\delta^{13}C$ -values (Eq. 2.12):

$$\delta^2H_S = \left( \frac{\delta^{13}C_S + 1000}{\delta^{13}C_M + 1000} \right)^\Phi \cdot (\delta^2H_M + 1000) - 1000 \quad (\text{S2.7})$$

with  $\Phi = \varepsilon_H/\varepsilon_C$ .

Figure S2.2 illustrates the trajectory of carbon and hydrogen isotope ratios given by Eq. 2.12 (Eq. S2.7) in a two-dimensional isotope plot.

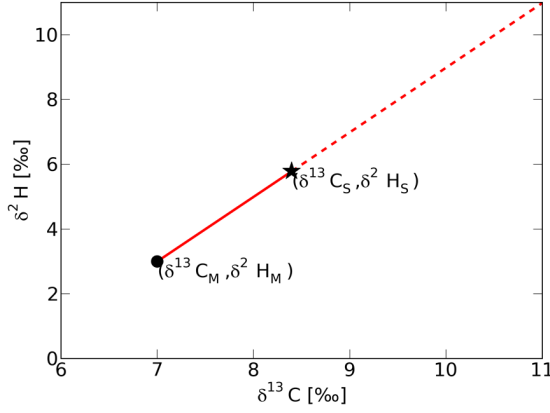


Figure S2.2: Two-dimensional isotope plot of the degradation trajectory given by Eq. 2.12/S2.7 (solid red line between mixing and sample signature). Enrichment factors are  $\varepsilon_{\text{H}} = -4 \text{ ‰}$  and  $\varepsilon_{\text{C}} = -2 \text{ ‰}$ .

### S2.3 Analytical Solution of Equations 2.12 and 2.17 for $\Phi = \varepsilon_{\text{H}}/\varepsilon_{\text{C}} = 1$

In the case of identical enrichment factors for a specific reaction, i.e.,  $\Phi = 1$ , Eq. 2.12 takes the form

$$\delta^2\text{H}_S = \left( \frac{10^{-3} \cdot \delta^{13}\text{C}_S + 1}{10^{-3} \cdot \delta^{13}\text{C}_M + 1} \right) \cdot (\delta^2\text{H}_M + 1000) - 1000 \quad (\text{S2.8})$$

Substituting Eq. 2.17 into Eq. S2.8 and rearranging terms yields the mixing signature (Eq. S2.11):

$$\delta^2\text{H}_S(10^{-3} \cdot \delta^{13}\text{C}_M + 1) = (10^{-3} \cdot \delta^{13}\text{C}_S + 1) \cdot (m\delta^{13}\text{C}_M + b + 1000) - (\delta^{13}\text{C}_M + 1000) \quad (\text{S2.9})$$

$$\begin{aligned} \delta^{13}\text{C}_M[1 + 10^{-3} \cdot \delta^2\text{H}_S - m(10^{-3} \cdot \delta^{13}\text{C}_S + 1)] + \delta^2\text{H}_S \\ = (10^{-3} \cdot \delta^{13}\text{C}_S + 1)(b + 1000) - 1000 \end{aligned} \quad (\text{S2.10})$$

$$(\delta^{13}\text{C}_M, \delta^2\text{H}_M) = \left( \frac{(10^{-3}b + 1)(\delta^{13}\text{C}_S + 1000) - 1000 - \delta^2\text{H}_S}{-m(10^{-3} \cdot \delta^{13}\text{C}_S + 1) + 10^{-3} \cdot \delta^2\text{H}_S + 1}, m\delta^{13}\text{C}_M + b \right) \quad (\text{S2.11})$$

The parameters  $m$  and  $b$  are known from the mixing line equation (Eqs. 2.15 and 2.16).

## S2.4 Analytical Solution of Equations 2.12 and 2.17 for $\Phi = \varepsilon_{\text{H}}/\varepsilon_{\text{C}} = 2$

For  $\Phi = \varepsilon_{\text{H}}/\varepsilon_{\text{C}} = 2$ , Eq. 2.12 takes the form

$$\delta^2\text{H}_{\text{S}} = \left( \frac{10^{-3} \cdot \delta^{13}\text{C}_{\text{S}} + 1}{10^{-3} \cdot \delta^{13}\text{C}_{\text{M}} + 1} \right)^2 \cdot (\delta^2\text{H}_{\text{M}} + 1000) - 1000 \quad (\text{S2.12})$$

Substituting Eq. 2.17 into Eq. S2.12 yields:

$$\delta^2\text{H}_{\text{S}} = \left( \frac{10^{-3} \cdot \delta^{13}\text{C}_{\text{S}} + 1}{10^{-3} \cdot \delta^{13}\text{C}_{\text{M}} + 1} \right)^2 \cdot (m\delta^{13}\text{C}_{\text{M}} + b + 1000) - 1000 \quad (\text{S2.13})$$

Rearranging Eq. S2.13 to obtain a quadratic equation of the form  $ax^2 + bx + c = 0$  (with  $x$  being the unknown carbon isotopic signature of the mixture,  $\delta^{13}\text{C}_{\text{M}}$ ) gives

$$\delta^2\text{H}_{\text{S}}(10^{-3} \cdot \delta^{13}\text{C}_{\text{M}} + 1)^2 = m\delta^{13}\text{C}_{\text{M}}(10^{-3} \cdot \delta^{13}\text{C}_{\text{S}} + 1)^2 + (b + 1000)(10^{-3} \cdot \delta^{13}\text{C}_{\text{S}} + 1)^2 - 1000(10^{-3} \cdot \delta^{13}\text{C}_{\text{M}} + 1)^2 \quad (\text{S2.14})$$

$$\begin{aligned} \delta^2\text{H}_{\text{S}}(10^{-6} \cdot \delta^{13}\text{C}_{\text{M}}^2 + 2 \cdot 10^{-3} \cdot \delta^{13}\text{C}_{\text{M}} + 1) &= m\delta^{13}\text{C}_{\text{M}}(10^{-3} \cdot \delta^{13}\text{C}_{\text{S}} + 1)^2 \\ &+ (b + 1000)(10^{-3} \cdot \delta^{13}\text{C}_{\text{S}} + 1)^2 - 1000(10^{-6} \cdot \delta^{13}\text{C}_{\text{M}}^2 + 2 \cdot 10^{-3} \cdot \delta^{13}\text{C}_{\text{M}} + 1) \end{aligned} \quad (\text{S2.15})$$

$$\begin{aligned} \delta^{13}\text{C}_{\text{M}}^2(10^{-6} \cdot \delta^2\text{H}_{\text{S}} + 10^{-3}) + \delta^{13}\text{C}_{\text{M}}[2 \cdot 10^{-3} \cdot \delta^2\text{H}_{\text{S}} - \\ m(10^{-3} \cdot \delta^{13}\text{C}_{\text{S}} + 1)^2 + 2] + \delta^2\text{H}_{\text{S}} - (10^{-3} \cdot \delta^{13}\text{C}_{\text{S}} + 1)^2(b + 1000) + 1000 = 0 \end{aligned} \quad (\text{S2.16})$$

The general solution of the quadratic equation  $ax^2 + bx + c = 0$  is  $x_{1,2} = \frac{-b \pm \sqrt{b^2 - 4ac}}{2a}$ . When applied to Eq. S2.16, this results in the following solution for the mixing signature:

$$(\delta^{13}\text{C}_{\text{M}1,2}, \delta^2\text{H}_{\text{M}1,2}) = \left( \frac{-q \pm \sqrt{q^2 - 4pr}}{2p}, m \cdot \left[ \frac{-q \pm \sqrt{q^2 - 4pr}}{2p} \right] + b \right) \quad (\text{S2.17})$$

where  $p = 10^{-6}\delta^2\text{H}_{\text{S}} + 10^{-3}$ ,  $q = 2 \cdot 10^{-3}\delta^2\text{H}_{\text{S}} - m(10^{-3}\delta^{13}\text{C}_{\text{S}} + 1)^2 + 2$ , and  $r = \delta^2\text{H}_{\text{S}} - (10^{-3}\delta^{13}\text{C}_{\text{S}} + 1)^2 \cdot (b + 1000) + 1000$ . The parameters  $m$  and  $b$  are defined by the mixing line equation. The isotopic signature that lies on the mixing line between the two sources (either  $(\delta^{13}\text{C}_{\text{M}1}, \delta^2\text{H}_{\text{M}1})$  or  $(\delta^{13}\text{C}_{\text{M}2}, \delta^2\text{H}_{\text{M}2})$ ) is the valid solution of Eq. S2.17.

## S2.5 Derivation of Equations 2.33 and 2.34

The sample concentration relates to the concentration of the contaminant pools from source A and B ( $C_{\text{A}}$  and  $C_{\text{B}}$ , respectively) as

$$C_{\text{S}} = C_{\text{A}}v_{\text{A}} + C_{\text{B}}v_{\text{B}} = C_{\text{A}}v_{\text{A}} + C_{\text{B}}(1 - v_{\text{A}}) \quad (\text{S2.18})$$

where  $v_A = V_A/V_S$  is the ratio between the volume of water coming from source A ( $V_A$ ) and total sample volume ( $V_S$ ), and  $v_B$  is the ratio between the volume of water coming from source B and total sample volume. For example, a sample concentration of  $C_S = 75 \text{ mg L}^{-1}$  might result from concentrations of  $C_A = 100 \text{ mg L}^{-1}$  and  $C_B = 50 \text{ mg L}^{-1}$  prior to mixing, and volumetric contributions of  $v_A = v_B = 0.5$ . Note that  $v_A$  is not equal to  $f_A$ , which gives the contribution from source A in terms of number of molecules (or mass), i.e.  $f_A = m_A/m_S$  (where  $m_S$  is the total contaminant mass in the sample, and  $m_A$  is the mass in the sample derived from source A). With  $C_S = m_S/V_S$ , it follows for the concentration of the contaminant pool from source A that

$$C_A = \frac{m_A}{V_A} = \frac{m_A}{v_A V_S} = \frac{f_A m_S}{v_A V_S} = C_S \frac{f_A}{v_A} \quad (\text{S2.19})$$

and, accordingly, for  $C_B$  that

$$C_B = C_S \frac{(1 - f_A)}{v_B} \quad (\text{S2.20})$$

If no degradation had occurred before mixing, the sample concentration would be given by (according to Eq. S2.18):

$$C_{S,0} = \frac{C_A}{f_{\text{deg},A}} v_A + \frac{C_B}{f_{\text{deg},B}} v_B \quad (\text{S2.21})$$

The total non-degraded fraction equals the ratio between sample concentration and theoretical sample concentration without degradation (given by Eq. S2.21):

$$f_{\text{deg,tot}} = \frac{C_S}{C_{S,0}} = \frac{C_S}{\frac{C_A}{f_{\text{deg},A}} v_A + \frac{C_B}{f_{\text{deg},B}} v_B} \quad (\text{S2.22})$$

Substitution of Eqs. S2.19 and S2.20 into S2.22 yields an equation for the total non-degraded fraction that is independent of concentration data (Eq. 2.33):

$$f_{\text{deg,tot}} = \frac{C_S}{\frac{C_S f_A}{f_{\text{deg},A}} + \frac{C_S (1-f_A)}{f_{\text{deg},B}}} = \frac{1}{\frac{f_A}{f_{\text{deg},A}} + \frac{(1-f_A)}{f_{\text{deg},B}}} \quad (\text{S2.23})$$

In the absence of sorption processes, the concentration of the contaminant pool from source A at the time of mixing ( $C_A$ ) relates to the source concentration ( $C_{A,0}$ ) as follows:

$$C_A = C_{A,0} f_{\text{deg},A} f_{\text{dil},A} \quad (\text{S2.24})$$

where  $f_{\text{deg},A}$  is the non-degraded fraction from source A, and  $f_{\text{dil},A}$  is the remaining fraction from source A after the effect of dilution. Substituting the right-hand side of Eq. S2.19 into S2.24 and rearranging yields Eq. 2.34:

$$C_{A,0} = \frac{C_A}{f_{\text{deg},A} f_{\text{dil},A}} = \frac{C_S f_A}{f_{\text{deg},A} f_{\text{dil},A} v_A} = \frac{F_{\text{dil},A} C_S f_A}{f_{\text{deg},A}} \quad (\text{S2.25})$$

with  $F_{\text{dil}} = \frac{1}{f_{\text{dil},A} v_A}$  being the dilution factor for source A.

## S2.6 Conservative estimate of overall degradation with scenario 1

Figure S2.3 shows the application of Eq. 2.33 to the following imaginary system: scenario 2 (mixing follows degradation) with two sources A and B with  $\delta^{13}\text{C}$ -values of  $-10\text{‰}$  and  $+10\text{‰}$ , respectively, and a  $\delta^2\text{H}$ -value of  $0\text{‰}$  for both sources. The degradation process is fractionating for hydrogen isotopes ( $\varepsilon_{\text{H}} = -15\text{‰}$ ), but not for carbon isotopes ( $\varepsilon_{\text{C}} = 0\text{‰}$ ). The environmental sample has a unit concentration of 1 and a hydrogen isotope shift of  $10\text{‰}$ . The minimum extent of overall degradation according to Eq. 2.33 coincides with equal assumed  $\delta^2\text{H}_{\text{A,t}}$  and  $\delta^2\text{H}_{\text{B,t}}$  (i.e.,  $f_{\text{deg,A}} = f_{\text{deg,B}}$ ) for each  $f_{\text{A}}$ , as the calculated overall ED increases with increasing deviation between  $\delta^2\text{H}_{\text{A,t}}$  and  $\delta^2\text{H}_{\text{B,t}}$  (Fig. S2.3b). As  $f_{\text{deg}}$  decreases exponentially with increasing isotopic shift ( $f_{\text{deg}} \approx \exp(\Delta/\varepsilon)$  with isotopic shift  $\Delta = \delta^2\text{H}_t - \delta^2\text{H}_0$  and  $\varepsilon < 0$ ), a larger NDF of one source (i.e., a smaller ED) is overcompensated by a much smaller NDF (i.e., a much larger ED) of the other source (Fig. S2.3c). Accordingly,  $\delta^2\text{H}_{\text{A,t}} = \delta^2\text{H}_{\text{B,t}}$  yields the smallest sum of minimum source concentrations for each  $f_{\text{A}}$  at a given sample concentration (Fig. S2.3d), which implies the lowest overall ED of all possible combinations of  $\delta^2\text{H}_{\text{A,t}}$  and  $\delta^2\text{H}_{\text{B,t}}$ . As the assumption of  $\delta^2\text{H}_{\text{A,t}} = \delta^2\text{H}_{\text{B,t}}$  is identical to the application of scenario 1, the latter gives a conservative estimate of the overall ED.

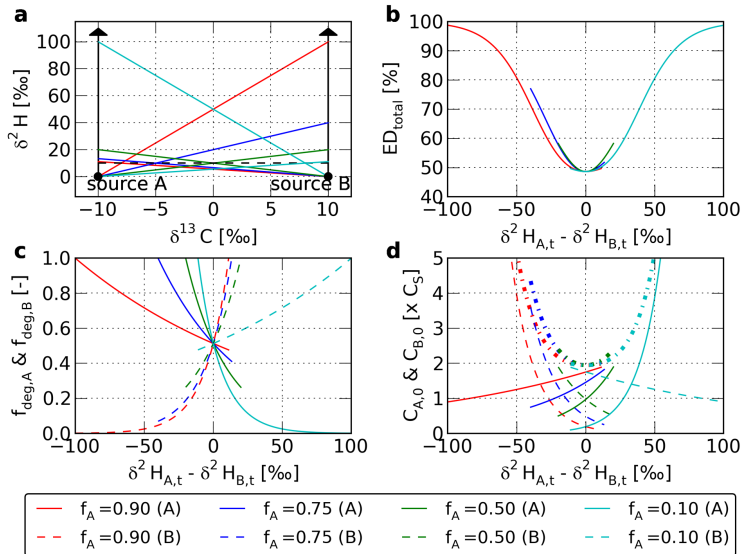


Figure S2.3: Analysis of Eq. 2.33. For various values of  $f_{\text{A}}$  (0.90, 0.75, 0.50, 0.10) are shown: mixing lines for  $\delta^2\text{H}_{\text{A,t}} = \delta^2\text{H}_{\text{B,t}}$  (black dashed line) and for the theoretically possible minima and maxima of  $\delta^2\text{H}_{\text{A,t}}$  and  $\delta^2\text{H}_{\text{B,t}}$  (solid lines) (a); total ED as a function of the difference between  $\delta^2\text{H}_{\text{A,t}}$  and  $\delta^2\text{H}_{\text{B,t}}$  (b); NDFs of sources A and B ( $f_{\text{deg,A}}$  and  $f_{\text{deg,B}}$ ) as a function of the difference between  $\delta^2\text{H}_{\text{A,t}}$  and  $\delta^2\text{H}_{\text{B,t}}$  (c); and minimum concentrations of sources A and B (solid and dashed lines; sum of those indicated as dash-dotted lines) following from Eq. 2.34 as a function of the difference between  $\delta^2\text{H}_{\text{A,t}}$  and  $\delta^2\text{H}_{\text{B,t}}$  for a given sample concentration of  $C_{\text{S}}$  (d).

## S2.7 Uniquely defined source contributions in the two-dimensional isotope plot

The slope of the trajectory of  $\delta^2\text{H}$ - versus  $\delta^{13}\text{C}$ -values in the two-dimensional isotope plot (Eq. 2.12/S2.7) is approximately given by the ratio between the corresponding enrichment factors, i.e., the value of  $\Phi$  (van Breukelen, 2007a; Fischer et al., 2008). This is illustrated in Fig. S2.4, where the solid lines are trajectories given by Eq. 2.12/S2.7 with  $(\delta^{13}\text{C}_M, \delta^2\text{H}_M) = (0, 0)$  and different  $\Phi$ -values (resulting from constant  $\varepsilon_{\text{C-}}$ , but different  $\varepsilon_{\text{H-}}$ -values), and the dashed black lines are straight lines through  $(0, 0)$  with a slope of the same  $\Phi$ -values. It becomes apparent that the deviation of the straight lines from the actual trajectory described by Eq. 2.12/S2.7 increases for an increasing ED (Jin et al., 2013) and for larger values of  $\Phi$  in Eq. 2.12/S2.7, i.e., for larger differences between the isotopic enrichment factors of the two elements. However, the deviation of the approximated from the correct values is minor even for a substantial ED: in the shown example, the approximated  $\delta^2\text{H}$ -value that corresponds to an ED of 99 % (dotted black line in Fig. S2.4) underestimates the true  $\delta^2\text{H}$ -value of 96.5 ‰ by only 3.9 ‰ even for  $\Phi = 10$ . Therefore, especially if the isotopic enrichment factors of both considered elements are of similar magnitude, Eq. 2.12/S2.7 gives in good approximation a straight line in the relevant range of isotope ratios.

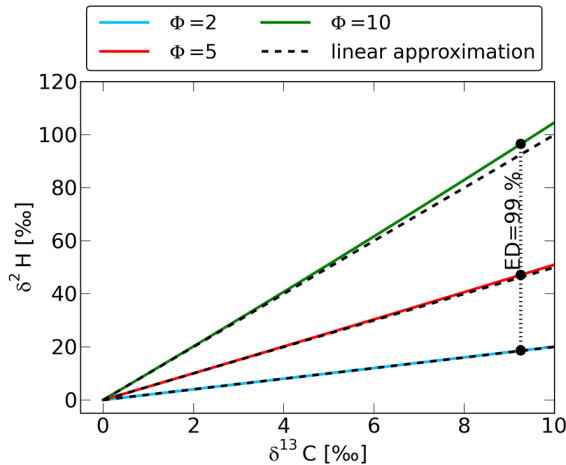


Figure S2.4: Trajectories in the  $(\delta^{13}\text{C}, \delta^2\text{H})$ -space (Eq. 2.12/S2.7; solid lines) and their approximation by straight lines with a slope of  $\Phi$  (dashed black lines). The black dots correspond to an ED of 99 %.

As Eq. 2.12/S2.7 can be in good approximation described by straight lines, we can use the Thales' theorem (Agricola et al., 2008), which states that if three parallel lines intercept a transversal, the ratio of the length of the resulting segments is equal for every transversal. This is illustrated in Fig. S2.5, where the parallel lines  $a$ ,  $b$ , and  $c$  represent the degradation trajectories for source A, source B, and a mixture of sources A and B, respectively, and the lines  $m_1$  and  $m_2$  indicate two different mixing lines between partially degraded contaminant pools that originate

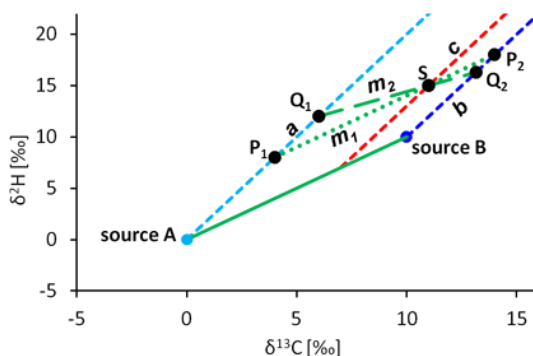


Figure S2.5: Application of the Thales' theorem to three parallel trajectories ( $a$ ,  $b$ , and  $c$ ) and two mixing lines ( $m_1$  and  $m_2$ ) in the two-dimensional isotope plot. The ratio of the segments  $|SP_2|$  and  $|P_1P_2|$  on mixing line  $m_1$  is equal to the ratio of the segments  $|SQ_2|$  and  $|Q_1Q_2|$  on mixing line  $m_2$ .

exclusively from one of the sources. It follows from the Thales' theorem that

$$\frac{|SP_2|}{|P_1P_2|} = \frac{|SQ_2|}{|Q_1Q_2|} = f_A \quad (\text{S2.26})$$

This means that the mixing lines  $m_1$  and  $m_2$  give the same proportional contribution of source A ( $f_A$ ) to the sample S, although they correspond to different NDFs of the two mixing contaminant pools (defined by  $P_1$  and  $P_2$ , and by  $Q_1$  and  $Q_2$ , respectively). Moreover, Eq. S2.26 holds true for any parallel of  $m_1$  (or  $m_2$ ). It follows that every point on the trajectory  $c$  yields the same contribution of source A. Hence, based on the approximation of the trajectories by straight lines, it is possible to uniquely determine the value of  $f_A$  for every point in the two-dimensional isotope plot. This allows for a division of the  $(\delta^{13}\text{C}, \delta^2\text{H})$ -space into ranges of  $f_A$  (Fig. 2.5).

## S2.8 Use of the SISS model for two emission sources and two reaction pathways

Extension of the SISS model with a second transformation pathway is attractive as degradation of pollutants might occur via two pathways such as aerobic and anaerobic degradation. We assume that dual-element CSIA data are available (e.g., carbon and hydrogen CSIA), and that the enrichment factors of the two potentially occurring reaction pathways are known for both elements. If we consider a scenario of mixing followed by degradation (scenario 1), this leads to the following set of equations:

$$\delta^{13}\text{C}_M = f_A \delta^{13}\text{C}_A + (1 - f_A) \delta^{13}\text{C}_B \quad (\text{S2.27})$$

$$\delta^2\text{H}_M = f_A \delta^2\text{H}_A + (1 - f_A) \delta^2\text{H}_B \quad (\text{S2.28})$$

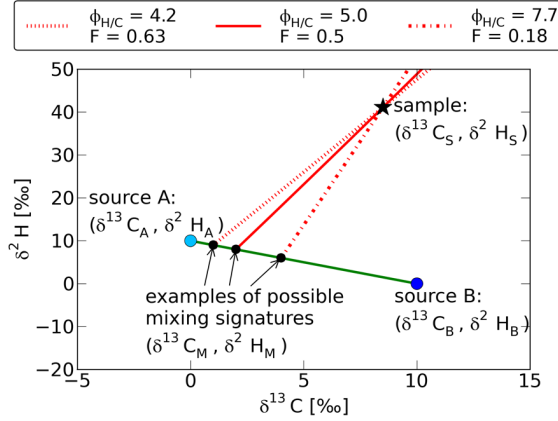


Figure S2.6: Three examples of possible combinations between  $\Phi_{H/C}$ -values and isotopic signatures at the mixing point (black dots) that give the same sample signature (black star).  $F$  indicates the contribution of reaction pathway 1 to overall degradation via two competing reaction pathways (Eq. S2.31 with  $\varepsilon_{C1} = -4.0$  ‰,  $\varepsilon_{H1} = -10.0$  ‰,  $\varepsilon_{C2} = -2.0$  ‰, and  $\varepsilon_{H2} = -20.0$  ‰).

$$\delta^2H_S = \left( \frac{10^{-3} \cdot \delta^{13}C_S + 1}{10^{-3} \cdot \delta^{13}C_M + 1} \right)^{\Phi_{H/C}} \cdot (\delta^2H_M + 1000) - 1000 \quad (S2.29)$$

where  $\Phi_{H/C}$  is the ratio between the apparent enrichment factors  $\varepsilon_{H,app}$  and  $\varepsilon_{C,app}$ , which describes isotope fractionation as a result of degradation via two competing reaction pathways (van Breukelen, 2007a).  $\Phi_{H/C}$  is equal to the ratio of the isotopic shifts in carbon and hydrogen isotopes between mixing (signature of  $(\delta^{13}C_M, \delta^2H_M)$ ) and sampling (signature of  $(\delta^{13}C_S, \delta^2H_S)$ ):

$$\Phi_{H/C} = \frac{\ln \left( \frac{10^{-3} \cdot \delta^2H_S + 1}{10^{-3} \cdot \delta^2H_M + 1} \right)}{\ln \left( \frac{10^{-3} \cdot \delta^{13}C_S + 1}{10^{-3} \cdot \delta^{13}C_M + 1} \right)} \quad (S2.30)$$

The distribution  $F_{H/C}$  between the two competing reaction pathways is defined as (van Breukelen, 2007a):

$$F_{H/C} = \frac{\Phi_{H/C} \cdot \varepsilon_{C2} - \varepsilon_{H2}}{(\varepsilon_{H1} - \varepsilon_{H2}) - \Phi_{H/C} \cdot (\varepsilon_{C1} - \varepsilon_{C2})} \quad (S2.31)$$

where the subscripts C and H indicate the enrichment factors for carbon and hydrogen isotopes, respectively, and the index number denotes the respective pathway.  $F_{H/C}$  is the relative contribution of reaction pathway 1 to overall degradation and ranges between 0 and 1.

$\Phi_{H/C}$  in Eq. S2.30 can take various values that satisfy Eqs. S2.27 – S2.29 and yield a value of  $F_{H/C}$  between 0 and 1. This is shown in Fig. S2.6, where the red lines represent possible trajectories given by Eq. S2.29 that yield different  $F_{H/C}$ -values and isotopic signatures at the mixing point  $(\delta^{13}C_M, \delta^2H_M)$ . There is thus no uniquely defined mixing point  $(\delta^{13}C_M, \delta^2H_M)$  as opposed to the case of one reaction pathway. Consequently, a system of two mixing sources and two competing reaction

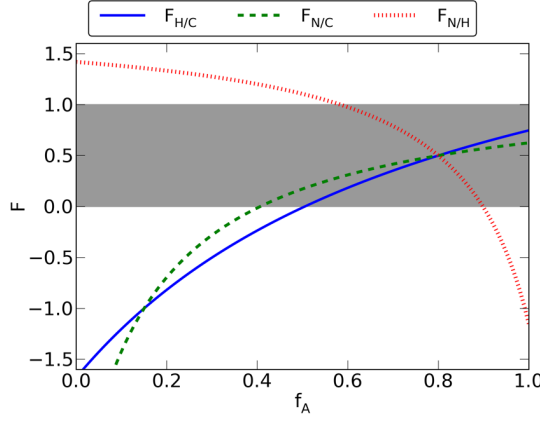


Figure S2.7: Equations S2.31, S2.34, and S2.36 as a function of  $f_A$  for the sample signature in Fig. S2.6. The intersection point between the blue (solid), green (dashed), and red (dotted) curve defines the distribution between two competing reaction pathways ( $F_{H/C} = F_{N/C} = F_{N/H}$ ) and the proportion from source A ( $f_A$ ), which gives a unique solution for the mixing signature ( $\delta^{13}C_M$ ,  $\delta^2H_M$ ,  $\delta^{15}N_M$ ). The valid range for  $F$  (between 0 and 1) is indicated in grey. Enrichment factors are  $\varepsilon_{C1} = -4.0$  ‰,  $\varepsilon_{H1} = -10.0$  ‰,  $\varepsilon_{N1} = -2.0$  ‰,  $\varepsilon_{C2} = -2.0$  ‰,  $\varepsilon_{H2} = -20.0$  ‰, and  $\varepsilon_{N2} = -5.0$  ‰.

pathways requires CSIA of more than two elements to allow for combined SA and QED.

Adding CSIA of a third element, e.g., nitrogen, leads to the following additional equations:

$$\delta^{15}N_M = f_A \delta^{15}N_A + (1 - f_A) \delta^{15}N_B \quad (\text{S2.32})$$

$$\Phi_{N/C} = \frac{\ln \left( \frac{10^{-3} \cdot \delta^{15}N_S + 1}{10^{-3} \cdot \delta^{15}N_M + 1} \right)}{\ln \left( \frac{10^{-3} \cdot \delta^{13}C_S + 1}{10^{-3} \cdot \delta^{13}C_M + 1} \right)} \quad (\text{S2.33})$$

$$F_{N/C} = \frac{\Phi_{N/C} \cdot \varepsilon_{C2} - \varepsilon_{N2}}{(\varepsilon_{N1} - \varepsilon_{N2}) - \Phi_{N/C} \cdot (\varepsilon_{C1} - \varepsilon_{C2})} \quad (\text{S2.34})$$

$$\Phi_{N/H} = \frac{\Phi_{N/C}}{\Phi_{H/C}} \quad (\text{S2.35})$$

$$F_{N/H} = \frac{\Phi_{N/H} \cdot \varepsilon_{H2} - \varepsilon_{N2}}{(\varepsilon_{N1} - \varepsilon_{N2}) - \Phi_{N/H} \cdot (\varepsilon_{H1} - \varepsilon_{H2})} \quad (\text{S2.36})$$

Eqs. S2.31, S2.34, and S2.36 have to give the same distribution between the two competing pathways for the sample mixture (i.e.,  $F_{H/C} = F_{N/C} = F_{N/H}$ ), which is only satisfied by a single value of  $f_A$ . This is illustrated in Fig. S2.7, which shows Eqs. S2.31, S2.34, and S2.36 as a function of  $f_A$  for the sample signature in Fig. S2.6.

Whereas  $F_{H/C}$  takes valid values (i.e., between 0 and 1; shaded area) for  $f_A > 0.5$ , the only point with  $F_{H/C} = F_{N/C} = F_{N/H}$  is the intersection between the blue, green, and red curve at  $f_A = 0.8$  and  $F_{H/C} = F_{N/C} = F_{N/H} = 0.5$ . The extension of the model for two reaction pathways by Eqs. S2.34 and S2.36 thus yields a unique solution for the proportion from source A ( $f_A$ ) as opposed to dual-element CSIA. Plugging  $f_A$  into Eq. S2.27, S2.28, and S2.32 determines the mixing point ( $\delta^{13}C_M$ ,  $\delta^2H_M$ ,  $\delta^{15}N_M$ ), which then defines the ED of the sample. Analogous to the case of one reaction pathway only, this ED also gives a conservative estimate of the overall ED in a scenario of mixing of two contaminant pools after degradation via two reaction pathways (scenario 2).

## S2.9 Use of the SISS model for three emission sources and one reaction pathway

If a sample signature results from degradation of a mixture between three sources, the first step in SA is to determine the signature at the mixing point prior to degradation. This can be done using the following geometric approach. Mixtures between three end members lie within a triangle on a plane that is defined by the three source signatures (Fig. S2.8; Phillips and Koch 2002). If we consider, for example, carbon, hydrogen, and nitrogen isotopes, the equation of this plane can be expressed in parametric form as

$$\mathbf{E}: \quad \vec{x} = \vec{p} + \alpha\vec{v}_1 + \beta\vec{v}_2 \quad (\text{S2.37})$$

$$\text{with } \vec{p} = \begin{pmatrix} \delta^{13}C_A \\ \delta^2H_A \\ \delta^{15}N_A \end{pmatrix}, \vec{v}_1 = \begin{pmatrix} \delta^{13}C_B - \delta^{13}C_A \\ \delta^2H_B - \delta^2H_A \\ \delta^{15}N_B - \delta^{15}N_A \end{pmatrix} \text{ and } \vec{v}_2 = \begin{pmatrix} \delta^{13}C_C - \delta^{13}C_A \\ \delta^2H_C - \delta^2H_A \\ \delta^{15}N_C - \delta^{15}N_A \end{pmatrix}.$$

The vector equation of the degradation trajectory, which is in good approximation a straight line that passes through the mixing ( $\delta^{13}C_M$ ,  $\delta^2H_M$ ,  $\delta^{15}N_M$ ) and sampling point ( $\delta^{13}C_S$ ,  $\delta^2H_S$ ,  $\delta^{15}N_S$ ), is given by

$$\mathbf{g}: \quad \vec{x} = \vec{r} + \lambda \cdot \vec{s} \quad (\text{S2.38})$$

$$\text{with } \vec{r} = \begin{pmatrix} \delta^{13}C_S \\ \delta^2H_S \\ \delta^{15}N_S \end{pmatrix} \text{ and } \vec{s} = \begin{pmatrix} \delta^{13}C_S - \delta^{13}C_M \\ \delta^2H_S - \delta^2H_M \\ \delta^{15}N_S - \delta^{15}N_M \end{pmatrix}.$$

The point of intersection between  $\mathbf{E}$  and  $\mathbf{g}$  defines the signature of the mixing point (Fig. S2.8). However, the point of intersection cannot be readily determined, as the vector  $\vec{s}$  in Eq. S2.38, which describes the slope of the degradation trajectory in three-dimensional space, contains the unknown mixing signature ( $\delta^{13}C_M$ ,  $\delta^2H_M$ ,  $\delta^{15}N_M$ ). Therefore, we approximate  $\vec{s}$  by the respective enrichment factors, as it has already been described for dual-element CSIA (see section S2.7):

$$\vec{s}^* = \begin{pmatrix} \varepsilon_C \\ \varepsilon_H \\ \varepsilon_N \end{pmatrix} \quad (\text{S2.39})$$

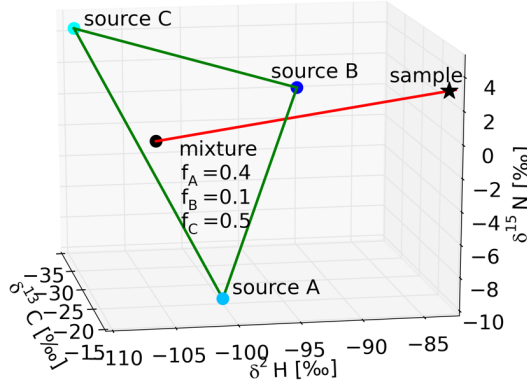


Figure S2.8: Isotopic signature of the mixing point ( $\delta^{13}\text{C}_M$ ,  $\delta^2\text{H}_M$ ,  $\delta^{15}\text{N}_M$ ) as the intersection between the mixing triangle of sources A, B, and C, and the trajectory of the degrading mixture in the three-dimensional isotope plot. Enrichment factors are  $\varepsilon_C = -5.0$  ‰,  $\varepsilon_H = -10.0$  ‰, and  $\varepsilon_N = -2.0$  ‰.

The scalar  $\lambda$  at the point of intersection is then given by:

$$\lambda = -\frac{\vec{v}_1 \times \vec{v}_2 \cdot (\vec{r} - \vec{p})}{\vec{v}_1 \times \vec{v}_2 \cdot \vec{s}^*} \quad (\text{S2.40})$$

Inserting  $\lambda$  and  $\vec{s}^*$  into Eq. S2.38 yields the signature at the mixing point ( $\delta^{13}\text{C}_M$ ,  $\delta^2\text{H}_M$ ,  $\delta^{15}\text{N}_M$ ).

Once the mixing signature ( $\delta^{13}\text{C}_M$ ,  $\delta^2\text{H}_M$ ,  $\delta^{15}\text{N}_M$ ) is determined, the ED can be calculated by applying Eq. 2.19. Solving the following equations for  $f_A$ ,  $f_B$ , and  $f_C$  yields the respective source contributions:

$$\delta^{13}\text{C}_M = f_A \delta^{13}\text{C}_A + f_B \delta^{13}\text{C}_B + f_C \delta^{13}\text{C}_C \quad (\text{S2.41})$$

$$\delta^2\text{H}_M = f_A \delta^2\text{H}_A + f_B \delta^2\text{H}_B + f_C \delta^2\text{H}_C \quad (\text{S2.42})$$

$$1 = f_A + f_B + f_C \quad (\text{S2.43})$$

Figure S2.9 shows a projection of Fig. S2.8 into the ( $\delta^{13}\text{C}$ ,  $\delta^2\text{H}$ )-space, where the mixing point is no longer uniquely defined as it could lie anywhere on the intersection line between the mixing triangle and the trajectory of the degrading mixture (dashed red line in Fig. S2.9). This implies that the SISS model requires CSIA of at least three elements to allow for SA and QED in the case of three end members and one reaction pathway (as illustrated in Fig. S2.8).

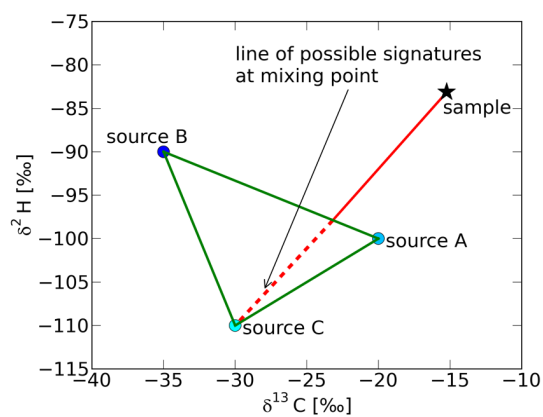


Figure S2.9: Projection of Fig. S2.8 into the  $(\delta^{13}\text{C}, \delta^2\text{H})$ -space. The intersection between the mixing triangle of sources A, B, and C and the trajectory of the degrading mixture gives an indefinite number of possible mixing signatures (dashed red line).

# 3

## A stable isotope model for combined source apportionment and degradation quantification of organic pollutants: model validation and application\*

**Abstract.** Compound-specific stable isotope analysis (CSIA) has proven a useful tool for the quantification of the extent of degradation (QED), and for source identification and source apportionment (SA) in contaminated environmental systems. However, the simultaneous occurrence of degradation processes and mixing of emission sources complicates the use of CSIA in combined SA and QED. In chapter 2, we developed a mathematical model that allows for combined SA and QED of organic pollutants (and inorganic compounds such as nitrate) in a scenario of two emission sources and degradation via one reaction pathway. This chapter presents a validation of the model against virtual data from a two-dimensional reactive transport model. The model calculations for SA and QED were in good agreement with the simulation results, which suggests the correctness of the model assumptions. However, the application of the model to field data of benzene contamination was challenged by large uncertainties in CSIA data and the unknown interplay between competing degradation pathways. Nonetheless, the use of the model allowed for the identification of a prevailing contribution of one emission source and revealed a low overall extent of degradation at the field site. This indicates that the model can, for example, facilitate the characterization of air pollution or aquifer contamination with organic pollutants.

---

\*This chapter is an edited version of: Lutz, S. R. and van Breukelen, B. M. Combined Source Apportionment and Degradation Quantification of Organic Pollutants with CSIA: 2. Model Validation and Application. *Environmental Science & Technology*, 48(11):6229-6236, 2014.

### 3.1 Introduction

Compound-specific stable isotope analysis (CSIA) has proven useful in the assessment of in situ degradation of organic pollutants (Schmidt et al., 2004; Elsner et al., 2012; Thullner et al., 2012). Moreover, it has been applied for source identification and apportionment in environmental systems with more than one potential emission source (Mancini et al., 2008; Deutsch et al., 2006; Sturchio et al., 2012; Okuda et al., 2002). However, degradation and mixing processes can lead to changes in isotopic compositions, such that their simultaneous occurrence might complicate the use of CSIA in the assessment of source contributions and the extent of degradation (ED) (Kellman and Hillaire-Marcel, 2003; Moore and Semmens, 2008; Xue et al., 2009; van Keer et al., 2012; Seiler, 2005). In chapter 2, we developed a mathematical model (stable isotope sources and sinks model; SISS model) for combined source apportionment (SA) and quantification of the extent of degradation (QED) of organic pollutants (and inorganic compounds such as nitrate) in a scenario of two emission sources and degradation via one reaction pathway. It was demonstrated that, given isotope data of at least two elements contained in the pollutant, the SISS model provides a tool for SA even in the presence of degradation-induced isotope fractionation effects. It was also shown that the SISS model allows for QED of a sample, and gives a conservative estimate of the ED if mixing follows independent degradation of the two mixing contaminant pools.

The SISS model was developed for two scenarios where mixing and degradation occur in a sequential order, i.e., where mixing follows degradation and vice versa. Moreover, it was assumed that mixing occurs at a localized mixing point. In reality, however, mixing between different contaminant pools might be accompanied by simultaneously occurring degradation processes, and it might occur gradually or only partially. In addition, field isotope data are generally associated with analytical uncertainties, which might affect the accuracy of the SISS model calculations. Field sites can also exhibit a large degree of physical and biogeochemical heterogeneity, which might influence the mixing between emission sources and alter the rate of contaminant degradation (Anneser et al., 2008; Cozzarelli et al., 1999; Rolle et al., 2010). Moreover, physical heterogeneity can lead to attenuation of the actual extent of isotope fractionation, which results in an underestimation of the ED based on field CSIA data (van Breukelen and Prommer, 2008; Abe and Hunkeler, 2006). Hence, this work seeks to analyze how these factors affect the applicability and correctness of the SISS model.

The objective of this study was to assess to what extent the theoretically derived SISS model holds for environmental systems. To this end, we first validated the SISS model against a virtual data set from reactive transport model simulations of a two-dimensional flow system with two emission sources, which enabled us to compare calculated and exact values of SA and ED. Second, we applied the SISS model to carbon and hydrogen CSIA data of a benzene-contaminated field site. On the basis of this, we discuss uncertainties and complications in the use of the SISS model for field isotope data.

## 3.2 Methods

### 3.2.1 Summary of the SISS model

The SISS model is applicable to compounds whose degradation follows the Rayleigh equation model (i.e., organic pollutants and inorganic compounds such as nitrate). This chapter makes use of scenario 1 of the SISS model, which assumes instantaneous mixing between two sources and subsequent degradation via one irreversible reaction pathway. Scenario 1 always provides conservative estimates of the overall ED of the sample irrespective of the order of mixing and degradation (see chapter 2 for a more detailed description). We briefly revisit the main concepts of the SISS model for scenario 1. The complete description of the SISS model equations can be found in chapter 2.

Scenario 1 requires dual-element isotope analysis for the determination of the isotopic signature at the time of mixing, which can then be calculated as the intersection point between the mixing line between the two sources (Eq. 3.1) and the trajectory of the degrading mixture (Eq. 3.2; see Fig. 2.2). Accordingly, the mixing signature (here given for carbon and hydrogen isotope values as  $(\delta^{13}\text{C}_M, \delta^2\text{H}_M)$ ) is the solution of the following system of two equations:

$$\delta^2\text{H}_M = m\delta^{13}\text{C}_M + b \quad (3.1)$$

$$\delta^2\text{H}_S = \left( \frac{\delta^{13}\text{C}_S + 1000}{\delta^{13}\text{C}_M + 1000} \right)^\Phi \cdot (\delta^2\text{H}_M + 1000) - 1000 \quad (3.2)$$

where  $m$  and  $b$  are parameters that define the mixing line between sources A and B (which can be obtained from the isotope ratios of sources A and B; see Eqs. 2.15 and 2.16 in chapter 2), subscripts M and S denote the isotope values of the mixture and the sample, respectively, and  $\Phi$  is the ratio of the enrichment factors for carbon and hydrogen isotopes (i.e.,  $\Phi = \varepsilon_{\text{H}}/\varepsilon_{\text{C}}$ ). The relative contribution of source A to the mixture ( $f_A$ ) is then given by

$$f_A = \frac{\delta^{13}\text{C}_M - \delta^{13}\text{C}_B}{\delta^{13}\text{C}_A - \delta^{13}\text{C}_B} \quad (3.3)$$

where  $(\delta^{13}\text{C}_A, \delta^2\text{H}_A)$  and  $(\delta^{13}\text{C}_B, \delta^2\text{H}_B)$  are the isotopic signatures of sources A and B, respectively.

The ED of the sample in scenario 1 gives a conservative estimate of the overall ED in scenario 2 (see chapter 2) or any other scenario, and is determined as follows:

$$ED (\%) = 100 \cdot \left( 1 - \left( \frac{10^{-3} \cdot \delta^{13}\text{C}_S + 1}{10^{-3} \cdot \delta^{13}\text{C}_M + 1} \right)^{1000/\varepsilon_{\text{C}}} \right) \quad (3.4)$$

Equation 3.4 is based on the Rayleigh equation, which is accurate for the calculation of the ED in closed systems, but generally leads to an underestimation of the ED when applied to field CSIA data (van Breukelen and Prommer, 2008; Abe and Hunkeler, 2006).

### 3.2.2 Reactive transport model setup

The model was validated against virtual data obtained through simulations with the reactive transport model (RTM) PHAST (Parkhurst et al., 2010). The model domain represents a plan view on an aquifer flow system with two partially overlapping groundwater pollution plumes (Fig. 3.1). It has a length of 500 m in the longitudinal (downgradient) direction ( $x$ -axis) with a spatial discretization of 5 m, and a width of 200 m in the horizontal direction ( $y$ -axis) with a spatial discretization of 2 m. Variations with depth were not simulated. A groundwater flow velocity of 50 m yr<sup>-1</sup> was chosen. The dispersivities were set to 5 m in the horizontal, and 0.5 m in the vertical direction. The contaminant was emitted by an upgradient source A and a downgradient source B (Fig. 3.1), which were assigned a zero-order dissolution rate of  $5.28 \cdot 10^{-11}$  mg/(s·L). This resulted, due to downgradient contaminant transport from source A, in a higher total concentration at source B than source A. The rest of the model domain represented initially pristine water. The total simulated time was set to 10 yr (with a time step of 0.1 yr) such that the system reached steady state.

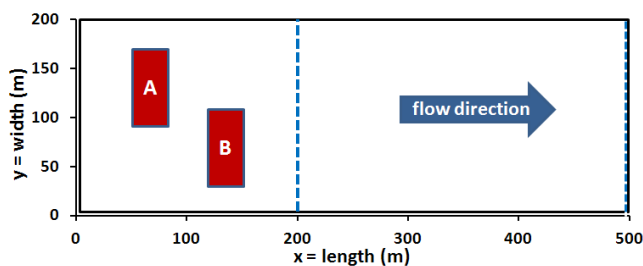


Figure 3.1: Plan view of the model domain of the two-dimensional PHAST simulations. The sources were located at  $x = [50 \text{ m}, 80 \text{ m}]$  and  $y = [90 \text{ m}, 150 \text{ m}]$  (source A), and  $x = [120 \text{ m}, 150 \text{ m}]$  and  $y = [30 \text{ m}, 110 \text{ m}]$  (source B). Monitoring fences at  $x = 200 \text{ m}$  and  $x = 500 \text{ m}$  are indicated by blue dashed lines. Key model parameters: groundwater flow velocity = 50 m yr<sup>-1</sup>; simulated time = 10 yr; source A:  $\delta^{13}\text{C} = -30 \text{ ‰}$ ,  $\delta^2\text{H} = -70 \text{ ‰}$ ; source B:  $\delta^{13}\text{C} = -25 \text{ ‰}$ ,  $\delta^2\text{H} = -100 \text{ ‰}$ ; first-order degradation rate constant  $k_{\text{eff}} = 0.3 \text{ yr}^{-1}$ ;  $\varepsilon_{\text{C}} = -2 \text{ ‰}$ ; and  $\varepsilon_{\text{H}} = -4 \text{ ‰}$ .

The model simulated the contaminant and its heavy carbon and heavy hydrogen isotopes as solute species. The concentrations of the corresponding light isotopes followed from the difference between the contaminant and its heavy isotope concentrations. The target concentrations for the heavy isotopes at the downgradient boundaries of the sources were chosen such that the initial isotopic signatures were  $\delta^{13}\text{C}_{\text{A},0} = -30 \text{ ‰}$  and  $\delta^2\text{H}_{\text{A},0} = -70 \text{ ‰}$  at source A, and  $\delta^{13}\text{C}_{\text{B},0} = -25 \text{ ‰}$  and  $\delta^2\text{H}_{\text{B},0} = -100 \text{ ‰}$  at source B. The simulation of an additional conservative and degrading tracer, respectively, for each source allowed for accurate information on source contributions and ED of the virtual data set. Sorption was not simulated, but this process will not affect model outcomes for steady state plumes (van Breukelen and Prommer, 2008). Isotopologue-specific diffusion coefficients were not considered in the simulation of dispersion, as diffusion-induced isotope fractionation might only be relevant in the vertical direction (and not in the horizontal direction as applicable here) and under relatively homogeneous conditions (van Breukelen and

Rolle, 2012).

The total contaminant pool and the tracers were assumed to degrade via a first-order reaction. According to Hunkeler et al. (2009), degradation of the heavy carbon and hydrogen isotopes was simulated as:

$$\frac{dC^H}{dt} = -\frac{k_{\text{eff}}}{\frac{C^H}{C^{\text{tot}}} + \frac{1}{\alpha}(1 - \frac{C^H}{C^{\text{tot}})}} C^H \quad (3.5)$$

### 3.3 Results and Discussion

#### 3.3.1 Model validation: virtual data set

Figure 3.2 shows the virtual data set that was produced in the PHAST simulations. Simulated concentrations were highest close to the sources, and decreased with increasing distance from the sources as a result of degradation and dilution during eastwards transport (Fig. 3.2a). Degradation-induced isotope fractionation resulted in enriched  $\delta^{13}\text{C}$ - and  $\delta^2\text{H}$ -values toward the east (Fig. 3.2b and c). Accordingly, the overall ED increased eastward and reached nearly 100% for large x-values (Fig. 3.2d). Due to the differing isotopic signatures at the sources, carbon and hydrogen isotope ratios show a strong north-south gradient (Fig. 3.2b and c). A north-south divide can also be seen in the relative proportion from source A ( $f_A$ ): it was approximately 1 in the northern part, and close to 0 in the southern part of the model domain (Fig. 3.2e).

At  $x = 120$  m (i.e., at the western boundary of source B), the average extent of degradation of source A was 35.6% (range of between 18.7% and 76.8%). Therefore, the simulation setup differed from scenario 1, which assumes instantaneous mixing before degradation. This is a potential source of inaccuracy of the SISS model results. Moreover, as is the case for field CSIA data from an aquifer, the simulated isotope ratios were affected by hydrodynamic dispersion, which generally leads to attenuation of apparent isotope fractionation and, consequently, to an underestimation of the actual ED (van Breukelen and Prommer, 2008; Abe and Hunkeler, 2006). Hence, we expected that the SISS model also underestimates the ED for the virtual data set.

#### 3.3.2 Model validation: extent of degradation

Figure 3.3 compares the SISS-model calculations with the RTM simulations for two monitoring fences at  $x = 200$  m (panel a) and  $x = 500$  m (panel b). With a maximum absolute deviation of below  $-2\%$  at  $x = 200$  m and  $-1\%$  at  $x = 500$  m, the calculated ED ( $ED_{\text{SISS}}$ ) is in good agreement with the actual ED (known from the simulations;  $ED_{\text{RTM}}$ ; top right corner of Fig. 3.3a and b). The deviation of  $ED_{\text{SISS}}$  from  $ED_{\text{RTM}}$  resulted from the assumption of instantaneous mixing before degradation (scenario 1), which always yields a conservative estimate of the ED (see chapter 2), and the application of the Rayleigh equation approach to isotope data that are affected by dispersion (van Breukelen and Prommer, 2008;

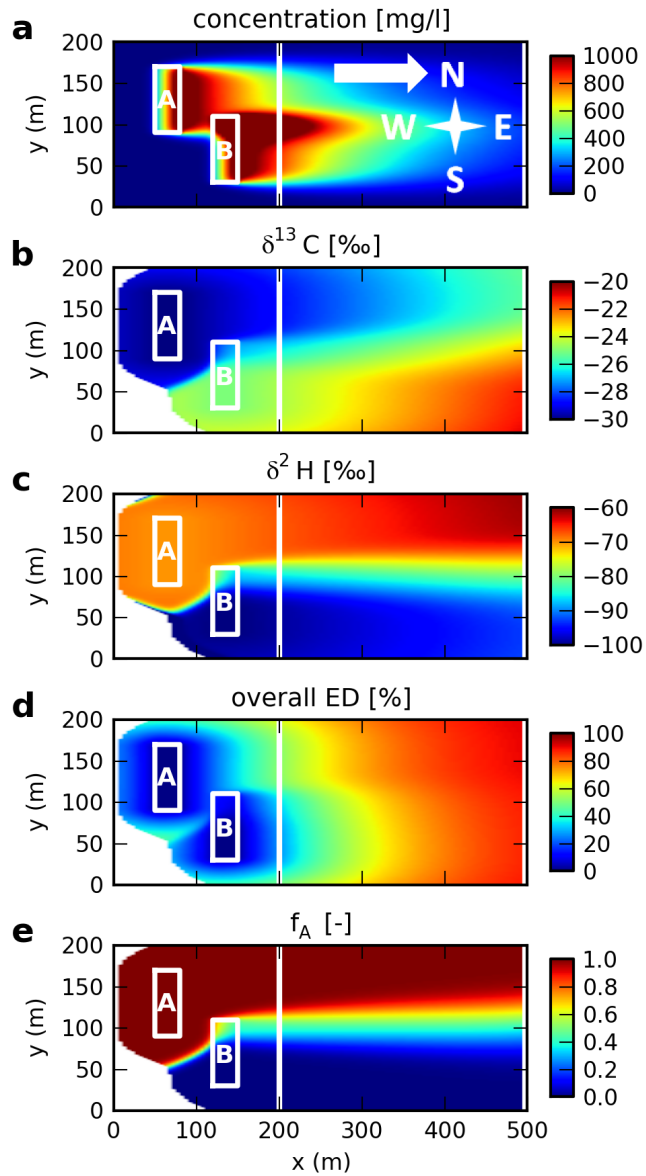


Figure 3.2: Virtual data (RTM simulation results) from the simulation of two partially overlapping groundwater pollution plumes: total contaminant concentration (a),  $\delta^{13}\text{C}$ -values (b),  $\delta^2\text{H}$ -values (c), overall ED (d), and relative proportion of source A,  $f_A$  (e). Monitoring fences at  $x = 200$  m and  $x = 500$  m are shown as vertical white lines. The white arrow in (a) indicates the groundwater flow direction. Cells with a concentration of below  $1 \mu\text{g L}^{-1}$  were blanked.

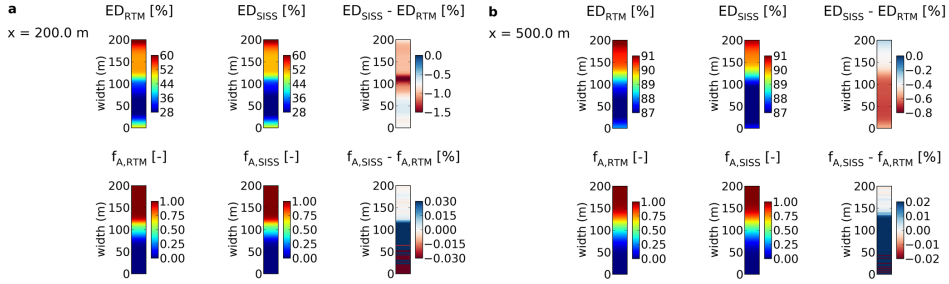


Figure 3.3: Virtual data (RTM simulation results) and SISS model calculations for the overall ED (upper panels) and SA (lower panels) at two monitoring fences:  $x = 200$  m (a) and  $x = 500$  m (b).

Abe and Hunkeler, 2006). At  $x = 200$  m, the absolute and relative error in  $ED_{SISS}$  decreased toward the fringes of the mixed contaminant plume (Fig. 3.3a), where the contribution of one of the sources (source A at the northern fringe, and source B at the southern fringe, respectively) was close to one. The SISS model accurately assessed the ED of the predominant source, and given the negligible contribution of the other source, this resulted in a more precise  $ED_{SISS}$  than at the middle part of the monitoring fence. At  $x = 500$  m, the absolute error in  $ED_{SISS}$  was largest between  $y = 20$  and 110 m (Fig. 3.3b), as this was the area of the largest non-degraded fraction due to the downgradient position of source B. Moreover, the application of scenario 1 in the northern part (between  $y = 86$  and 176 m) yielded an overall ED that was lower than the actual ED of source A and higher than the actual ED of source B, which resulted in a smaller deviation of  $ED_{SISS}$  from  $ED_{RTM}$ . In general, the relative and absolute error in  $ED_{SISS}$  decreased eastwards from the sources (i.e., at  $x = 500$  m compared to  $x = 200$  m), as the relative contribution of degradation before mixing to overall degradation decreased with further distance from the source areas. This diminished, in turn, the effect of the error introduced by assuming no degradation before mixing (scenario 1; see explanation in section S3.2 of the supplementary information).

### 3.3.3 Model validation: source apportionment

With an absolute error of below  $\pm 0.05\%$  from the actual values, the SISS model yielded accurate results for the contribution of source A ( $f_{A,SISS} - f_{A,RTM}$ ; bottom right corner of Fig. 3.3a and b). Apart from the southern part of the monitoring fences, the SISS model slightly overestimated  $f_A$ . This overestimation was largest in the middle part, as this area shows a relatively high contribution of both sources, and thus gave the largest error in absolute values (bottom right corner of Fig. 3.3a and b). In contrast,  $f_{A,RTM}$  was underestimated in the southern part due to the negligible contribution of source A.

In general, the accuracy of the SISS model in SA and QED increased for larger  $x$ -values (Fig. 3.3), as the difference between the non-degraded fractions of the sources decreased eastwards, which is more in line with the model assumption of an equal ED for both sources (scenario 1). Additional RTM simulations with different

contaminant input rates at the sources (not shown) demonstrated that SA and QED with the SISS model is also accurate for different source concentrations, as the SISS-model calculations are independent of concentration data. However, simulations with a greater distance between the sources (Fig. S3.1 in the supplementary information) yielded slightly larger errors in  $f_{A,SISS}$  and  $ED_{SISS}$ , as a greater distance between the sources implies more degradation for source A before mixing, and thus a larger error introduced by assuming instantaneous mixing. In summary, the validation against virtual data indicated the accuracy of the SISS model despite the simplifying assumptions of localized and instantaneous mixing prior to degradation (scenario 1), and thus supports its use for SA and QED in systems of two emission sources with different isotopic signatures and one prevailing degradation pathway.

### 3.3.4 Model application: description of the case study

The number of field studies with detailed dual-element CSIA data that investigated mixing and degradation in systems with two end members was generally limited. The study by van Keer et al. (2012) represented, however, a suitable example application, as it investigated two distinct BTEX source areas, and provided a detailed field site description, information on prevailing degradation mechanisms and respective enrichment factors, comprehensive dual-element isotope data ( $\delta^{13}\text{C}$ - and  $\delta^2\text{H}$ -values) for benzene at the source areas and downgradient wells, and information on geochemical conditions (see Tables S3.1 and S3.2 in the supplementary information).

Figure 3.4 shows the two sources of BTEX contamination at the field site, with source area A being positioned downgradient from source area B, and the position of the well filters (i.e., different screening depths at the monitoring wells, indicated by a capital "F"). van Keer et al. (2012) associated source area B with considerably higher benzene concentrations ( $11.6 \text{ mg L}^{-1}$  at W2F1 versus  $5.1 \text{ mg L}^{-1}$  at W7; see also Table S3.2 in the supplementary information) and a larger area than source area A. They were able to identify the two source areas based on well-filter depths, and analysis of concentrations and CSIA data, and suggested that degradation of benzene at the field site occurred under sulfate-reducing conditions (mainly at the plume fringe) and methanogenic conditions. Moreover, considering concentrations and CSIA data, the location in the aquifer, and the presence or absence of chlorinated aliphatic hydrocarbons (only associated with source B), they could attribute the contamination at most of the downgradient well filters to one of the two source areas. However, they could not conclusively identify the main contamination source for well filters in the mixing zone between the contaminant plumes from sources A and B (Fig. 3.4), as both mixing and degradation processes likely affected the isotopic signatures. Hence, these well filters are especially qualified for the application of the SISS model.

### 3.3.5 Model application: preliminary qualitative analysis

Prior to the application of the SISS-model, we first analyzed the carbon and hydrogen isotope ratios of benzene at the well filters in a qualitative manner. Following van

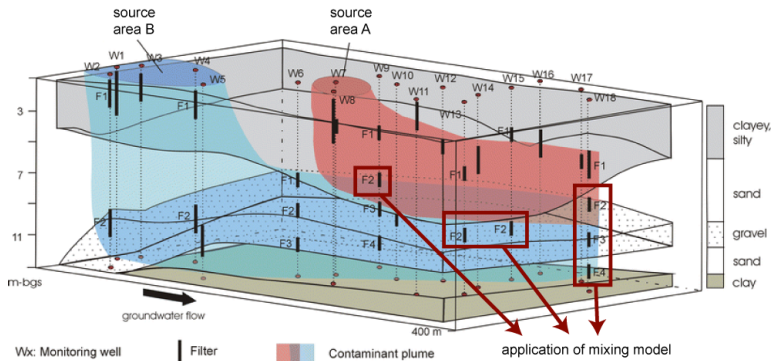


Figure 3.4: BTEX-contaminated field site with two source areas. Carbon and hydrogen isotope data for benzene were available at 27 well filters with an average screen length of 1.5 m. The SISS model was applied to isotope data from the well filters in the mixing zone indicated by red rectangles (modified from van Keer et al., 2012).

Keer et al. (2012), we considered well filters W7 and W8 representative of source area A, and W2F1 and W3 of source area B. Given the isotopic signatures of the potential source well-filters and assuming either methanogenesis or sulfate-reduction (which are associated with different isotope enrichment factors; Mancini et al., 2003), it is possible to delineate the theoretical range of isotope ratios of benzene at downgradient wells (shaded area in Fig. 3.5). To obtain the boundaries of this range,  $\Phi$  in Eq. 3.2 was set to the values representative of the methanogenic and sulfate-reducing reaction pathway, respectively.  $\Phi$ -values in between these boundaries can result from simultaneous occurrence of both reaction pathways (van Breukelen, 2007a). Remarkably, however, more than half of the well filters show isotope ratios that lie outside of this range. This applies, in particular, to all well filters that van Keer et al. (2012) attributed to the mixing zone between the two contaminant plumes (see Fig. 3.4 and green diamonds in Fig. 3.5). The main factors that presumably cause this discrepancy are the analytical uncertainties in the isotope ratios (standard deviations of duplicate or triplicate measurements of up to 1.1 ‰ for  $\delta^{13}\text{C}$  and 61 ‰ for  $\delta^2\text{H}$ ; see error bars in Fig. 3.5 and Table S3.2 in the supplementary information), and the appropriate choice of enrichment factors and representative source well-filters. The enriched  $\delta^{13}\text{C}$ -values of the well filters outside of the shaded area in Fig. 3.5 might also indicate degradation via an unknown third reaction pathway that led to pronounced carbon, but minor hydrogen isotope fractionation.

van Keer et al. (2012) considered source area A as the predominant emission source for the filters indicated by red diamonds in Fig. 3.5 (see also red contaminant plume in Fig. 3.4). However, the isotopic signature of some of these filters (especially W12, W15F1, and W17) is closer to the value of source area B (Fig. 3.5), although the shallow depth of these filters implies that they are mainly located in the contaminant plume from source A. In fact, W13F1 is the only downgradient well filter whose isotopic signature can be clearly attributed to source area A (Fig. 3.5). This indicates that source B is the predominant source area at the field site, and that mixing with the contaminant plume from source B might also affect the isotope

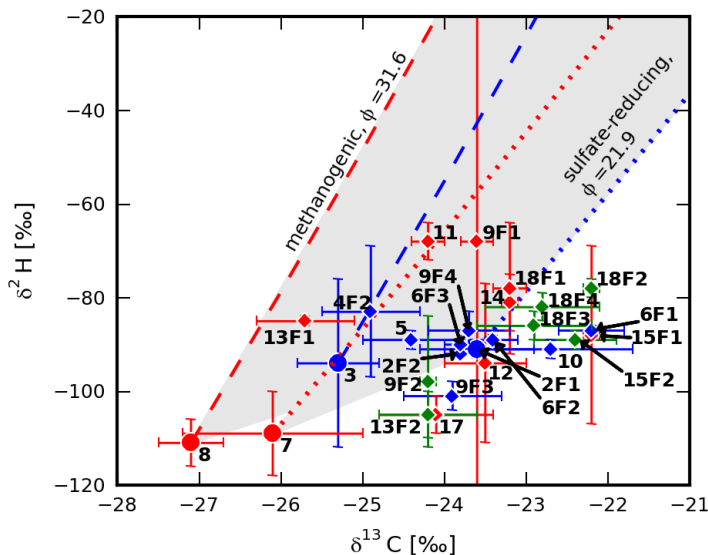


Figure 3.5:  $\delta^{13}\text{C}$ - and  $\delta^2\text{H}$ -ratios of benzene at source area A (large red dots); source area B (large blue dots); well filters attributed to source area A (red diamonds); well filters attributed to source area B (blue diamonds); and well filters in the mixing zone (green diamonds) for the BTEX-contaminated field site according to the classification of well filters by van Keer et al. (2012). Standard deviations of  $\delta^{13}\text{C}$ - and  $\delta^2\text{H}$ -values of duplicate or triplicate measurements are shown with horizontal and vertical bars, respectively. Trajectories of degrading benzene are indicated by dashed lines for methanogenic conditions ( $\varepsilon_{\text{H}} = -60 \text{ ‰}$  and  $\varepsilon_{\text{C}} = -1.9 \text{ ‰}$ ,  $\Phi = 31.6$ ) and dotted lines for sulfate-reducing conditions ( $\varepsilon_{\text{H}} = -79 \text{ ‰}$  and  $\varepsilon_{\text{C}} = -3.6 \text{ ‰}$ ,  $\Phi = 21.9$ ; Mancini et al., 2003). The shaded area constrains the theoretical range of isotope ratios for degraded mixtures between source areas A and B under the assumed conditions.

ratios of well filters in the contaminant plume from source A. Alternatively, the relative shift of isotope values of these filters toward source B could also result from an unknown third reaction pathway.

The isotope ratios of the well filters that van Keer et al. (2012) attributed to source area B (blue diamonds in Fig. 3.5) are, indeed, mostly consistent with the signature of source area B. This holds, in particular, for well filters W2F2, W4F2, W5, W6F2, W6F3, and W9F4. Correspondingly, these well filters are (apart from W9F4) located upgradient of source area A (Fig. 3.4), which precludes significant mixing effects with this source. In contrast, well filter W6F1, which is also located upgradient of the mixing zone, shows an enriched  $\delta^{13}\text{C}$ -value that lies outside of the plausible range (Fig. 3.5). This cannot be explained by large analytical uncertainties, as the standard deviation for  $\delta^{13}\text{C}$  at W6F1 is  $0.4 \text{ ‰}$ . The isotope ratios of well filter W10 also exceed the valid range, but the standard deviation in  $\delta^{13}\text{C}$  is larger ( $1.0 \text{ ‰}$ ) compared to W6F1.

### 3.3.6 Model application: SA and QED in the mixing zone

We applied the SISS model to the groundwater well filters W9F2, W13F2, W15F2, and W18F2-F4, which van Keer et al. (2012) assumed to be located in the mixing zone of the two contaminant plumes. We considered the isotopic signature of W8 representative of source area A, as the relatively enriched carbon isotope ratio at the alternative well filter W7 would conflict with the more depleted  $\delta^{13}\text{C}$ -value at W13F1 (Fig. 3.5). Likewise, we chose the isotopic signature of W2F1 for source area B because it allows us to capture well filters with relatively enriched carbon isotope ratios as opposed to W3 (Fig. 3.5).

As discussed before, some of the isotopic signatures fall outside of the limits defined by the trajectories for sulfate-reducing and methanogenic degradation, respectively. In order to increase the number of captured signatures, the data set was modified in two ways prior to the application of the SISS model. First, the source signatures were adjusted to more enriched  $\delta^{13}\text{C}$ -values within the range of their reported standard deviations (adjusted values source A\* and source B\*; green dots in Fig. 3.6). Second, the isotopic signatures of the well filters that still fell outside the valid limits (W13F2, W15F2, and W18F2) were changed to more depleted  $\delta^{13}\text{C}$ -values within the range of their respective standard deviations (adjusted values indicated by orange rectangles in Fig. 3.6). This approach was based on the assumption that the  $\delta^{13}\text{C}$ -values outside the applicable range resulted from analytical uncertainties, and not from degradation via an unknown third reaction pathway that merely led to carbon isotope fractionation. The shaded area in Fig. 3.6 indicates the valid limits for the application of the SISS model resulting from this adjustment.

Following the adjustment of some data points as described above, the mixing signature ( $\delta^{13}\text{C}_M$ ,  $\delta^2\text{H}_M$ ) was determined by numerical solution of Eqs. 3.1 and 3.2 (module `nsolve` of python package `SymPy`). Application of Eq. 3.3 then yielded the relative contribution of source A\*, and Eq. 3.4 provided a conservative estimate of the ED. We obtained two results of SA and QED for each well filter by considering methanogenic and sulfate-reducing conditions separately. Table 3.1 shows the SISS-model based SA and QED for the investigated well filters in the mixing zone. The ED is reported as the range between the conservative (scenario 1) and maximum estimate. The maximum estimate was obtained by assuming the largest possible ED of benzene from source A\* (constrained by  $\delta^{13}\text{C}$ - and  $\delta^2\text{H}$ -values of benzene), and no degradation of benzene from source B\*. In reality, it is, however, more likely that both contaminant pools degrade during downgradient transport, which results in a lower overall ED.

Despite the adjustment of isotope ratios, the signature of well filter W18F2\* was still outside of the possible range for degradation under purely methanogenic conditions (Fig. 3.6). This indicates that, provided isotope ratios of source B\* and filter W18F2 are correct, other reaction pathways than only methanogenesis (e.g., sulfate-reduction) might have played a role. Under sulfate-reducing conditions, the overall ED at W18F2\* based on the SISS model was the highest of all well filters (Table 3.1). Moreover, W18F2\* shows, similar to the other investigated filters of well 18, a secondary influence of source area A ( $f_A = 0.05$ ). Filter W15F2 is located upgradient of well W18 and should therefore show a lower ED than W18. The SISS

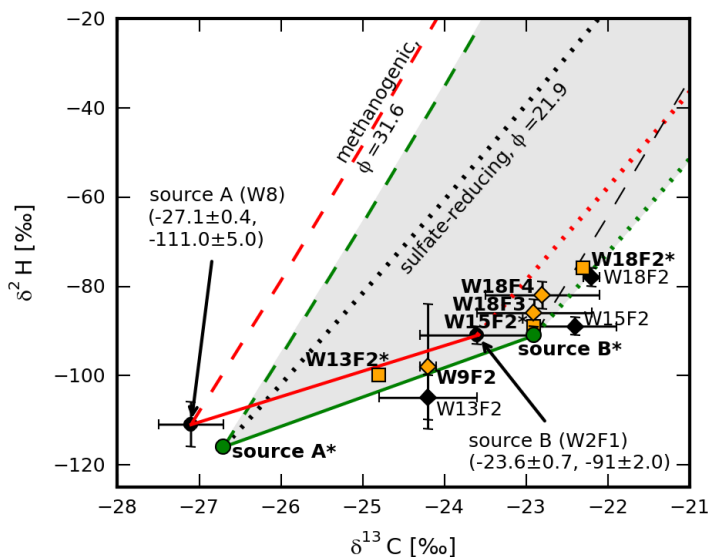


Figure 3.6:  $\delta^{13}\text{C}$ - and  $\delta^2\text{H}$ -values of benzene with standard deviations (horizontal and vertical bars, respectively) at the emission sources and groundwater well-filters that were used to test the SISS model (based on van Keer et al., 2012; see Figs. 3.4 and 3.5). The source signatures were shifted from their mean values indicated by black dots (source A and source B) to the values indicated by green dots (source A\* and source B\*). The shaded area represents the valid range for the application of the model after this adjustment. Black diamonds show well filters with mean isotope ratios outside this range; they were replaced by the isotope ratios indicated by orange rectangles. The remaining isotopic signatures were kept at the reported values (orange diamonds). Trajectories for methanogenic and sulfate-reducing conditions are shown by dashed and dotted lines, respectively (red: before the adjustment of source signatures; green and black: after the adjustment of source signatures). Enrichment factors are  $\varepsilon_{\text{H}} = -60$  ‰ and  $\varepsilon_{\text{C}} = -1.9$  ‰ for methanogenesis, and  $\varepsilon_{\text{H}} = -79$  ‰ and  $\varepsilon_{\text{C}} = -3.6$  ‰ for sulfate-reduction (Mancini et al., 2003).

model yielded, indeed, a minimum ED at W15F2\* of about 4.0% and 4.6% under sulfate-reducing and methanogenic conditions, respectively. In comparison, van Keer et al. (2012) calculated, depending on the assumed reaction pathway (sulfate-reduction or methanogenesis), an ED at W15F2 of 66 to 93% with carbon isotope data and 25 to 34% with hydrogen isotope data. As opposed to this SISS-model application, they assessed the ED for the originally measured isotope ratios and one contamination source. The analysis of isotope ratios at other groundwater wells in van Keer et al. (2012) shows a comparable inconsistency between the  $\delta^{13}\text{C}$ - and  $\delta^2\text{H}$ -based ED. In contrast, the SISS model considers mixing between sources A and B, and incorporates both carbon and hydrogen isotopic data, which thus yielded a single value for the minimum and maximum ED, respectively. This suggests that single-element CSIA (and thus the assumption of one end member) is insufficient for QED of the well filters in the mixing zone.

The relatively enriched carbon isotope ratio of W15F2\* led to a minor contribution of source A\*, which agrees with the small  $f_{\text{A}}$  at the analyzed filters of well 18 (Table 3.1). In contrast, W13F2\* shows a proportional contribution of above 0.5 of source A\* (Table 3.1). As W13F2 and W15F2 are located at a similar depth and distance

Table 3.1: Application of the SISS Model to  $\delta^{13}\text{C}$ - and  $\delta^2\text{H}$ -values of benzene<sup>a</sup> from van Keer et al. (2012).

well filter	sulfate-reducing conditions		methanogenic conditions	
	ED (%)	$f_A$	ED (%)	$f_A$
W9F2	3.2 <sup>b</sup> –3.3 <sup>c</sup>	0.37	3.6–3.8	0.36
W13F2*	7.1–7.3	0.57	8.1–8.4	0.54
W15F2*	4.0–6.9	0.04	4.6–13.5	0.02
W18F2*	20.1–82.8	0.05	n.d. <sup>d</sup>	n.d.
W18F3	9.7–15.6	0.09	11.1–28.1	0.06
W18F4	15.7–26.2	0.13	17.8–54.7	0.07

<sup>a</sup> Source values A\* ( $-26.7\text{‰}$ ,  $-116.0\text{‰}$ ) and B\* ( $-22.9\text{‰}$ ,  $-91.0\text{‰}$ ),  $m = 6.6$ ,  $b = 59.7$ .

<sup>b</sup> Conservative estimate (scenario 1).

<sup>c</sup> Maximum estimate (assuming mixing follows maximum degradation of source A\* and no degradation of source B\*).

<sup>d</sup> Not determined as isotopic signature lies outside of applicable range.

from the source areas, this might result from a different position of these well filters relative to the groundwater flow direction, or physical heterogeneity of the aquifer. Nonetheless, the SISS model indicates a comparably low overall ED for W13F2\* and W15F2\*, as opposed to the analyzed filters of well W18, which agrees with their upgradient position relative to W18 (Fig. 3.4). Correspondingly, the ED at W9F2 is the lowest among the investigated well filters, which is consistent with its upgradient location in the aquifer.

In general, the results of the SISS model were similar for sulfate-reduction and methanogenesis (apart from the maximum ED). Hence, the appropriate choice of the active reaction pathway was not crucial for SA or QED of benzene at this field site, which can be ascribed to relatively similar  $\Phi$ -values for the two considered reaction pathways (21.9 ‰ and 31.6 ‰, respectively). With an increase in the ED from below 10% to about 20% (conservative estimate; Table 3.1), the results indicate enhanced degradation between well W13 (or W15) and W18. The model generally yielded a much lower ED than the single-element isotope analysis by van Keer et al. (2012). Nonetheless, according to the  $f_A$ -value of W9F2 and W13F2\*, the model results corroborate the hypothesis by van Keer et al. (2012) that some of the well filters are situated in the mixing zone of the two contaminant plumes. They also indicate that the contamination at the well filters in the mixing zone seems to predominantly originate from source area B despite the larger distance from this source area. This might result from a combination of various factors: (i) the higher concentration and considerably larger source area (Fig. 3.4) of source B compared to source A, (ii) a potentially higher local permeability of the top layer at source B compared to source A, which would promote mass transfer to the aquifer from source B, and (iii) presence of DNAPL at source area B, which may have facilitated BTEX transport to larger depths.

Shifting the isotopic signatures of some of the well filters into the valid model range caused an overestimation of  $f_A$ , as this reduced the difference between the

$\delta^{13}\text{C}$ -values of source A and the well filters. However, the characteristics of the original isotope data (Fig. 3.5) were preserved: for example, despite the adjustments of isotopic signatures, the SISS model calculated a small  $f_A$  at well filters W15F2\* and W18F2\*, and indicated substantial mixing between the contaminant plumes at W13F2\* (Fig. 3.6 and Table 3.1). In addition, despite the large degree of uncertainty in measured isotope ratios and assumed enrichment factors, the model confirmed trends from the qualitative analysis of the isotope data such as a prevailing contribution of source B and a larger ED with increasing distance from the source areas.

### 3.3.7 Uncertainties and complications in the use of the SISS model

Figure 3.7 illustrates possible uncertainties and complications in the use of the SISS model by the previously discussed example of benzene contamination. It shows that, if the distribution between the competing reaction pathways (methanogenesis and sulfate-reduction) is unknown, the hypothetical sample signature indicated by the black star could be interpreted in different ways: it could be entirely attributed to source A and indicate an ED of 58.0% under sulfate-reducing conditions only (black dotted line), or it could result from mixing between sources A and B in a ratio of 50:50 ( $f_A = 0.5$ ; green dot) and subsequent degradation under purely methanogenic conditions ( $ED = 57.0\%$ ; green dashed line). In addition, considering the uncertainties in source signatures, the sample signature could also point to a  $f_A$ -value of 0.29 (red dot) and methanogenic transformation (red dashed line) with a slightly lower ED of 53.5%. Two factors particularly complicate SA in this example: the uncertainties in the measured source signatures, and the unknown contribution of each pathway to overall degradation. Moreover, in cases where the  $\Phi$ -values of the two competing pathways differ more than in this example, the area of overlap between possible trajectories from source A and B (dark gray area in Fig. S3.3) would be larger, which would further complicate SA and QED for the sample signature (see section S3.4 in the supplementary information). Another important factor is the angle between the mixing line and the degradation trajectories in the two-dimensional isotope plot (see section S3.5 in the supplementary information): the SISS model is most reliable when the mixing line between the sources is perpendicular to the degradation trajectories (Fig. S3.4a), whereas it cannot be applied if the mixing line and the degradation trajectories have the same slope (Fig. S3.4b).

Despite the discussed uncertainties and complications, the SISS model represents a unique tool for SA and QED in cases where the separate analysis of isotope data for SA and QED is inappropriate. Besides, Fig. 3.7 illustrates complications in the application of the SISS model to extreme values of source signatures and enrichment factors, which yields a large range of possible source contributions. Statistical analyses, on the contrary, would allow for the consideration of uncertainties in source signatures and enrichment factors, and thus reduce their impact on the model results (see chapter 2).

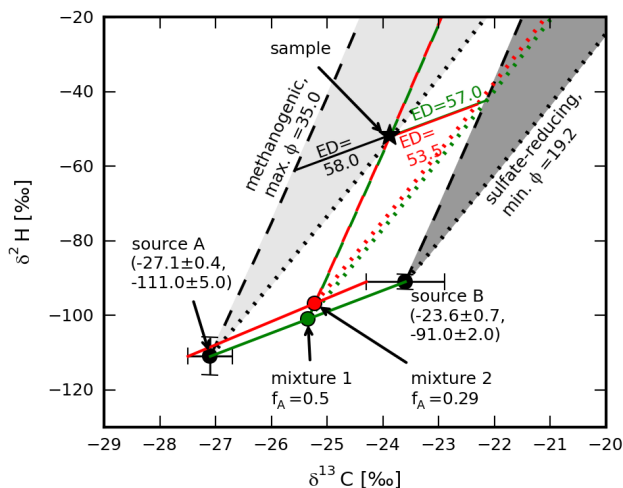


Figure 3.7:  $\delta^{13}\text{C}$ - and  $\delta^2\text{H}$ -values of benzene at the emission sources (black dots) with standard deviations (horizontal and vertical bars, respectively) from the study by van Keer et al. (2012); range of possible trajectories for the source signatures under methanogenic and sulfate-reducing conditions (shaded areas) with minimum (dotted lines) and maximum  $\Phi$ -values (dashed lines); hypothetical sample signature (black star); two example mixtures (green and red dots); corresponding mixing lines (solid lines in green and red) that result from different proportional contributions and signatures of the two sources; and corresponding degradation trajectories for minimum (dotted lines in green and red) and maximum  $\Phi$ -values (dashed lines in green and red) with respective ED. Enrichment factors are  $\varepsilon_{\text{H}} = -60 \pm 3 \text{ ‰}$  and  $\varepsilon_{\text{C}} = -1.9 \pm 0.1 \text{ ‰}$  for methanogenesis, and  $\varepsilon_{\text{H}} = -79 \pm 4 \text{ ‰}$  and  $\varepsilon_{\text{C}} = -3.6 \pm 0.3 \text{ ‰}$  for sulfate-reduction ( $\pm 95\%$  confidence interval; Mancini et al., 2003). The minimum  $\Phi$ -value for sulfate-reduction was set to the ratio between the lowest  $\varepsilon_{\text{H}}$  and highest  $\varepsilon_{\text{C}}$  within the respective confidence intervals, and the maximum  $\Phi$ -value for methanogenesis was set to the ratio between the highest  $\varepsilon_{\text{H}}$  and lowest  $\varepsilon_{\text{C}}$  within the respective confidence intervals.

### 3.4 Conclusions

The SISS model allows for source apportionment and gives a conservative estimate of the ED for organic pollutants (and inorganic compounds such as nitrate) in a scenario of two mixing sources and degradation via one reaction pathway. It showed very good agreement with actual values of source contributions and ED when validated against virtual data from a RTM. Similarly, the model application to field isotope data underlined how the SISS model can help in the identification of the predominant contamination source and assessment of the extent of in situ degradation. However, this field application was challenged by uncertainties in source signatures, CSIA data, enrichment factors, and the unknown interplay between competing degradation pathways. These factors of uncertainty are, nonetheless, inherent to the interpretation of CSIA data and would affect any approach that relies on field CSIA data. Overall, it became apparent how the use of the SISS model can allow for a qualitative and quantitative analysis of field data and improves the understanding of the interplay between degradation processes and mixing of emission sources at contaminated field sites.

Future research could test the SISS model in a coupled subsurface-surface hydro-

logical model that incorporates isotope fractionation effects (see chapters 4 and 5), which would include different routes of contaminant transport and a larger degree of heterogeneity. Similarly, additional model applications to actual CSIA data might reveal whether the discussed example represents a particularly complex case, or whether it is likely to encounter similar difficulties at other locations. In addition, the SISS model was only tested for two emission sources and one degradation pathway. Follow-up studies could, therefore, aim for the application of the model to a combination of multiple emission sources and reaction pathways (see the supplementary information of chapter 2). Despite the encountered challenges, this study indicates that the SISS model forms a useful basis for a combined analysis of source contributions and in situ degradation, which can substantially facilitate the characterization of complex cases of groundwater, surface water, or atmospheric pollution.

## Supplementary information to chapter 3

### S3.1 Alternative model setup with greater distance between the sources

The model was also validated against PHAST simulations according to Fig. S3.1 in order to analyze the effect of a larger difference between the non-degraded fractions of the mixing contaminant pools.

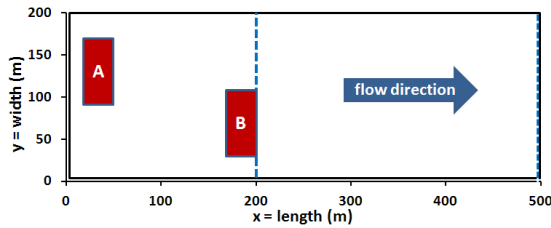


Figure S3.1: Plan view of the alternative simulation with a greater distance between the sources: source A at  $x = [20 \text{ m}, 90 \text{ m}]$  and  $y = [50 \text{ m}, 170 \text{ m}]$ , and source B at  $x = [170 \text{ m}, 200 \text{ m}]$  and  $y = [30 \text{ m}, 110 \text{ m}]$ . Dissolution rates and isotopic signatures at the sources were kept as in the original simulations. Monitoring fences at  $x = 200 \text{ m}$  and  $x = 500 \text{ m}$  are indicated by blue dashed lines.

### S3.2 Comparison of model estimates of non-degraded fractions at $x = 200 \text{ m}$ and $x = 500 \text{ m}$

The SISS-model estimate of the extent of degradation ( $ED_{\text{SISS}}$ ) in the validation against the RTM data set was more accurate at larger distances from the source areas. This is illustrated in Fig. S3.2 for the two monitoring fences at  $x = 200 \text{ m}$  and  $x = 500 \text{ m}$ : the deviation of the non-degraded fraction assumed in scenario 1 of the SISS model ( $f_{\text{deg}}(\text{SISS})$  in Fig. S3.2) from the actual values of the two sources ( $f_{\text{deg,A}}(\text{RTM})$  and  $f_{\text{deg,B}}(\text{RTM})$  in Fig. S3.2) was smaller at  $x = 500 \text{ m}$  than at  $x = 200 \text{ m}$ . This can be explained by a decreasing contribution of degradation (of source A mainly) before mixing to overall degradation with further distance from the source areas. This is, in turn, more consistent with the assumption of no degradation before mixing (scenario 1), and thus resulted in a more precise estimate of the actual extent of degradation ( $ED_{\text{RTM}}$ ).

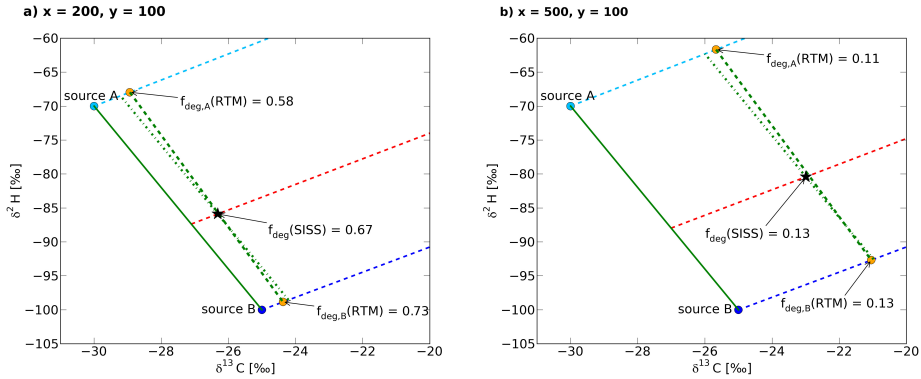


Figure S3.2: Conservative SISS-model estimate of the non-degraded fraction from source A and B ( $f_{\text{deg}}(\text{SISS})$ ); mixing line in the SISS-model calculations (dash-dotted green line); simulated non-degraded fractions (orange dots) from source A ( $f_{\text{deg},A}(\text{RTM})$ ) and source B ( $f_{\text{deg},B}(\text{RTM})$ ); and mixing line corresponding to the simulated  $f_{\text{deg},A}(\text{RTM})$  and  $f_{\text{deg},B}(\text{RTM})$  (dashed green line) at  $x = 200$  m and  $y = 100$  m (a), and at  $x = 500$  m and  $y = 100$  m (b).

### S3.3 Parameters of field site application

Hydrochemical, concentration and CSIA data were taken from van Keer et al. (2012). Table S3.1 shows the main hydrochemical parameters of the investigated aquifer, and Table S3.2 lists benzene concentrations and isotope ratios at the well filters according to van Keer et al. (2012).

Table S3.1: Hydrochemical parameters in the aquifer (van Keer et al., 2012).

$\text{O}_2$	mostly $< 1 \text{ mg L}^{-1}$
redox conditions	$-186$ to $-72 \text{ mV}$
$\text{NO}_3^-$	$< \text{LOD}^{\text{a}}$ ( $0.23 \text{ mg L}^{-1}$ )
$\text{SO}_4^{2-}$	outside the contaminant plume: $\leq 440 \text{ mg L}^{-1}$ , center of the contaminant plume: $< 6 \text{ mg L}^{-1}$ or $< \text{LOD}$ ( $1 \text{ mg L}^{-1}$ )
Fe	$\leq 417 \text{ mg L}^{-1}$
$\text{CH}_4$	$\leq 28 \text{ mg L}^{-1}$

<sup>a</sup> limit of detection

Table S3.2: Benzene concentrations,  $\delta^{13}\text{C}$ - and  $\delta^2\text{H}$ -values, and classification of benzene source at well filters according to van Keer et al. (2012).

well filter	filter depth (m below ground surface)	benzene concentration ( $\mu\text{g L}^{-1}$ )	$\delta^{13}\text{C}$ (‰)	$\delta^2\text{H}$ (‰)	classification
W1	0.8–4.3	600	NA	$-91 \pm 12$	source B
W2F1	1.5–2.5	11600	$-23.6 \pm 0.7$	$-91 \pm 2$	source B
W3	0.5–2.5	560	$-25.3 \pm 0.5$	$-94 \pm 18$	source B
W4F1	2.0–4.0	60	$-25.2 \pm 0.3$	NA	source B
W7	2.8–3.8	5100	$-26.1 \pm 1.1$	$-109 \pm 9$	source A
W8	1.0–4.0	3000	$-27.1 \pm 0.4$	$-111 \pm 5$	source A
W9F1	4.0–5.0	440	$-23.6 \pm 0.2$	$-68 \pm 61$	plume A
W11	1.0–3.0	290	$-24.2 \pm 0.2$	$-68 \pm 4$	plume A
W12	4.0–5.0	860	$-23.5 \pm 0.5$	$-94 \pm 17$	plume A
W13F1	5.0–6.0	1600	$-25.7 \pm 0.6$	$-85 \pm 1$	plume A
W14	4.0–6.0	390	$-23.2 \pm 0.1$	$-81 \pm 6$	plume A
W15F1	3.5–4.5	170	$-22.2 \pm 0.1$	$-88 \pm 19$	plume A
W16	4.0–6.0	80	$-22.6 \pm 0.6$	NA	plume A
W17	4.5–5.5	600	$-24.1 \pm 0.7$	$-105 \pm 4$	plume A
W18F1	4.0–6.0	460	$-23.2 \pm 0.2$	$-78 \pm 14$	plume A
W2F2	9.5–11.5	6000	$-23.8 \pm 0.2$	$-92 \pm 0.4$	plume B
W4F2	9.5–11.5	200	$-24.9 \pm 0.6$	$-83 \pm 14$	plume B
W5	10.0–12.0	2100	$-24.4 \pm 0.6$	$-89 \pm 2$	plume B
W6F1	6.5–7.5	2100	$-22.2 \pm 0.4$	$-87 \pm 1$	plume B
W6F2	8.6–9.6	5500	$-23.4 \pm 0.3$	$-89 \pm 1$	plume B
W6F3	10.5–11.5	5600	$-23.8 \pm 0.2$	$-90 \pm 1$	plume B
W9F2	7.0–8.0	170	$-24.2 \pm 0.1$	$-98 \pm 14$	mixing zone
W9F3	9.0–10.0	1100	$-23.9 \pm 0.6$	$-101 \pm 3$	plume B
W9F4	11.0–12.0	2100	$-23.7 \pm 0.5$	$-87 \pm 4$	plume B
W10	9.0–10.0	1570	$-22.7 \pm 1.0$	$-91 \pm 2$	plume B
W13F2	9.0–10.0	417	$-24.2 \pm 0.6$	$-105 \pm 5$	mixing zone
W15F2	9.5–10.5	3400	$-22.4 \pm 0.5$	$-89 \pm 2$	mixing zone
W18F2	7.0–8.0	800	$-22.2 \pm 0.1$	$-78 \pm 2$	mixing zone
W18F3	9.0–10.0	1900	$-22.9 \pm 0.7$	$-86 \pm 3$	mixing zone
W18F4	11.0–12.0	1800	$-22.8 \pm 0.7$	$-82 \pm 3$	mixing zone

### S3.4 Model complications for two competing pathways with widely differing $\Phi$ -values

Figure S3.3 shows an example of two sources and two competing reaction pathways that results in a large area of overlap (dark grey area) between possible degradation trajectories from source A and B. The larger overlap compared to the discussed example of benzene contamination (Fig. 3.7) results from the greater difference between the  $\Phi$ -values of the two reaction pathways (increase of  $\Phi_1$  from 35.0 to 50.0, and decrease of  $\Phi_2$  from 19.2 to 10.0). Points within the area of overlap can be exclusively attributed to one of the sources, or indicate a mixture of both sources. This complicates the use of the SISS model in comparison to cases where the  $\Phi$ -values of the competing reaction pathways are similar. However, if the contribution of each reaction pathway to overall degradation is known, the extension of the SISS model by isotope data of a third element can allow for precise SA and QED (see section S2.8 in the supplementary information of chapter 2).

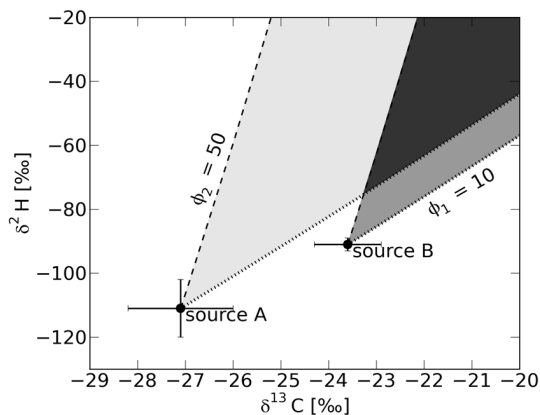


Figure S3.3: Two-dimensional isotope plot with a large area of overlap between possible trajectories from sources A and B (dark grey area), which results from widely differing  $\Phi$ -values ( $\Phi_1 = 10$  and  $\Phi_2 = 50$ ).

### S3.5 Model applicability for different angles between mixing line and degradation trajectories

An important factor for the applicability of the SISS model in a scenario of two sources and one reaction pathway is the angle between mixing line and degradation trajectories in the two-dimensional isotope plot. A  $90^\circ$ -angle between mixing line and degradation trajectories (Fig. S3.4a) represents the ideal case, where the isotopic signature of non-degraded mixtures (green line) does not overlap with the isotopic signature of degraded ones. In contrast, the SISS model cannot be applied if the mixing line and the degradation trajectories have the same slope (i.e., an angle of  $0^\circ$ ; Fig. S3.4b), as the isotopic signatures of non-degraded and degraded contaminant pools are then indistinguishable.

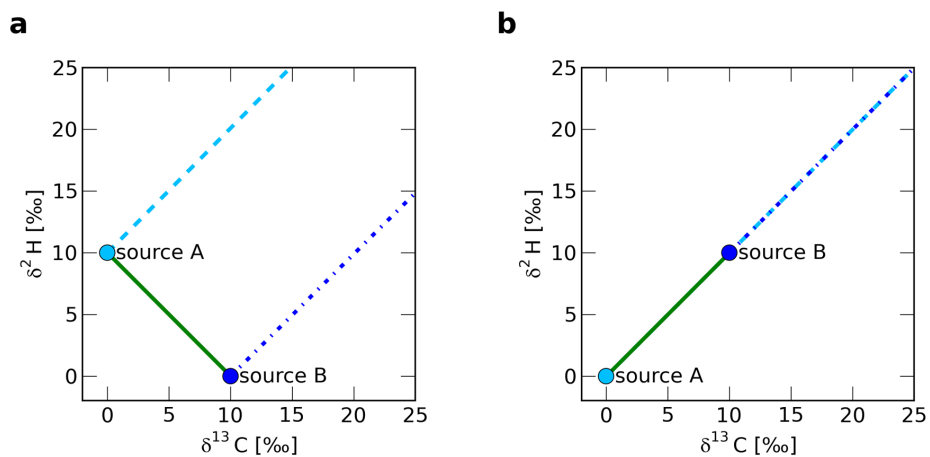


Figure S3.4: Two extreme configurations of the angle between the mixing line (green line) and degradation trajectories (dash-dotted blue line and dashed light blue line): 90°-angle as ideal case (a), and 0°-angle as worst case (b) for the application of the SISS model.



# A model-based assessment of the potential use of CSIA in the analysis of diffuse pesticide pollution\*

**Abstract.** Compound-specific stable isotope analysis (CSIA) has, in combination with model-assisted interpretation, proven to be a valuable approach to quantify the extent of organic contaminant degradation in groundwater systems. CSIA data may also provide insights into the origin and transformation of diffuse pollutants, such as pesticides and nitrate, at the catchment scale. While CSIA methods for pesticides have increasingly become available, they have not yet been deployed to interpret isotope data of pesticides in surface water. We applied a coupled subsurface-surface reactive transport model (HydroGeoSphere) at the hillslope scale to investigate the usefulness of CSIA in the assessment of pesticide degradation. We simulated the transport and transformation of a pesticide in a hypothetical but realistic two-dimensional hillslope transect. The steady-state model results illustrate a strong increase of isotope ratios at the hillslope outlet, which resulted from degradation and long travel times through the hillslope during average hydrological conditions. In contrast, following an extreme rainfall event that induced overland flow, the simulated isotope ratios dropped to the values of soil water in the pesticide application area. These results suggest that CSIA can help to identify rainfall-runoff events that entail significant pesticide transport to the stream via surface runoff. Simulations with daily rainfall and evapotranspiration data and one pesticide application per year resulted in small seasonal variations of concentrations and isotope ratios at the hillslope outlet, which fell within the uncertainty range of current CSIA methods. This implies a good reliability of in-stream isotope data in the absence of transport via surface runoff or other fast transport routes, since the time of measurement appears to be of minor importance for the assessment of pesticide degradation. The analysis of simulated isotope ratios also allowed quantification of the contribution of two different reaction pathways (aerobic and anaerobic) to overall degradation, which gave further insight into the transport routes in the modeled system. The simulations supported the use of the commonly applied Rayleigh equation for the interpretation of CSIA data, since this led to an underestimation of the real extent of degradation of less than 12% at the hillslope outlet. Overall, this study emphasizes the applicability and usefulness of CSIA in the assessment of diffuse river pollution, and represents a first step towards a theoretical framework for the interpretation of CSIA data in agricultural catchments.

---

\*This chapter is an edited version of: Lutz, S. R.; van Meerveld, H. J.; Waterloo, M. J.; Broers, H. P., and van Breukelen, B. M. A model-based assessment of the potential use of compound-specific stable isotope analysis in river monitoring of diffuse pesticide pollution. *Hydrology and Earth System Sciences*, 17:4505-4524, 2013.

## 4.1 Introduction

Modern agriculture makes use of a variety of pesticides to increase crop yield and reduce pests and the growth of weeds. As a result, pesticides have become ubiquitous organic contaminants in agricultural catchments. Diffuse pollution by pesticides can pose a risk for the terrestrial and aquatic environment, and human health. Pesticide residuals and their metabolites have been found in groundwater and surface water, and affect drinking water quality (Donald et al., 2007; Kolpin et al., 1998; Kjær et al., 2005). It is therefore vital to assess the fate of diffuse pollutants, and to identify major pesticide sources in a catchment.

After application, pesticides are subject to various transfer, transformation, and transport processes (Gavrilescu, 2005; Flury, 1996). Important transfer processes are volatilization (the transfer of compounds from the solid or liquid phase to the gas phase), and sorption (the transfer from the liquid to the solid phase of the soil matrix). Pesticide molecules that have not been volatilized can undergo transformation processes on the ground surface and in the soil, which leads to destruction of the compound. The transformation of pesticides is either ascribed to microbial activity or abiotic processes. Microbial degradation in the soil matrix can occur under aerobic or anaerobic conditions. The transport of pesticides in the aqueous phase towards surface water bodies can occur via surface runoff or subsurface flow. If the pesticide is not directly removed by surface runoff, it leaches into the subsurface. Drainage systems, preferential flow (e.g., in earthworm burrows and cracks) and subsurface storm flow can thereupon cause fast transport to surface water (Gavrilescu, 2005; Müller et al., 2003; Leu et al., 2004b). In contrast, pesticide leaching to groundwater represents a slow subsurface transport mechanism (Holvoet et al., 2007; Flury, 1996).

Previous research has shown that rainfall events increase the risk of surface water contamination by pesticides (Taghavi et al., 2011; Müller et al., 2003). The highest pesticide loads happen in response to rainfall events shortly after pesticide application, and are attributed to surface runoff and preferential flow (Leu et al., 2004a). A secondary contribution to overall pesticide export is ascribed to the baseflow component (Louchart et al., 2001; Squillace and Thurman, 1992).

Monitoring of pesticide concentrations in rivers enables us to assess the extent of diffuse pollution at the catchment scale. However, concentration data do not provide clear evidence of degradation processes, since a reduction in concentration might, for example, indicate degradation of the contaminant, changes in the application pattern and amount, or dilution (Battaglin and Goolsby, 1999; Schreglmann et al., 2013). In contrast to degradation, non-destructive processes such as dilution do not reduce the contaminant loads to subsurface and surface water. In this context, compound-specific isotope analysis (CSIA) has emerged as a valuable tool for the analysis of the transformation of organic contaminants.

CSIA is the measurement of the isotopic composition, i.e. the ratio between the abundance of a heavy and a light stable isotope of an element in a compound. This isotope ratio tends to increase during degradation since chemical bonds that contain a heavy isotope are less amenable to degradation processes than those that solely consist of light isotopes (Meckenstock et al., 2004; Elsner, 2010). This phenomenon,

called isotope fractionation, does not occur during dilution (van Breukelen, 2007b), and it is only relevant under specific conditions for other physical non-destructive processes such as diffusion (van Breukelen and Rolle, 2012) and sorption (van Breukelen and Prommer, 2008). In contrast to concentration monitoring, CSIA thus serves as a direct indicator of the transformation of a contaminant and, by measuring multiple elements, even allows for the determination of the degradation mechanism that leads to the transformation (Elsner, 2010).

CSIA has been used to study the fate of various groundwater pollutants, such as monoaromatic and polyaromatic hydrocarbons (Blum et al., 2009; Vieth et al., 2005; Griebler et al., 2004), MTBE (Kolhatkar et al., 2002; Zwank et al., 2005), chlorinated ethenes (Hunkeler et al., 2005; Sherwood Lollar et al., 2001), perchlorate (Sturchio et al., 2012), nitrate (Deutsch et al., 2006; Ging et al., 1996; Seiler, 2005; Zhang et al., 2012), and chromium(VI) (Wanner et al., 2012a). However, except for the identification of nitrate sources, it has so far not been used to examine diffuse pollution at the catchment scale. Similarly, although analytical methods for CSIA of different elements have been developed and applied for several pesticides and pesticide metabolites (Badea et al., 2009; Hartenbach et al., 2008; Meyer et al., 2008; Milosevic et al., 2013; Penning and Elsner, 2007; Reinnicke et al., 2011; Schreglmann et al., 2013; Wu et al., 2014; Elsayed et al., 2014), isotopes of pesticides have not yet been continuously monitored and analyzed in rivers.

Reactive transport models that incorporate isotope fractionation effects (isotope fractionation reactive transport models, IF-RTMs) have become a popular method to model and interpret CSIA data from point-source pollutants in groundwater systems (Atteia et al., 2008; D’Affonseca et al., 2011; Pooley et al., 2009; Prommer et al., 2009; van Breukelen et al., 2005; Wanner et al., 2012b). In particular, assumptions concerning reaction kinetics can be validated by comparing model results to measured concentration and CSIA data (D’Affonseca et al., 2011; Pooley et al., 2009; Prommer et al., 2009; Atteia et al., 2008). IF-RTMs have also proven useful to study the transformation of the agrochemical pollutant nitrate (Chen and MacQuarrie, 2004; Green et al., 2010). These studies have demonstrated that IF-RTMs allow for the quantification of in situ degradation and the distinction between destructive and non-destructive processes. Moreover, IF-RTMs permit the assessment of the performance of the Rayleigh equation, which is the mathematical basis of CSIA. The Rayleigh equation tends to underestimate the extent of biodegradation in real flow systems because of the attenuation of isotopic enrichment due to dispersion or mixing processes (Abe and Hunkeler, 2006; van Breukelen and Prommer, 2008).

So far, IF-RTM studies have solely focused on groundwater systems. This chapter presents the first incorporation of isotope fractionation effects into a reactive transport model of a coupled surface-subsurface system, which involves more complex transport routes. The aim of this modeling study was to determine whether CSIA measured in surface water can help to identify transport routes and quantify the extent of degradation of diffuse agricultural pollutants in subsurface-surface systems. We modeled a hypothetical but realistic situation of pesticide application, transport, and degradation, including isotope fractionation at the hillslope scale. To this end, we applied a distributed physically-based model, which allowed for the simulation of hydrological processes in different flow domains in a detailed and spatially

explicit way (Kampf and Burges, 2007) and the description of pesticide fluxes and concentrations (Thorsen et al., 1996). This study thus ties in with the virtual experiment approach in hillslope hydrology of Weiler and McDonnell (2004), Hopp et al. (2009), and Mirus et al. (2011), and additionally considers reactive transport and isotope fractionation. We opted for a hillslope transect because hillslopes are a fundamental landscape element and form the basic hydrological unit of catchments. Hence, understanding processes at the hillslope scale is an important and relevant first step towards interpreting CSIA at the catchment scale. By means of scenario modeling, we examined the evolution of isotope ratios under average hydrological conditions, in response to an extreme rainfall event, and under transient, daily varying hydrological conditions. In order to advance the transition from these virtual experiments to real applications, we give, based on the simulation results for this hillslope model, general guidelines for the monitoring and interpretation of isotope data in the context of diffuse pollution.

## 4.2 Methods

### 4.2.1 Model code description: HydroGeoSphere

We simulated isotope fractionation during transport and transformation of a hypothetical pesticide with the software HydroGeoSphere (HGS) (Therrien et al., 2010; Brunner and Simmons, 2012). HGS is a fully-coupled, subsurface-surface flow and solute transport model. Surface flow is described by the diffusion-wave approximation of the Saint Venant equation, while the variably saturated form of the Richards' equation is used for the subsurface. The Newton-Raphson technique is implemented to solve the non-linear equations of variably-saturated flow. Solute transport is simulated by solving the advection-dispersion equation; degradation of the solute is modeled with first-order kinetics. Furthermore, it is possible to include interception, transpiration and evaporation processes. Applications of HGS include large watershed modeling (Goderniaux et al., 2009; Li et al., 2008), simulations of aquifer-river interactions in hypothetical model domains (Doble et al., 2012; McCallum et al., 2010), and the analysis of contaminant transport in groundwater (Rivett et al., 2006; Sudicky et al., 2010).

### 4.2.2 Hillslope geometry and model grid

The model domain consists of a two-dimensional hillslope that is 200 m long and stretches 15 m in the vertical direction (Fig. 4.1). Conceptually, the hillslope represents part of a headwater catchment. The hillslope outlet corresponds to a river monitoring point. Inflow of water and pesticides from upstream parts was not considered in this model. The hillslope is convex with an average gradient of 5%, which is comparable to the average slope in previously studied agricultural catchments (Doppler et al., 2012; Leu et al., 2004a). A river bank was incorporated as a vertical drop of 2 m over the last 5 m in the x-direction, which increased the average slope to 5.8%. The model domain does not represent, nor was calibrated for a specific field site, but is supposed to resemble a realistic agricultural hillslope.

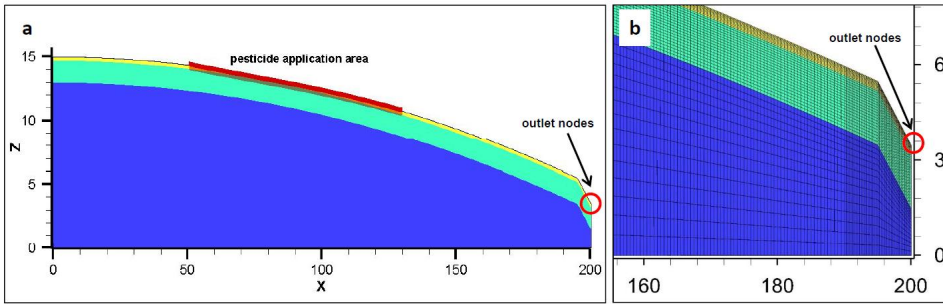


Figure 4.1: Model domain with the pesticide application area (red) and three subsurface zones: topsoil (yellow), subsoil (green) and bedrock (blue) (a). The discretization is finer in the upper soil and close to the hillslope outlet (b). The hillslope outlet is represented by two boundary nodes (red circle).

Figure 4.1a shows the model mesh and the three subsurface zones (see section 4.2.3) in the hillslope. The subsurface comprises a total of 43 layers. The vertical grid spacing is a few centimeters in the topsoil and increases with depth, which results in a maximum cell height of more than one meter at the bottom of the model domain. The mesh nodes are 0.5 m apart in the horizontal direction, except for the zone near the river, which has a horizontal discretization of 0.25 m (Fig. 4.1b).

### 4.2.3 Hydraulic properties and flow simulation

We opted for modeling a layered system with variable hydraulic properties, as many sites are characterized by relatively shallow soils on fractured bedrock. The hillslope model therefore consists of three zones with different properties: the topsoil extends 0.3 m below the ground surface, the subsoil is located between 0.3 and 2 m below the ground surface, and the remaining part of the subsurface represents the bedrock. A similar layering was used for the numerical simulation of runoff generation mechanisms in different catchments by Mirus et al. (2011). The saturated hydraulic conductivity for the three subsurface zones was set as follows:  $1.0 \text{ m d}^{-1}$  in the topsoil,  $0.5 \text{ m d}^{-1}$  in the subsoil, and  $0.1 \text{ m d}^{-1}$  in the bedrock (Table 4.1). These values represent the frequently observed decline in hydraulic conductivity with depth and are comparable to those used by Christiansen et al. (2004) to simulate pesticide transport in a small agricultural catchment in Denmark. The hydraulic parameters for the soil were obtained from an experimental site at Canadian Forces Base Borden (north of Toronto, Ontario, Canada) because HGS has been validated against irrigation experiments at this site (Abdul, 1985; Therrien et al., 2010). These simulations therefore provided verified HGS parameters for the porosity, the residual saturation, and the parameters  $\alpha$  and  $\beta$  of the Van Genuchten model (which determine the saturation-pressure relation). Previous HGS simulations of the Borden site used uniform soil parameters and only considered the upper 4 m of the profile (Therrien et al., 2010), but we preferred to explicitly represent the bedrock. The bedrock parameters were therefore taken from simulations of the forested Coos Bay site in Oregon, USA (Mirus et al., 2011). They represent weathered bedrock and fractured sandstone. The specific storage coefficient was kept at its default

Table 4.1: Hydraulic properties of the hillslope subsurface domain.

	Topsoil	Subsoil	Bedrock
saturated hydraulic conductivity ( $\text{m d}^{-1}$ )	1.0	0.5	0.1
porosity (-)	0.37 <sup>a</sup>	0.37 <sup>a</sup>	0.12 <sup>b</sup>
residual saturation (-)	0.18 <sup>a</sup>	0.18 <sup>a</sup>	0.01 <sup>b</sup>
<i>Van Genuchten parameters</i>			
$\alpha$ ( $\text{m}^{-1}$ )	1.9 <sup>a</sup>	1.9 <sup>a</sup>	4.3 <sup>b</sup>
$\beta$	6 <sup>a</sup>	6 <sup>a</sup>	1.3 <sup>b</sup>

<sup>a</sup> Abdul (1985)<sup>b</sup> Mirus et al. (2011)

value ( $1 \cdot 10^{-4} \text{m}^{-1}$ ) for all three zones.

HGS explicitly represents the overland flow domain as a layer on top of the subsurface domain. The nodes of the overland flow domain coincide with the top elements of the subsurface domain. The overland flow parameters rill storage height and coupling length were both set to 0.01 m based on previous studies using HGS (Goderniaux et al., 2009; Therrien et al., 2010). The rill storage height defines the depth of depressions on the ground surface, which inhibit the generation of surface runoff. The coupling length determines the degree of continuity in pressure heads between the surface and the subsurface domain and thus defines the exchange flux between these domains (Verbist et al., 2012). A smaller coupling length results in increased coupling of the overland flow domain to the subsurface domain.

The lateral and bottom boundaries of the hillslope were set to zero-flux boundaries such that the water could leave the hillslope only via the overland flow domain. This was realized by applying a critical depth boundary at the hillslope outlet, which yields a time varying flux that is given by Manning's equation (Therrien et al., 2010). The hillslope outlet was represented by two nodes in the surface layer, since the hillslope extends one cell into the y-direction. Rainfall was applied at a spatially uniform rate on the entire model domain.

Rainfall and potential evapotranspiration data were supplied as model input. The actual evapotranspiration in HGS depends on the moisture content and several vegetation-related parameters. The difference between precipitation and actual evapotranspiration is then added to or abstracted from the model domain, depending on which component is dominant. The parameters for evapotranspiration were kept at their default values, except for the leaf area index, which was set to the value for temperate and tropical crops given in the HGS manual (leaf area index of 4.2), and the interception by canopy, which was assumed to be negligible.

#### 4.2.4 Reactive solute transport

We used HGS to simulate the reactive transport of a soluble, non-volatile, and non-sorbing hypothetical pesticide. These properties are characteristic of the widely used compounds MCPA, bentazone, metam-sodium and clopyralid (University of

Table 4.2: Parameters for degradation and isotope fractionation.

	$k_{\text{eff}}^{\text{a}}$ ( $\text{a}^{-1}$ )	$\varepsilon_{\text{C}}^{\text{b}}$ (‰)	$\varepsilon_{\text{H}}^{\text{c}}$ (‰)	$\varepsilon_{\text{H}}/\varepsilon_{\text{C}}$
aerobic (topsoil)	5	-5	-10	2
anaerobic (subsoil and bedrock)	0.2	-1	-20	20

<sup>a</sup> overall degradation rate constant (Eq. 4.3)

<sup>b</sup> enrichment factor for carbon isotope fractionation

<sup>c</sup> enrichment factor for hydrogen isotope fractionation

Hertfordshire, 2013), as well as nitrate. We therefore neglected volatilization and sorption processes. The pesticide was applied to the cells at the ground surface between x-coordinates 50 m and 130 m (Fig. 4.1a). Depending on the simulated scenario, the solute transport boundary condition was either set to a specified concentration or a specified mass flux (see section 4.2.6). The transport parameters were chosen as follows: an aqueous diffusion coefficient of  $7.8 \cdot 10^{-5} \text{m}^2 \text{d}^{-1}$ , which is the value that was assumed for diffusion of the herbicides metolachlor and alachlor in groundwater by Lee and Benson (2004); and the default values for dispersivities in HGS of 1.0 m in the longitudinal direction and 0.1 m in the vertical transverse direction.

The hypothetical pesticide was assumed to degrade via two different pathways: an aerobic reaction in the topsoil and an anaerobic reaction in the subsoil and bedrock. A pesticide half life of 51 days, corresponding to an overall degradation rate constant of 5 per year, was chosen for the aerobic reaction (Table 4.2), which is within the range of reported half lives of widely used pesticides (e.g., linuron and clopyralid; University of Hertfordshire, 2013). The half life for the anaerobic reaction was assumed to be much longer (1265 days; rate constant of  $0.2 \text{yr}^{-1}$ ).

The model yielded concentrations for the entire model domain. Additionally, for each time step and solute, the concentration at the hillslope outlet was obtained by tracking the solute and water fluxes through the boundary nodes. These concentrations were verified against the model-based concentrations in the overland flow domain at the boundary nodes.

The simulations were run in finite difference mode with upstream weighting. The adaptive time stepping scheme was used; the maximum time step was set to one day for the steady state simulations and 0.01 days for the transient simulation (see section 4.2.6). A maximum concentration change of 0.1 relative to the source concentration was allowed in each time step for the steady state simulation; this value had to be increased to 500 for the transient simulation because of the temporary high mass load.

#### 4.2.5 Simulation of isotope fractionation effects

Isotope fractionation effects were included in the model by simulating the concentrations of the light and heavy isotopes of the pesticide. Since the assumption of two degradation pathways requires the analysis of two isotopic elements (van Breukelen, 2007a), this resulted in the simulation of four solutes. The two-dimensional isotope

analysis was implemented by simulating carbon and hydrogen isotopes because carbon represents the element with the most isotope data available for pesticides (Annable et al., 2007; Badea et al., 2009; Meyer et al., 2009; Penning et al., 2010), and the cleavage of chemical bonds in pesticide molecules with hydrogen atoms induces a significantly stronger isotope fractionation effect than, for example, with nitrogen atoms (Hartenbach et al., 2008; Penning et al., 2010).

Following Hunkeler et al. (2009), van Breukelen et al. (2005), and van Breukelen and Prommer (2008), the differential equations for degradation of the light carbon and hydrogen isotopes were simulated as first-order reaction with the degradation rate constant  $k^L$ :

$$\frac{dC^L}{dt} = k^L \cdot C^L \quad (4.1)$$

with  $C^L$  being the concentration of the light carbon or hydrogen isotopes, respectively. The reaction kinetics of the heavy isotopes, involving a different degradation rate constant  $k^H$ , were specified as:

$$\frac{dC^H}{dt} = k^H \cdot C^H \quad (4.2)$$

where  $C^H$  is the concentration of the heavy carbon and hydrogen isotopes, respectively.

The kinetic isotopic fractionation factor,  $\alpha$ , represents the ratio between the degradation rate constants of the heavy and light isotopes (i.e.  $k^H/k^L$ ). It thus determines the strength of the isotope fractionation effect for a specific reaction. Since it typically has a value close to one, it is reported in per mil (‰) as the kinetic isotopic enrichment factor  $\varepsilon$  (‰) =  $(\alpha - 1) \cdot 1000$ . The degradation rate constant of the light isotopes ( $k^L$ ) was set to the overall degradation rate constant ( $k_{\text{eff}}$ , Table 4.2). Given  $\alpha = k^H/k^L$  and  $k^L = k_{\text{eff}}$ , degradation of the heavy carbon and hydrogen isotopes was thus simulated as

$$\frac{dC^H}{dt} = k_{\text{eff}} \cdot \alpha \cdot C^H = k_{\text{eff}} \cdot \left( \frac{\varepsilon}{1000} + 1 \right) \cdot C^H \quad (4.3)$$

The enrichment factors ( $\varepsilon$ ) for aerobic and anaerobic degradation for the carbon isotopes were chosen to be representative for fractionation effects during biotic pesticide degradation (Meyer et al., 2009; Penning et al., 2010). Data about fractionation effects for hydrogen isotopes are much scarcer; the enrichment factors for hydrogen were therefore set to values following the general trend of stronger enrichment in hydrogen compared to carbon isotopes (Hunkeler and Elsner, 2009).

In a system with two transformation pathways, the ratio between the enrichment factors of two isotopic elements, for example of hydrogen and carbon ( $\varepsilon_H/\varepsilon_C$ ), can be indicative of a specific degradation mechanism (Meyer et al., 2009; Fischer et al., 2008). The enrichment factors for the two reaction pathways were therefore chosen such that they yield distinct  $\varepsilon_H/\varepsilon_C$ -ratios (Table 4.2). This is in agreement with considerably diverging  $\varepsilon_H/\varepsilon_C$ -ratios that were, for example, observed for aerobic and anaerobic biodegradation of MTBE (Zwank et al., 2005).

Combining and integrating Eqs. 4.1 and 4.2 leads to the Rayleigh equation, which allows for the quantification of in situ degradation on the basis of isotope ratios (see also section 2.2.1). Its simplified form can be expressed as:

$$\frac{R_{\text{sample}}}{R_{\text{source}}} = f^{(\alpha-1)} \quad (4.4)$$

where  $R$  represents the ratio between the abundance of a heavy and a light isotope of an element in a compound for a sample ( $R_{\text{sample}}$ ) and at the emission source ( $R_{\text{source}}$ ), respectively, and  $f$  denotes the non-degraded fraction of the compound in the sample with respect to the emission source.

To facilitate inter-sample comparison, the isotope ratio of a sample ( $R_{\text{sample}}$ ) is expressed in the  $\delta$ -notation, which is the relative difference of  $R_{\text{sample}}$  from a standard ratio  $R_{\text{standard}}$  (Schmidt and Jochmann, 2012):

$$\delta_{\text{sample}} = \frac{R_{\text{sample}} - R_{\text{standard}}}{R_{\text{standard}}} = \frac{R_{\text{sample}}}{R_{\text{standard}}} - 1 \quad (4.5)$$

where the  $\delta$ -value or isotopic signature is commonly reported in per mil (‰). The standard isotope ratios that were used in this study are the international standards for carbon and hydrogen, i.e. Vienna Pee Dee Belemnite (VPDB;  $R_{\text{standard}} = 0.0112372$ ) and Vienna Standard Mean Ocean Water (VSMOW;  $R_{\text{standard}} = 1.5575 \cdot 10^{-4}$ ), respectively.

The  $\delta^{13}\text{C}$ -value at the source was fixed at  $-30$  ‰, which corresponds to typical values for carbon isotopes in pesticides (Annable et al., 2007; Kawashima and Katayama, 2010; Badea et al., 2009). Since no typical source values were available for hydrogen isotopes in pesticides, a value of  $-100$  ‰ was chosen, which is consistent with  $\delta^2\text{H}$ -values reported for other organic contaminants (Mancini et al., 2008; Wang et al., 2004). These initial  $\delta$ -values determined the ratio of the concentrations of light and heavy isotopes at the pesticide source (Eq. 4.5). The simulated concentrations of the light and heavy isotopes were used to calculate the  $\delta$ -values for the entire hillslope domain and the hillslope outlet.

#### 4.2.6 Simulated scenarios

In a preliminary model run, a recharge rate of  $250 \text{ mm yr}^{-1}$  was applied to the whole surface domain in order to achieve a steady-state flow field. This value was considered representative for average hydrological conditions for the Netherlands and northern Germany (Otto, 2001; Querner, 2000) and did not cause any surface saturation, except for a few nodes at the hillslope outlet that represent the river bank and bottom. The distribution of the hydraulic head values at the end of this simulation was used as the initial condition for subsequent simulations with solute transport. We simulated three different scenarios with solute transport: scenario 1 represents steady state conditions and aims at analyzing the pattern of isotopic enrichment of the pesticide during transport and degradation under average hydrological conditions; scenario 2 focuses on the response of concentrations and isotope ratios to an extreme rainfall event to determine the effect of surface runoff;

and scenario 3 incorporates periods of baseflow conditions and extreme rainfall events to study transient pesticide concentrations and isotope ratios in the course of the year.

### **Scenario 1: steady-state flow conditions**

The first scenario was designed to mimic diffuse pollution under average hydrological conditions. The emission source was implemented as a specified concentration boundary with a constant relative concentration of  $C_0 = 1.0$  for the sum of the light and heavy isotopes of each isotopic element. In addition, one conservative tracer with  $C_0 = 1.0$  was applied across the entire surface of the model domain and another tracer (also with  $C_0 = 1.0$ ) at the application area only, to allow for the calculation of the mean travel time of groundwater. This scenario was run until the concentrations at the hillslope outlet reached steady-state.

### **Scenario 2: extreme rainfall event**

As a hillslope system is in reality exposed to varying hydrological conditions, it was subsequently studied how concentrations and isotope ratios responded to a single extreme rainfall that leads to surface runoff. To facilitate the occurrence of surface runoff, the coupling length for this scenario was increased from 0.1 to 0.8 m. Rainfall was applied with a uniform intensity of  $60 \text{ mm h}^{-1}$  for 30 min. Based on a rainfall depth-duration-frequency curve (Overeem et al., 2009), the return period for such an event in the Netherlands is more than 58 years. For the rest of the simulation time, the recharge rate was held constant at the same value as for the steady-state scenario (scenario 1). Solute transport was initialized with the concentration results from the steady-state simulation; the concentration in the source area was kept at a constant value of  $C_0 = 1.0$  for the total concentration of each isotopic element.

### **Scenario 3: transient simulation for water flow and solute input**

Finally, a time-varying hydrological system was simulated by applying the daily rainfall and evapotranspiration data of 2010 from the meteorological station "Twente" (Database of the Royal Netherlands Meteorological Institute, Koninklijk Nederlands Meteorologisch Instituut KNMI) for 20 years. This time series (Fig. 4.2a) includes an extraordinary rainfall event at the end of August with a maximum intensity of  $27.6 \text{ mm h}^{-1}$  and a total rainfall amount of 106.4 mm; the rainfall event lasted for 20.8 hours. Based on Overeem et al. (2009), the return period of this event exceeds 260 years. The use of these data thus allowed for the simulation of a broad range of possible rainfall intensities and runoff responses for Mid-European climates; it resulted in a net groundwater recharge of approximately  $360 \text{ mm yr}^{-1}$  (Fig. 4.2b). The annual rainfall and evapotranspiration data set was repeated for a total of 20 simulation years. This facilitated the interpretation of the results as opposed to an actual data set for 20 consecutive years, which would have produced a different hydrological and isotopic response for every simulation year.

Since pesticides are not applied at a constant rate throughout the year, a more realistic setup comprises short emission pulses. To this end, the pesticide was applied once a year on a dry day in spring (day 100; 11 April) using a specified relative mass flux of 1 for the sum of light and heavy isotopes of each isotopic element for every grid cell at the pesticide source. The specified mass flux was

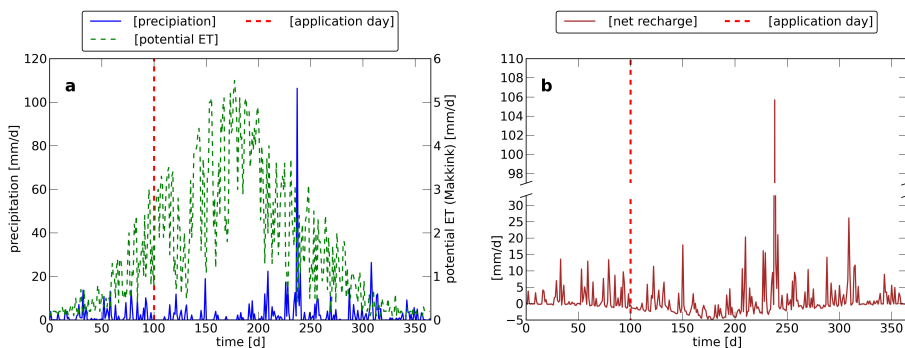


Figure 4.2: Daily rainfall and evapotranspiration data for the meteorological station Twente (a); and net infiltration as the difference between precipitation and modeled actual evapotranspiration (b). The data set shown in panel a was repeated for 20 yr in the transient simulation (scenario 3). The pesticide application (11 April; day 100) is marked by the red dashed vertical line. The simulation was started on this day to ensure the presence of pesticide in the hillslope system.

chosen as the boundary condition for this scenario because the pesticide application is supposed to occur on a day without precipitation. If the boundary condition had been set to a specified concentration, the pesticide would not have been transferred to the subsurface because of the lack of infiltration on dry days. The model domain did not contain any pesticide at the beginning of the simulation. In order to assure the presence of pesticide in the system, which is required for the simulation of degradation, the model run was started on the first application day.

#### 4.2.7 Post-model calculations

For the steady-state conditions, the cumulative transit time distribution at the hillslope outlet was derived from the concentration of the conservative tracer that was applied to the entire surface of the model domain using the relation between the transit time distribution and conservative solute breakthrough described by Duffy and Lee (1992) and further explored by Eberts et al. (2012). The mean travel time (MTT) of the system was calculated by integrating the transit time distribution. The MTT for the pesticide at steady-state was obtained from the concentration at the outlet of the conservative tracer that was only applied at the pesticide application area.

Two-dimensional CSIA permits the assessment of the relative contribution of each transformation pathway to the overall degradation in a system of two competing reactions. For the simulated system, which involves an aerobic and an anaerobic reaction affecting carbon and hydrogen isotope ratios, this contribution was calculated according to van Breukelen (2007a):

$$F = \frac{\Phi \cdot \varepsilon_{C\text{anaerobic}} - \varepsilon_{H\text{anaerobic}}}{(\varepsilon_{H\text{aerobic}} - \varepsilon_{H\text{anaerobic}}) - \Phi \cdot (\varepsilon_{C\text{aerobic}} - \varepsilon_{C\text{anaerobic}})} \quad (4.6)$$

where the subscripts C and H indicate the enrichment factors for carbon and hydrogen isotopes, the subscripts aerobic and anaerobic denote the respective

pathway, and  $\Phi$  is the ratio of the isotopic shifts  $\Delta^2\text{H}$  and  $\Delta^{13}\text{C}$  for carbon and hydrogen:  $\Phi = \Delta^2\text{H}/\Delta^{13}\text{C}$ . The isotopic shift, i.e. the change in the  $\delta$ -value, is defined as

$$\Delta = 1000 \cdot \ln \left( \frac{10^{-3} \cdot \delta_{\text{sample}} + 1}{10^{-3} \cdot \delta_{\text{source}} + 1} \right) \quad (4.7)$$

where  $\delta_{\text{sample}}$  and  $\delta_{\text{source}}$  are the  $\delta$ -values for the carbon or hydrogen isotopes at a point in the model domain and at the pollution source, respectively.

The non-degraded fraction of the compound at a point in the model domain,  $f_{\text{deg}}$ , was obtained by substituting  $F$  (Eq. 4.6) into the Rayleigh equation for two-dimensional CSIA (van Breukelen, 2007a):

$$f_{\text{deg}} = \left( \frac{10^{-3} \cdot \delta_{\text{sample}} + 1}{10^{-3} \cdot \delta_{\text{source}} + 1} \right)^{\frac{1000}{F \cdot \varepsilon_{\text{Caerobic}} + (1-F) \cdot \varepsilon_{\text{Canaerobic}}}} \quad (4.8)$$

The fraction  $f_{\text{deg}}$  yields the extent of degradation based on the Rayleigh equation approach:

$$B (\%) = (1 - f_{\text{deg}}) \cdot 100 \quad (4.9)$$

The exact value of the fraction of non-degraded pesticide,  $f_{\text{deg,m}}$ , was calculated from the simulated concentrations of the pesticide and the conservative tracer, and was used to quantify the underestimation of the extent of degradation that would result from the application of the Rayleigh equation to the simulated isotope data (Abe and Hunkeler, 2006). Given that the rate constant,  $k$ , of a first-order reaction satisfies  $-kt = \ln(f)$ , this underestimation,  $\theta$ , was determined as (van Breukelen and Prommer, 2008):

$$\theta (\%) = \left( 1 - \frac{k_{\text{Rayleigh}}}{k_{\text{model}}} \right) \cdot 100 = \left( 1 - \frac{\ln f_{\text{deg}}}{\ln f_{\text{deg,m}}} \right) \cdot 100 \quad (4.10)$$

The simulation results were also used to derive the residual fractions of the pesticide that remain at the hillslope outlet after dilution ( $f_{\text{dil}}$ ) and degradation ( $f_{\text{deg}}$ ) following the assumption of an open system (van Breukelen, 2007b). The parameter  $f_{\text{deg}}$  was determined by applying Eq. 4.8 to the simulated isotope ratios at the hillslope outlet. The dilution factor  $f_{\text{dil}}$  was then obtained as

$$f_{\text{dil}} = \frac{f_{\text{tot}}}{f_{\text{deg}}} \quad (4.11)$$

where  $f_{\text{tot}}$  is the ratio between the concentration at the hillslope outlet and the source concentration.

## 4.3 Results

### 4.3.1 Scenario 1: steady-state flow conditions

The constant recharge rate in scenario 1 produced a steady-state flow and transport regime with a mean travel time (MTT) of 6.7 years for the groundwater and of

5.0 years for the pesticide. At the hillslope outlet, this resulted in a steady-state concentration of 0.09 for the degrading pesticide and 0.41 for the conservative tracer that was applied at the pesticide application area relative to the initial concentration of 1.0 at the pollution source. Pesticide concentrations were lower than concentrations of the conservative tracer in the entire model domain. They were highest below the application area and decreased with depth and distance from the source (Fig. 4.3a). In contrast to the shallow subsurface beneath the application area, the shallow soil layers at the hillslope bottom were characterized by low solute concentrations.

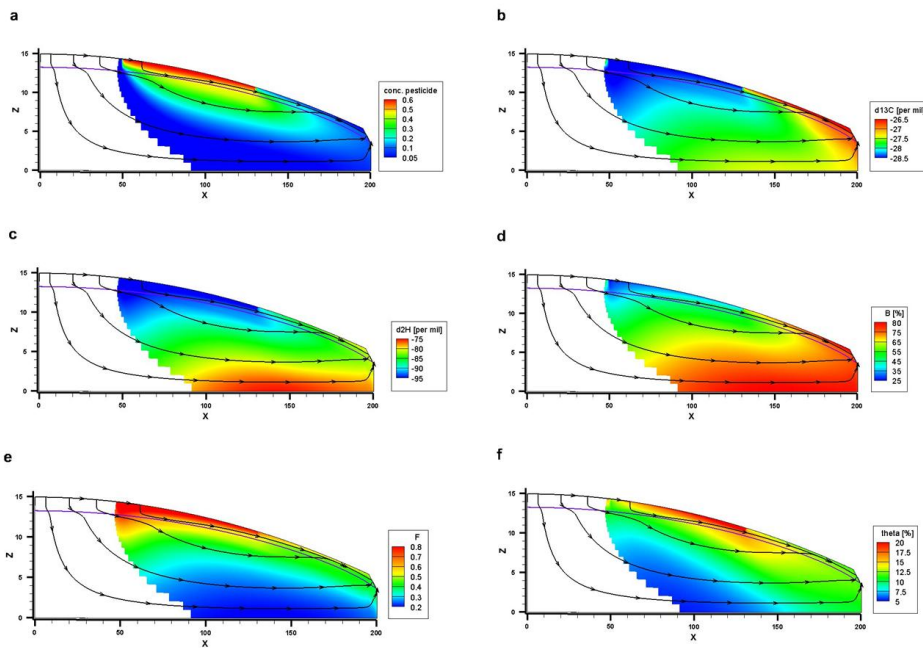


Figure 4.3: Steady-state results for the pesticide concentration (a);  $\delta^{13}\text{C}$ -values (‰) of the pesticide (b);  $\delta^2\text{H}$ -values (‰) of the pesticide (c); extent of degradation (%; d); relative contribution of the aerobic reaction to overall pesticide degradation (e); and underestimation (%) of the true extent of degradation when the Rayleigh equation is used (f). Areas with a concentration reduction of more than three orders of magnitude relative to the source are blanked because CSIA would not be possible due to detection limits. The black arrows indicate streamlines of the steady-state flow field. The purple line shows the position of the water table. Vertical exaggeration is five times.

Figure 4.3b shows the carbon isotope ratios in the hillslope domain, which became progressively enriched with distance from the source area. With a shift of up to 4 ‰ from the initial value of  $-30$  ‰, the shallow subsurface at the lower hillslope was characterized by the largest enrichment in  $\delta^{13}\text{C}$ . Hydrogen isotopes were enriched by about 20 ‰ in the shallow soil layers close to the hillslope outlet (Fig. 4.3c). In contrast to carbon isotopes, the strongest fractionation effects occurred in the deeper bedrock, which showed an enrichment of up to 25 ‰.

Degradation during transport induced isotope fractionation, which resulted in a steady state isotope ratio of  $-26.7$  ‰ for  $\delta^{13}\text{C}$  and  $-80.8$  ‰ for  $\delta^2\text{H}$  at the

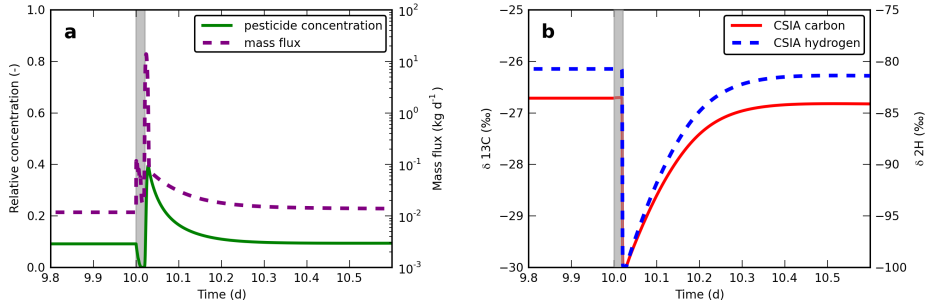


Figure 4.4: Response to the extreme rainfall event at the hillslope outlet immediately before and after the rainfall event: pesticide concentration and mass flux (a; note the logarithmic scale for the mass flux); and carbon and hydrogen isotope ratios of the pesticide (b). The timing of the rainfall event is shaded in grey.

hillslope outlet. According to the two-dimensional Rayleigh equation (Eq. 4.8), this corresponds to an extent of degradation of 73% at the hillslope outlet. It follows from Eq. 4.11 that the non-degraded fraction was approximately 27% ( $f_{\text{deg}} = 0.27$  in Eq. 4.11), while the residual fraction after the effect of dilution was 34% ( $f_{\text{dil}} = 0.34$  in Eq. 4.11). Dilution therefore contributed slightly less to the concentration decrease than degradation. The extent of degradation, derived from the simulated isotope values (Eq. 4.9), increased with depth and distance from the pollution source (Fig. 4.3d). With a value of 80%, it was highest in the deep bedrock and in the shallow soil layers at the footslope. The  $\theta$ -value, which compares the extent of degradation given by the two-dimensional Rayleigh equation to the model-based extent of degradation (Eq. 4.10), was largest below the application area (up to 25%). Apart from this area, the underestimation was  $< 20\%$ ; it was approximately 5% in the deep bedrock (Fig. 4.3f) and 11.5% at the hillslope outlet.

Figure 4.3e shows the relative contribution ( $F$ ) of the aerobic reaction to the overall degradation of the pesticide according to Eq. 4.6.  $F$  decreased rapidly with depth from a fraction of more than 0.9 in the topsoil below the pesticide application area to less than 0.2 in the deeper bedrock. At the hillslope outlet, it reached a value of 0.39.

### 4.3.2 Scenario 2: extreme rainfall event

Figure 4.4a illustrates the pesticide concentrations and mass flux at the hillslope outlet in response to the extreme rainfall event. It can be seen that with the onset of rainfall, concentrations first dropped and subsequently reached a distinct maximum. In contrast, the pesticide mass flux shows two peaks, with the second peak being much more pronounced than the first. In response to the rainfall event, the isotope signatures at the hillslope outlet dropped from their steady-state values of  $\delta^{13}\text{C} = -26.7\text{‰}$  and  $\delta^2\text{H} = -80.8\text{‰}$  to  $\delta^{13}\text{C} = -30.0\text{‰}$  and  $\delta^2\text{H} = -100.0\text{‰}$  (Fig. 4.4b). The latter values are the characteristic isotopic signatures of the pollution source. The minima in the isotope ratios coincided with the maximum in pesticide concentrations and the second peak in pesticide mass flux (Fig. 4.4a).

### 4.3.3 Scenario 3: transient simulation for water flow and solute input

The changing hydrological conditions and the annual pesticide application in scenario 3 induced a transient concentration response in the subsurface. We consider the first fifteen years of the transient simulation as spin-up period and focus on the results of the last five simulation years. Figure 4.5 shows a comparison of the pesticide concentration at two different times: after 19 years (panel a) and after 19 years and 50 days (panel b), thus 50 days after the last pesticide application. It illustrates that the pesticide plume from the new application mixed with the residual plume from the previous applications.

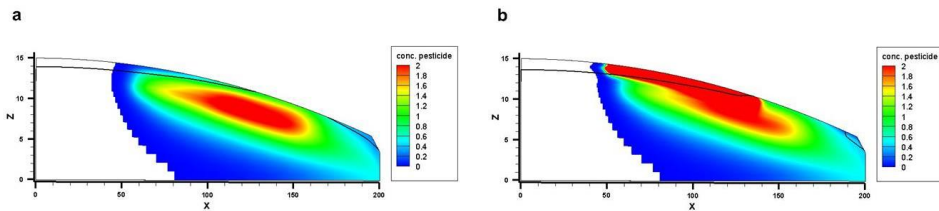


Figure 4.5: Pesticide plume before and after the last application: concentrations after 19 yr (a) and after 19 yr and 50 days (b). Areas with a concentration reduction of more than three orders of magnitude relative to a concentration of 1.0 are blanked because CSIA would not be possible due to detection limits. The black line indicates the position of the water table.

The inclusion of evapotranspiration into the simulation resulted in several periods of negative net infiltration, which followed the time of pesticide application (shaded areas in Fig. 4.6). Hereafter, this phase will be denoted as the dry period. The dry period was characterized by an increase in pesticide concentrations till the extreme rainfall event in August (Fig. 4.6b). Two other concentration peaks occurred later in each simulation year (beginning of November and end of February), while concentrations sharply dropped following increased rainfall in November. After the third concentration peak in February, the pesticide concentrations decreased again until the next pesticide application. In contrast to the steady state scenario, the pesticide concentrations at the hillslope outlet thus varied significantly and followed the same seasonal pattern every year. In particular, some of the days with high rainfall induced distinct minima in the pesticide concentrations.

Figure 4.6c shows the  $\delta^{13}\text{C}$  and  $\delta^2\text{H}$ -values, which alternated between periods of enrichment and depletion. Moreover, despite the 15-year spin-up period, the isotope ratios still increased slightly. The hydrogen isotope ratios declined to their minimum in the middle of the wet season and reached the highest value at the end of the dry season (shaded area). In contrast, the peak in carbon isotope ratios occurred at the onset of the dry season. While the sharp drops in pesticide concentrations correlate with the minima in  $\delta^2\text{H}$ , they correspond to maxima in  $\delta^{13}\text{C}$ .

The contribution of the aerobic degradation to overall degradation ( $F$ ) mirrored the seasonal pattern of the  $\delta^{13}\text{C}$ -values: the maximum occurred at the beginning of the dry season (Fig. 4.6d). In contrast, the extent of degradation ( $B$ ) increased with

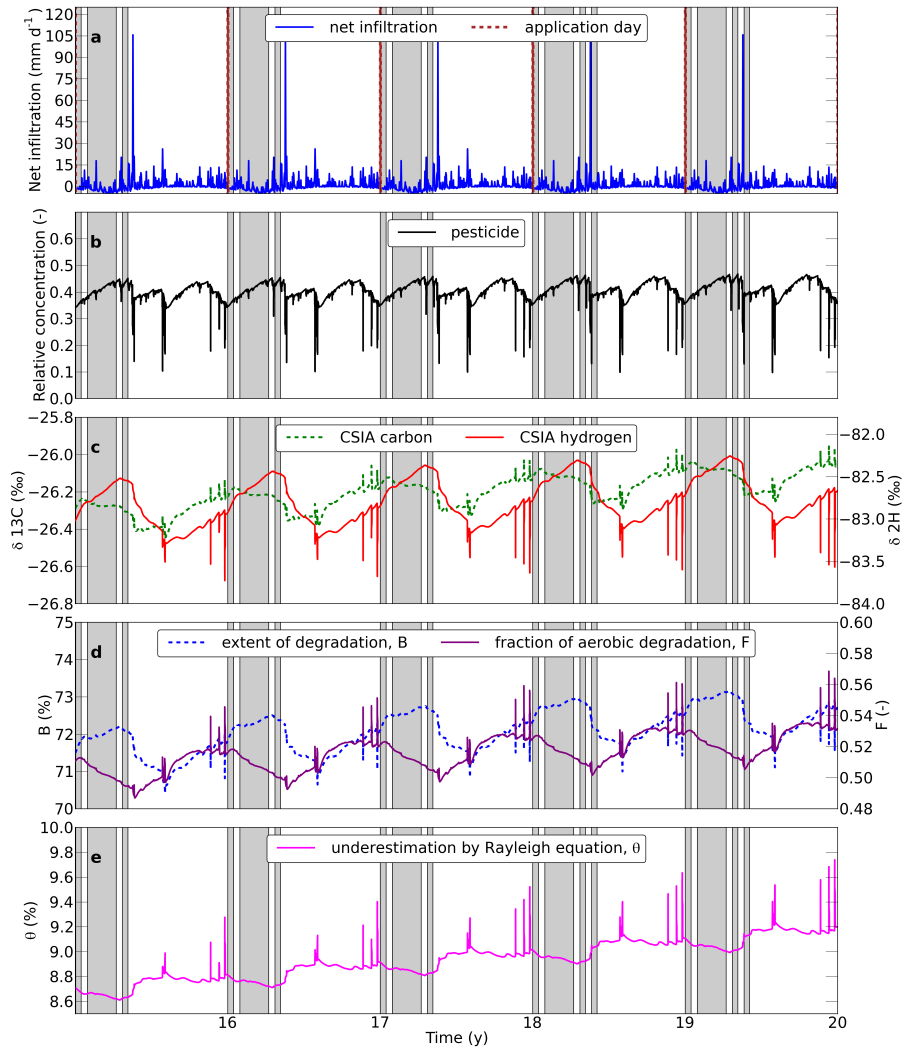


Figure 4.6: Results of the last five years of the transient simulation at the hillslope outlet (after 15 yr of spin-up): application days and net infiltration (a); pesticide concentrations (b);  $\delta^{13}\text{C}$  and  $\delta^2\text{H}$  isotope ratios (c); extent of degradation ( $B$ ) and relative contribution of the aerobic reaction pathway to overall degradation ( $F$ ) based on the two-dimensional Rayleigh equation approach (d); and underestimation of the extent of degradation resulting from the use of the Rayleigh equation (e). Periods with a negative net infiltration (dry periods) are shaded in grey.

increasing concentrations during the dry season and reached its maximum at the end of the dry season before the extreme rainfall event in August and subsequent precipitation. It thus shows a similar response as the  $\delta^2\text{H}$ -values (Fig. 4.6c). In addition, the parameters  $B$  and  $F$  reflect the response of the isotope ratios to rainfall events: while the distinct peaks in  $\delta^{13}\text{C}$ -values correspond to maxima in  $F$ , the drops in  $\delta^2\text{H}$ -values coincided with minima in  $B$ .

The underestimation of the extent of degradation ( $\theta$ ) that results from the use of the two-dimensional Rayleigh equation approach increased during the wet period and with subsequent simulation years; it reached a value of 9.2% at the hillslope outlet at the end of the transient simulation (Fig. 4.6e). In addition,  $\theta$  shows distinct peaks that are correlated with the concentration minima during rainfall events. With respect to the entire model domain, the maximum in  $\theta$  occurred in the shallow subsurface below the application area in response to every pesticide input. Subsequently, this zone of the highest  $\theta$  moved downgradient with the plume center (not shown).

## 4.4 Discussion

### 4.4.1 Pesticide movement through the hillslope

Scenario 1 yielded an average travel time of five years for the pesticide, which implies a relatively long response time to the emission of diffuse pollutants. This is consistent with elevated atrazine concentrations in a spring in a small catchment several years after the use of the herbicide had been abandoned (Gutierrez and Baran, 2009). Similarly, the pesticide reached the hillslope outlet approximately 1.4 years after the first application in the spin-up period of the transient scenario (scenario 3). This, in turn, highlights the potential time lag between the first use and the first detection of a newly introduced pesticide in stream flow. Analogous to the continuous detection of an abandoned compound, the extent of contamination caused by a new compound might manifest itself only after several consecutive application years. Moreover, the isotope ratios and derived parameters in the transient scenario did not reach an oscillatory steady state at the end of the 20-year simulation. Correspondingly, the extent of degradation ( $B$ ) still increased over the course of the last five simulation years (Fig. 4.6d). This is another indicator of the long response time of the modeled hydrological system to diffuse pollution.

At steady state, the pesticide concentrations in the shallow soil layers at the footslope were low (Fig. 4.3a), which resulted from their position above the water table during steady-state conditions: the transfer of pesticides into the unsaturated shallow soil close to the outlet could only occur via dispersion and diffusion from deeper layers, whereas the transport through the saturated zone was driven by faster advective transport. The part of the pesticide that was transported to the shallow subsurface at the footslope had, therefore, undergone more degradation than the pesticide that was present directly below the water table (Fig. 4.3d). Correspondingly, the shallow subsurface soil at the footslope also shows more enriched isotope ratios relative to other parts of the model domain (Fig. 4.3b and c).

The first two periods of increasing concentrations in each simulation year in transient scenario 3 ended abruptly in response to rainfall events (Fig. 4.6b). These rainfall events thus led to a pronounced dilution effect in the pesticide concentrations. In contrast, the third concentration peak in every simulation year did not precede a large rainfall event, but was related to a transition to wetter conditions (Fig. 4.6a), which induced a stronger dilution of pesticide concentrations. In summary, concentrations seem to be rather driven by the hydrological conditions than by the application pattern of the pesticide. However, the application pattern might have influenced the second phase of rising concentrations following the extreme rainfall event because the pesticide reached the hillslope outlet 1.4 years after the first application. The second increase thus coincided with the arrival of the pesticide plume from the previous year. Consequently, the hydrological conditions immediately affected the concentration pattern, whereas the response to the emission of the contaminant into the system was much more delayed and subdued.

The results of the steady-state simulation illustrate how the relative contribution of the aerobic degradation pathway ( $F$ ) rapidly decreased with depth (Fig. 4.3e). This is due to the fact that aerobic conditions solely occurred in the topsoil. Accordingly, flow lines that display long travel times through the bedrock exhibit a significant extent of degradation under anaerobic conditions. However, even directly below the application area,  $F$  did not attain its maximum value of one because of the effect of vertical dispersion that caused pesticide transport from the anaerobic subsoil into topsoil layers.  $F$  reached a steady-state value of 39.0% at the hillslope outlet, although the topsoil accounts for less than 3% of the total subsurface volume. This mainly resulted from the higher degradation rate in the topsoil (5 per year) than in the subsoil and bedrock (0.2 per year), which disproportionately increased the contribution of the aerobic reaction to overall degradation. Furthermore, the pesticide traversed the topsoil (i.e. aerobic zone) during infiltration and exfiltration, which enhanced the imprint of the aerobic degradation pathway. Correspondingly, the relatively small influence of anaerobic transformation indicates that a considerable part of the pesticide was transported via shallow flow pathways, which did not traverse the deeper bedrock and thus had a relatively short residence time in the anaerobic zone. The significant contribution of shallow flow pathways to hillslope discharge resulted, in turn, from the decrease in saturated hydraulic conductivity with depth. Hence, the chosen hydraulic properties also influenced the relative contribution of the aerobic reaction pathway to overall degradation.

#### 4.4.2 Carbon and hydrogen isotope ratios

In general, isotope ratios increased with travel distance, as more degradation leads to more pronounced isotope fractionation. This becomes apparent when considering the progressive enrichment in carbon and hydrogen isotope ratios with distance from the source area during steady state (Fig. 4.3b and c). However, carbon and hydrogen isotopes show a different strength of enrichment in the deep bedrock, which can be ascribed to the choice of enrichment factors for the aerobic and the anaerobic zones. In contrast to the hydrogen isotopes, the isotopic enrichment of carbon was stronger for the aerobic reaction pathway in the topsoil than for the anaerobic reaction

pathway in the subsoil and bedrock. Hence, the pesticide that crossed the topsoil for the second time during exfiltration shows the most pronounced enrichment in  $\delta^{13}\text{C}$ . In addition, this re-entrance into the topsoil was driven by a dispersive flux, which is, as explained before, associated with a higher degree of degradation than the advective flux. In contrast, the most enriched  $\delta^2\text{H}$ -values occurred in the deep bedrock, since long travel times through the subsurface induced, together with the high hydrogen enrichment factor under anaerobic conditions, the strongest fractionation effect for the hydrogen isotopes. Corresponding to these different areas of largest isotope fractionation for carbon and hydrogen, the two-dimensional Rayleigh equation (Eq. 4.8) yielded a high degree of degradation for the deep bedrock and the shallow soil layers at the footslope (Fig. 4.3d).

In scenario 3, the overall extent of degradation increased with longer residence times of the pesticide in the hillslope (i.e., with pesticide transport via deeper flow pathways). Therefore,  $B$  increased under drier conditions and was highest at the end of the dry season (Fig. 4.6d). The concentration increase during the dry season (Fig. 4.6b) thus resulted from less dilution due to little rainfall, and not from less degradation. Similar to scenario 1, the choice of enrichment factors also explains the differences in the seasonal patterns of the hydrogen and carbon ratios in scenario 3. Since the enrichment for hydrogen was assumed to be stronger in the anaerobic zone than in the aerobic zone, the increase in  $\delta^2\text{H}$  during the dry season reflects the increasing contribution of deeper groundwater. This agrees with the shape of the curve of the extent of degradation (Fig. 4.6d), which resembles more the pattern of  $\delta^2\text{H}$  than the pattern of  $\delta^{13}\text{C}$ . In general, an increasing contribution of deeper flow pathways, which implies longer travel times, also caused a higher degree of fractionation for the carbon isotopes. Nevertheless, a smaller relative contribution of the aerobic reaction pathway can account for a less pronounced overall fractionation effect for carbon because of the higher enrichment factor in the topsoil. Accordingly,  $\delta^{13}\text{C}$ -values increased during the wet season as a result of more degradation in the topsoil (Fig. 4.6d), which demonstrates that shallow flow through the topsoil was more pronounced under wet conditions. This finding agrees with Brown et al. (1999) and Rozemeijer and Broers (2007), who emphasized the increasing importance of shallow subsurface flow during rain events in headwater catchments and lowlands, respectively.

The simulation of isotope ratios allowed for quantification of the extent of pesticide degradation ( $B$ ). It was thus possible to compare the concentration reduction by dilution to the concentration reduction by transformation processes. In addition, the Rayleigh equation approach yielded the distribution between the aerobic and anaerobic reaction pathway ( $F$ ), which suggests that isotope data of two elements can, under favorable conditions, allow for the distinction between two reaction mechanisms. Moreover,  $F$  was used for the analysis of the relative importance of shallow and deeper flow pathways to pesticide fluxes to the stream. In summary, these analyses support the additional benefit of CSIA, as pesticide concentration data alone would not have allowed for the derivation of  $B$  and  $F$  in a real hillslope system.

### 4.4.3 Responses to rainfall events

The response of concentrations and isotope ratios to the extreme rainfall event in scenario 2 highlights the advantages of combined concentration and CSIA data. Judging by the peak in pesticide mass flux, the concentration minimum at the onset of the rainfall event has to be ascribed to initial dilution by rainwater (Fig. 4.4a). The subsequent concentration peak occurred shortly after the rain had ceased. Given that the mass flux shows a second maximum, this concentration peak stemmed from increased pesticide transport. However, it cannot be concluded from the concentration and mass flux data which mechanism led to increased pesticide transport. In contrast, the analysis of isotope ratios at the hillslope outlet reveals the underlying mechanism. During the rainfall event, the isotope ratios remained at the constant pre-event level despite the occurrence of surface runoff. This indicates that the surface runoff reaching the hillslope outlet did not contain any pesticide yet, which is due to the uphill location of the pollution source and the pesticide-free area at the lower hillslope. Subsequently, the isotope ratios decreased to the source values of  $-30\text{ ‰}$  and  $-100\text{ ‰}$ , respectively (Fig. 4.4b). This resulted from the arrival of contaminated surface runoff at the hillslope outlet, which occurred, by coincidence, at the end of rainfall. As the time lag between the release from the pollution source and the arrival at the hillslope outlet was too short (less than 30 minutes) to allow for significant degradation, the pesticide did not undergo any detectable fractionation. It follows that transport via surface runoff dominated the overall pesticide flux to the stream at that time. This scenario thus shows how the combined analysis of concentrations and isotope data can reveal the occurrence of surface runoff.

The first peak in mass flux prior to the arrival of contaminated surface runoff suggests that the rainfall event initially caused enhanced pesticide transport via exfiltration of shallow groundwater. This illustrates the concept of emission of "old" contaminant residues with pre-event water at the onset of rain (Burt and Pinay, 2005). Discharge of pre-event water can also be inferred from the analysis of the parameter  $F$ , which indicates a slightly enhanced contribution of topsoil degradation after the onset of rainfall and prior to the discharge of contaminated surface runoff (not shown).

Surface runoff in scenario 2 occurred as infiltration excess overland flow, which can be an important mechanism of pesticide transport from agricultural land (Doppler et al., 2012). The infiltration excess overland flow was generated by increasing the coupling length from 0.1 m to 0.8 m, which decreased the coupling between overland flow domain and subsurface domain. This can be considered an analogue for the decreased infiltration capacity of the soil as a result of surface sealing during high-intensity rainfalls. The same approach was applied in the HGS simulation by Verbist et al. (2012) to generate infiltration excess overland flow. A layer of low hydraulic conductivity at the surface would have had the same effect, but this would have required a modification of the model domain. Alternatively, the rainfall intensity could have been increased, but without changing the coupling length, a sufficiently long period of overland flow could have only been achieved with an unrealistically high rainfall amount (data not shown).

With a return period of nearly 60 years, the simulated rainfall event in scenario 2 corresponds to an exceptional event for mid-European climate. This extreme rainfall event was required to generate continuous overland flow from the area of the pesticide application to the hillslope outlet and thereby produce a discernible response in the isotope ratios in the stream. Nonetheless, scenario 2 can be considered representative of situations where the surface is sealed or has been disturbed (see above), or where a pesticide product is spilled on impermeable areas such as paved farmyard. In this case, subsequent surface runoff from these contaminated areas may lead to concentration peaks even during relatively dry periods (Holvoet et al., 2007; Kreuger, 1998). Similarly, preferential flow to drainage systems represents a fast transport route of pesticides that can lead to elevated pesticide concentrations in the absence of surface runoff at the application area (David et al., 2003). Pesticide transport via drain flow and surface runoff from impermeable areas can thus occur in response to rainfall of lower intensity. The response in isotope ratios would be comparable to the one simulated in scenario 2, and has already been observed for oxygen isotope ratios of nitrate: Ging et al. (1996) found elevated  $\delta^{18}\text{O}$ -values in a storm sewer, which were indicative of an atmospheric nitrate source, and ascribed them to surface runoff from impervious areas. Correspondingly, CSIA data that is measured during rain events could also be used for forensic source determination, i.e. for the distinction between different pesticide products and application areas that are characterized by different isotopic compositions.

The sharp drops in pesticide concentrations in response to large rain events in scenario 3 (Fig. 4.6b) resulted from dilution. Moreover, these drops also occurred on days with smaller events, provided that the rainfall (in combination with previous wet conditions) was sufficient to saturate the footslope. This had a similar dilution effect as high intensity rainfalls. The concentration minima correlate with minima in hydrogen isotope ratios, as high intensity rainfall and footslope saturation were accompanied by the discharge of more shallow groundwater, which had a shorter residence time and thus shows less hydrogen isotope fractionation. In contrast, the concentration minima correspond to peaks in the carbon isotope ratios, since they are associated with a relatively large contribution of topsoil degradation and thus more pronounced carbon isotope fractionation. Consequently, analogous to the seasonal pattern of isotope ratios, the different strength of isotope fractionation for the aerobic and the anaerobic reaction pathway resulted in the opposite behavior of carbon and hydrogen isotope ratios during single rainfall events. This demonstrates how CSIA can give insights into transport routes of a contaminant in a hydrological system, provided that reaction pathways can be attributed to different zones.

The rainfall events in scenario 3 that led to footslope saturation were accompanied by minima in the extent of degradation (Fig. 4.6d), since they induced discharge of more recently applied and thus less degraded pesticide. This agrees with previous findings about nitrate contamination where rainfall events led to a fast mobilization of soil nitrate with a relatively depleted  $\delta^{15}\text{N}$ -value, while increasing denitrification in soil between rainfall events resulted in progressively enriched  $\delta^{15}\text{N}$ -values (Kellman and Hillaire-Marcel, 2003). In contrast to the simulation of the extreme rainfall event in scenario 2, the isotope ratios did not drop to the initial values of the pesticide application area in scenario 3, which implies the absence of pesticide transport via surface runoff. This can be explained by the time lag of 137 days between the

pesticide application and the extreme rainfall event in August, which allowed for infiltration and degradation of the pesticide prior to intense rainfall as opposed to the simultaneous application of rain and pesticide in scenario 2.

#### 4.4.4 Validity of model assumptions

As shown above, the relative importance of the aerobic and anaerobic reaction pathways ( $F$ ) allowed for the analysis of the role of shallow and deeper flow pathways for pesticide transport. This analysis was facilitated by the model assumption of mutually exclusive reaction pathways with distinct enrichment factors that were active in specific hillslope layers. We considered this a reasonable assumption for aerobic and anaerobic degradation. In reality, however, reaction mechanisms might not be spatially exclusive, or their spatial distribution might be unknown. The analysis of transport routes based on  $F$  might therefore be restricted to cases where the reaction mechanisms occur in specific subsurface zones (e.g., anaerobic beneath the aerobic zone), and would be more complex for competing degradation pathways that occur simultaneously in space, entail a similar extent of isotope fractionation, or whose spatial distribution is unknown.

The simulations did not explicitly account for pesticide sorption, volatilization, or preferential flow pathways. Volatilization was not considered, as it would mainly lead to a decrease in the pesticide mass load at the pollution source. Moreover, as rainfall occurred soon after pesticide application in the simulations, we assumed a rapid mobilization of the applied compound and thus minor losses due to volatilization for the modeled system. This implies negligible volatilization-induced isotope fractionation under comparable hydrological conditions. However, depending on the properties of the pesticide, soil parameters, and meteorological conditions, volatilization losses can be up to 50% of the applied amount for some pesticides (van den Berg et al., 1999). If isotope fractionation at the pollution source due to volatilization is not considered in this case, CSIA might yield an inaccurate assessment of the extent of degradation.

Sorption to the solid phase can be relevant for pesticide transport in two ways: as sorption to suspended matter (e.g., in surface runoff), and as sorption to the soil matrix. Calculations under the assumption of equilibrium sorption revealed that transport with suspended matter in surface runoff is only relevant for highly sorbing compounds ( $\log K_{OC} > 4$ ; not shown). We therefore decided to disregard this transport route in our simulations. Simulation of sorption to the soil matrix would have had a retardation effect on pesticide transport to the hillslope outlet. If sorption had been included, it would have been possible to also simulate sorption-induced isotope fractionation in the soil matrix. This can result in an enrichment in heavy isotopes at the front and a depletion at the tail of a migrating groundwater plume (Kopinke et al., 2005; van Breukelen and Prommer, 2008). If isotopic enrichment is only attributed to degradation, CSIA can thus yield an overestimation of degradation for the plume front. However, we did not explicitly simulate sorption-related isotope fractionation, as this is only relevant in non-stationary plumes when degradation is slow (van Breukelen and Prommer, 2008), and would thus be insignificant in the modeled hillslope system. We also disregarded diffusion-induced

isotope fractionation effects, as their importance for the simulated system should be minor given the widespread nature of the emission and the relatively large spatial scope (van Breukelen and Rolle, 2012).

Similar to other virtual experiments with physically-based models (e.g., Hopp and McDonnell, 2009, 2011; James et al., 2010; Mirus et al., 2011; Mirus and Loague, 2013), we did not include preferential flow in the simulations. We anticipate that vertical preferential flow leads to a faster transition of water through the soil, and thus a decrease in the extent of degradation in the soil layers. This will, in turn, increase pesticide concentrations and decrease the isotope ratios at the hillslope outlet. Furthermore, vertical preferential flow would result in a lower contribution of the aerobic reaction pathway to overall degradation. The simulation of lateral preferential flow in the soil would decrease flow to the bedrock and result in a faster subsurface flow response to rainfall. This would, similar to vertical preferential flow, lead to less degradation and isotopic enrichment. However, the effect of lateral preferential flow pathways on the relative contribution of aerobic and anaerobic degradation to overall degradation, and thus on carbon and hydrogen isotope ratios at the hillslope outlet, depends on their location in the soil.

Even if the influence of preferential flow on concentrations and isotope fractionation is small, it may still affect the accuracy of the CSIA method, as it would cause enhanced mixing between recently applied pesticide and partially degraded pesticide in the soil. This might result in a stronger attenuation of apparent isotopic enrichment, and thus amplify the underestimation of degradation by the Rayleigh equation approach (Kopinke et al., 2005).

CSIA at downstream river monitoring points might be affected by polluted influent water from upstream parts, which could mask isotope fractionation effects in hillslope discharge at the stream monitoring point and, therefore, bias the quantification of pesticide degradation. Similarly, dry conditions can cause infiltration of polluted river water into the streambank or aquifer, which would perturb the pattern of gradual enrichment with increasing travel time in the hillslope. Hence, the simulation results primarily apply to gaining streams in headwater catchments or river sections that do not show mixing with residues of the same pesticide from upstream sources.

#### **4.4.5 Implications for the applicability of CSIA to assess pesticide transport and transformation**

In order to examine the applicability of compound-specific isotope analysis in the context of diffuse agricultural pollutants, the concentration decrease in scenario 1 needs to be compared to the difference between soil water concentrations and detection limits of CSIA. Initial soil water concentrations of up to a few milligrams per liter have been reported for pesticides at realistic application rates (Liu et al., 2012), while carbon isotopes of organic contaminants, including the pesticide atrazine and its metabolite desethylatrazine, could be measured at concentrations of around 100 ng L<sup>-1</sup> (Jochmann et al., 2006; Schreglmann et al., 2013). Consequently, the difference between pore water concentrations and the detection limit for carbon isotope analysis can be four orders of magnitude. By way of comparison, the simulation

yielded a concentration reduction by a factor 10 between the application area and the hillslope outlet. Therefore, the model results indicate that, given appropriate sampling and preconcentration techniques, low environmental concentrations of pesticides would not impede CSIA of diffuse river pollutants.

The magnitude of the simulated enrichment between the source area and the hillslope outlet in scenario 1 exceeds the uncertainty range of CSIA. Isotope ratios increased by 4 ‰ for  $\delta^{13}\text{C}$  and by 20 ‰ for  $\delta^2\text{H}$ , while the instrumental uncertainty is about 0.5 ‰ for carbon and 5 ‰ for hydrogen isotope analysis (Sherwood Lollar et al., 2007). This indicates that the enrichment in the isotopic composition at the hillslope outlet relative to the source values is detectable, which supports the use of CSIA in the analysis of diffuse river pollution under average hydrological conditions. We suggest that isotope ratios during baseflow conditions indicate the maximum potential for degradation, as they are not influenced by fast pesticide transport routes such as surface runoff (see scenario 2). It should be noted, however, that the magnitude of isotope enrichment depends, among others, on the site-specific travel times and isotope fractionation effects.

In contrast to the response to the extreme event in scenario 2, the isotope ratios in scenario 3 display only small variations, which did not exceed 0.3 ‰ for  $\delta^{13}\text{C}$  and 1.4 ‰ for  $\delta^2\text{H}$  during each simulation year. Hence, these small fluctuations would not be detectable based on the current accuracy of carbon and hydrogen CSIA. In the absence of overland flow, the assessment of the extent of in situ degradation on the basis of CSIA would thus yield the same results throughout the year. This suggests that grab samples for CSIA measurements are sufficient for a representative assessment of pesticide transformation between the pollution source and river monitoring point, except during events that result in direct transport via overland flow. This might, however, not apply to systems that show a larger temporal variation in the relative contribution of baseflow versus stormflow to streamflow, which could, for example, result from the activation of preferential flow pathways during rainfall events or a larger difference between the permeabilities of the soil and bedrock. A more pronounced variation in in-stream CSIA might also arise from pesticide use closer to the river than for the modeled hillslope, as rainfall events would then be more likely to lead to transport of recently applied pesticide into the river, while the dry season would be characterized by transport of strongly degraded pesticide via baseflow. Moreover, catchments with well-drained soils, long mean travel times and a high groundwater contribution to streamflow tend to dampen solute input signals to a much larger extent than catchments that exhibit more responsive soils and short mean transit times (Hrachowitz et al., 2013). Consequently, the latter systems might show a significant seasonal variability in isotope data that reflects the short emission pulses of pesticide application and the fast subsurface transport mechanisms in response to rainfall events. The determination of factors that would cause larger seasonal variabilities in in-stream CSIA was not the objective of this study, but should be addressed in future research.

During extreme rainfall events, only a fine temporal sampling resolution can allow for the detection of transient surface runoff, as the latter might only occur for a short time. According to the comparable response in concentrations and isotope ratios in scenario 2, the detection of surface runoff by CSIA requires the same temporal

resolution as concentration measurements. Analysis of isotope ratios in addition to concentrations during rain events requires the use of automatic sampling devices, which would also allow capturing surface runoff from potentially contaminated areas. If a concentration peak in the monitoring data occurs, CSIA could then additionally be performed in order to detect isotope ratios that correspond to typical values for pesticide products. This analysis can, however, only allow for the detection of contamination via surface runoff if the isotopic signature of the diffuse pollution source is known and distinguishable from isotope ratios that are associated with pesticide transport via subsurface flow pathways.

The model results for the isotope ratios allowed for a detailed analysis of the seasonal pattern of the extent of degradation ( $B$ ), the relative contribution of the aerobic reaction pathway ( $F$ ), and the underestimation by the use of the Rayleigh equation approach ( $\theta$ ). In the case of measured CSIA data, these parameters might, however, appear constant over time because of minor seasonal fluctuations in isotope ratios within analytical uncertainties. Nonetheless, even a constant value of these parameters can facilitate the analysis of the underlying transport and transformation mechanisms in the studied flow system. Since CSIA represents a unique method for the determination of these parameters, this highlights an additional benefit of isotope analysis in the context of diffuse river pollutants.

The extent of degradation during pesticide transport through the hillslope was determined by applying the Rayleigh equation to the simulated isotope ratios. Nevertheless, the Rayleigh equation is in principle only applicable to closed and fully mixed systems (e.g., to degradation experiments in microcosms; van Breukelen and Prommer, 2008). Hydrological systems such as the modeled hillslope are, however, open systems, which display a variety of transport and transfer processes. For example, dispersion leads to different transport routes with varying flow velocities to the same measurement point. Therefore, while some molecules might have been subject to strong isotope fractionation during transport along a flow pathway, others might have traveled much faster via a different pathway. The latter molecules exhibit less fractionation because of less exposure to degradation processes (Aravena and Hunkeler, 2009). In other words, physical heterogeneities of the aquifer and hydrodynamic dispersion can result in the attenuation of isotope fractionation effects that occurred in a part of the sample mixture only (van Breukelen and Prommer, 2008). This masking effect might also appear in areas where flow pathways from different layers mix (Kopinke et al., 2005). Consequently, if the Rayleigh equation approach is applied in such open flow systems, it tends to result in an underestimation of the extent of in situ degradation (Abe and Hunkeler, 2006; van Breukelen and Prommer, 2008). For the simulated hillslope system, the extent of degradation at steady state was significantly underestimated for the topsoil below the application area. This is due to the high degradation rate under aerobic conditions, which induced larger concentration gradients and thus larger dispersive fluxes than the slower reaction rate under anaerobic conditions. Large dispersive fluxes cause, in turn, an attenuation of isotopic shifts and, therefore, result in a more significant underestimation of the actual extent of degradation (van Breukelen and Prommer, 2008). Correspondingly, the zone of the strongest underestimation in scenario 3 was located at the plume center, as the pesticide plume is associated with the strongest concentration gradients in the system (not shown).

Although transient hydrological conditions are likely to cause enhanced mixing of different flow pathways, the degree of underestimation at the hillslope outlet in the steady state simulation was slightly larger than for the transient scenario. This might result from a greater importance of deeper flow pathways to pesticide transport at steady state, which agrees with a smaller contribution of the aerobic pathway at steady state than in the transient scenario. Pathways with a long travel time thus controlled the isotope ratios at the hillslope outlet to a larger degree in scenario 1 than in scenario 3. Consequently, the contribution of pesticide that displays advanced degradation and thus strong isotope fractionation to overall pesticide export was more significant at steady state. This, in turn, favored the masking of strong isotope fractionation in scenario 1, which resulted in a higher  $\theta$  for scenario 1 compared to scenario 3. Scenario 3 shows a higher  $\theta$  during the wet period than during the dry period (Fig. 4.6e), which illustrates the effect of mixing of different flow pathways on the accuracy of the Rayleigh equation: the growing relative contribution of more shallow flow pathways during wet conditions resulted in increased discharge of more recently applied pesticide, which led to an enhanced masking of the isotopic enrichment in deeper groundwater. The same mechanism caused the distinct peaks in  $\theta$  following rainfall events.

The underestimation of degradation due to the use of the Rayleigh equation is typically below 5% for groundwater plumes (Abe and Hunkeler, 2006). However, it has been shown that the underestimation can exceed 50% at fringes of pollution plumes, especially for high degradation rates and at large distances from the contaminant source (van Breukelen and Prommer, 2008; van Breukelen and Rolle, 2012). In view of the large underestimation for groundwater systems, the maximum  $\theta$ -value at the hillslope outlet of 11.5% and 10.0% in scenario 1 and scenario 3, respectively, can be considered negligible. Therefore, the simulation results suggest that CSIA yields a good assessment of in situ degradation, not only for aquifer systems, but also for more complex subsurface-surface systems that are subject to mixing of different flow pathways.

## 4.5 Conclusions

In this chapter, we present a model study of compound-specific stable isotope analysis (CSIA) in the context of diffuse pollution. The objective was to examine whether CSIA qualifies as a feasible and expedient technique for the analysis of transport pathways and the assessment of the extent of degradation of diffuse pollutants. We simulated reactive solute transport and isotope fractionation effects for a hypothetical hillslope. The model results support the usefulness of CSIA data in this context: the simulated isotope data allowed for the quantification of the extent of in situ degradation and the relative contribution of two competing pathways to overall degradation, which would not have been possible on the basis of simulated concentration data only.

The two-dimensional Rayleigh equation provided a reliable estimate of the overall extent of degradation under transient conditions. In particular, the inherent underestimation of the Rayleigh equation approach was small, considering the high degree of mixing of groundwater flow pathways from different depths at the hillslope

toe. The attenuation of isotope signals, which partly results from this mixing, did not exceed the degree of attenuation reported in previous studies of groundwater pollution plumes.

The simulation of an extreme rainfall event illustrated how isotope data can, as opposed to concentration data alone, reveal the occurrence of surface runoff and thereby indicate the fast transport of a diffuse pollutant to a river. In this way, CSIA might allow for the distinction between pollution via surface runoff or direct spillage, and via groundwater exfiltration solely. However, the simulation results also showed that surface flow might only be discernible in CSIA data for a very short period, which requires the use of automated sampling procedures during large rainfall events.

The simulation of transient hydrological conditions resulted in small seasonal variations in isotope ratios and derived parameters, which would not be detectable in CSIA data because they would fall within the uncertainty range of current analytical methods (with the exception of pesticide transport via surface runoff in response to rain events). For systems with a larger seasonal variation in isotope ratios (e.g., resulting from shallower and more permeable soils or the activation of preferential flow pathways in response to rain events), CSIA could yield a time-dependent estimate of the extent of degradation. In the case of a system with low seasonal variability such as the modeled hillslope, however, CSIA would give a stable result throughout the year, regardless of the temporal sampling resolution. This, in turn, supports the feasibility of CSIA in the analysis of pollutants in stream flow. Provided that the relevant underlying degradation mechanisms and associated isotope fractionation factors are known, CSIA thus offers a unique tool for the assessment of pesticide transformation, and, if the spatial distribution of the degradation mechanisms is known, even for a qualitative description of the interplay between transport via shallow and deep flow pathways.

Future modeling studies might extend this study to a three-dimensional catchment and incorporate in-stream degradation, or include several pollution sources to test CSIA as a tool for source identification and apportionment. Furthermore, transport via suspended matter should be considered for highly sorptive pesticides and erosion-prone sites. In addition to modeling studies, it is crucial to further test CSIA in experimental studies, especially in view of the low environmental concentrations (see chapter 5). In conclusion, the model results advocate the applicability and advantages of CSIA, and this study emphasized the potential benefits of CSIA in the characterization of diffuse river pollution.



# 5

## CSIA of pesticides: a combined monitoring and modeling approach to assess pesticide fate and degradation at catchment scale\*

**Abstract.** As pesticides are frequently found in stream water, it is crucial to assess pesticide transformation under field conditions. Compound-specific stable isotope analysis (CSIA) has proven useful in the characterization of contaminant transformation, but it has mainly been applied for groundwater contaminants, and not yet in the assessment of diffuse pesticide pollution. This chapter presents the first application of CSIA of pesticides at catchment scale. Concentration and carbon isotope data of two chloroacetanilide pesticides (S-metolachlor and acetochlor) were collected in a 47-ha agricultural catchment (Alteckendorf, Alsace, France) between March and August 2012 at three different spatial scales (plot, drainage outlet, catchment outlet). Measured pesticide concentrations at the catchment outlet were highest ( $65 \mu\text{gL}^{-1}$ ) following an intense rainfall event in the first month after pesticide application. Carbon isotope ratios increased by more than 2 ‰ between May and July 2012. In addition to these field CSIA data, this chapter also describes the first model-assisted interpretation of CSIA data at catchment scale. Discharge, pesticide concentrations and carbon isotope ratios in the Alteckendorf catchment were modeled with a conceptual two-compartment model based on non-stationary travel time distributions. Calibration against the field CSIA data allowed the assessment of the isotopic enrichment factor ( $\epsilon_C$ ), and slightly reduced model uncertainty in the quantification of pesticide degradation. We suggest that a finer temporal resolution than feasible in this study would more significantly reduce model uncertainty. Nonetheless, this chapter demonstrates how CSIA can provide clear evidence of pesticide degradation, and illustrates the benefits of a combined monitoring and modeling approach of concentration and CSIA data at catchment scale.

---

\*This chapter is in preparation for submission to a scientific journal with the following list of authors: Lutz, S. R.; van der Velde, Y.; Elsayed, O. F.; Imfeld, G.; Lefrancq, M.; Payraudeau, S., and van Breukelen, B. M.

## 5.1 Introduction

Diffuse pollution of groundwater and rivers is a common problem in agricultural catchments due to the extensive and deliberate application of pesticides to arable land. Therefore, numerous studies have analyzed pesticide concentration data to characterize degradation and transport of pesticides at catchment scale (Beernaerts et al., 2003; Doppler et al., 2012; Kreuger, 1998; Leu et al., 2004a; Richards and Baker, 1993). Understanding degradation at catchment scale is of high importance, as this process removes the applied pesticide product from the environment and, provided that the pesticide is completely mineralized or forms innocuous degradation products, annihilates its impact on the ecosystem. However, concentration data alone cannot conclusively indicate pesticide degradation and thus help distinguish destructive from non-destructive processes, as these data depend on various factors such as the application amount and timing (Battaglin and Goolsby, 1999) or the extent of dilution by pristine water (Schreglmann et al., 2013). Similarly, laboratory studies can elucidate the potential of specific mechanisms for pesticide degradation, but they can hardly indicate if and to what extent these mechanisms contribute to pesticide degradation under field conditions (Fenner et al., 2013). These limitations can be overcome by compound-specific isotope analysis (CSIA), which can serve as a clear indicator of contaminant degradation. CSIA measures the isotopic composition of the contaminant (i.e., the abundance of heavy isotopes relative to light isotopes of an element contained in the compound, e.g.  $^{13}\text{C}$  relative to  $^{12}\text{C}$ ). The isotopic composition tends to change under the influence of contaminant transformation (Elsner, 2010; Meckenstock et al., 2004), which is referred to as isotope fractionation. In contrast, non-destructive processes such as dispersion or sorption do, in general, not lead to significant isotope fractionation effects (van Breukelen, 2007b; van Breukelen and Prommer, 2008). Therefore, CSIA can allow for the detection and even quantification of natural degradation of the pesticide.

CSIA has been applied to study in situ degradation of organic groundwater contaminants such as monoaromatic and polyaromatic hydrocarbons (Blum et al., 2009; Vieth et al., 2005), MTBE (Kolhatkar et al., 2002; Zwank et al., 2005) and chlorinated ethenes (Hunkeler et al., 2005; Sherwood Lollar et al., 2001). In the context of diffuse agricultural pollution, it has mainly been applied to identify natural and anthropogenic nitrate sources, and provide evidence of denitrification (Divers et al., 2014; Johannsen et al., 2008; Kellman and Hillaire-Marcel, 2003; Voss et al., 2006). Although CSIA may confirm the occurrence of pesticide degradation (Fenner et al., 2013), CSIA data of pesticides remain restricted to the measurement of the isotopic composition of pesticide products (Annable et al., 2007; Weller et al., 2011), the change of the isotopic composition due to specific reaction mechanisms under laboratory conditions (Hartenbach et al., 2008; Meyer and Elsner, 2013; Meyer et al., 2009; Penning et al., 2010; Reinicke et al., 2011; Wu et al., 2014), grab samples of groundwater (Schreglmann et al., 2013), and the analysis of groundwater and stream water samples near a landfill (Milosevic et al., 2013). Chloroacetanilide herbicide degradation and associated isotope fractionation have been recently studied in lab-scale wetlands (Elsayed et al., 2014), but CSIA has not yet been repeatedly measured in stream water to evaluate in situ degradation of pesticides at catchment scale. This chapter presents the first field isotope data of

pesticides in surface runoff and stream water from an agricultural catchment. It discusses concentration and carbon CSIA data of two chloroacetanilide herbicides (S-metolachlor and acetochlor), which were collected in a 47-ha agricultural catchment (Alsace, France) at three different spatial scales (i.e., at a plot, at the outlet of a drain, and in the stream at the catchment outlet).

In addition to the field CSIA data, this chapter also describes the use of these data in a catchment-scale hydrological model. CSIA data and associated isotope fractionation effects have been previously simulated to characterize groundwater pollution (Atteia et al., 2008; D’Affonseca et al., 2011; Pooley et al., 2009; Prommer et al., 2009; van Breukelen et al., 2005; Wanner et al., 2012b). Moreover, this approach has been applied in chapter 4 in a virtual experiment of pesticide pollution at hillslope scale. In view of the acquired CSIA data of pesticides, we now present a two-compartment flow and transport model that describes pesticide transport, degradation and associated isotope fractionation at catchment scale. The transport formulation in this model is based on travel-time distributions, which allows calculating flux concentrations and mass fluxes of conservative and reactive solutes with a parsimonious model structure (Botter et al., 2010; van der Velde et al., 2012). This modeling approach has been applied to, e.g., simulate atrazine and chloride transport in agricultural catchments (Benettin et al., 2013; Bertuzzo et al., 2013).

In the current study, the objective of the modeling was to identify dominant processes affecting herbicide transport and degradation. In particular, the aim was to examine how the field CSIA data from the three different spatial scales can inform the modeling (e.g., by indicating which transport pathways and degradation kinetics have to be simulated), and thus to identify potential benefits of CSIA data in modeling compared to concentration data only. Moreover, the purpose of the modeling study was to analyze what additional information about herbicide transport and degradation can be gained from the model results (e.g., by comparing model and field-data based assessment of pesticide degradation and isotope fractionation). This chapter thus seeks to determine whether the use of CSIA data in a complementary monitoring and modeling approach allows for an improved assessment of the fate and degradation of diffuse pesticide pollution at catchment scale.

This chapter first describes the experimental setup and provides the field concentration and CSIA data of S-metolachlor and acetochlor. Second, it presents the model concepts for the simulation of pesticide transport, degradation and associated isotope fractionation. The chapter then discusses the results of the model calibration to the field data. This leads to a discussion of the added value of CSIA data in monitoring and modeling of pesticide transport and degradation.

## 5.2 Methods

### 5.2.1 Field measurements

#### Study catchment

The study was conducted in a 47-ha headwater catchment, located 30 km north of Strasbourg (Alteckendorf, Alsace, France). The mean annual temperature between

2005 and 2011 was 11.7°C, and mean annual precipitation and potential evapotranspiration were 704 mm ( $\pm 151$  mm) and 820 mm ( $\pm 28$  mm), respectively (data from Météo France station in Waltenheim sur Zorn at 7 km distance from the catchment). Arable land comprises 88% of the catchment area (of which 68% is corn, 16% winter wheat, and 4% sugar beets). The catchment is prone to mudslides; its mean slope is 6.7%, and the main soil type is loess. The catchment is drained by an artificial drainage network of unknown size; at least one drainpipe was active during the study period and continuously discharged into the ditch upstream of the catchment outlet (D1; Fig. 5.1). During the study period, an area of 77.2 m<sup>2</sup> was isolated on a sugar beet field (with a 60 cm high shield to a depth of 30 cm below the ground surface) for a controlled plot experiment (Fig. 5.1). A detailed description of the study catchment and experimental setup can be found in Lefranq (2014).

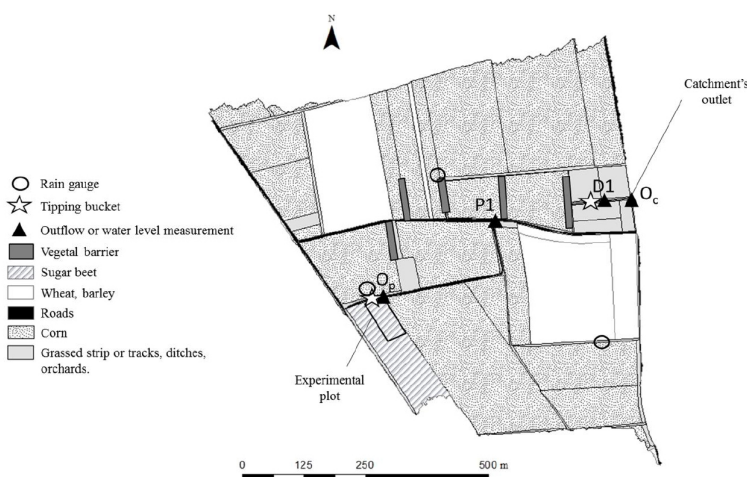
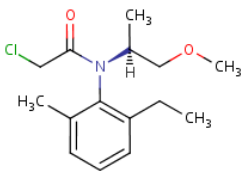
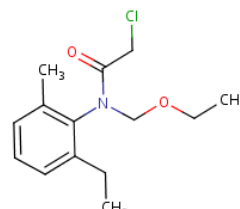


Figure 5.1: Scheme of the Alteckendorf catchment (Alsace, France).  $O_C$  and D1 indicate the outlet of the catchment and the drainage system, respectively. P1 shows the location of a pipe that conducts runoff water below a path. Surface runoff from the experimental plot was collected and measured at  $O_P$ .

## Study compounds

This study considers the two chloroacetanilide herbicides metolachlor (2-chloro-N-(2-ethyl-6-methylphenyl)-N-(2-methoxy-1-methylethyl)acetamide) and acetochlor (2-chloro-N-(ethoxymethyl)-N-(2-ethyl-6-methylphenyl)acetamide; Table 5.1). They rank among the most commonly applied pesticides (Grube et al., 2011) and are mainly used for pre-emergence weed control. Metolachlor consists of four stable stereoisomers; S-metolachlor (Table 5.1) denotes the two herbicidally active stereoisomers of metolachlor. Since the late 1990s, metolachlor products comprising all isomers have been progressively replaced by formulations that typically contain more than 80% of S-metolachlor (Buser et al., 2000). S-metolachlor is classified as moderately water-soluble ( $480 \text{ mg L}^{-1}$ ) and moderately mobile in soil ( $\log K_{OC}$  between 1.79 and 2.57). Acetochlor has a moderate solubility ( $282 \text{ mg L}^{-1}$ ) and mobility in soil ( $\log K_{OC}$  of 2.19). In the study year 2012, S-metolachlor was applied as the commercial formulations Mercantor Gold, Dual Gold, and Camix (Syngenta),

Table 5.1: Compound properties of the two study compounds S-metolachlor and acetochlor. Sources: University of Hertfordshire (2013); TOXNET database<sup>a</sup>.

	S-metolachlor	Acetochlor
		
Chemical formula	C <sub>15</sub> H <sub>22</sub> ClNO <sub>2</sub>	C <sub>14</sub> H <sub>20</sub> ClNO <sub>2</sub>
Molecular mass (g mol <sup>-1</sup> )	283.8	269.8
Solubility in water at 20°C (mg l <sup>-1</sup> )	480	282
Henry's law constant at 25°C (Pa m <sup>3</sup> mol <sup>-1</sup> )	2.2·10 <sup>-3</sup>	2.1·10 <sup>-3</sup>
log K <sub>OC</sub> <sup>b</sup>	1.79 – 2.57 <sup>c</sup>	2.19
Soil half life (d)	15	14
Half life for hydrolysis in water (d)	stable	stable

<sup>a</sup> U.S. National Library of Medicine; <http://toxnet.nlm.nih.gov>

<sup>b</sup> soil organic carbon-water partition coefficient

<sup>c</sup> Alletto et al., 2013

and acetochlor as the commercial formulation Harness (Dow Agrosciences).

### Data collection and sampling

Metolachlor and acetochlor have been used in the study catchment since the 1990s. To estimate the application of these compounds in the study year 2012, a survey was conducted among the farmers within the catchment. The survey showed that the two herbicides were mainly applied in the first two weeks of May; the total estimated application amount for the catchment was 10.4 kg of acetochlor and 11.0 kg of S-metolachlor. At the experimental plot, only metolachlor was applied (on April 12 and May 1). Discharge and concentrations of S-metolachlor and acetochlor were measured between March and August 2012 at the three different scales (plot experiment, O<sub>P</sub>; drain outlet, D1; and catchment outlet, O<sub>C</sub>; Fig. 5.1). At the catchment outlet, discharge was measured using a Doppler flowmeter (2150 Isco, Lincoln, Nebraska, USA), and flow-proportional samples were taken every 20 m<sup>3</sup> with a cooled automatic sampler (Isco Avalanche, Lincoln, Nebraska, USA). At the plot, only surface runoff was captured; it was collected in a polyethylene gutter, and water levels were determined with a Venturi channel and a surface water level sensor (ISMA, Forbach, France). Flow-proportional water samples at the plot were taken every 7 L with a cooled automatic sampler (Isco Avalanche, Lincoln, Nebraska, USA). Weekly grab samples were collected from the drain outlet.

### Concentration and CSIA analysis

S-metolachlor and acetochlor concentrations were determined according to the method described in (Lefranq, 2014). In brief, water samples were filtered through a 0.7  $\mu\text{m}$  glass-fiber filter and extracted by solid-phase extraction (AutoTrace 280 SPE system, Dionex, CA, USA). They were analyzed in a GC-MS/MS system (ITQ 700 model, Thermo Fisher Scientific, Les Ulis, France) using a OPTIMA 5MS column (30 m x 0.25 mm ID, 0.25  $\mu\text{m}$  film thickness, Macherey Nagel GmbH, Düren, Germany) with helium as carrier gas (flow rate of 1  $\text{mL min}^{-1}$ ). This yielded a mean analytical uncertainty of 8%, and quantification limits of 0.05 and 0.02  $\mu\text{g L}^{-1}$  for acetochlor and S-metolachlor, respectively.

The detailed method of carbon stable isotope analysis of S-metolachlor and acetochlor can be found in Elsayed et al. (2014). In brief, carbon isotope ratios of samples were determined in triplicates with a GC-C-IRMS system coupling a gas chromatograph (Agilent 6890) to an isotope ratio mass spectrometer (Finnigan MAT 252, Thermo Fischer Scientific). Analytes (4  $\mu\text{L}$  volume) were injected using a split/splitless injector run in splitless mode (held at 280°C), combusted with a GC/C III interface (set to 980°C), and transferred to a BPX5 chromatographic column (60 m x 0.32 mm, 0.5  $\mu\text{m}$  film thickness, SGE, Ringwood, Australia; heated stepwise from 50°C to 320°C) with helium as carrier gas (flow rate of 2.0  $\text{mL min}^{-1}$ ). Quality control of this procedure was achieved by regularly measuring reference carbon isotope ratios of S-metolachlor and acetochlor standards, which had been determined earlier with an elemental analyzer-isotopic ratio mass spectrometer (EA-IRMS, eurovector, Milan, Italy).

Carbon isotope ratios of samples  $\left(\left(\frac{^{13}\text{C}}{^{12}\text{C}}\right)_{\text{sample}}\right)$  are reported in per mil (‰) relative to the VPDB (Vienna Pee Dee Belemnite) standard ratio  $\left(\left(\frac{^{13}\text{C}}{^{12}\text{C}}\right)_{\text{VPDB}} = 0.0112372\right)$ :

$$\delta^{13}\text{C} = \frac{\left(\frac{^{13}\text{C}}{^{12}\text{C}}\right)_{\text{sample}}}{\left(\frac{^{13}\text{C}}{^{12}\text{C}}\right)_{\text{VPDB}}} - 1 \quad (5.1)$$

Carbon isotope ratios were obtained for six plot and six catchment samples for S-metolachlor (between one and nine weeks after the main application day), and three plot and five catchment samples for acetochlor (between two and six weeks after the main application day). Additionally,  $\delta^{13}\text{C}$ -values of the S-metolachlor formulation used in the plot experiment were determined (for a sample from the application tank and the applied pesticide). No  $\delta^{13}\text{C}$ -values of either herbicide were available for the drain outlet due to low concentrations and small sample volumes.

In the context of groundwater contamination, a conservative estimate of the extent of natural attenuation can be obtained from the Rayleigh equation approach:

$$\frac{R_S}{R_0} = f^{\alpha-1} \quad (5.2)$$

where  $R_0$  is the isotope ratio (e.g.,  $^{13}\text{C}/^{12}\text{C}$ ) of the contaminant at the contamination source,  $R_S$  is the isotope ratio of the contaminant in a groundwater sample

downgradient from the source,  $f_{\text{deg}}$  represents the remaining fraction of the contaminant in the sample relative to the source, and  $\alpha$  is the kinetic isotope fractionation factor (reported in per mil (‰) as the kinetic isotopic enrichment factor;  $\varepsilon = (\alpha - 1)$ ). In this study, we applied Eq. 5.2 to the field CSIA data at the catchment outlet, and calculated the extent of degradation based on the measured CSIA data ( $ED_{\text{meas}}$ ) as follows:

$$ED_{\text{meas}}(\%) = (1 - f_{\text{deg}}) \cdot 100 \quad (5.3)$$

In order to evaluate the potential use of the Rayleigh equation approach for catchment-scale application, we compared  $ED_{\text{meas}}$  to the simulated extent of degradation known from the mass balance of the pesticide model (see below).

### 5.2.2 Hydrological model

Similar to (Benettin et al., 2013; Bertuzzo et al., 2013), the parsimonious hydrological model comprises two storage reservoirs: a shallow reservoir, which represents crop leaves and the upper soil layers, and a lower groundwater reservoir (Fig. 5.2). The storage of the shallow reservoir ( $S_s$ ) is fed by precipitation ( $P$ ), and the groundwater reservoir by recharge from the shallow reservoir ( $R_{\text{gw}}$ ). Water in shallow storage can leave the reservoir as evapotranspiration ( $ET_s$ ) or discharge ( $Q_s$ ).  $Q_s$  is zero as long as the amount of water does not exceed the capacity of shallow storage. If the latter is reached, discharge flows to groundwater with a maximum recharge rate of  $R_{\text{max}}$ . Excessive discharge above  $R_{\text{max}}$  from the shallow reservoir is directly diverted to the stream as overland flow ( $OF$ ). Groundwater storage ( $S_{\text{gw}}$ ) is a function of recharge from the shallow reservoir ( $R_{\text{gw}}$ ), evapotranspiration from the groundwater reservoir ( $ET_{\text{gw}}$ ), and discharge to the stream ( $Q_{\text{gw}}$ ). We assumed that discharge from the groundwater reservoir is solely a function of storage (Kirchner, 2009). The model simulated discharge at the catchment outlet on a daily time step. The detailed equations of storage and fluxes for the hydrological model are given in Table S5.1 in the supplementary information to this chapter.

#### Travel time distributions

Travel time distributions characterize flow dynamics in a reservoir; they give the probability density function of the time that a water parcel spends inside the reservoir before leaving it via  $Q$  or  $ET$ , respectively (van der Velde et al., 2012; Botter et al., 2010). Travel time distributions also allow for the calculation of solute concentrations in  $Q$  and  $ET$  by convolution of travel time distributions and the relation between travel times and concentrations (Benettin et al., 2013; Botter et al., 2010). The shape of travel time distributions depends on the assumed mixing scheme, which specifies the time-variance of travel times, and the preference of  $Q$  and  $ET$  to remove water of a certain age from storage. For example, it may be sufficient for the description of a specific catchment to assume identical travel time distributions for  $Q$ ,  $ET$ , and any water parcel in the reservoir (i.e., complete mixing). In other cases, however, it might be required to simulate that  $ET$  predominantly removes young water and thus yields relatively older water in the reservoir (van der

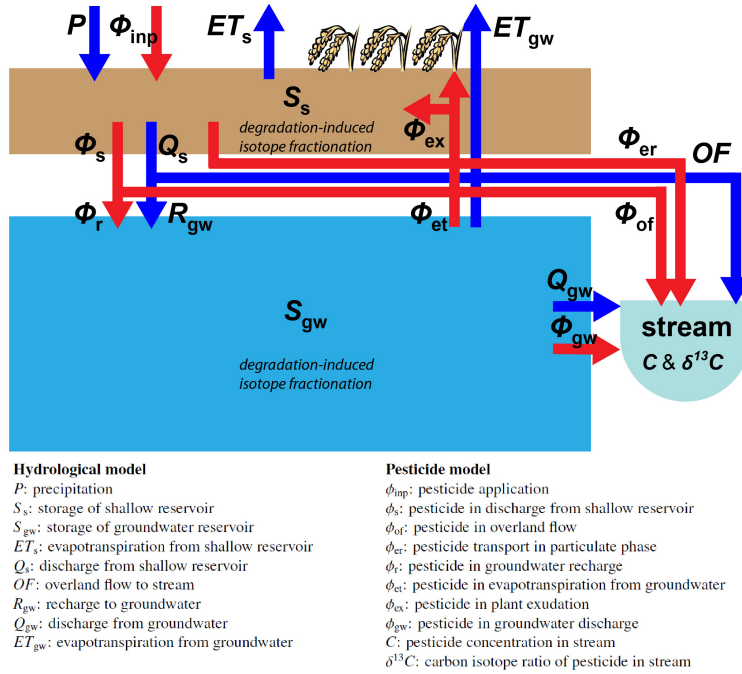


Figure 5.2: Scheme of flow (blue arrows) and pesticide transport routes (red arrows) from the shallow reservoir (brown box) and groundwater (blue box) to the stream (light blue semicircle). Pesticide concentrations were modeled separately for light and heavy carbon isotopes to simulate degradation-induced isotope fractionation.

Velde et al., 2012). In this study, we assumed variable flow with variable incomplete mixing, which means that travel time distributions are time-variant and different for ET, Q, and storage, and that the preference of Q for water of a certain age depends on storage (i.e., on wetness conditions in the catchment). A detailed description of the used mixing scheme and derivation of travel times can be found in van der Velde et al. (2014). Based on this mixing scheme, travel time distributions were numerically calculated for the modeled fluxes from the groundwater and shallow reservoir, which, in turn, yielded pesticide concentrations in  $Q_s$ ,  $Q_{gw}$ , and  $ET_{gw}$  (Table S5.2).

### 5.2.3 Pesticide model

The applied pesticide enters the model system via the shallow reservoir (mass flux  $\phi_{inp}$  in Fig. 5.2) and is assumed to immediately sorb to soil. Infiltration of precipitation leads to pesticide desorption and dissolution in the shallow reservoir. Pesticide in the dissolved phase of the shallow reservoir can leave this storage via discharge ( $\phi_s$ ), which leads to pesticide input to groundwater storage ( $\phi_r$ ) and, if this transport way is active, also to the stream via overland flow ( $\phi_{of}$ ). Pesticide in groundwater storage can be discharged to the stream ( $\phi_{gw}$ ), or enter plants and the shallow reservoir via evapotranspiration from groundwater ( $\phi_{et}$ ). Evapotranspira-

tion from groundwater was assumed to only transport a fraction of the pesticide mass into the shallow storage ( $\phi_{\text{ex}}$ ; Benettin et al., 2013; Bertuzzo et al., 2013). This mirrors incomplete uptake of pesticide in ET water by plants, and pesticide release to the soil after uptake (i.e., exudation by plant roots; Al-Khatib et al., 2002; Henderson et al., 2007). As the study catchment is prone to surface runoff and erosion, the model also accounts for direct pesticide transport from shallow storage to the catchment outlet via overland flow. This can occur in the dissolved phase after desorption ( $\phi_{\text{of}}$ ) or in the particulate phase via eroded material in overland flow ( $\phi_{\text{er}}$ ; without desorption). The eroded pesticide amount is proportional to discharge via overland flow and stored pesticide mass in the shallow reservoir. Pesticide in  $\phi_{\text{er}}$  plays an important role for the overall mass balance as it removes the pesticide from the shallow reservoir. As the pesticide can enter the stream via overland flow and groundwater discharge, concentrations in the stream (dissolved phase) were calculated from concentrations in overland flow and groundwater. S-metolachlor concentrations and carbon isotope ratios (see Eq. 5.4 below) were calculated on a daily time step. Table S5.2 in the supplementary information to this chapter shows the detailed equations for pesticide storage, mass fluxes and concentrations.

### Pesticide degradation and isotope fractionation

The model simulates pesticide degradation in the shallow and groundwater reservoir. We only considered degradation of metolachlor in the aqueous phase. Following Bertuzzo et al. (2013), we assumed first-order kinetics with a time-invariant degradation rate constant for the shallow reservoir. In contrast, we opted for a time-variant degradation rate constant in groundwater: the degradation rate constant in groundwater declines exponentially with travel time, which resembles a linear decrease in the degradation rate with depth given an exponential decrease in travel time with depth (van der Velde et al., 2010). This simulates slower pesticide degradation in groundwater compared to the topsoil (Albrechtsen et al., 2001), which is associated with the frequently observed decrease in microbial activity with increasing distance to the topsoil (Rodríguez-Cruz et al., 2006; Si et al., 2009).

The model was applied to calculate concentrations of light and heavy carbon isotopes contained in the pesticide separately, which allowed for the simulation of degradation-induced isotope fractionation: the light isotopes degraded with a rate constant  $r_0^{\text{L}}$ , which is related to the rate constant of the heavy isotopes ( $r_0^{\text{H}}$ ) by the isotope fractionation factor  $\alpha$  ( $\alpha < 1$ ) as  $r_0^{\text{H}} = \alpha \cdot r_0^{\text{L}}$ . For simplicity, we assumed identical fractionation factors for biodegradation in the shallow reservoir and groundwater. Simulated carbon isotope ratios were determined as

$$\delta^{13}\text{C}_{\text{sim}} = \frac{\left(\frac{^{13}\text{C}_{\text{sim}}}{^{12}\text{C}_{\text{sim}}}\right)_{\text{sample}}}{\left(\frac{^{13}\text{C}}{^{12}\text{C}}\right)_{\text{VPDB}}} - 1 \quad (5.4)$$

where  $^{13}\text{C}_{\text{sim}}$  and  $^{12}\text{C}_{\text{sim}}$  are the simulated concentrations of the heavy and light carbon isotopes of the pesticide, respectively, at the catchment outlet.

We disregarded abiotic degradation processes (e.g., photolysis) and potentially associated isotope fractionation effects in the modeling because of the lack of information about their importance for this study. We also assumed a negligible role of photolysis on the ground surface, as the application of metolachlor in a spray

formulation on bare soil presumably resulted in rapid infiltration of the herbicide into the topsoil and thus reduced susceptibility to photodegradation (Fenner et al., 2013; Rivard, 2003). Moreover, soil photolysis appears to play a minor role for metolachlor compared to biodegradation (Health & Consumer Protection Directorate, 2004; Joly et al., 2012; Parochetti, 1978).

### Pesticide volatilization and sorption

The model disregards pesticide transfer to and from the atmosphere (i.e., volatilization and deposition). We assume a minor role of volatilization for the field study, as pesticide application as spray formulation and precipitation soon after application presumably led to rapid infiltration of S-metolachlor into the soil. In addition, volatilization of metolachlor is generally considered low (Parochetti, 1978; Rice et al., 2002; Rivard, 2003), which also follows from its relatively small Henry's law constant (Table 5.1). As metolachlor only shows moderate sorption to solids (Rivard, 2003; University of Hertfordshire, 2013), we also neglected sorption in the groundwater reservoir. However, we considered sorption in the shallow reservoir to simulate the observed persistence of S-metolachlor in soil (see below). To this end, we assumed that water flowing through the shallow reservoir can only dissolve and transport a fraction of the adsorbed pesticide in the shallow reservoir depending on the contact time between water and soil, with decreasing dissolved pesticide concentrations with increasing water flow through the shallow reservoir. This mimics that water bypassing the soil matrix (i.e., preferential flow) dissolves little of the sorbed pesticide residues. Pesticide sorbed to suspended material entering the stream was not considered in the calculation of pesticide concentrations and isotope ratios in the dissolved phase (i.e., pesticide desorption from particles was neglected). Sorption-induced isotope fractionation was not simulated.

## 5.2.4 Input data and calibration

The model simulated discharge, pesticide concentrations and carbon isotope ratios from 1 September 2004 to 31 December 2012. It was run with daily data for precipitation and potential evapotranspiration ( $ET_{\text{pot}}$ ) from the meteorological station Waltenheim sur Zorn. The initial storage in the shallow and groundwater reservoir were calculated from the parameter values of  $S_{\text{max}}$  and  $S_0$ , respectively (Table 5.2). Pesticide input rates and dates of pesticide application for each simulation year were set to the application rates and dates in 2012 (known from the farmers surveys). The initial pesticide concentration was zero in the whole model domain.

Table 5.2 shows the range of parameter values used for the calibration of 16 of the 18 model parameters. The following data were used for calibration: daily average of discharge at the catchment outlet ( $O_C$ ; Fig. 5.1) between 9 March and 14 August 2012; 34 flow-proportional samples of S-metolachlor concentrations at  $O_C$  between 20 March and 21 August 2012, among which six with  $\delta^{13}\text{C}$ -values; and one grab sample of S-metolachlor concentrations at  $O_C$  on 20 November 2012. Model performance of each parameter set was evaluated with respect to the Nash-Sutcliffe coefficients for discharge ( $NS_Q$ ), concentrations ( $NS_C$ ) and carbon isotope ratios of S-metolachlor ( $NS_{\delta^{13}\text{C}}$ ; see section S5.3 in the supplementary information for a

Table 5.2: Parameters of the hydrological and pesticide model with the lower and upper bounds of the parameter value for model calibration.

Parameter	Symbol	Calibration	
		Lower bound	Upper bound
<i>Shallow reservoir</i>			
Storage capacity (mm)	$S_{\max}$	0.1	10
<i>Groundwater reservoir</i>			
Maximum recharge rate (mm d <sup>-1</sup> )	$R_{\max}$	5	50
First fitting parameter of storage-discharge relation (-)	$a$	10	20
Second fitting parameter of storage-discharge relation (-)	$b$	1	1.8
Storage for which discharge ceases (mm)	$S_0$	30	100
Storage for which ET starts to reduce (mm)	$S_{\text{red}}$	25	320
Storage for which ET ceases (mm); constrained to < $S_{\text{red}}$	$S_{\text{ext}}$	15	120
<i>Calculation of travel time distributions</i>			
Preference for young (< 1) or old (> 1) water in groundwater discharge during dry periods (-)	$\alpha_Q$	0.2	1.9
Change fraction of $\alpha_Q$ from the driest to wettest conditions <sup>a</sup> (-)	$\beta_Q$	0	0.95
Preference for young water in ET from groundwater (-)	$\alpha_{\text{ET}}$	0.01	0.8
<i>Pesticide model</i>			
Calibration factor for applied pesticide amount (-)	$m_{\text{IN}}$	0.95	1.05
Degradation rate constant (d <sup>-1</sup> )	$r_0$	0.02	0.14
Coefficient for decrease of degradation rate constant in groundwater with travel time (d <sup>-1</sup> )	$k$	$5 \cdot 10^{-3}$	0.03
Coefficient describing pesticide sorption in the shallow reservoir (d <sup>-1</sup> )	$l$	0.05	0.37
Fraction of pesticide transfer from groundwater to the shallow reservoir via ET and plant exudation (-)	$f_{\text{ex}}$	0.01	0.5
Eroded fraction of pesticide mass in the shallow reservoir with overland flow (mm <sup>-1</sup> )	$f_{\text{er}}$	$3.4 \cdot 10^{-4}$	0.02
Isotopic enrichment factor (‰)	$\varepsilon_C$	fixed at -1	
Carbon isotope ratio of the applied pesticide product (‰)	$\delta^{13}\text{C}_0$	fixed at -32.5	

<sup>a</sup> VIM model; van der Velde et al. (2014)

detailed description). First, preliminary model calibrations were run to determine the parameter set with the best model fit in terms of  $NS_Q$ ,  $NS_C$ , and  $NS_{\delta^{13}C}$  similar to the GLUE approach (Beven, 2012). Subsequently, in view of the relatively few field data points, we did not consider this parameter set as the only suitable one, but defined a range of values for the  $NS$ -efficiency around the best fit that indicated an equally suitable (i.e., behavioral) parameter set. Model parameters were then determined in 10000 calibration runs, which yielded 10000 behavioral parameter sets. In order to investigate the added value of the CSIA measurements, the calibration runs were classified into two sets: the first set contains simulations with  $NS_Q \leq 0.85$  and  $NS_C \leq 0.9$  (hereafter referred to as set 1); the second set of calibration runs is a subset of the first one with the additional constraint of  $NS_{\delta^{13}C} \leq 0.9$  (hereafter referred to as set 2). With this setup, it was tested whether set 2 yields a reduction in model-output uncertainty compared to set 1.

Preliminary calibration showed that the field CSIA data were not sufficient for calibration of the isotopic enrichment factor ( $\varepsilon_C$ ), as they contained too few samples to constrain the  $\delta^{13}C$ -values. Hence, to reduce equifinality of model parameters in the calibration procedure, the two parameters that only affect simulated  $\delta^{13}C$ -values were kept at predefined values for the final model calibration (i.e.,  $\varepsilon_C = -1 \text{ ‰}$  and  $\delta^{13}C_0 = -32.5 \text{ ‰}$ , respectively; Table 5.2). The value for the isotopic enrichment factor ( $\varepsilon_C$ ) was chosen such that large fluctuations in the simulated  $\delta^{13}C$ -values in periods between  $\delta^{13}C$ -measurements were avoided. This resulted in an  $\varepsilon_C$ -value at the lower end of the range of experimentally derived  $\varepsilon_C$ -values for the chloroacetanilide alachlor ( $-1.5 \pm 0.9 \text{ ‰}$  to  $-2.1 \pm 0.4 \text{ ‰}$ ), and below the range for acetochlor ( $-3.2 \pm 1.2 \text{ ‰}$  to  $-3.6 \pm 1.1 \text{ ‰}$ ), respectively (Elsayed et al., 2014). The isotopic signature of the applied pesticide ( $\delta^{13}C_0$ ) was assumed to be more negative than the one of the metolachlor formulation exclusively used in the plot experiment ( $\delta^{13}C = -31.9 \pm 0.3 \text{ ‰}$ ), which allowed simulation of measured  $\delta^{13}C$ -values as low as  $-32.4 \text{ ‰}$  at the catchment outlet.

## 5.3 Results and Discussion

### 5.3.1 Monitoring results

#### Drain outlet

Figure 5.3 displays S-metolachlor and acetochlor concentrations and carbon isotope ratios at the three spatial scales (i.e., drain outlet, plot, and catchment outlet). With a maximum concentration of 2.2 and 0.9  $\mu\text{gL}^{-1}$  for S-metolachlor and acetochlor, respectively, the weekly grab samples at the drain outlet (Fig. 5.3a and b) show low concentrations compared to concentrations at the catchment outlet (Fig. 5.3e and f) and in surface runoff at the plot (Fig. 5.3c and d). The low concentrations can be ascribed to the attenuating effect of dilution, degradation, and sorption during transport through the soil to the drain. Due to sorption and slow percolation through the soil matrix (apart from preferential flow), it is also possible that the pesticide that was applied in spring had not yet entirely reached the drainage network by the end of the sampling period (mid July).

The concentration maxima for S-metolachlor (2.2  $\mu\text{gL}^{-1}$ ) and acetochlor (0.9  $\mu\text{gL}^{-1}$ )

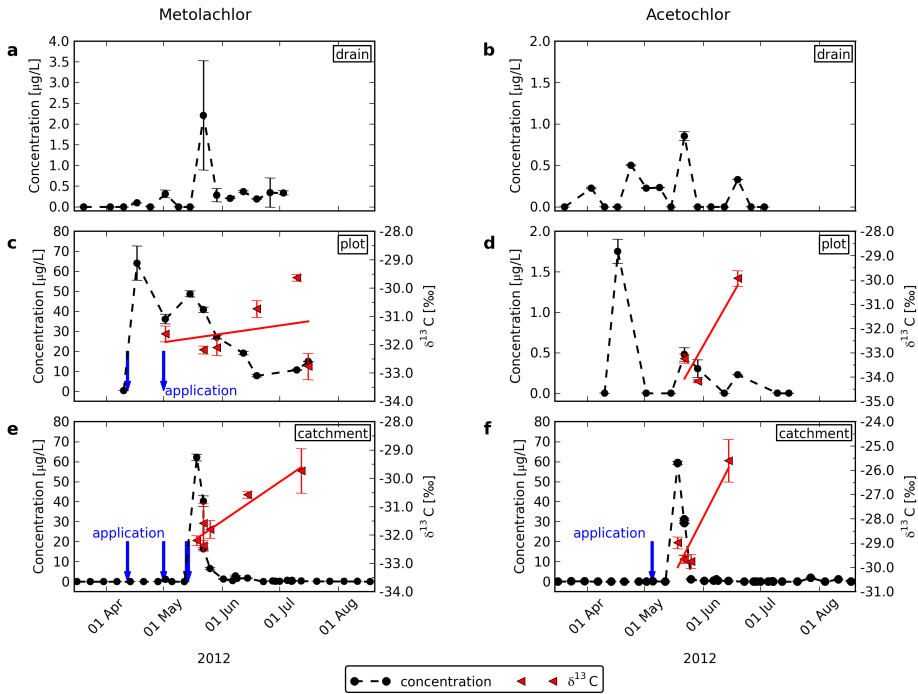


Figure 5.3: Measured concentrations (black dots) and carbon isotope ratios (red triangles) of S-metolachlor (panels on the left) and acetochlor (panels on the right) at the drain outlet (a and b), plot (c and d), and catchment outlet (e and f). Standard deviations of replicate measurements are indicated by vertical bars. Linear regression lines of carbon isotope ratios are indicated in red (coefficients of determination:  $R^2 = 0.06$  (c);  $R^2 = 0.81$  (d);  $R^2 = 0.92$  (e); and  $R^2 = 0.85$  (f)).

on 21 May can be attributed to the occurrence of an intense rainfall-runoff event (54 mm, return period of 40 years), which led to extensive overland flow and soil erosion. This event might have activated preferential flow pathways, which caused additional input of water with high pesticide concentrations from upper soil layers into the drainage system. However, the drain concentrations during this extreme event were much lower than the concentrations at the plot (Fig. 5.3c and d) and catchment outlet (Fig. 5.3e and f), as the drainage system did presumably not receive pesticide input via surface runoff or soil erosion.

As the drainage outflow was perennial, the concentrations during baseflow conditions can be considered representative of the background concentration in groundwater. Accordingly, background concentrations were below  $1 \mu\text{gL}^{-1}$  for both compounds, which highlights that groundwater exfiltration represents a secondary emission route for pesticides in the Alteckendorf catchment. Nonetheless, acetochlor was detected in the drain water in early April, which has to be attributed either to an early application in 2012, or to the use of the compound in previous years. According to the survey among the farmers, acetochlor was not applied before May 2012. Hence, this implies a high persistence of the compound in the soil, and would also explain the detection of acetochlor at the catchment outlet in late March.

### Plot experiment

Figure 5.3c and d show concentrations and carbon isotope ratios of S-metolachlor (left) and acetochlor (right) in surface runoff from the plot between mid April and mid July. S-metolachlor concentrations were highest during the first runoff event ( $64.1 \mu\text{gL}^{-1}$  on 17 April) following the first controlled metolachlor application (12 April). The second highest concentration ( $48.7 \mu\text{gL}^{-1}$  on 15 May) was associated with surface runoff in mid May, which mobilized metolachlor from the second controlled application (1 May) as well. Acetochlor concentrations also peaked during the first runoff event on 17 April, but at a much lower level ( $1.8 \mu\text{gL}^{-1}$ ), as this compound had not been applied at the plot. Its frequent detection in the plot samples must, therefore, be ascribed to contamination from surrounding fields, or, possibly, to applications in previous years.

After the first runoff event, plot concentrations of S-metolachlor remained above  $10 \mu\text{gL}^{-1}$  throughout the study period (except for 19 June), which indicates repeated mobilization of metolachlor residues from the topsoil by surface runoff or erosion. Metolachlor was thus persistent in the soil throughout the summer, which agrees with the field-derived degradation half life of 54 d based on soil samples from the plot experiment (Lefranq, 2014). The high concentration for the plot samples in comparison to the catchment outlet, which is mainly fed by drain flow except for surface runoff events, indicates that surface runoff is a major transport route for metolachlor in the Alteckendorf catchment. Moreover, the decreasing plot concentrations of S-metolachlor and acetochlor for subsequent runoff events suggest a gradual depletion of chloroacetanilide-herbicide residues in the topsoil. This can be attributed to mobilization by erosion and surface runoff, and degradation in between runoff events.

The  $\delta^{13}\text{C}$ -value of the pesticide product in the application tank was  $-31.9 \pm 0.31 \text{‰}$ . The gradual enrichment of  $^{13}\text{C}$  of S-metolachlor in surface runoff (Fig. 5.3c) indicates degradation of the compound at the plot. However, a significant increase in  $\delta^{13}\text{C}$ -values is only apparent for two runoff events at the end of the study period (19 June and 10 July). This suggests that substantial degradation might have only occurred in summer after a period of little microbial activity in April and May, which might be caused by low soil temperature or availability of nutrients, or a phase of adaptation of microorganisms to the applied pesticide (Albrechtsen et al., 2001). Therefore, the first runoff events caused mobilization of barely degraded S-metolachlor, whose  $\delta^{13}\text{C}$ -value was still in the range of the applied pesticide product. Acetochlor shows a faster and more pronounced enrichment between two samples from the end of May and mid June (Fig. 5.3d), but as it was not applied on the plot in 2012, other processes than transformation might be at the origin of this enrichment.

The  $\delta^{13}\text{C}$ -value of S-metolachlor in the last sample at the plot (16 July) dropped below the initial values of the applied product ( $\delta^{13}\text{C} = -32.8 \text{‰}$ ). This decrease was accompanied by a concentration increase relative to the two previous runoff events (Fig. 5.3c). A decrease in  $\delta^{13}\text{C}$  combined with a concentration increase can result from enhanced desorption of light carbon isotopes at later times, as these might preferably sorb to the soil matrix after pesticide application (Qiu et al., 2013). However, this effect is not likely to cause a decrease in  $\delta^{13}\text{C}$  of more than 3 ‰

within one week ( $\delta^{13}\text{C} = -29.6 \text{ ‰}$  on 10 July). It is thus not clear what caused this change in  $\delta^{13}\text{C}$  for the last sample.

### **Catchment scale**

S-metolachlor concentrations at the catchment outlet were highest ( $62.1 \mu\text{gL}^{-1}$ ) at the beginning of the extreme rainfall-runoff event on 21 May (Fig. 5.3e). Prior to this event, S-metolachlor was only detected once in late March at background concentration level. The rainfall-runoff event on 21 May caused extensive surface runoff and soil erosion, which, in turn, entailed metolachlor transport from the agricultural fields to the catchment outlet in the aqueous and particulate phase. Subsequent concentration maxima during later runoff events did not exceed  $10 \mu\text{gL}^{-1}$ . Moreover, concentrations gradually decreased from around  $2 \mu\text{gL}^{-1}$  in June to around  $0.1 \mu\text{gL}^{-1}$  in August. This indicates that metolachlor was mainly mobilized by the first runoff event after pesticide application (21 May), which is consistent with the estimated contribution of 96% of this event to total chloroacetanilide export during the study period (equal to 3.2% of the applied amount of S-metolachlor; Lefranq, 2014). Major pesticide losses to streams following the first rainfall events after pesticide application have been found in previous studies on pesticide transport in other agricultural catchments as well (Kreuger, 1998; Leu et al., 2004a; Louchart et al., 2001; Rabiet et al., 2010).

Similar to the plot scale, the relatively low S-metolachlor concentrations during runoff events in July indicate that the majority of metolachlor residues had already been removed from the topsoil before via surface runoff, infiltration, and/or degradation. However, the catchment-scale concentrations reflect a more complex system than the plot-scale concentrations, as the contamination at the catchment outlet can result from various agricultural plots within the catchment, where the herbicide was applied on different dates and in different amounts. The catchment outlet receives water from surface and subsurface flow, and the drain. We suggest that catchment discharge was essentially fed by surface runoff during storm events, and by drain outflow and groundwater seepage during low flow conditions. Accordingly, concentrations at the catchment outlet were similar to concentrations in surface runoff from the plot during the first runoff event. S-metolachlor was still detected at a concentration of  $0.1 \mu\text{gL}^{-1}$  in a grab sample at the catchment outlet in November (not shown), which indicates a high persistence of metolachlor residues in the system, given that the herbicide was only applied in spring.

Concentrations of acetochlor at the catchment outlet were comparable to those of S-metolachlor (Fig. 5.3f). For example, as observed for S-metolachlor, concentrations of acetochlor were highest in response to the rainfall event on 21 May, and rapidly decreased afterwards. However, the last two samples show a concentration increase following very low concentrations in July. This could result from a second application of the compound, but, to our knowledge, a summer application of acetochlor did not occur in the catchment. Another explanation for this late concentration increase might, therefore, be a delayed arrival of the pesticide in the drainage network due to slow pesticide transport through the soil matrix.

The total mass export in the dissolved phase at the catchment outlet between the end of March and mid of August was 3.3% for acetochlor and 1.8% for S-metolachlor

relative to the application amount (Lefranq, 2014), which indicates a higher mobility of acetochlor compared to S-metolachlor. The particulate phase accounted for 2.5% of acetochlor and 1.6% of S-metolachlor export. The more pronounced particulate transport for acetochlor compared to S-metolachlor might result from a slightly higher sorptivity of acetochlor compared to S-metolachlor ( $\log K_{OC}$  of 2.19 for acetochlor versus 1.79 – 2.57 for S-metolachlor; Table 5.1). A larger export in the particulate phase might increase the amount of acetochlor in the dissolved phase via desorption during transport to the catchment outlet, and thus cause a higher total export of acetochlor compared to S-metolachlor. Besides, a larger overall export for acetochlor might have also resulted from application-specific factors such as application practices, plant cover, or predominant use of acetochlor on fields near the catchment outlet (although not suggested by the survey). Another cause could be faster metolachlor degradation, which would result in less metolachlor residue available for transport to the outlet in comparison to acetochlor. However, more than 96% of total pesticide export occurred within two weeks after the main pesticide applications, which suggests that differences in degradation rates will only play a minor role for the total mass export compared to hydrological forcing, especially as both compounds have similar half lives in soil (Table 5.1).

Carbon isotope ratios of S-metolachlor and acetochlor at the catchment outlet became increasingly enriched with time, and show a difference of 2.7 ‰ and 4.1 ‰, respectively, between 21 May and 17 July (Fig. 5.3e and f). This increase in  $\delta^{13}C$ -values is indicative of gradual isotope fractionation due to degradation processes, which appears to be more pronounced for acetochlor than for S-metolachlor. Carbon isotope ratios of S-metolachlor were similar for the plot and catchment outlet:  $\delta^{13}C$ -values were in the range of the applied product during the first runoff events in May (-32.2 to -31.6 ‰ at the plot and -32.4 to -31.6 ‰ at the catchment outlet, respectively), and became gradually enriched in June and July (maximum of -29.6 ‰ and -29.7 ‰ at the plot and catchment outlet, respectively). This indicates a comparable extent of degradation at both spatial scales. The only exception to the general trend of isotopic enrichment is the significant decrease in  $\delta^{13}C$ -values between the last two plot samples, which was not observed at the catchment outlet. This suggests that local effects such as late desorption, which might have caused the decrease in  $\delta^{13}C$ -values at the plot, became masked at catchment scale due to the general increase of carbon isotope ratios with time. However, the CSIA data at catchment scale might be subject to variations resulting from the use of different metolachlor formulations: although the same commercial product accounts for about 80% of metolachlor applications in the study year, the remainder may have caused metolachlor input with a different initial isotopic composition (no information available) at different times. This would cause variations in  $\delta^{13}C$ -values at catchment scale even without any degradation-induced change in the isotopic composition. The relatively coarse temporal resolution of  $\delta^{13}C$ -measurements did not allow to discern such an effect.

As also seen for S-metolachlor,  $\delta^{13}C$ -values of acetochlor at the plot and catchment scale became significantly enriched between May and July (above 3 ‰). This confirms the hypothesis of similar isotope fractionation effects at both spatial scales. However, in the case of acetochlor, plot samples show a systematic shift of approximately 4 ‰ towards more depleted values compared to the catchment

samples (Fig. 5.3d and f). This might result from the use of an acetochlor formulation near the plot that has a more depleted  $\delta^{13}\text{C}$ -value than the predominantly used product at catchment scale, although the farmers survey suggests application of a single commercial product on all fields during the study year. Therefore, a more plausible explanation would be volatilization of acetochlor from surrounding fields and subsequent deposition on the experimental plot, which would favor the deposition of pesticide with a relatively depleted  $\delta^{13}\text{C}$ -value. As acetochlor was not applied on the experimental plot, this might have resulted in the detection of solely deposited and thus isotopically depleted acetochlor at the plot scale.

### 5.3.2 Modeling results

#### Feedbacks from monitoring to modeling

The monitoring results were used for building and validating the conceptual flow and transport model. First, the low drain concentrations of the two herbicides (Fig. 5.3a and b) suggested that pesticide export via groundwater discharge is of secondary importance. This could only be achieved by assuming pesticide degradation not only in the shallow reservoir, but also in the groundwater reservoir. However, the field CSIA data from the catchment outlet indicated that degradation in groundwater is slower than in the shallow reservoir: trial model runs with the same degradation rate constant in both compartments resulted in a too large enrichment in modeled  $\delta^{13}\text{C}$  compared to the measurements, even with  $\varepsilon_{\text{C}}$ -values at the lower end of the plausible range ( $\varepsilon_{\text{C}} = -1.0\text{‰}$ ; not shown). Moreover, whereas decreasing this degradation rate constant would have led to less enrichment, it would have also produced high pesticide concentrations until late autumn, which is inconsistent with the measured concentrations. Therefore, we assumed first-order degradation kinetics in the shallow reservoir, and applied a time-dependent exponential decrease of the degradation rate constant in the groundwater compartment (see section 5.2.3 and Table S5.2).

The monitoring results highlighted the role of overland flow as most important pesticide transport way during the study period. Correspondingly, the measured carbon isotope ratios demonstrated the need for a direct transport route from the shallow reservoir to the stream, which would avoid further degradation-induced isotope fractionation in groundwater and, consequently, allow modeled  $\delta^{13}\text{C}$ -values in the range of the applied pesticide product following the extreme rainfall event on May 21. Therefore, we incorporated overland flow and associated pesticide transport in the dissolved phase into the model structure. In addition, pesticide transport in the particulate phase appeared to be significant during intense precipitation. Hence, we also included soil erosion from the shallow reservoir, which is proportional to the amount of overland flow (see section 5.2.3).

The relatively long persistence of both pesticides and the late enrichment in carbon isotope ratios at the plot indicated the presence of a limiting factor for pesticide degradation in the soil. This was included in the modeling by assuming no degradation for sorbed pesticides, which allowed for repeated pesticide release with discharge from the shallow reservoir in response to rainfall events. This agrees with the observed concentration peaks at the plot and catchment scale following rainfall

events. The repeated pesticide release from the shallow reservoir resulted, in turn, in a long tailing of modeled S-metolachlor concentrations in groundwater discharge, which is in line with concentrations above the quantification limit until late autumn, as suggested by the grab sample from the catchment outlet in November.

### Multiple model calibrations

Figure 5.4 displays the measurements (red lines) and model results for discharge, S-metolachlor concentrations and carbon isotope ratios at the catchment outlet. The calibration run with the best fit in terms of the mean of  $NS_Q$ ,  $NS_C$ , and  $NS_{\delta^{13}C}$  is shown as black line; the ranges of all calibration runs in calibration set 1 (i.e.,  $NS_Q > 0.85$  and  $NS_C > 0.9$ ) and calibration set 2 (i.e.,  $NS_Q > 0.85$ ,  $NS_C > 0.9$ , and  $NS_{\delta^{13}C} > 0.9$ ) are indicated as light and dark grey area, respectively. Whereas the ranges of set 1 and 2 for modeled discharge, concentrations, and isotope ratios are narrow during the calibration period (March to August), they are much larger outside the calibration period, where model results were not constrained by their fit to measurements. The model generally captured the measured discharge (Fig. 5.4a), and also succeeded in reproducing the general concentration pattern: concentrations were low prior to pesticide application, and increased during high-flow conditions, with the maximum following the extreme rainfall event on May 21 (Fig. 5.4b). However, as the occurrence of overland flow in the model requires discharge from the shallow reservoir above the maximum recharge rate, it underestimated peaks in discharge and concentrations. Some calibrations yielded concentrations in the low  $\text{ng L}^{-1}$  range in late summer due to the absence of outflow from the shallow reservoir (i.e., no pesticide release), which matches periods of measured concentrations below the quantification limits. Subsequently, concentrations increased again due to pesticide input from the shallow reservoir following precipitation in early autumn. This simulates persistence of metolachlor in topsoil throughout summer, which would explain the detection of pesticide at the catchment outlet several months after the application period.

Modeled carbon isotope ratios gradually increased after pesticide application in April and May, which reflects the progressive enrichment of  $\delta^{13}C$ -values in groundwater discharge due to pesticide degradation. Due to the scarcity of the field CSIA data, calibration results for  $\delta^{13}C$ -values are associated with a wide range of possible values outside the period with measurements (Fig. 5.4c). Whereas the relatively small enrichment in observed  $\delta^{13}C$ -values restricts the increase in carbon isotope ratios during the study period, the range of behavioral simulations suggests a more pronounced enrichment in early autumn.

Although degradation in both model compartments induces isotope fractionation with the same  $\varepsilon_C$ -value, the modeled curve of  $\delta^{13}C$ -values is not monotonously increasing, but shows local minima following rainfall events. These rainfall events caused pesticide transfer from the shallow reservoir to groundwater. Pesticide in discharge from the shallow reservoir is, despite the larger degradation rate constant, associated with a smaller extent of degradation than pesticide in groundwater, as degradation does not occur for the sorbed pesticide. Therefore, transport of recently desorbed pesticide from the shallow reservoir to groundwater is reflected in lower carbon isotope ratios at the catchment outlet. In addition, rainfall events result in a temporal decrease in travel times in the groundwater reservoir, which, in turn,

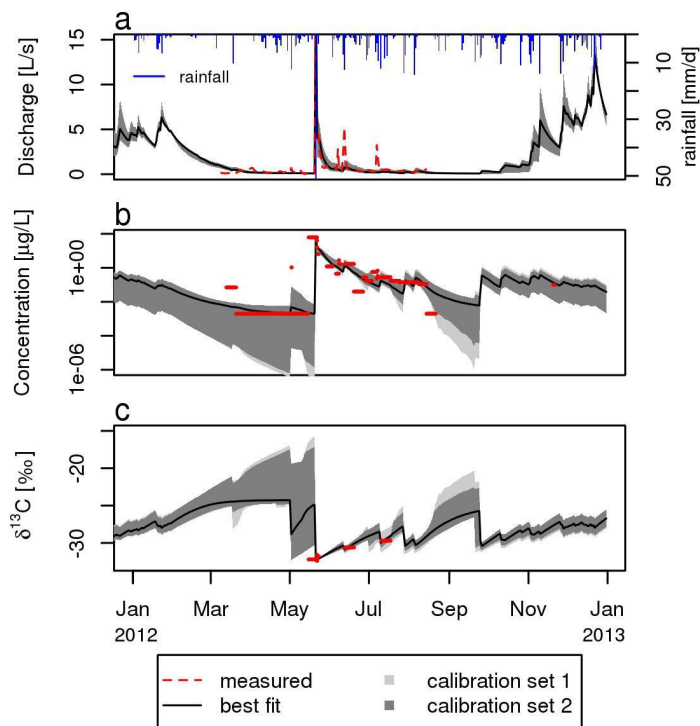


Figure 5.4: Measured (red lines) and modeled time series for discharge (a), S-metolachlor concentrations (b), and carbon isotope ratios (c) in 2012. The black line indicates the results of the calibration run with the best fit in terms of the mean of  $NS_Q$ ,  $NS_C$ , and  $NS_{\delta^{13}C}$ . The shaded areas show the ranges of behavioral calibration set 1 ( $NS_Q \leq 0.85$  and  $NS_C \leq 0.9$ ; light grey) and 2 ( $NS_Q \leq 0.85$ ,  $NS_C \leq 0.9$ , and  $NS_{\delta^{13}C} \leq 0.9$ ; dark grey), respectively. Blue bars in (a) indicate daily precipitation.

shortens the time for degradation and associated isotope fractionation to occur during transport through groundwater. Consequently, rainfall events during spring and summer resulted in a decrease in carbon isotope ratios relative to low-flow conditions. This decrease was strongest following the rainfall event on May 21. In contrast, the effect of precipitation on  $\delta^{13}C$ -values was much less apparent in late autumn and winter, as most of the pesticide had already been removed from the shallow reservoir. A stronger isotope fractionation (i.e., a more negative  $\varepsilon_C$ ) would have resulted in even larger fluctuations in modeled  $\delta^{13}C$ -values in response to pesticide release from the shallow reservoir. Due to the limited temporal resolution of the field CSIA data, it is not possible to conclude whether these fluctuations occurred in reality.

According to the range of simulation results and the simulation with the best fit, carbon isotope ratios show two distinct minima in spring: after the second metolachlor application at the plot (May 1), and after the extreme rainfall event on May 21 (Fig. 5.4c). These minima reflect the arrival of recently applied pesticide at the catchment outlet, which had undergone little degradation and, therefore,

shows little isotope fractionation. Prior to the first minimum, the increase in  $\delta^{13}\text{C}$ -values for the best fit leveled off, which indicates that isotope fractionation became negligible prior to pesticide application. This can be attributed to discharge of pesticide from the previous year, which is associated with long travel times. These long travel times imply a significant decrease in the rate of pesticide degradation in groundwater (exponential decrease with travel time in groundwater), which resulted, in turn, in negligible isotope fractionation and thus flattening of the  $\delta^{13}\text{C}$ -curve before May. Hence, the results for the best model fit suggest little degradation of the pesticide once it has passed through the upper soil layers. This would also explain S-metolachlor detection several months after its application in the study catchment, and agrees with experiments of pesticide degradation in groundwater, which have shown decreasing rates of pesticide degradation with decreasing pesticide concentration (Albrechtsen et al., 2001).

### Quantification of pesticide transport and degradation

The mean amount of applied pesticide that was transported to the catchment outlet in dissolved and particulate form in 2012 was  $1.9 \pm 1.5\%$  in simulations with  $NS_{\delta^{13}\text{C}} > 0.9$  (set 2), of which 1.6% occurred via overland flow (Table 5.3). The remaining 0.3% indicates low pesticide export by groundwater discharge, which is in line with the low concentrations in the drain outlet (Fig. 5.3a). The average extent of pesticide degradation in 2012 for calibration set 2 was  $97.4 \pm 1.9\%$  of the applied amount (84.9% in the shallow reservoir and 12.5% in groundwater, respectively). Correspondingly, only 0.7% of the applied pesticide was still retained in the modeled catchment at the end of 2012. For the study period only, the model simulated the same mass export as for the whole year for both calibration sets (1.9%; Table 5.3), which closely matches a mass export of 1.8% calculated from measured concentrations. The mass balance also highlights the role of overland flow for pesticide transport. This becomes apparent when comparing the modeled contribution of overland flow in the years 2011 and 2012: erosion accounted for the bulk of pesticide transport in 2012, whereas it did not occur in the simulation of 2011 (Table 5.3). Therefore, modeled pesticide transport to the stream only occurred via groundwater, and was thus negligible in 2011. This resulted in a more significant pesticide retention in the catchment at the end of 2011 (around 5%) compared to the year 2012 (less than 1%).

Information about retained and degraded pesticide amount cannot easily be obtained from the measurements alone. Application of the Rayleigh equation to the field CSIA data can, however, yield a rough estimate of the extent of degradation. If we assume the same enrichment factor and initial isotopic signature of the applied product as in the model (i.e.,  $\varepsilon_{\text{C}} = -1 \text{‰}$  and  $\delta^{13}\text{C}_0 = -32.5 \text{‰}$ , respectively), the Rayleigh equation approach gives an extent of degradation of  $ED_{\text{meas}} = 94.2\%$  (Eq. 5.3) for the last CSIA sample (17 July). The mass balance of the model (set 2) suggests a lower extent of degradation of  $76.0 \pm 6.3\%$  between 1 May and 17 July. However, the result of the Rayleigh equation approach is presumably not representative of the extent of degradation occurring in the whole system, as it describes the extent of degradation specifically for the environmental sample, which will, in general, differ from that for the bulk of the diffuse pollutant in the entire system. For example, while application of Eq. 5.3 only accounts for isotope

Table 5.3: Amount of degraded and transported pesticide for behavioral calibration set 1 ( $NS_Q > 0.85$  and  $NS_C > 0.9$ ) and set 2 ( $NS_Q > 0.85$ ,  $NS_C > 0.9$ , and  $NS_{\delta^{13}C} > 0.9$ ) in the simulation years 2011, 2012, and study period.

	Study period (CSIA) <sup>a</sup>		2012		2011	
	Set1	Set2	Set1	Set2	Set1	Set2
<b>Degradation (%)</b>	<b>72.0±9.2<sup>b</sup></b>	<b>76.0±6.3</b>	<b>97.1±2.2</b>	<b>97.4±1.9</b>	<b>94.7±2.5</b>	<b>95.0±1.9</b>
Shallow reservoir (%)	67.7±9.7	72.1±6.3	83.7±3.9	84.9±3.0	88.7±4.3	89.6±2.8
Groundwater (%)	4.3±1.2	4.0±0.9	13.5±3.4	12.5±2.5	6.0±2.2	5.4±1.5
<b>Transport to stream (%)</b>	<b>1.9±1.5</b>	<b>1.9±1.5</b>	<b>1.9±1.5</b>	<b>1.9±1.5</b>	<b>0.1±0.0</b>	<b>0.1±0.0</b>
Overland flow – dissolved (%)	0.2±0.1	0.2±0.1	0.2±0.1	0.2±0.1	0	0
Overland flow – eroded (%)	1.4±1.5	1.4±1.5	1.4±1.5	1.4±1.5	0	0
Groundwater discharge (%)	0.3±0.1	0.3±0.1	0.3±0.1	0.3±0.1	0.1±0.0	0.1±0.0
<b>Total (%)</b>	<b>73.9±9.2</b>	<b>77.9±6.3</b>	<b>99.0±1.7</b>	<b>99.3±1.3</b>	<b>94.7±2.5</b>	<b>95.1±1.9</b>

<sup>a</sup> 1 May to 17 July

<sup>b</sup> mean ± standard deviation of all runs

fractionation of the pesticide that was transported to the catchment outlet (only 1.9% of the applied amount), the pesticide that is still retained in the system (e.g., due to sorption or slow transport via groundwater) might be more or less susceptible to degradation. This part of the applied pesticide might get discharged at a later point, or be dominant in the  $\delta^{13}C$ -values during low-flow periods that were not captured in the CSIA data. This is opposed to closed laboratory systems or steady-state groundwater plumes, where the calculated extent of degradation can be used as estimate for the entire contaminated system.

Although we assume a monotonous isotopic enrichment when applying the Rayleigh equation to the four CSIA samples, a higher temporal resolution or longer sampling period of CSIA might reveal variations in the  $\delta^{13}C$ -values as seen in the model results. Hence, whereas the Rayleigh equation approach generally yields a conservative estimate of contaminant transformation in studies of groundwater pollution plumes (Abe and Hunkeler, 2006; van Breukelen and Prommer, 2008), application of Eq. 5.3 to a few CSIA data points from a catchment outlet might result in an overestimation of the extent of degradation. Correspondingly, as modeled  $\delta^{13}C$ -values show local minima, application of the Rayleigh equation to these values would yield a different extent of degradation depending on which data point during the study period is taken as  $R_S$  (Eq. 5.2). These minima also explain the relatively low extent of degradation in the simulations: they result from repeated input of recently desorbed (i.e., barely degraded) pesticide from the shallow reservoir, which thus results in a lower overall extent of degradation compared to the estimate obtained from the Rayleigh equation approach.

Another source of uncertainty for the application of the Rayleigh equation approach is the assumption of a unique isotope ratio of the applied pesticide: in reality, different metolachlor products were applied in the study year, which may have different isotope ratios and, thus, cause additional variations of  $\delta^{13}\text{C}$ -values at catchment scale. Moreover, it was required to assume a certain value of the isotopic enrichment factor for the catchment ( $\varepsilon_C$ ) in order to apply the Rayleigh equation to the field CSIA. This value can be based on laboratory studies, but when used for the simulation of field CSIA data, one should take into account that dispersion and mixing of various flowpaths in catchments might attenuate actual isotope fractionation (Abe and Hunkeler, 2006; van Breukelen and Prommer, 2008) and thus require the assumption of a smaller isotopic enrichment factor (in terms of its absolute value). In this study, the assumption of the  $\varepsilon_C$ -value for S-metolachlor had to be based on prior calibration results of the pesticide transport model, and laboratory-derived  $\varepsilon_C$ -values for similar compounds.

### Distribution of calibrated model parameters

In general, the distribution of model parameters was similar for calibration set 1 and 2. However, the  $NS_{\delta^{13}\text{C}}$ -efficiency affected the calibration results for the storage capacity of the shallow reservoir ( $S_{\text{max}}$ ) and maximum recharge rate ( $R_{\text{max}}$ ). Whereas the distribution of these parameters has one clear maximum and a relatively evenly distributed parameter range in set 1 (especially for  $S_{\text{max}}$ ), set 2 shows two distinct peaks and less spread in the parameter ranges (Fig. 5.5). These peaks are correlated: in most calibrations,  $S_{\text{max}}$  and  $R_{\text{max}}$  either both take values from the secondary peak (around 6 mm and 39 mm d<sup>-1</sup>, respectively), or the primary peak (around 9 mm and 35 mm d<sup>-1</sup>, respectively). These differences in the distribution of  $S_{\text{max}}$  and  $R_{\text{max}}$  between set 1 and 2 imply that incorporation of field CSIA data into the calibration would lower the uncertainty in calibrated parameter ranges of these parameters. Correspondingly, the  $NS_{\delta^{13}\text{C}}$ -efficiency also affects the assessment of pesticide degradation. This cannot only be observed for the simulation results of the year 2012, but also for those of the other simulation years, which were not calibrated to field data. For example, simulation results for 2011 belonging to set 2 are associated with less uncertainty in the quantification of pesticide degradation for both reservoirs compared to set 1 (standard deviation of 1.9 versus 2.5, respectively; Fig. 5.6). This also becomes apparent from Table 5.3, where set 2 always shows equal or lower standard deviations in the mass balance terms than set 1. In contrast, preliminary calibrations that restricted  $\varepsilon_C$  to a range instead of a value (i.e., inclusion of  $\varepsilon_C$  in the calibration procedure) yielded no difference in uncertainty of model output between calibration sets 1 and 2. This indicates that detailed knowledge of the isotopic enrichment factor is required to achieve a reduction of model uncertainty by calibration against CSIA data.

Despite the measurable reduction in uncertainty, differences in the parameter ranges and mass balance terms between calibration sets 1 and 2 were small, and the uncertainty of most of the parameter values did not decrease by including the field CSIA data into the calibration. Accordingly, model results of calibration sets 1 and 2 are similar except for a period in autumn, where set 1 shows lower concentrations and more enriched  $\delta^{13}\text{C}$ -values than possible in set 2 (Fig. 5.4b and c). We suggest that the scarcity of the field CSIA data limited the decrease in uncertainty for

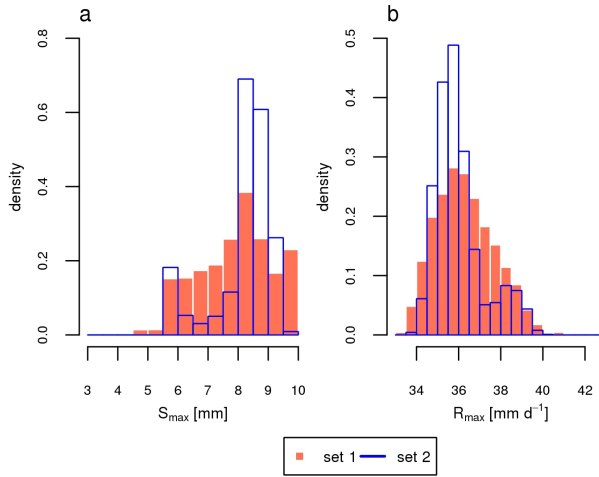


Figure 5.5: Distribution of the parameter values for the storage capacity of the shallow reservoir ( $S_{\max}$ ; a) and the maximum recharge rate ( $R_{\max}$ ; b) for all calibrations (behavioral calibration set 1; red bars) and calibrations with  $NS_{\delta^{13}C} > 0.9$  (behavioral calibration set 2; blue bars).

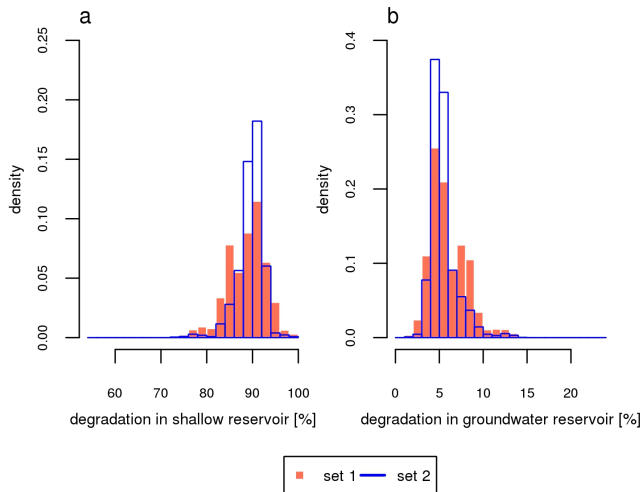


Figure 5.6: Distribution of the calculated extent of degradation in the shallow (a) and groundwater reservoir (b) for all behavioral calibration sets (red bars, set 1) and behavioral calibration sets with  $NS_{\delta^{13}C} > 0.9$  (blue bars, set 2) in 2011.

set 2: the values stem from six flow-proportional samples only, which are likely to overrepresent the isotopic signature during runoff events, and underrepresent periods of low flow (drain flow only). Correspondingly, 3342 out of the 10.000 calibration runs were behavioral with respect to set 2, which illustrates that the criterion of  $NS_{\delta^{13}C} > 0.9$  could easily be met for calibrations with a good fit for

discharge and concentrations. We propose that much more information about pesticide degradation than from concentration data only might have been obtained from samples representative of base flow conditions, and measurements that imply a larger extent of degradation than those taken soon after pesticide application. Hence, additional CSIA data at a higher temporal resolution could have significantly reduced the uncertainty in calibration results.

### **Benefits of the modeling approach**

In summary, both the monitoring and modeling results indicate extensive pesticide degradation during the study period, which highlights that CSIA can yield additional information in comparison to concentration measurements only. Pesticide concentrations following rainfall events were high enough to allow for carbon isotope analysis of several samples at the plot and catchment scale. The parsimonious modeling approach was able to reproduce concentration dynamics at the catchment outlet, with the highest concentrations occurring in response to rainfall events shortly after pesticide application. It also showed a good fit with the measured carbon isotope ratios. However, due to the scarcity of CSIA data points (especially in autumn), calibration to these data could only partly reduce model uncertainties. For example, pesticide fate in the shallow reservoir appeared to govern the extent of pesticide degradation and mass export in the system, but the field CSIA data do not illustrate whether the model accurately mirrors the dynamics of pesticide degradation and isotope fractionation in the source zone (e.g., no degradation in the shallow reservoir for sorbed pesticides). Pesticide release from the source zone also affects the role of the groundwater reservoir for pesticide degradation and discharge, which could have been described in more detail if CSIA data had been available for baseflow conditions. Another important factor is pesticide transport via overland flow, which leads to direct input of barely degraded pesticide into the stream. In the model, overland flow only occurs when the shallow reservoir is filled and flow to the groundwater reservoir exceeds the maximum recharge rate. This results in the simulation of only one event with overland flow in 2012 and the absence of overland flow in 2011. However, the model does not account for localized generation of overland flow, which can, for example, occur if the rainfall intensity during storm events surpasses the infiltration capacity of the topsoil. It is, therefore, likely that overland flow, and, consequently, fast pesticide transport to the catchment outlet occurred in response to several rainfall events during the study period, which was, indeed, observed at local scale in the plot experiment.

Despite the shortcomings of the modeling approach, it allowed for an estimate of pesticide degradation and retention in the catchment, which is presumably more applicable than the use of the Rayleigh equation approach at catchment scale. Model calibration also helped in assessing the isotopic enrichment factor ( $\varepsilon_C$ ). At the same time, the combination of field concentration and CSIA data allowed for the setup of the parsimonious model approach, which enabled us to better understand pesticide degradation and transport in the study catchment. In particular, field CSIA data improved our conceptualization of pesticide transport at catchment scale. Overall, these results showed how monitoring and modeling of CSIA data can be combined and inform each other, which proves advantageous in the characterization of diffuse pollution at catchment scale.

## 5.4 Conclusions

In this chapter, we presented a combined monitoring and modeling approach of pesticide concentrations and CSIA data at catchment scale. Concentrations of the chloroacetanilide herbicides S-metolachlor and alachlor from an agricultural headwater catchment were highest in response to an extreme rainfall event shortly after pesticide application, and decreased subsequently. In contrast, measured carbon isotope ratios increased gradually, which is indicative of pesticide degradation in the soil and during transport to the catchment outlet. This illustrates that CSIA data of diffuse pollutants can yield additional information in comparison to concentration data only. However, as supposed to CSIA-based assessment of contaminant degradation in aquifers, it is questionable due to the heterogeneous nature of the investigated system whether the Rayleigh equation approach yields a reliable estimate of pesticide degradation at catchment scale. In order to gain more insight in pesticide degradation and transport in the study catchment, we, therefore, developed a parsimonious model approach based on the description of flow and transport by travel time distributions. This model was calibrated in multiple model runs against measured discharge, S-metolachlor concentrations and carbon isotope ratios. Model results indicated an average extent of degradation above 70% during the study period, which mainly occurred in the topsoil compartment, and an average mass export of less than 2% with respect to the initially applied amount. This is in good agreement with the measured mass export of 1.8% for S-metolachlor. The model approach was also used to examine the added value of CSIA data in modeling of pesticide degradation at catchment scale. Simulations with a good fit against the CSIA data showed lower uncertainty in calibrated parameter values and calculated extent of degradation compared to simulations with solely a good fit to discharge and concentration data. However, the decrease in model uncertainty was generally small and only significant for two model parameters. This might result from the scarcity of the field CSIA data, such that calibration to CSIA data with finer temporal resolution might reveal a more significant reduction of parameter uncertainty.

Although the presented field CSIA data could be used as an indicator of pesticide degradation, it was not possible to analyze the dynamics of isotope ratios at a higher resolution (e.g. during single rainfall events) due to the scarcity of the CSIA data points. The model results indicated, however, that dynamics of CSIA data are highly responsive to changing hydrological conditions (e.g., following rainfall events). Future studies might, therefore, aim for a more extensive monitoring of CSIA data, which would also improve the applicability of CSIA-based assessment of degradation of diffuse pollutants. A finer temporal resolution of field CSIA data would, in addition, increase data availability for model calibration and might thus significantly improve the representation of pesticide degradation in models. Besides the analysis of more samples, measuring isotope fractionation for a second element (i.e., dual-element isotope analysis) might confirm the occurrence of degradation, and also allow a more precise assessment of the extent of degradation (Wiegert et al., 2012; Zwank et al., 2005). The quantification of degradation based on CSIA data relies, however, on the specification of an accurate enrichment factor for pesticide degradation in the investigated environmental system. This demonstrates

the need for additional laboratory studies of isotope fractionation associated with pesticide degradation. Despite the limited information on isotope fractionation of the investigated compounds, this study, nonetheless, highlighted how CSIA can advance our understanding of pesticide degradation at catchment scale, especially when applied in a combined monitoring and modeling approach.

## Supplementary information to chapter 5

### S5.1 Equations of the hydrological and pesticide model

Tables S5.1 and S5.2 show the equations of the hydrological and pesticide model, respectively. See Fig. 5.2 and Table 5.2 for further explanation of parameters.

### S5.2 Calculation of Nash-Sutcliffe coefficients

$NS_Q$  compares measured with modeled discharge at the catchment outlet, considering the best fit in a window of plus or minus one day to account for potential time lags of measured discharge in response to rainfall events:

$$NS_Q = 1 - 0.03 \cdot f - \frac{\min \left( \sum_{t=1}^n (Q_{t,\text{mod}} - Q_{t,\text{meas}})^2, \sum_{t=1}^n (Q_{t-1,\text{mod}} - Q_{t,\text{meas}})^2, \sum_{t=1}^n (Q_{t+1,\text{mod}} - Q_{t,\text{meas}})^2 \right)}{\sum_{t=1}^n (Q_{t,\text{meas}} - \overline{Q_{\text{meas}}})^2} \quad (\text{S5.1})$$

where  $n$  is the total number of days with discharge measurements,  $Q_{t,\text{mod}}$  and  $Q_{t,\text{meas}}$  are the modeled and measured discharge on day  $t$ , respectively,  $Q_{t-1,\text{mod}}$  and  $Q_{t+1,\text{mod}}$  are the modeled discharge one day before and after day  $t$ , respectively,  $\overline{Q_{\text{meas}}}$  is the mean of the measured discharge values, and  $f$  counts the number of days where the modeled discharge is zero while the measured discharge is not, or vice versa (weighted by the factor 0.03).

$NS_C$  considers errors in normal and ln-transformed concentration values, with the latter emphasizing deviations at low concentrations:

$$NS_C = 1 - 0.5 \left( \frac{\sum_{i=1}^n tw_i \cdot (C_{i,\text{mod}} - C_{i,\text{meas}})^2}{\sum_{i=1}^n tw_i \cdot (C_{i,\text{mod}} - \overline{C_{\text{meas}}})^2} + \frac{\sum_{i=1}^n tw_i \cdot (\ln C_{i,\text{mod}} - \ln C_{i,\text{meas}})^2}{\sum_{i=1}^n tw_i \cdot (\ln C_{i,\text{mod}} - \ln \overline{C_{\text{meas}}})^2} \right) \quad (\text{S5.2})$$

where  $n$  is the total number of concentration samples,  $C_{i,\text{meas}}$  is the concentration of sample  $i$ ,  $\overline{C_{i,\text{mod}}}$  is the flow-weighted average concentration over all days comprised in sample  $i$ ,  $\ln \overline{C_{\text{meas}}}$  is the mean of the ln-transformed measured concentrations, and  $tw_i$  is the time-proportional weight of sample  $i$  (with flow-proportional samples spanning more than a day considered as a daily sample). Note that the grab sample in November was considered as daily value. The same  $tw_i$  is also used in the calculation of  $NS_{\delta^{13}C}$ , which gives the deviations of the flow-proportionally weighted modeled ( $\delta^{13}C_{i,\text{mod}}$ ) from the measured carbon isotope ratios ( $\delta^{13}C_{i,\text{meas}}$ ):

$$NS_{\delta^{13}C} = 1 - \frac{\sum_{i=1}^n tw_i \cdot (\delta^{13}C_{i,\text{mod}} - \delta^{13}C_{i,\text{meas}})^2}{\sum_{i=1}^n tw_i \cdot (\delta^{13}C_{i,\text{mod}} - \overline{\delta^{13}C_{\text{meas}}})^2} \quad (\text{S5.3})$$

Table S5.1: Hydrological model.

---

**Shallow reservoir**

Storage  $\frac{dS_s(t)}{dt} = P(t) - ET_s(t) - Q_s(t)$

Fluxes  $ET_s(t) = \begin{cases} ET_{\text{pot}}(t) & \text{if } ET_{\text{pot}}(t) \leq \frac{dS_s(t)}{dt} \\ \frac{dS_s(t)}{dt} & \text{if } ET_{\text{pot}}(t) > \frac{dS_s(t)}{dt} \end{cases}$

$$Q_s(t) = \begin{cases} 0 & \text{if } P(t) - ET_s(t) - \frac{d(S_{\text{max}} - S_s(t))}{dt} \leq 0 \\ P(t) - ET_s(t) - \frac{d(S_{\text{max}} - S_s(t))}{dt} & \text{otherwise} \end{cases}$$

$$OF(t) = \begin{cases} 0 & \text{if } Q_s(t) \leq R_{\text{max}} \\ Q_s(t) - R_{\text{max}} & \text{if } Q_s(t) > R_{\text{max}} \end{cases}$$

**Groundwater reservoir**

Storage  $\frac{dS_{\text{gw}}(t)}{dt} = R_{\text{gw}}(t) - ET_{\text{gw}}(t) - Q_{\text{gw}}(t)$

Fluxes  $R_{\text{gw}}(t) = \begin{cases} Q_s(t) & \text{if } Q_s(t) \leq R_{\text{max}} \\ R_{\text{max}} & \text{if } Q_s(t) > R_{\text{max}} \end{cases}$

$$ET_{\text{gw}}(t) = \begin{cases} \min \left( ET_{\text{pot}}(t) - ET_s(t), \frac{dS_{\text{gw}}(t)}{dt} \right) & \text{if } S_{\text{gw}}(t) \geq S_{\text{red}} \\ \min \left( \frac{S_{\text{gw}}(t) - S_{\text{red}}}{S_{\text{ext}} - S_{\text{red}}}, (ET_{\text{pot}}(t) - ET_s(t)), \frac{dS_{\text{gw}}(t)}{dt} \right) & \text{if } S_{\text{ext}} < S_{\text{gw}}(t) < S_{\text{red}} \\ 0 & \text{if } S_{\text{gw}}(t) \leq S_{\text{ext}} \end{cases}$$

$$Q_{\text{gw}}(t) = [(2 - b)a(S_{\text{gw}}(t) - S_0)]^{\frac{1}{2-b}}$$


---

Table S5.2: Pesticide transport model.

	Parameter	Equation
<b>Shallow reservoir</b>		
Storage	change of pesticide mass $M_s$	$\frac{dM_s(t)}{dt} = \phi_{\text{inp}}(t) - \phi_s(t) + \phi_{\text{ex}}(t) - \phi_{\text{er}}(t) - D_s(t)$
Fluxes	application	$\phi_{\text{inp}}(t)$
	via discharge	$\phi_s(t) = Q_s(t) C_s(t)$
	via plant exudation	$\phi_{\text{ex}}(t) = f_{\text{ex}} ET_{\text{gw}}(t) C_{\text{ET}}(t)$
	via particulate phase	$\phi_{\text{er}}(t) = f_{\text{er}} OF(t) M_s(t)$
	degradation	$D_s(t) = r_0 M_s(t)$
Concentration	average concentration in reservoir	$C_0(t) = \frac{M_s(t)}{S_s(t)}$
	in discharge	$C_s(t) = \int_0^\infty p_{Q,s}(T_s, t) \cdot C_0(t - T_s) \cdot (1 - e^{-lT_s}) \cdot e^{-r_0 T_s} dT_s$
	probability density function of travel times $T_s$ of pesticide in $Q_s$ at time $t$	$p_{Q,s}(T_s, t)$
<b>Groundwater reservoir</b>		
Storage	change of pesticide mass $M_{\text{gw}}$	$\frac{dM_{\text{gw}}(t)}{dt} = \phi_r(t) - \phi_{\text{et}}(t) - \phi_{\text{gw}}(t) - D_{\text{gw}}(t)$
Fluxes	via groundwater recharge	$\phi_r(t) = R_{\text{gw}}(t) C_s(t)$
	via evapotranspiration	$\phi_{\text{et}}(t) = ET_{\text{gw}}(t) C_{\text{ET}}(t)$
	via discharge	$\phi_{\text{gw}}(t) = Q_{\text{gw}}(t) C_{\text{gw}}(t)$
	degradation	$D_{\text{gw}}(t) = r_0 e^{-kt} M_{\text{gw}}(t)$
	in discharge	$C_{\text{gw}}(t) = \int_0^\infty p_{Q,\text{gw}}(T_{\text{gw}}, t) \cdot C_s(t - T_{\text{gw}}) \cdot e^{-\frac{r_0}{k} (1 - e^{-kT_{\text{gw}}})} dT_{\text{gw}}$
Concentration	in evapotranspiration	$C_{\text{ET}}(t) = \int_0^\infty p_{\text{ET},\text{gw}}(T_{\text{gw}}, t) \cdot C_s(t - T_{\text{gw}}) \cdot e^{-\frac{r_0}{k} (1 - e^{-kT_{\text{gw}}})} dT_{\text{gw}}$
	probability density function of travel times $T_{\text{gw}}$ of pesticide in $Q_{\text{gw}}$ at time $t$	$p_{Q,\text{gw}}(T_{\text{gw}}, t)$
	probability density function of travel times $T_{\text{gw}}$ of pesticide in $ET_{\text{gw}}$ at time $t$	$p_{\text{ET},\text{gw}}(T_{\text{gw}}, t)$
	dissolved phase	$C(t) = \frac{C_{\text{gw}}(t) Q_{\text{gw}}(t) + C_s(t) OF(t)}{Q_{\text{gw}}(t) + OF(t)}$
<b>Stream</b>		
Concentration	dissolved phase	$C(t) = \frac{C_{\text{gw}}(t) Q_{\text{gw}}(t) + C_s(t) OF(t)}{Q_{\text{gw}}(t) + OF(t)}$



# 6

## Synthesis

This chapter provides a summary of the main results and conclusions of this thesis, which examines the use of compound-specific stable isotope analysis (CSIA) in the analysis of sources and sinks of organic pollutants. Following this summary, it discusses the implications of the thesis results for the use of the presented methods and model concepts: it gives recommendations for potential applications of the SISS model, and the use of CSIA in the assessment of diffuse pesticide pollution. Moreover, this chapter presents an outlook for future research that might follow from the results of this research.

## 6.1 Summary

Previous studies have challenged the applicability of the Rayleigh equation approach and CSIA-based source apportionment in cases where isotope ratios change due to both contaminant degradation and mixing between contaminant sources. These cases were discussed in chapters **2** and **3**, which investigated the use of a CSIA-based mathematical model for the assessment of sources and sinks of organic contaminants (stable isotopes sources and sinks model; SISS model). The SISS model represents a combination of the Rayleigh equation (for degradation quantification) and the linear stable isotope mixing model (for source apportionment), and thus allows for combined source apportionment and quantification of in situ degradation. Chapter 2 presented a detailed derivation of the SISS model for a scenario with two sources and one reaction pathway. Chapter 3 provided a validation of the SISS model against reactive transport model simulations, and an example application to previously published CSIA data from a BTEX-contaminated aquifer.

**Chapter 2** highlighted two major benefits of the SISS model. First, the SISS model accurately assesses the extent of degradation if contaminant transformation follows instantaneous mixing of two sources, and provides a conservative estimate of the extent of degradation otherwise. Second, the SISS model allows for an accurate estimate of source contributions even if degradation occurs prior to mixing between the two contaminant pools. It is thus, in general, possible to partition the dual-element isotope plot of a contaminant that originates from two sources according to the relative contributions of these sources. This finding contrasts with previous studies that challenge the use of CSIA-based source apportionment for situations where degradation-induced isotope fractionation occurs. Source apportionment (i.e., partitioning of the dual-element isotope plot) with the SISS model was illustrated by the example of CSIA data of perchlorate. The model showed little uncertainty in the calculated source contributions of natural and synthetic perchlorate sources.

The validation of the SISS model against the results of a reactive transport model that simulates isotope fractionation effects (**chapter 3**) illustrated the accuracy of the SISS model in source apportionment and quantification of contaminant degradation. However, a field application of the model to a benzene-contaminated aquifer revealed challenges in the use of the SISS model, which resulted from the inherent uncertainties in field CSIA data and heterogeneity of the field site. Despite these challenges, the SISS model illustrated that benzene contamination mainly stemmed from one of the two sources, and allowed for the assessment of the minimum and maximum extent of in-situ degradation at the field site. The

latter became especially beneficial in view of the contradictory estimates that the classical Rayleigh equation approach yielded for the investigated field site. The field application thus illustrated the role of the SISS model as a unique tool of CSIA-based source apportionment and quantification of contaminant degradation in systems with more than one contaminant source or reaction pathway (or both).

Whereas chapters 2 and 3 discussed CSIA-based methods that are independent of a specific environmental system or spatial scope, **chapter 4** narrowed the focus to the potential use of CSIA for diffuse pollutants at catchment scale. The aim was to analyze the evolution of CSIA data of diffuse pollutants under various hydrological conditions. To this end, virtual experiments of pesticide transport, degradation and isotope fractionation at hillslope scale were performed with a physically-based coupled subsurface-surface model (HydroGeoSphere). Pesticide concentrations and isotope ratios were simulated for steady-state hydrologic conditions, in response to an extreme rainfall event, and under transient hydrological conditions.

The main conclusions to be drawn from the virtual experiments were that (i) the modeled isotope ratios allowed for the quantification of the extent of in-situ degradation and the relative contribution of two competing pathways to overall degradation; (ii) the decrease in isotopic signatures during extreme rainfall events can be used as an indicator of pesticide transport via surface runoff; (iii) the modeled extent of isotope fractionation was large enough to be measured by current analytical methods; and (iv) the inherent underestimation of the extent of degradation by the Rayleigh equation approach remained small even under transient conditions. The virtual experiments thus indicate the usefulness and feasibility of CSIA in the analysis of diffuse pollution, especially given that concentration data alone would not allow for analyses such as mentioned under points (i) and (ii). Nonetheless, these promising results need to be confirmed in experimental studies of CSIA of diffuse pollutants. Such an experimental study was presented in chapter 5.

**Chapter 5** illustrated a combined measurement and modeling approach of concentrations and carbon isotope ratios of two herbicides (i.e., S-metolachlor and acetochlor) aimed at examining the added value of CSIA data in monitoring and modeling of pesticide transport and degradation. These field data were collected in a 47-ha agricultural catchment in Alsace (France; Altekendorf catchment), and represent the first systematically measured CSIA data of pesticides at catchment scale. Concentrations at the catchment outlet ranged from the low  $\text{ng L}^{-1}$  level before the application period to  $65 \mu\text{g L}^{-1}$  following an extreme rainfall event in the first month after herbicide application. While concentrations show several peaks associated with rainfall events, carbon isotope ratios gradually increased during the study period, leading to an enrichment of more than 2 ‰ within two months. Consequently, whereas concentrations did not provide clear evidence of transformation processes, the increase in isotope ratios indicates the occurrence of herbicide degradation in the soil and during transport to the catchment outlet. This illustrates the added value of CSIA in the analysis of pesticide pollution at catchment scale.

To underpin and extend the analysis of the field CSIA data, pesticide concentrations and isotope ratios at the catchment outlet were simulated in a conceptual (parsimonious) model (chapter 5). This model is based on the description of flow and

transport by travel time distributions, and is able to simulate transient hydrological conditions, pesticide degradation, and pesticide transport to the stream via overland flow and groundwater discharge. The model was calibrated against discharge, pesticide concentration, and CSIA data. The calibration results demonstrated that incorporation of CSIA data into model calibration can reduce model uncertainty by restricting the range of parameter values and constraining the simulated extent of degradation. Model results were used to assess the isotopic enrichment factor ( $\varepsilon_C$ ), and to specify the extent of degradation, which could not be derived from the measured CSIA data only. At the same time, the field data informed the modeling, as measured concentration and CSIA data illustrated which processes had to be included in the model. For example, the best model fit to the field data was achieved by assuming inhibition of degradation in the topsoil for sorbed pesticide, and a decreasing rate of pesticide degradation with increasing depth.

## 6.2 Implications and Outlook

### 6.2.1 Assessment of contaminant sources and sinks with the SISS model

Despite the detailed field site characterization, the application of the SISS model in **chapter 3** was complicated by uncertainties in the field CSIA data. Consequently, there is still considerable room for additional model testing, which might indicate how to address and minimize these complications. Chapter 3 mentions several factors that facilitate the application of the SISS model: (i) small analytical uncertainties in CSIA data, (ii) clearly distinct source signatures, (iii) a single reaction process or a combination of reaction processes with known relative contributions to overall degradation, and, ideally, (iv) a perpendicular mixing line between the sources with respect to the degradation trajectories in the dual-element isotope plot. As the SISS model has also been outlined for more than two sources and one reaction pathway, respectively, future research might aim for application of the model to a combination of multiple emission sources and reaction pathways. In addition, it might be interesting to evaluate the performance of the SISS model in the characterization of diffuse pollution, as studied in **chapters 4** and **5**. These systems involve different flowpaths and a larger degree of heterogeneity than aquifers. Validation of the SISS model for these systems would thus require virtual experiments with a more complex coupled subsurface-surface model that incorporates isotope fractionation effects. If the SISS model proves applicable for such systems, it might support the identification and quantification of pesticide sources and sinks, especially in catchments with detailed information about applied pesticide products, corresponding isotope ratios, and isotope fractionation effects of the considered pesticide.

In addition to research purposes, CSIA has also attracted the interest of consultants and regulators for the assessment of, e.g., groundwater pollution beneath industrial sites. In this context, the SISS model might improve the CSIA-based assessment of contaminant degradation, as it helps in distinguishing degradation-induced isotope fractionation from changes in isotope ratios due to mixing of sources. Future applications of the SISS model might, therefore, also include commercial purposes

that focus on monitored natural attenuation. Finally, the SISS model is not restricted to applications in contaminant hydrology, but it might also be employed in other disciplines such as atmospheric pollution.

## 6.2.2 Applicability of CSIA for diffuse pollutants

CSIA of pesticides in the study catchment (**chapter 5**) was only feasible for samples with relatively high pesticide concentrations (in the  $\mu\text{g L}^{-1}$  range except for one sample) due to analytical detection limits. The interpretation of the CSIA data was, therefore, solely based on six data points. A higher temporal resolution might have allowed for a more detailed interpretation, including the analysis of isotope ratios before the application period and during baseflow periods, and multiple samples during single rainfall events. However, the low concentrations of these samples did not allow for CSIA. Similarly, additional CSIA data points might have been beneficial for the calibration of the parsimonious pesticide model. CSIA-based studies of pesticide transport and degradation as presented in chapter 5 should, therefore, aim at a fine temporal resolution of CSIA data, and, preferably, also include isotope ratios during baseflow conditions. The latter is, however, challenged by current detection limits of CSIA, as baseflow conditions usually imply low pesticide concentrations. At present, CSIA of environmental samples requires large sample volumes, and special extraction and preconcentration techniques (Elsner et al., 2012). By employing these techniques, it has, nonetheless, been possible to determine carbon isotope ratios of organic contaminants (including one pesticide) at concentrations below  $100 \text{ ng L}^{-1}$  (Jochmann et al., 2006; Schreglmann et al., 2013). In view of in-stream concentrations of pesticides commonly reaching a few  $\mu\text{g L}^{-1}$  (Kreuger, 1998; Müller et al., 2002; Fenner et al., 2013), concentrations of pesticides can be expected to frequently exceed these limits.

Although **chapters 4** and **5** both suggest the applicability of CSIA in the analysis of diffuse pollutants, the studied hydrological systems show fundamental differences: whereas hillslope discharge was dominated by groundwater (chapter 4), the agricultural study catchment was characterized by a high responsiveness to rainfall via overland flow (chapter 5). Accordingly, pesticide transport was governed by groundwater in the virtual hillslope model, and by overland flow in the Alteckendorf catchment. Therefore, simulated isotope ratios show a highly fluctuating pattern in the Alteckendorf catchment, whereas seasonal variations in isotope ratios were small in the virtual hillslope model. These contrasting results suggest that the detail needed in CSIA sampling is dependent on the characteristics of the hydrological system. Catchments with well-drained soils and long response times will dampen variations in the isotope ratios, and thus yield a stable CSIA pattern as seen for the simulated hillslope. For these systems, application of the Rayleigh equation to one CSIA data point might, therefore, already give an accurate estimate of pesticide degradation in the catchment (see chapter 4). In contrast, extreme events or highly responsive systems that are prone to the generation of overland flow and erosion (such as the Alteckendorf catchment in chapter 5) might require a fine temporal resolution of CSIA samples, as the sampled pesticide might have undergone a different extent of degradation depending on which flowpath dominates stream discharge.

In the case of the Alteckendorf catchment, CSIA could only be applied to samples with high pesticide concentrations, which were associated with the occurrence of pesticide transport via overland flow and erosion. This restriction might affect the CSIA-based assessment of degradation in opposing ways. Pesticides that are transported via surface runoff stem from the microbially active upper soil layers, and might thus show a larger extent of degradation than pesticides that have quickly percolated to groundwater. However, the model results suggest that pesticides in surface runoff are associated with less degradation compared to pesticides in groundwater discharge. This might be the case if sorption in the upper soil layers limits bioavailability of the pesticide and thus results in reduced pesticide degradation (as assumed in the model in chapter 5); or if pesticides discharged via groundwater also stem from applications in previous years, and have thus undergone significantly more degradation than recently applied pesticide emitted via surface runoff (as in the virtual hillslope system in chapter 4). In other cases, redox conditions in groundwater might be more favorable to pesticide degradation than those in the soil, which would also result in a larger extent of degradation for pesticide in groundwater discharge compared to pesticide in surface runoff.

Regardless of the type of hydrological system, model results and field data from **chapters 4 and 5** suggest that the isotopic enrichment between the applied pesticide product and a river sample is large enough to be detected by CSIA (given instrumental uncertainties of about 0.5 ‰ for carbon and 5 ‰ for hydrogen isotope analysis, respectively; Sherwood Lollar et al., 2007). Moreover, although more than 90% of the total mass export in the Alteckendorf catchment occurred within two weeks after the main pesticide application, enough pesticide was retained in the catchment to allow for CSIA several weeks later. This indicates the applicability of CSIA for diffuse pollutants even in highly responsive catchments.

### 6.2.3 Recommendations for modeling of CSIA of diffuse pollutants

**Chapter 5** demonstrates the usefulness of a combined measurement and modeling approach for CSIA data, as the model gave further insight into pesticide transport and degradation in comparison to the measurements alone. However, it is crucial that such a modeling approach includes all important pesticide transfer processes. For example, in chapter 5, pesticide application was modeled as a homogeneous input into the shallow reservoir. This representation was sufficient in view of the purpose of this study and the limited CSIA data. For other applications, however, it might prove useful to apply a spatially-distributed model instead, as this would allow simulation of the hydrologic connectivity between agricultural fields and the catchment outlet, and thus help in identifying areas that pose a high risk of surface water contamination. Similarly, spatially-distributed models might assist in source identification of pesticide pollution. Moreover, more complex models than the one in chapter 5 might be able to incorporate additional processes affecting pesticide fate at catchment scale (such as in-stream degradation), or explicitly simulate soil erosion and associated particulate pesticide transport. Nonetheless, distributed models, and especially physically-based models, are computationally intensive and

require many input data and parameters (Holvoet et al., 2007; Kampf and Burges, 2007). In general, the choice between different models of pesticide pollution greatly depends on the objectives and scope of the modeling approach (Payraudeau and Gregoire, 2012). As seen in chapter 5, it can prove advantageous to begin with a very simple model concept, and gradually increase its complexity by updating the model with information gained from the analysis of field data. Hence, it is inadvisable to favor, a priori, a certain model type for the interpretation of CSIA data.

The model validation and calibration in chapter 5 was challenged by a lack of information about isotope fractionation associated with S-metolachlor transformation. Isotopic enrichment factors were only available for other chloroacetanilide pesticides (Elsayed et al., 2014), and it is unknown to what extent these laboratory values are representative of processes occurring at catchment scale. Hence, there is a clear need for additional studies that determine isotope fractionation effects specifically for the considered compound. As shown in chapter 5, the determination of appropriate enrichment factors can also be assisted by modeling of field CSIA data. However, this can only yield accurate estimates in combination with sufficient CSIA data, which restrict equifinality of model parameters.

In summary, this thesis presents novel CSIA-based methods in the analysis of sources and sinks of organic pollutants. **Chapters 2** and **3** illustrated how source apportionment and degradation quantification with CSIA can be combined and refined by employing the SISS model. **Chapters 4** and **5** illustrated the unprecedented use of CSIA in the characterization of transport and transformation of diffuse pollutants, which was underpinned by analysis and modeling of field CSIA data. While the discussed CSIA-based methods are not free of limitations, the presented example applications clearly demonstrate how these methods allow for an improved assessment of sources and sinks of organic pollutants.



# Acknowledgments

My time as a PhD candidate has been a great experience full of important lessons within and beyond my research field. This would not have been possible without the excellent supervision I have received from my supervisor Dr. Boris van Breukelen. Boris, thank you a lot for keeping the right balance between letting me find my way on my own and leading me when I got stuck. Especially in the last year of my PhD, when I ran a bit out of time, you helped me out a lot in a very efficient and constructive way! Your masterstroke of splitting one manuscript into two SISS model papers really turned the tide!

Ilja, thank you for keeping up the female hydrologist power in our group, and for your help with the modeling, especially when some expertise in the setup and parameterization of the hillslope model was called for. Also, your help with scientific writing in English was crucial to (or would it be for?) improving the conciseness of my manuscripts. Maarten, thanks so much for providing our floor with a lot of liveliness, motivation, and coffee, but also for telling me when it was really time to go home.

Ype, thanks a lot for your brilliant work with the pesticide model. I really appreciate that you always took the time to explain the model and discuss results with me. I feel as if I was stealing first authorship from you. Marie, Gwenaël, Sylvain, thanks for your hospitality when I came to Strasbourg, your interest in my work, countless enlightening e-mails, and the willingness to leave one of the most innovative parts of your study to me - the precious CSIA data! I would also like to thank Joachim Rozemeijer and Rob McLaren for their help with HydroGeoSphere.

I am very grateful for all the opportunities the CSI:environment network provided. It was very inspiring to learn from the diverse expertise of all the scientists in the network. And of course I enjoyed the traveling and looking behind the scenes at other institutes. Thanks to the network, I also got to know a very good friend. Tania, thank you so much for all the fun we shared in Europe and elsewhere, and for your help with my Leipzig mission!

My special thanks also go to the members of the reading committee, Dr. Hans Peter Broers, Dr. Martin Elsner, Prof.Dr. Daniel Hunkeler, Prof.Dr. Stefan Uhlenbrook, and Prof.Dr. Sjoerd van der Zee, for the diligent assessment of this thesis.

I am most thankful for the help I got with editing and formatting this book. Vielen, vielen Dank, Doris, für die schnelle und professionelle Gestaltung von einem großartigen Cover! Veelmals bedankt, Anne, voor je hulp met de Nederlandse samenvatting - dat is conversation exchange op zijn best!

Thanks for the company to everyone who has worked with me in the Hydro Copyshop. David, muchas gracias for all the encouragement and confidence in me! I admire your passion for science and unshakable positive thinking. So happy to have you as a friend and cherished pen pal! Jun and Liang, I think we formed the best Eurasian office ever! Thanks for your support and patience in the final phase of my PhD.

Patricia, I thoroughly enjoyed all the dancing you and others brought to our office. Thanks also to Herman who discovered my talent as paranimf.

Mari, you are simply the best! Danke für dein grenzenloses Verständnis und all die Unterstützung, für die tollsten Kaffeepausen, Abendessen, Ausflüge ins Amsterdamer Nachtleben, und unser grandioses Urlaubsabenteuer. Yanjiao, thanks for all the good chats - I would not have made it through all this without your invaluable help and encouragement, and the occasional glass of wine we drank! Héloïse, my closest colleague and dearest friend, thank you so much for countless chats, (iso)top food at your place, adventures and fun nights out! Keep up the honor of us hydrology girls! Brett, cheers for regularly checking whether I have to be rescued from underneath a pile of hydrology papers, and for being the best company to enjoy cultural happenings in Amsterdam.

Alex, Andreas, Angela, Artem, Callum, Diego, Hylke, Katerina, Katrin (wir sehen uns wieder in Leipzig!), Margreet, Marjan, Martin, Lintao, Luca, Michi, Ove, Paolo, Paula, Philip, Wouter, Yvonne, Zaman, I am incredibly thankful for all the support, discussions and good times I had with you at the VU and elsewhere. My deepest gratitude also goes to all friends outside of work, you made Amsterdam an unforgettable and unique experience! I will miss you all.

I am most grateful for the support of my family and friends in Germany. Frank, Ani, Gisela, liebe Eltern, vielen Dank für die bedingungslose Unterstützung und Hilfe. Dank euch hatte ich immer einen Zufluchtsort in Deutschland, an dem ich durchatmen und neue Kraft schöpfen konnte. Darum widme ich euch diese Doktorarbeit.

# Bibliography

- Abdul, A. S. *Experimental and Numerical studies of the effect of the capillary fringe on streamflow generation*. PhD thesis, University of Waterloo, 1985.
- Abe, Y. and Hunkeler, D. Does the Rayleigh equation apply to evaluate field isotope data in contaminant hydrogeology? *Environmental Science & Technology*, 40(5):1588–1596, 2006.
- Aeppli, C.; Berg, M.; Cirpka, O. A.; Holliger, C.; Schwarzenbach, R. P., and Hofstetter, T. B. Influence of mass-transfer limitations on carbon isotope fractionation during microbial dechlorination of trichloroethene. *Environmental Science & Technology*, 43(23):8813–8820, 2009.
- Aeppli, C.; Hofstetter, T. B.; Amaral, H. I. F.; Kipfer, R.; Schwarzenbach, R. P., and Berg, M. Quantifying in situ transformation rates of chlorinated ethenes by combining compound-specific stable isotope analysis, groundwater dating, and carbon isotope mass balances. *Environmental Science & Technology*, 44(10):3705–3711, 2010.
- Agricola, I.; Friedrich, T., and Spain, P. G. *Elementary geometry*. American Mathematical Society, Providence, R.I., 2008.
- Al-Khatib, K.; Baumgartner Unland, J.; Olson, B. L. S., and Graham, D. W. Alachlor and metolachlor transformation pattern in corn and soil. *Weed Science*, 50(5):581–586, 2002.
- Albrechtsen, H.-J.; Mills, M. S.; Aamand, J., and Bjerg, P. L. Degradation of herbicides in shallow Danish aquifers: an integrated laboratory and field study. *Pest Management Science*, 57(4):341–350, 2001.
- Alletto, L.; Benoit, P.; Bolognesi, B.; Couffignal, M.; Bergheaud, V.; Dumény, V.; Longueval, C., and Barriuso, E. Sorption and mineralisation of S-metolachlor in soils from fields cultivated with different conservation tillage systems. *Soil and Tillage Research*, 128(0):97–103, 2013.
- Amaral, H. I. F.; Aeppli, C.; Kipfer, R., and Berg, M. Assessing the transformation of chlorinated ethenes in aquifers with limited potential for natural attenuation: Added values of compound-specific carbon isotope analysis and groundwater dating. *Chemosphere*, 85(5):774–781, 2011.
- Andersson, A. A systematic examination of a random sampling strategy for source apportionment calculations. *Science of The Total Environment*, 412-413(0):232–238, 2011.
- Annable, W. K.; Frape, S. K.; Shouakar-Stash, O.; Shanoff, T.; Drimmie, R. J., and Harvey, F. E.  $^{37}\text{Cl}$ ,  $^{15}\text{N}$ ,  $^{13}\text{C}$  isotopic analysis of common agro-chemicals for identifying non-point source agricultural contaminants. *Applied Geochemistry*, 22(7):1530–1536, 2007.
- Anneser, B.; Einsiedl, F.; Meckenstock, R. U.; Richters, L.; Wisotzky, F., and Griebler, C. High-resolution monitoring of biogeochemical gradients in a tar oil-contaminated aquifer. *Applied Geochemistry*, 23(6):1715–1730, 2008.
- Aravena, R. and Hunkeler, D. Investigating the origin and fate of organic contaminants in groundwater using stable isotope analysis. In *Environmental Isotopes in Biodegradation and Bioremediation*, pages 249–291. CRC Press, 2009.
- Arias-Estévez, M.; López-Periago, E.; Martínez-Carballo, E.; Simal-Gándara, J.; Mejuto, J.-C., and García-Río, L. The mobility and degradation of pesticides in soils and the

- pollution of groundwater resources. *Agriculture, Ecosystems & Environment*, 123(4): 247–260, 2008.
- Atteia, O.; Franceschi, M., and Dupuy, A. Validation of reactive model assumptions with isotope data: Application to the Dover case. *Environmental Science & Technology*, 42(9):3289–3295, 2008.
- Badea, S. L.; Vogt, C.; Weber, S.; Danet, A. F., and Richnow, H. H. Stable isotope fractionation of gamma-hexachlorocyclohexane (lindane) during reductive dechlorination by two strains of sulfate-reducing bacteria. *Environmental Science & Technology*, 43(9): 3155–3161, 2009.
- Battaglin, W. A. and Goolsby, Donald A. Are shifts in herbicide use reflected in concentration changes in midwestern rivers? *Environmental Science & Technology*, 33(17): 2917–2925, 1999.
- Beernaerts, S.; Gerard, M.; Debongnie, P.; Barthelemy, J.-P.; Pussemier, L., and Copin, A. Two years of pesticides monitoring in a Belgian watershed. *International Journal of Environmental Analytical Chemistry*, 83(6):469–480, 2003.
- Benettin, P.; van der Velde, Y.; van der Zee, S. E. A. T. M.; Rinaldo, A., and Botter, G. Chloride circulation in a lowland catchment and the formulation of transport by travel time distributions. *Water Resources Research*, 49(8):4619–4632, 2013.
- Bertuzzo, E.; Thomet, M.; Botter, G., and Rinaldo, A. Catchment-scale herbicides transport: Theory and application. *Advances in Water Resources*, 52(0):232–242, 2013.
- Beven, K. Parameter estimation and predictive uncertainty. In *Rainfall-Runoff Modelling*, pages 231–287. John Wiley & Sons, Ltd, 2012.
- Blessing, M.; Schmidt, T. C.; Dinkel, R., and Haderlein, S. B. Delineation of multiple chlorinated ethene sources in an industrialized area—a forensic field study using compound-specific isotope analysis. *Environmental Science & Technology*, 43(8):2701–2707, 2009.
- Blum, P.; Hunkeler, D.; Weede, M.; Beyer, C.; Grathwohl, P., and Morasch, B. Quantification of biodegradation for o-xylene and naphthalene using first order decay models, michaelis-menten kinetics and stable carbon isotopes. *Journal of Contaminant Hydrology*, 105(3-4):118–130, 2009.
- Botter, G.; Bertuzzo, E., and Rinaldo, A. Transport in the hydrologic response: Travel time distributions, soil moisture dynamics, and the old water paradox. *Water Resources Research*, 46(3):W03514, 2010.
- Bouchard, D.; Hunkeler, D.; Gaganis, P.; Aravena, R.; Höhener, P.; Broholm, M. M., and Kjeldsen, P. Carbon isotope fractionation during diffusion and biodegradation of petroleum hydrocarbons in the unsaturated zone: Field experiment at Vaerløse Airbase, Denmark, and modeling. *Environmental Science & Technology*, 42(2):596–601, 2008.
- Brown, V. A.; McDonnell, J. J.; Burns, D. A., and Kendall, C. The role of event water, a rapid shallow flow component, and catchment size in summer stormflow. *Journal of Hydrology*, 217(3-4):171–190, 1999.
- Brunner, P. and Simmons, C. T. Hydrogeosphere: A fully integrated, physically based hydrological model. *Ground Water*, 50(2):170–176, 2012.
- Burt, T. P. and Pinay, G. Linking hydrology and biogeochemistry in complex landscapes. *Progress in Physical Geography*, 29(3):297–316, 2005.
- Buser, H.-R.; Poiger, T., and Müller, M. D. Changed enantiomer composition of metolachlor in surface water following the introduction of the enantiomerically enriched product to the market. *Environmental Science & Technology*, 34(13):2690–2696, 2000.
- Chen, D. J. Z. and MacQuarrie, K. T. B. Numerical simulation of organic carbon, nitrate,

- and nitrogen isotope behavior during denitrification in a riparian zone. *Journal of Hydrology*, 293(1-4):235–254, 2004.
- Christiansen, J. S.; Thorsen, M.; Clausen, T.; Hansen, S., and Refsgaard, J. C. Modelling of macropore flow and transport processes at catchment scale. *Journal of Hydrology*, 299(1-2):136–158, 2004.
- Cifuentes, L. A. and Eldridge, P. M. *A mass- and isotope-balance model of DOC mixing in estuaries*, volume 43. American Society of Limnology and Oceanography, Waco, TX, ETATS-UNIS, 1998.
- Coplen, T. B. Guidelines and recommended terms for expression of stable-isotope-ratio and gas-ratio measurement results. *Rapid Communications in Mass Spectrometry*, 25(17):2538–2560, 2011.
- Cozzarelli, I. M.; Herman, J. S.; Baedecker, M. J., and Fischer, J. M. Geochemical heterogeneity of a gasoline-contaminated aquifer. *Journal of Contaminant Hydrology*, 40(3):261–284, 1999.
- D’Afonseca, F. M.; Prommer, H.; Finkel, M.; Blum, P., and Grathwohl, P. Modeling the long-term and transient evolution of biogeochemical and isotopic signatures in coal tar-contaminated aquifers. *Water Resources Research*, 47(5):W05518, 2011.
- David, M. B.; Gentry, L. E.; Starks, K. M., and Cooke, R. A. Stream transport of herbicides and metabolites in a tile-drained, agricultural watershed. *Journal of Environmental Quality*, 32(5):1790–1801, 2003.
- Deutsch, B.; Mewes, M.; Liskow, I., and Voss, M. Quantification of diffuse nitrate inputs into a small river system using stable isotopes of oxygen and nitrogen in nitrate. *Organic Geochemistry*, 37(10):1333–1342, 2006.
- Divers, M. T.; Elliott, E. M., and Bain, D. J. Quantification of nitrate sources to an urban stream using dual nitrate isotopes. *Environmental Science & Technology*, 2014.
- Doble, R.; Brunner, P.; McCallum, J., and Cook, P. G. An analysis of river bank slope and unsaturated flow effects on bank storage. *Ground Water*, 50(1):77–86, 2012.
- Donald, D. B.; Cessna, A. J.; Sverko, E., and Glozier, N. E. Pesticides in surface drinking-water supplies of the Northern Great Plains. *Environmental Health Perspectives*, 115(8), 2007.
- Doppler, T.; Camenzuli, L.; Hirzel, G.; Krauss, M.; Lück, A., and Stamm, C. Spatial variability of herbicide mobilisation and transport at catchment scale: insights from a field experiment. *Hydrology and Earth System Sciences*, 16(7), 2012.
- Duffy, C. J. and Lee, D.-H. Base flow response from nonpoint source contamination: Simulated spatial variability in source, structure, and initial condition. *Water Resources Research*, 28(3):905–914, 1992.
- Eberts, S. M.; Braun, C., and Jones, S. Compound-specific isotope analysis: Questioning the origins of a trichloroethene plume. *Environmental Forensics*, 9(1):85–95, 2008.
- Eberts, S. M.; Böhlke, J. K.; Kauffman, L. J., and Jurgens, B. C. Comparison of particle-tracking and lumped-parameter age-distribution models for evaluating vulnerability of production wells to contamination. *Hydrogeology Journal*, 20(2):263–282, 2012.
- Elsayed, O. F.; Maillard, E.; Vuilleumier, S.; Nijenhuis, I.; Richnow, H. H., and Imfeld, G. Using compound-specific isotope analysis to assess the degradation of chloroacetanilide herbicides in lab-scale wetlands. *Chemosphere*, 99(0):89–95, 2014.
- Elsner, M. Stable isotope fractionation to investigate natural transformation mechanisms of organic contaminants: principles, prospects and limitations. *Journal of Environmental Monitoring*, 12(11):2005–2031, 2010.
- Elsner, M.; Jochmann, M. A.; Hofstetter, T. B.; Hunkeler, D.; Bernstein, A.; Schmidt, T. C., and Schimmelmann, A. Current challenges in compound-specific stable isotope

- analysis of environmental organic contaminants. *Analytical and Bioanalytical Chemistry*, 403(9):2471–91, 2012.
- Fausser, P.; Thomsen, M.; Sørensen, P., and Petersen, S. Predicted concentrations for pesticides in drainage dominated catchments. *Water, Air, & Soil Pollution*, 187(1): 149–156, 2008.
- Fenner, K.; Canonica, S.; Wackett, L. P., and Elsner, M. Evaluating pesticide degradation in the environment: Blind spots and emerging opportunities. *Science*, 341(6147):752–758, 2013.
- Fischer, A.; Herklotz, I.; Herrmann, S.; Thullner, M.; Weelink, S. A. B.; Stams, A. J. M.; Schlömann, M.; Richnow, H.-H., and Vogt, C. Combined carbon and hydrogen isotope fractionation investigations for elucidating benzene biodegradation pathways. *Environmental Science & Technology*, 42(12):4356–4363, 2008.
- Flipe, N.; Even, S.; Poulin, M.; Théry, S., and Ledoux, E. Modeling nitrate fluxes at the catchment scale using the integrated tool cawaqs. *Science of The Total Environment*, 375(1-3):69–79, 2007.
- Flury, M. Experimental evidence of transport of pesticides through field soils - a review. *Journal of Environmental Quality*, 25(1):25–45, 1996.
- Gassmann, M.; Stamm, C.; Olsson, O.; Lange, J.; Kümmerer, K., and Weiler, M. Model-based estimation of pesticides and transformation products and their export pathways in a headwater catchment. *Hydrology and Earth System Sciences*, 17(12):5213–5228, 2013.
- Gavrilescu, M. Fate of pesticides in the environment and its bioremediation. *Engineering in life sciences*, 5(6):497–526, 2005.
- Giebel, B. M.; Swart, P. K., and Riemer, D. D. New insights to the use of ethanol in automotive fuels: A stable isotopic tracer for fossil- and bio-fuel combustion inputs to the atmosphere. *Environmental Science & Technology*, 45(15):6661–6669, 2011.
- Ging, P.B.; Lee, R.W., and Silva, S.R. Water chemistry of Shoal Creek and Waller Creek, Austin, Texas, and potential sources of nitrate. Water-Resources Investigations Report 96-4167. Technical report, U.S. Geological Survey, 1996.
- Goderniaux, P.; Brouyère, S.; Fowler, H. J.; Blenkinsop, S.; Therrien, R.; Orban, P., and Dassargues, A. Large scale surface-subsurface hydrological model to assess climate change impacts on groundwater reserves. *Journal of Hydrology*, 373(1-2):122–138, 2009.
- Green, C. T.; Böhlke, J. K.; Bekins, B. A., and Phillips, S. P. Mixing effects on apparent reaction rates and isotope fractionation during denitrification in a heterogeneous aquifer. *Water Resources Research*, 46(8), 2010.
- Griebler, C.; Safinowski, M.; Vieth, A.; Richnow, H. H., and Meckenstock, R. U. Combined application of stable carbon isotope analysis and specific metabolites determination for assessing in situ degradation of aromatic hydrocarbons in a tar oil-contaminated aquifer. *Environmental Science & Technology*, 38(2):617–631, 2004.
- Grube, A.; Donaldson, D.; Kiely, T., and Wu, L. Pesticides industry sales and usage 2006 and 2007 market estimates. Technical report, U.S. Environmental Protection Agency, 2011.
- Gutierrez, A. and Baran, N. Long-term transfer of diffuse pollution at catchment scale: Respective roles of soil, and the unsaturated and saturated zones (Brévilles, France). *Journal of Hydrology*, 369(3-4):381–391, 2009.
- Hartenbach, A. E.; Hofstetter, T. B.; Tentscher, P. R.; Canonica, S.; Berg, M., and Schwarzenbach, R. P. Carbon, hydrogen, and nitrogen isotope fractionation during light-induced transformations of atrazine. *Environmental Science & Technology*, 42(21): 7751–7756, 2008.

- Health & Consumer Protection Directorate, . Review report for the active substance S-metolachlor. Technical report, European Commission, 2004.
- Henderson, K. L.; Belden, J. B., and Coats, J. R. Mass balance of metolachlor in a grassed phytoremediation system. *Environmental Science & Technology*, 41(11):4084–4089, 2007.
- Holvoet, K. M. A.; Seuntjens, P., and Vanrolleghem, P. A. Monitoring and modeling pesticide fate in surface waters at the catchment scale. *Ecological Modelling*, 209(1): 53–64, 2007.
- Hopp, L. and McDonnell, J. J. Connectivity at the hillslope scale: Identifying interactions between storm size, bedrock permeability, slope angle and soil depth. *Journal of Hydrology*, 376(3-4):378–391, 2009.
- Hopp, L. and McDonnell, J. J. Examining the role of throughfall patterns on subsurface stormflow generation. *Journal of Hydrology*, 409(1-2):460–471, 2011.
- Hopp, L.; Harman, C.; Desilets, S. L. E.; Graham, C. B.; McDonnell, J. J., and Troch, P. A. Hillslope hydrology under glass: confronting fundamental questions of soil-water-biota co-evolution at Biosphere 2. *Hydrology and Earth System Sciences*, 13(11):2105–2118, 2009.
- Hrachowitz, M.; Savenije, H.; Bogaard, T. A.; Tetzlaff, D., and Soulsby, C. What can flux tracking teach us about water age distribution patterns and their temporal dynamics? *Hydrology and Earth System Sciences*, 17(2):533–564, 2013.
- Hunkeler, D. and Elsner, M. Principles and mechanisms of isotope fractionation. In Marjorie Aelion, C.; Aravena, R.; Hunkeler, D., and Höhener, P., editors, *Environmental Isotopes in Biodegradation and Bioremediation*, pages 43–77. CRC Press, 2009.
- Hunkeler, D.; Aravena, R.; Berry-Spark, K., and Cox, E. Assessment of degradation pathways in an aquifer with mixed chlorinated hydrocarbon contamination using stable isotope analysis. *Environmental Science & Technology*, 39(16):5975–5981, 2005.
- Hunkeler, D.; van Breukelen, B. M., and Elsner, M. Modeling chlorine isotope trends during sequential transformation of chlorinated ethenes. *Environmental Science & Technology*, 43(17):6750–6756, 2009.
- James, A. L.; McDonnell, J. J.; Tromp-van Meerveld, H. J., and Peters, N. E. Gypsies in the palace: experimentalist’s view on the use of 3-D physics-based simulation of hillslope hydrological response. *Hydrological Processes*, 24(26):3878–3893, 2010.
- Jin, B.; Haderlein, S. B., and Rolle, M. Integrated carbon and chlorine isotope modeling: Applications to chlorinated aliphatic hydrocarbons dechlorination. *Environmental Science & Technology*, 47(3):1443–1451, 2013.
- Jochmann, M. A.; Blessing, M.; Haderlein, S. B., and Schmidt, T. C. A new approach to determine method detection limits for compound-specific isotope analysis of volatile organic compounds. *Rapid Communications in Mass Spectrometry*, 20(24):3639–3648, 2006.
- Johannsen, A.; Dähnke, K., and Emeis, K. Isotopic composition of nitrate in five German rivers discharging into the North Sea. *Organic Geochemistry*, 39(12):1678–1689, 2008.
- Joly, P.; Besse-Hoggan, P.; Bonnemoy, F.; Batisson, I.; Bohatier, J., and Mallet, C. Impact of maize formulated herbicides mesotrione and S-metolachlor, applied alone and in mixture, on soil microbial communities. *ISRN Ecology*, 2012:9, 2012.
- Jones, R.L. and Norris, F.A. Factors affecting degradation of aldicarb and ethoprop. *Journal of Nematology*, 30(1):45–55, 1998.
- Kampf, S. K. and Burges, S. J. A framework for classifying and comparing distributed hillslope and catchment hydrologic models. *Water Resources Research*, 43(5), 2007.

- Kawashima, H. and Katayama, Y. Source evaluation of diazinon using stable carbon isotope ratio. *Environmental Forensics*, 11(4):363–371, 2010.
- Kellman, L. M. and Hillaire-Marcel, C. Evaluation of nitrogen isotopes as indicators of nitrate contamination sources in an agricultural watershed. *Agriculture, Ecosystems & Environment*, 95(1):87–102, 2003.
- Kjær, J.; Olsen, P.; Henriksen, T., and Ullum, M. Leaching of metribuzin metabolites and the associated contamination of a sandy Danish aquifer. *Environmental Science & Technology*, 39(21):8374–8381, 2005.
- Kolhatkar, R.; Kuder, T.; Philp, P.; Allen, J., and Wilson, J. T. Use of compound-specific stable carbon isotope analyses to demonstrate anaerobic biodegradation of MTBE in groundwater at a gasoline release site. *Environmental Science & Technology*, 36(23): 5139–5146, 2002.
- Kolpin, D. W.; Thurman, E. M., and Linhart, S. M. The environmental occurrence of herbicides: The importance of degradates in ground water. *Archives of Environmental Contamination and Toxicology*, 35(3):385–390, 1998.
- Konstantinou, I. K.; Zarkadis, A. K., and Albanis, T. A. Photodegradation of selected herbicides in various natural waters and soils under environmental conditions. *Journal of Environmental Quality*, 30(1):121–130, 2001.
- Kopinke, F.-D.; Georgi, A.; Voskamp, M., and Richnow, H. H. Carbon isotope fractionation of organic contaminants due to retardation on humic substances: Implications for natural attenuation studies in aquifers. *Environmental Science & Technology*, 39(16):6052–6062, 2005.
- Kreuger, J. Pesticides in stream water within an agricultural catchment in southern sweden, 1990-1996. *The Science of The Total Environment*, 216(3):227–251, 1998.
- Kronimus, A.; Schwarzbauer, J.; Dsikowitzky, L., and Littke, R. Compound-specific stable carbon isotope analyses of riverine water organic contaminants. *Environmental Chemistry Letters*, 4(1):23–28, 2006.
- Kuder, T.; Wilson, J. T.; Kaiser, P.; Kolhatkar, R.; Philp, P., and Allen, J. Enrichment of stable carbon and hydrogen isotopes during anaerobic biodegradation of MTBE: Microcosm and field evidence. *Environmental Science & Technology*, 39(1):213–220, 2004.
- Le Bot, B.; Oulhote, Y.; Deguen, S., and Glorennec, P. Using and interpreting isotope data for source identification. *TrAC Trends in Analytical Chemistry*, 30(2):302–312, 2011.
- Lee, T. and Benson, C. H. Sorption and degradation of alachlor and metolachlor in ground water using green sands. *Journal of Environmental Quality*, 33(5):1682–1693, 2004.
- Lefranq, M. *Transport and attenuation of pesticides in runoff from agricultural headwater catchments: from field characterisation to modelling*. PhD thesis, Université de Strasbourg, 2014.
- Leu, C.; Singer, H.; Stamm, C.; Müller, S. R., and Schwarzenbach, R. P. Simultaneous assessment of sources, processes, and factors influencing herbicide losses to surface waters in a small agricultural catchment. *Environmental Science & Technology*, 38(14): 3827–3834, 2004a.
- Leu, C.; Singer, H.; Stamm, C.; Müller, S. R., and Schwarzenbach, R. P. Variability of herbicide losses from 13 fields to surface water within a small catchment after a controlled herbicide application. *Environmental Science & Technology*, 38(14):3835–3841, 2004b.
- Li, Q.; Unger, A. J. A.; Sudicky, E. A.; Kassenaar, D.; Wexler, E. J., and Shikaze, S. Simulating the multi-seasonal response of a large-scale watershed with a 3D physically-based hydrologic model. *Journal of Hydrology*, 357(3-4):317–336, 2008.

- Liu, K.; Cao, Z.; Pan, X., and Yu, Y. Using in situ pore water concentrations to estimate the phytotoxicity of nicosulfuron in soils to corn (*Zea mays* L.). *Environmental Toxicology and Chemistry*, 31(8):1705–11, 2012.
- Liu, T.; Wang, F.; Michalski, G.; Xia, X., and Liu, S. Using  $^{15}\text{N}$ ,  $^{17}\text{O}$ , and  $^{18}\text{O}$  to determine nitrate sources in the Yellow River, China. *Environmental Science & Technology*, 47(23):13412–13421, 2013.
- Louchart, X.; Voltz, M.; Andrieux, P., and Moussa, R. Herbicide transport to surface waters at field and watershed scales in a Mediterranean vineyard area. *Journal of Environmental Quality*, 30(3):982–991, 2001.
- Mancini, S. A.; Lacrampe-Couloume, G.; Jonker, H.; van Breukelen, B. M.; Groen, J.; Volkering, F., and Sherwood Lollar, B. Hydrogen isotopic enrichment: An indicator of biodegradation at a petroleum hydrocarbon contaminated field site. *Environmental Science & Technology*, 36(11):2464–2470, 2002.
- Mancini, S. A.; Ulrich, A. C.; Lacrampe-Couloume, G.; Sleep, B.; Edwards, E. A., and Sherwood Lollar, B. Carbon and hydrogen isotopic fractionation during anaerobic biodegradation of benzene. *Applied and Environmental Microbiology*, 69(1):191–198, 2003.
- Mancini, S. A.; Lacrampe-Couloume, G., and Lollar, B. S. Source differentiation for benzene and chlorobenzene groundwater contamination: A field application of stable carbon and hydrogen isotope analyses. *Environmental Forensics*, 9(2-3):177–186, 2008.
- Mariotti, A.; Germon, J. C.; Hubert, P.; Kaiser, P.; Letolle, R.; Tardieux, A., and Tardieux, P. Experimental determination of nitrogen kinetic isotope fractionation: Some principles; illustration for the denitrification and nitrification processes. *Plant and Soil*, 62(3): 413–430, 1981.
- McCallum, J. L.; Cook, P. G.; Brunner, P., and Berhane, D. Solute dynamics during bank storage flows and implications for chemical base flow separation. *Water Resources Research*, 46(7):W07541, 2010.
- Meckenstock, R. U.; Morasch, B.; Griebler, C., and Richnow, H. H. Stable isotope fractionation analysis as a tool to monitor biodegradation in contaminated aquifers. *Journal of Contaminant Hydrology*, 75(3-4):215–255, 2004.
- Meyer, A. H. and Elsner, M.  $^{13}\text{C}/^{12}\text{C}$  and  $^{15}\text{N}/^{14}\text{N}$  isotope analysis to characterize degradation of atrazine: Evidence from parent and daughter compound values. *Environmental Science & Technology*, 47(13):6884–6891, 2013.
- Meyer, A. H.; Penning, H.; Lowag, H., and Elsner, M. Precise and accurate compound specific carbon and nitrogen isotope analysis of atrazine: Critical role of combustion oven conditions. *Environmental Science & Technology*, 42(21):7757–7763, 2008.
- Meyer, A. H.; Penning, H., and Elsner, M. C and N isotope fractionation suggests similar mechanisms of microbial atrazine transformation despite involvement of different enzymes (AtzA and TrzN). *Environmental Science & Technology*, 43(21):8079–8085, 2009.
- Milosevic, N.; Qiu, S.; Elsner, M.; Einsiedl, F.; Maier, M. P.; Bensch, H. K. V.; Albrechtsen, H. J., and Bjerg, P. L. Combined isotope and enantiomer analysis to assess the fate of phenoxy acids in a heterogeneous geologic setting at an old landfill. *Water Research*, 47(2):637–649, 2013.
- Mirus, B. B. and Loague, K. How runoff begins (and ends): Characterizing hydrologic response at the catchment scale. *Water Resources Research*, 49(5):2987–3006, 2013.
- Mirus, B. B.; Ebel, B. A.; Heppner, C. S., and Loague, K. Assessing the detail needed to capture rainfall-runoff dynamics with physics-based hydrologic response simulation. *Water Resources Research*, 47(3):1944–1973, 2011.

- Moore, J. W. and Semmens, B. X. Incorporating uncertainty and prior information into stable isotope mixing models. *Ecology Letters*, 11(5):470–480, 2008.
- Morasch, B.; Hunkeler, D.; Zopfi, J.; Temime, B., and Höhener, P. Intrinsic biodegradation potential of aromatic hydrocarbons in an alluvial aquifer – potentials and limits of signature metabolite analysis and two stable isotope-based techniques. *Water Research*, 45(15):4459–4469, 2011.
- Müller, K.; Bach, M.; Hartmann, H.; Spiteller, M., and Frede, H. G. Point- and nonpoint-source pesticide contamination in the Zwesten Ohm catchment, Germany. *Journal of Environmental Quality*, 31(1):309–18, 2002.
- Müller, K.; Deurer, M.; Hartmann, H.; Bach, M.; Spiteller, M., and Frede, H. G. Hydrological characterisation of pesticide loads using hydrograph separation at different scales in a German catchment. *Journal of Hydrology*, 273(1-4):1–17, 2003.
- Okuda, T.; Kumata, H.; Zakaria, M. P.; Naraoka, H.; Ishiwatari, R., and Takada, H. Source identification of Malaysian atmospheric polycyclic aromatic hydrocarbons nearby forest fires using molecular and isotopic compositions. *Atmospheric Environment*, 36(4): 611–618, 2002.
- Otto, R. Estimating groundwater recharge rates in the southeastern Holstein region, northern Germany. *Hydrogeology Journal*, 9(5):498–511, 2001.
- Overeem, A.; Buishand, T. A., and Holleman, I. Extreme rainfall analysis and estimation of depth-duration-frequency curves using weather radar. *Water Resources Research*, 45(10):W10424, 2009.
- Parkhurst, D. L.; Kipp, K. L., and Charlton, S. R. PHAST version 2–A program for simulating groundwater flow, solute transport, and multicomponent geochemical reactions. Technical report, U.S. Geological Survey Techniques and Methods 6-A35, 2010.
- Parochetti, J. V. Photodecomposition, volatility and leaching of atrazine, simazine, alachlor and metolachlor from soil and plant material. Weed Science Society of America, abstract no. 17, 1978.
- Payraudeau, S. and Gregoire, C. Modelling pesticides transfer to surface water at the catchment scale: a multi-criteria analysis. *Agronomy for Sustainable Development*, 32(2):479–500, 2012.
- Penning, H. and Elsner, M. Intramolecular carbon and nitrogen isotope analysis by quantitative dry fragmentation of the phenylurea herbicide isoproturon in a combined injector/capillary reactor prior to GC separation. *Analytical Chemistry*, 79(21):8399–8405, 2007.
- Penning, H.; Sørensen, S. R.; Meyer, A. H.; Aamand, J., and Elsner, M. C, N, and H isotope fractionation of the herbicide isoproturon reflects different microbial transformation pathways. *Environmental Science & Technology*, 44(7):2372–2378, 2010.
- Phillips, D. and Gregg, J. Uncertainty in source partitioning using stable isotopes. *Oecologia*, 127:171–179, 2001.
- Phillips, D. and Koch, P. Incorporating concentration dependence in stable isotope mixing models. *Oecologia*, 130:114–125, 2002.
- Pooley, K. E.; Blessing, M.; Schmidt, T. C.; Haderlein, S. B.; Macquarrie, K. T. B., and Prommer, H. Aerobic biodegradation of chlorinated ethenes in a fractured bedrock aquifer: Quantitative assessment by compound-specific isotope analysis (CSIA) and reactive transport modeling. *Environmental Science & Technology*, 43(19):7458–7464, 2009.
- Prommer, H.; Anneser, B.; Rolle, M.; Einsiedl, F., and Griebler, C. Biogeochemical and isotopic gradients in a BTEX/PAH contaminant plume: Model-based interpretation of

- a high-resolution field data set. *Environmental Science & Technology*, 43(21):8206–8212, 2009.
- Qiu, S.; Eckert, D.; Cirpka, O. A.; Huenniger, M.; Knappett, P.; Maloszewski, P.; Meckenstock, R. U.; Griebler, C., and Elsner, M. Direct experimental evidence of non-first order degradation kinetics and sorption-induced isotopic fractionation in a mesoscale aquifer:  $^{13}\text{C}/^{12}\text{C}$  analysis of a transient toluene pulse. *Environmental Science & Technology*, 47(13):6892–6899, 2013.
- Querner, E. P. The effects of human intervention in the water regime. *Ground Water*, 38(2):167–171, 2000.
- Quilbe, R.; Rousseau, A. N.; Lafrance, P.; Leclerc, J., and Amrani, M. Selecting a pesticide fate model at the watershed scale using a multi-criteria analysis. *Water Quality Research Journal of Canada*, 41(3):283–295, 2006.
- Rabiet, M.; Margoum, C.; Gouy, V.; Carluer, N., and Coquery, M. Assessing pesticide concentrations and fluxes in the stream of a small vineyard catchment – effect of sampling frequency. *Environmental Pollution*, 158(3):737–748, 2010.
- Rawn, D F. K. and Muir, Derek C. G. Sources of chlorpyrifos and dacthal to a small Canadian prairie watershed. *Environmental Science & Technology*, 33(19):3317–3323, 1999.
- Reinnicke, S; Simonsen, A; Sørensen, S R.; Aamand, J, and Elsner, M. C and N isotope fractionation during biodegradation of the pesticide metabolite 2,6-dichlorobenzamide (BAM): Potential for environmental assessments. *Environmental Science & Technology*, 46(3):1447–1454, 2011.
- Rice, P. J.; Anderson, T. A., and Coats, J. R. Degradation and persistence of metolachlor in soil: Effects of concentration, soil moisture, soil depth, and sterilization. *Environmental Toxicology and Chemistry*, 21(12):2640–2648, 2002.
- Richards, R. P. and Baker, D. B. Pesticide concentration patterns in agricultural drainage networks in the lake erie basin. *Environmental Toxicology and Chemistry*, 12(1):13–26, 1993.
- Rivard, L. Environmental fate of metolachlor, 2003.
- Rivett, M. O.; Chapman, S. W.; Allen-King, R. M.; Feenstra, S., and Cherry, J. A. Pump-and-treat remediation of chlorinated solvent contamination at a controlled field-experiment site. *Environmental Science & Technology*, 40(21):6770–6781, 2006.
- Rodríguez-Cruz, M. S.; Jones, J. E., and Bending, G. D. Field-scale study of the variability in pesticide biodegradation with soil depth and its relationship with soil characteristics. *Soil Biology and Biochemistry*, 38(9):2910–2918, 2006.
- Rolle, M.; Chiogna, G.; Bauer, R.; Griebler, C., and Grathwohl, P. Isotopic fractionation by transverse dispersion: Flow-through microcosms and reactive transport modeling study. *Environmental Science & Technology*, 44(16):6167–6173, 2010.
- Rozemeijer, J. C. and Broers, H. P. The groundwater contribution to surface water contamination in a region with intensive agricultural land use (Noord-Brabant, The Netherlands). *Environmental Pollution*, 148(3):695–706, 2007.
- Schmidt, T. C. and Jochmann, M. A. Origin and fate of organic compounds in water: characterization by compound-specific stable isotope analysis. *Annual Review of Analytical Chemistry*, 5:133–55, 2012.
- Schmidt, T. C.; Zwank, L.; Elsner, M.; Berg, M.; Meckenstock, R. U., and Haderlein, S. B. Compound-specific stable isotope analysis of organic contaminants in natural environments: a critical review of the state of the art, prospects, and future challenges. *Analytical and Bioanalytical Chemistry*, 378(2):283–300, 2004.

- Schreglmann, K.; Hoeche, M.; Steinbeiss, S.; Reinicke, S., and Elsner, M. Carbon and nitrogen isotope analysis of atrazine and desethylatrazine at sub-microgram per liter concentrations in groundwater. *Analytical and Bioanalytical Chemistry*, 405(9): 2857–2867, 2013.
- Seiler, R. L. Combined use of  $^{15}\text{N}$  and  $^{18}\text{O}$  of nitrate and  $^{11}\text{B}$  to evaluate nitrate contamination in groundwater. *Applied Geochemistry*, 20(9):1626–1636, 2005.
- Sherwood Lollar, B.; Slater, G. F.; Sleep, B.; Witt, M.; Klecka, G. M.; Harkness, M., and Spivack, J. Stable carbon isotope evidence for intrinsic bioremediation of tetrachloroethene and trichloroethene at area 6, Dover Air Force Base. *Environmental Science & Technology*, 35(2):261–9, 2001.
- Sherwood Lollar, B.; Hirschorn, S. K.; Chartrand, M. M. G., and Lacrampe-Couloume, G. An approach for assessing total instrumental uncertainty in compound-specific carbon isotope analysis: Implications for environmental remediation studies. *Analytical Chemistry*, 79(9):3469–3475, 2007.
- Si, Y.; Takagi, K.; Iwasaki, A., and Zhou, D. Adsorption, desorption and dissipation of metolachlor in surface and subsurface soils. *Pest Management Science*, 65(9):956–962, 2009.
- Squillace, P. J. and Thurman, E. M. Herbicide transport in rivers: Importance of hydrology and geochemistry in nonpoint-source contamination. *Environmental Science and Technology*, 26:538–545, 1992.
- Sturchio, N. C.; Böhlke, J. K.; Gu, B.; Horita, J.; Brown, G. M.; Beloso, A. D. Jr.; Patterson, L. J.; Hatzinger, P. B.; Jackson, W. A., and Batista, J. Stable isotopic composition of chlorine and oxygen in synthetic and natural perchlorate. In Baohua, G. and Coates, J. D., editors, *Perchlorate*, pages 93–109. Springer US, 2006.
- Sturchio, N. C.; Böhlke, J. K.; Beloso, A. D.; Streger, S. H.; Heraty, L. J., and Hatzinger, P. B. Oxygen and chlorine isotopic fractionation during perchlorate biodegradation: Laboratory results and implications for forensics and natural attenuation studies. *Environmental Science & Technology*, 41(8):2796–2802, 2007.
- Sturchio, N. C.; Hoaglund, J. R.; Marroquin, R. J.; Beloso, A. D.; Heraty, L. J.; Bortz, S. E., and Patterson, T. L. Isotopic mapping of groundwater perchlorate plumes. *Ground Water*, 50(1):94–102, 2012.
- Sudicky, E. A.; Illman, W. A.; Goltz, I. K.; Adams, J. J., and McLaren, R. G. Heterogeneity in hydraulic conductivity and its role on the macroscale transport of a solute plume: From measurements to a practical application of stochastic flow and transport theory. *Water Resources Research*, 46(1):W01508, 2010.
- Taghavi, L.; Merlina, G., and Probst, J.-L. The role of storm flows in concentration of pesticides associated with particulate and dissolved fractions as a threat to aquatic ecosystems - case study: the agricultural watershed of Save river (Southwest of France). *Knowledge and Management of Aquatic Ecosystems*, (400):06, 2011.
- Therrien, R.; McLaren, R. G.; Sudicky, E. A., and Panday, S. M. HydroGeoSphere, a three-dimensional numerical model describing fully integrated subsurface and surface flow and solute transport, draft. Technical report, Groundwater Simulation Group, University of Waterloo, 2010.
- Thompson, A.; Rudolph, J.; Rohrer, F., and Stein, O. Concentration and stable carbon isotopic composition of ethane and benzene using a global three-dimensional isotope inclusive chemical tracer model. *Journal of Geophysical Research: Atmospheres*, 108 (D13):4373, 2003.
- Thorsen, M.; Feyen, J., and Styczen, M. Agrochemical modelling. In Abbott, M.B. and Refsgaard, J.C., editors, *Distributed Hydrological Modelling*, pages 121–141. Kluwer Academic Publishers, Dordrecht, The Netherlands, 1996.

- Thullner, M.; Centler, F.; Richnow, H.-H., and Fischer, A. Quantification of organic pollutant degradation in contaminated aquifers using compound specific stable isotope analysis - review of recent developments. *Organic Geochemistry*, 42(12):1440–1460, 2012.
- University of Hertfordshire, The Pesticide Properties DataBase (PPDB) developed by the Agriculture & Environment Research Unit (AERU), University of Hertfordshire, 2013.
- van Breukelen, B. M. Extending the Rayleigh equation to allow competing isotope fractionating pathways to improve quantification of biodegradation. *Environmental Science & Technology*, 41(11):4004–4010, 2007a.
- van Breukelen, B. M. Quantifying the degradation and dilution contribution to natural attenuation of contaminants by means of an open system Rayleigh equation. *Environmental Science & Technology*, 41(14):4980–4985, 2007b.
- van Breukelen, B. M. and Prommer, H. Beyond the Rayleigh equation: Reactive transport modeling of isotope fractionation effects to improve quantification of biodegradation. *Environmental Science & Technology*, 42(7):2457–2463, 2008.
- van Breukelen, B. M. and Rolle, M. Transverse hydrodynamic dispersion effects on isotope signals in groundwater chlorinated solvents' plumes. *Environmental Science & Technology*, 46(14):7700–7708, 2012.
- van Breukelen, B. M.; Hunkeler, D., and Volkering, F. Quantification of sequential chlorinated ethene degradation by use of a reactive transport model incorporating isotope fractionation. *Environmental Science & Technology*, 39(11):4189–4197, 2005.
- van den Berg, F.; Kubiak, R.; Benjey, W. G.; Majewski, M. S.; Yates, S. R.; Reeves, G. L.; Smelt, J. H., and van der Linden, A. M. A. Emission of pesticides into the air. *Water, Air, & Soil Pollution*, 115(1):195–218, 1999.
- van der Velde, Y.; de Rooij, G. H.; Rozemeijer, J. C.; van Geer, F. C., and Broers, H. P. Nitrate response of a lowland catchment: On the relation between stream concentration and travel time distribution dynamics. *Water Resources Research*, 46(11):W11534, 2010.
- van der Velde, Y.; Torfs, P. J. J. F.; van der Zee, S. E. A. T. M., and Uijlenhoet, R. Quantifying catchment-scale mixing and its effect on time-varying travel time distributions. *Water Resources Research*, 48(6):W06536, 2012.
- van der Velde, Y.; Heidbüchel, I.; Lyon, S. W.; Nyberg, L.; Rodhe, A.; Bishop, K., and Troch, P. A. Consequences of mixing assumptions for time-variable travel time distributions. Accepted by *Hydrological Processes*, DOI: 10.1002/hyp.10372, 2014.
- van Keer, I.; Bronders, J.; Verhack, J.; Schwarzbauer, J., and Swennen, R. Limitations in the use of compound-specific stable isotope analysis to understand the behaviour of a complex BTEX groundwater contamination near Brussels (Belgium). *Environmental Earth Sciences*, 66(2):457–470, 2012.
- Verbist, K. M. J.; Pierreux, S.; Cornelis, W. M.; McLaren, R., and Gabriels, D. Parameterizing a coupled surface-subsurface three-dimensional soil hydrological model to evaluate the efficiency of a runoff water harvesting technique. *Vadose Zone Journal*, 11(4), 2012.
- Vieth, A.; Kästner, M.; Schirmer, M.; Weiß, H.; Gödeke, S.; Meckenstock, R. U., and Richnow, H. H. Monitoring in situ biodegradation of benzene and toluene by stable carbon isotope fractionation. *Environmental Toxicology and Chemistry*, 24(1):51–60, 2005.
- Voss, M.; Deutsch, B.; Elmgren, R.; Humborg, C.; Kuuppo, P.; Pastuszak, M.; Rolff, C., and Schulte, U. Source identification of nitrate by means of isotopic tracers in the Baltic Sea catchments. *Biogeosciences*, 3(4):663–676, 2006.

- Wang, Y.; Huang, Y. S.; Huckins, J. N., and Petty, J. D. Compound-specific carbon and hydrogen isotope analysis of sub-parts per billion level waterborne petroleum hydrocarbons. *Environmental Science & Technology*, 38(13):3689–3697, 2004.
- Wanner, C.; Eggenberger, U.; Kurz, D.; Zink, S., and Mäder, U. A chromate-contaminated site in southern Switzerland—Part 1: Site characterization and the use of Cr isotopes to delineate fate and transport. *Applied Geochemistry*, 27(3):644–654, 2012a.
- Wanner, C.; Eggenberger, U., and Mäder, U. A chromate-contaminated site in southern Switzerland—Part 2: Reactive transport modeling to optimize remediation options. *Applied Geochemistry*, 27(3):655–662, 2012b.
- Weiler, M. and McDonnell, J. Virtual experiments: a new approach for improving process conceptualization in hillslope hydrology. *Journal of Hydrology*, 285(1-4):3–18, 2004.
- Weller, P.; Boner, M.; Foerstel, H.; Becker, H.; Peikert, B., and Dreher, W. Isotopic fingerprinting for the authenticity control of crop protection active compounds using the representative insecticide fipronil. *Journal of Agricultural and Food Chemistry*, 59(9):4365–4370, 2011.
- Wiegert, C.; Aeppli, C.; Knowles, T.; Holmstrand, H.; Evershed, R.; Pancost, R. D.; Macháčková, J., and Gustafsson, Ö. Dual carbon-chlorine stable isotope investigation of sources and fate of chlorinated ethenes in contaminated groundwater. *Environmental Science & Technology*, 46(20):10918–10925, 2012.
- Wijker, R. S.; Adamczyk, P.; Bolotin, J.; Paneth, P., and Hofstetter, T. B. Isotopic analysis of oxidative pollutant degradation pathways exhibiting large H isotope fractionation. *Environmental Science & Technology*, 47(23):13459–13468, 2013.
- Wriedt, G.; Spindler, J.; Neef, T.; Meißner, R., and Rode, M. Groundwater dynamics and channel activity as major controls of in-stream nitrate concentrations in a lowland catchment system? *Journal of Hydrology*, 343(3-4):154–168, 2007.
- Wu, L.; Yao, J.; Trebse, P.; Zhang, N., and Richnow, H. H. Compound specific isotope analysis of organophosphorus pesticides. *Chemosphere*, 111(0):458–463, 2014.
- Wu, Q.; Riise, G.; Lundekvam, H.; Mulder, J., and Haugen, L. E. Influences of suspended particles on the runoff of pesticides from an agricultural field at Askim, SE-Norway. *Environmental Geochemistry and Health*, 26(2):295–302, 2004.
- Xue, D.; Botte, J.; De Baets, B.; Accoe, F.; Nestler, A.; Taylor, P.; van Cleemput, O.; Berglund, M., and Boeckx, P. Present limitations and future prospects of stable isotope methods for nitrate source identification in surface- and groundwater. *Water Research*, 43(5):1159–1170, 2009.
- Zehe, E.; Maurer, T.; Ihringer, J., and Plate, E. Modeling water flow and mass transport in a loess catchment. *Physics and Chemistry of the Earth Part B-Hydrology Oceans and Atmosphere*, 26(7-8):487–507, 2001.
- Zhang, Y.-C.; Slomp, C. P.; Broers, H. P.; Bostick, B.; Passier, H. F.; Böttcher, M. E.; Omoregie, E. O.; Lloyd, J. R.; Polya, D. A., and van Cappellen, P. Isotopic and microbiological signatures of pyrite-driven denitrification in a sandy aquifer. *Chemical Geology*, 300-301(0):123–132, 2012.
- Zwank, L.; Berg, M.; Schmidt, T. C., and Haderlein, S. B. Compound-specific carbon isotope analysis of volatile organic compounds in the low-microgram per liter range. *Analytical Chemistry*, 75(20):5575–5583, 2003.
- Zwank, L.; Berg, M.; Elsner, M.; Schmidt, T. C.; Schwarzenbach, R. P., and Haderlein, S. B. New evaluation scheme for two-dimensional isotope analysis to decipher biodegradation processes: Application to groundwater contamination by mtbe. *Environmental Science & Technology*, 39(4):1018–1029, 2005.

